Proceedings

Guang-Zhong Yang and Ara Darzi (Eds.)

The Hamlyn Symposium on Medical Robotics

19-20 June 2011

Imperial College London, UK

Proceedings of
The Hamlyn Symposium on Medical Robotics
19-20 June 2011, Imperial College
London, UK
ISBN: 978-0-9563776-2-3

Preface

The 4th Hamlyn Symposium on Medical Robotics was held at the Hamlyn Centre for Robotic Surgery and The Royal Geographical Society in London, UK on 19-20 June 2011.

The Hamlyn Symposium grew out of Imperial College's Cross Faculty Workshops on Medical Robotics funded by the Hamlyn Centre for Robotic Surgery. The focus of the 2011 Symposium continued with the similar theme of previous years - to develop healthcare technologies that are safe, intelligent, cost effective and accessible to patients. The Symposium is now established as an annual international forum for clinicians, engineers and researchers to exchange ideas and explore new challenges and opportunities in healthcare technologies, and this year's meeting was extended to a two day meeting. All of this would of course, not be possible without the generous philanthropic support from both the Helen Hamlyn Trust and Lady Hamlyn personally.

This year, we attracted 63 papers from 8 countries and after systematic peer review, 42 papers were selected for presentation at the Symposium. The topics covered ranged from clinical outcomes, planning and navigation, perception and vision, emerging hardware platforms, training and neuroergonomics, and general considerations of robotic surgery in routine clinical settings.

A series of invited talks from distinguished speakers, including Professor Russ Taylor, Dr Lee Swanstrom, Professor Andreas Melzer, Professor Dennis Fowler, Professor Kirby Vosburgh and Dr Ashutosh Tewari, provided insights into the cutting edge developments in this field. The keynote was delivered by Professor Nam Pho Suh, President of KAIST, who started this year's panel debate by providing an overview of "Invention Process, Innovation Continuum, and Case Studies: What we can learn from OLEV, MH, and MuCell for Medical Robotics." Lively discussions followed, focusing on the innovation processes of technology design and what we can learn from other engineering disciplines; as well as the need for both engineers and clinicians who are familiar with the translational processes, to take the lead in the clinical translation of new technologies to improve patient outcomes.

We would like to thank the entire Programme Committee, the Best Paper Awards Committee and the Local Organising Committee for giving up their precious time ensuring timely review of all the papers submitted and helping to provide an excellent symposium programme. The meeting would not be possible without the commitment and hard work of a dedicated team. In particular, we are grateful to Karen Kerr, Ruzanna Gulakyan, Sejal Jiwan, Raphaele Raupp, Daniel Elson, Su-Lin Lee, Danail Stoyanov, and Ling Li for working behind the scene and for their tireless effort in managing all aspects of the symposium organisation.

It was our pleasure to welcome the Symposium attendees to London.

June 2011, London

Guang-Zhong Yang
Ara Darzi

Organisation

General and Programme Co-Chairs

Professor Guang-Zhong Yang
Lord Ara Darzi

Programme Committee

Nick Cheshire	*Imperial College London*
Paolo Dario	*Scuola Superiore Sant'Anna, Pisa*
Prokar Dasgupta	*King's College London*
Hubertus Feussner	*Technical University Munich*
Dennis Fowler	*Columbia University*
Blake Hannaford	*University of Washington*
Branislav Jaramaz	*Carnegie Mellon University*
Jacques Marescaux	*University Hospital, Strasbourg*
Alex Mottrie	*Catholic University of Leuven, Belgium*
Azad Najmaldin	*St James University Hospital, Leeds*
Nassir Navab	*Technical University Munich*
Bradley Nelson	*ETH-Zürich*
Vipul Patel	*Global Robotic Institute*
Geoff Pegman	*R U Robots Limited*
Cameron Riviere	*Carnegie Mellon University*
Lee Swanstrom	*University of Oregon*
Mark Talimini	*University of California*
Russ Taylor	*Johns Hopkins University*
Chris Thompson	*Harvard Medical School*
Justin Vale	*Imperial College London*
Steve Wexner	*Cleveland Clinic Florida*

Local Organising Committee

Karen Kerr
Sejal Jiwan
Ruzanna Gulakyan
Hutan Ashrafian
Thanos Athanasiou
Colin Bicknell
Brian Davies
Daniel Elson
Leonard Fass
Mohamad Hamady
Su-Lin Lee
Daniel Leff
Erik Mayer
George Mylonas
Celia Riga
Ferdinando Rodriguez y Baena
Mikael Sodergren
Danail Stoyanov
Julian Teare

Table of Contents

Emerging Hardware Platforms

Clinical Outcomes

Training and Neuroergonomics

Poster Presentations

Invention Process, Innovation Continuum, and Case Studies: OLEV, MH, and MuCell

Nam P. Suh

KAIST, Daejeon, Korea
npsuh@kaist.edu

ABSTRACT

The field of medical robotics has grown significantly during the past two decades from the R&D phase to commercialization. This growth is likely to continue, expanding into more complicated application areas. This expected growth will require both creative designers and medical practitioners who are familiar with both the systematic processes that can lead to creative products and with the innovation processes that can transform an invention into a commercially successful innovation. The purpose of this presentation is twofold: to illustrate the invention process using the theoretic framework of Axiomatic Design (AD) and to outline the pre-requisites that must be fulfilled in converting inventions into innovations based on a theory of innovation. Three case studies will be used to illustrate both the design and innovation processes.

INTRODUCTION

A fundamental understanding of a design theory such as Axiomatic Design (AD) minimizes the time and effort required to develop new creative products and systems [1, 2]. AD requires the designer to do the following: identify the right set of "customer needs"; establish a right set of functional requirements (FRs) and design parameters (DPs) for the final product; conceptualize creative designs; decompose FRs and DPs; satisfy the independence of FRs by choosing a correct set of DPs that can satisfy the FRs throughout the decomposition process; and minimize the information content. During the design process, the independence of FRs must be checked explicitly throughout the decomposition process to develop diagonal or triangular design matrices. When this design process is properly followed, it leads to a creative product that has high reliability, incurs low development costs, enables low-cost manufacturing, and involves a minimum life-cycle cost.

The systematic approach to design applies to a diverse set of systems, ranging from mechanical, electromechanical, medical, communications, electrical, transportation, chemical, biological, and hybrid. All of these systems are structurally similar from the AD perspective. They involve the following key concepts: definition of "needs," the existence of the four domains, FRs, DPs, constraints, the need to satisfy the two axioms of AD, and the development of design matrices. Field specific knowledge needed to deal with these diverse systems can be acquired through study or collaboration with others who have the requisite knowledge. Three case studies presented in this paper illustrate this design process.

Innovation of OLEV

One of the case studies is the development of an electric vehicle called the On-Line Electric Vehicle (OLEV) [3-5]. The design of OLEV involved eight highest-level FRs and DPs, which were decomposed to many lower-level FRs and DPs. Unlike typical electric vehicles (EV) that carry the electric energy needed for mobility in the vehicle in the form of rechargeable batteries, OLEV is designed to receive its electric energy externally from an underground electric power system while in motion without any mechanical contact (i.e., wirelessly). This external supply of electric energy to the vehicle overcomes the major shortcoming of EV, which is the use of large batteries that are expensive, heavy, and bulky.

OLEV carries a small battery on board that enables the vehicle to operate autonomously even on roads without the underground electric cable. When OLEV operates with the power supplied from the underground cable, the battery is recharged. Because of the small battery on board, the underground cable is not needed everywhere, reducing the infrastructure cost. In Seoul Grand Park where an OLEV system has been installed, only 16% of the 2.2 km roadway has the underground cable installed in four sections of the road. The fraction of the road imbedded with underground cable depends on the speed of the vehicle, the fraction of the time spent at stations for passenger loading and unloading, the number of stops at signal lights, and air-conditioning and heating requirements.

The basic technology that enables the transmission of a large amount of electric energy from the underground electric cable to OLEV is named the Shaped Magnetic Field in Resonance (SMFIR). It converts the electrical energy (20 KHz at 200 amps and 440 V) supplied to the underground cable to an alternating magnetic field above ground, which is picked up by a resonating pick-up device attached to the vehicle. The efficiency of power transfer depends on the distance between the ground surface and the pick-up unit on the vehicle, the shape of the magnetic field, and the pick-up device. At a distance of 20 cm, the efficiency can be as high as 85%. It can be made higher by varying design parameters. OLEV is one of the many applications for SMFIR. It satisfies the world's most stringent specifications on EMF irradiation, safety, etc. OLEV was selected by

TIME magazine as one of the "50 Best Inventions of 2010."

The Innovation Process

The invention and development of OLEV does not guarantee that it will be commercially successful. The process of commercializing OLEV followed the guidelines provided by a theory of innovation that consists of three laws of innovation [6].

The first law of innovation states that all the elements (or steps) of the "Innovation Continuum" must be present for innovation to occur. The innovation continuum includes a series of sequential and concurrent elements: discovery, invention, angel and venture investment, marketing, manufacturing, etc. The second law of innovation states that an innovation hub must be nucleated by overcoming an activation energy barrier for innovation and that the rate of nucleation follows an exponential relationship similar to the Arrhenius relationship. The third law of innovation states that for a city or a region to become an innovation hub, the rate of nucleation of innovation must be faster than the rate of diffusion of talented people, investment, and ideas away from the region. In commercializing OLEV, the implications of these three laws were considered, especially the first law that requires the existence of all the elements of the innovation continuum.

The Boston and the Silicon Valley area of the United States satisfy the three laws of innovation better than any other regions of the world. They satisfy the innovation continuum (i.e., the first law of innovation) and the second and the third laws of innovation.

New venture firms were established in Korea and the United States to commercialize OLEV, since it was difficult to convince existing automobile manufacturers to commercialize the OLEV technologies. This situation is not unique to the medical robotics field. When disruptive technologies are introduced, they are often overlooked by the manufactures of well-established products (e.g., electronic digital photography vs traditional analog photography) [7].

Implications to Medial Robotics Field

Of the many creative designs that will be advanced in the field of medical robotics, only a few inventions will become commercially successful innovations. This low success rate in converting research results and inventions into successful innovations is not unique to the medical field.

Examining the innovation process leads us to the conclusion that for a product to become a successful innovation, we must develop products that truly satisfy the customer needs at all times, which is aided by a theoretic framework for rational design. Then for the invented product to be commercially successful, it must be nurtured in an entrepreneurial environment that has all the required elements of the innovation continuum.

In order to illustrate both the design process and the innovation process further, two other case studies will be briefly mentioned in this presentation. One – microcellular plastics (MuCell) -- is a commercially well established product that was invented at MIT [8]. The other invention – Mobile Harbor (MH) -- is in the early phase of commercialization at KAIST [9]. The Mobile Harbor project was initiated in 2009 together with the OLEV project at KAIST, but its conversion from a creative product to innovation has been more difficult due to the massive investment required to build a commercial-scale product for demonstration.

CONCLUSION

The three case studies and the theories of design and innovation presented in this paper may provide useful references and prove useful as the field of medical robotics takes on increasingly challenging new tasks in the future.

REFERENCES

[1] Suh, N. P. The Principles of Design. Oxford University Press, New York. 1990.

[2] Suh, N. P. Axiomatic Design: Advances and Applications. Oxford University Press, New York. 2001.

[3] Suh, N. P., Cho, D.H., and Rim, C.T. Design of On-Line Electric Vehicle (OLEV), Global Product Development (ed. Alain Bernard). Proceedings of the 20th CIRP Design Conference. Ecole Centrale de Nantes, Nantes, France. (Keynote paper). Springer. April 2010. (ISBN 978-3-642-15972-5 e-ISBN 978-3-642-15973-2).

[4] Suh, N. P. 2011, Design of Wireless Electric Power Transfer Technology: Shaped Magnetic Field in Resonance (SMFIR). Proceedings of the 2011 CIRP Design Conference, March 28, 2011, KAIST, Daejeon, Korea. 2011.

[5] Kim, J.H., Cho, D.H., Suh, N.P., Byun, J.K., Lee, H.J., Kang, D.S., Ahn, S.Y., and Choi, C.S. Wireless Power Transmission Device with Minimum EMF Leakage. Patent Application. 2010.

[6] Suh, N. P. A Theory of Innovation and Case Study. International Journal of Innovation Management. Vol. 14, No. 5 (October 2010) 893–913

[7] Christensen, Clayton M. The Innovator's Dilemma: When New Technologies Cause Great Firms to Fail. Boston, MA, Harvard Business School Press. 1997.

[8] Park, C.B., Baldwin, D.F., and Suh N.P. "A Method of Providing Continuous Processing of Microcellular and Supermicrocellular Foamed Materials." U.S. Patent 5,866,053, February 2, 1999.

[9] Suh, N. P. "Mobile Harbor", 2008, Korean Patent Office, 1020080012428, Date filed 2008.02.1

Recent Work Toward a Microsurgical Assistant for Retinal Surgery

R. Taylor[1*], J. Kang[1], I. Iordachita[1], G. Hager[1], P. Kazanzides[1], C. Riviere[2], E. Gower[1], R. Richa[1], M. Balicki[1], X. He[1], X. Liu[1], K. Olds[1], R. Sznitman[1], B. Vagvolgyi[1], P. Gehlbach[1], J. Handa[1]

[1]Engineering Research Center for Computer-Integrated Surgical Systems and Technology, Johns Hopkins University

[2] Robotics Institute, Carnegie-Mellon University

** rht@jhu.edu*

INTRODUCTION

This short paper describes recent work to develop technology and systems addressing fundamental limitations in current microsurgical practice, using vitreoretinal surgery as our focus. Vitreoretinal surgery is the most technically demanding ophthalmologic discipline and addresses prevalent sight-threatening conditions in areas of growing need. With the aging of our population, the prevalence of sight-threatening conditions will continue to escalate. Retinal surgery is currently performed under an operating microscope with free-hand instrumentation. Limitations include limited visual resolution, and physiological hand tremor. The surgeon also struggles with a lack of tactile feedback, proximity sensing, and real-time sensing of physiological parameters of the retina. Surgical technique and efficiency would be enhanced by the integration of preoperative images with the intraoperative view. Poor ergonomics for the surgeon in current practice result in surgeon fatigue and potential disability. All of these factors contribute to extended operating times, attendant light toxicity, and higher than needed complication rates.

MATERIALS AND METHODS

At the center of our planned approach is a "surgical workstation" system interfaced to a stereo visualization subsystem and a family of novel sensors, instruments, and robotic devices. The capabilities of these components individually address important limitations of current practice; together they provide a modular, synergistic, and extendable system that enables computer-interfaced technology and information processing to work in partnership with surgeons to improve clinical care and enable novel therapeutic approaches.

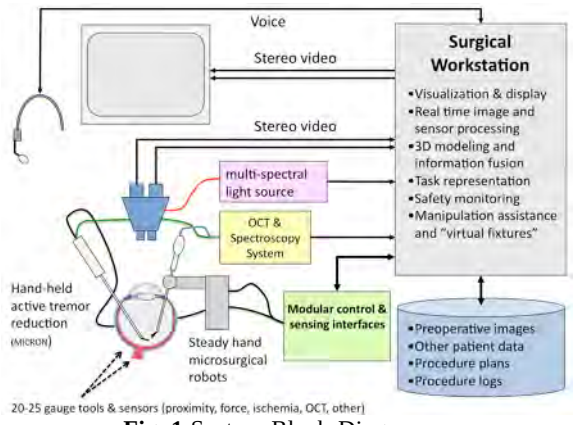

Fig. 1 System Block Diagram

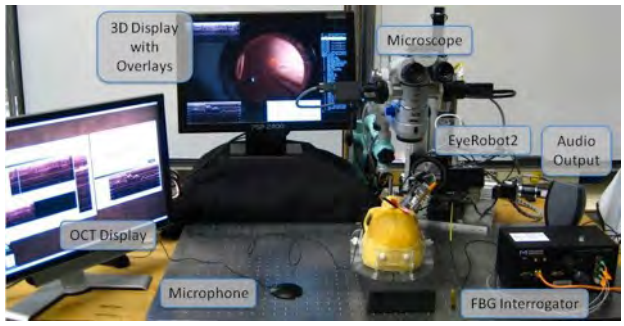

Fig. 2 Current system embodiment in our laboratory

RESULTS

Fig. 1 shows a block diagram of our system, and Fig. 2 shows a current embodiment in our laboratory.

Video Microscopy and Video Processing: In our current implementation, we have attached two Firewire HD video cameras to a Zeiss surgical microscope through custom optical couplers. The cameras are attached to a high end PC workstation, which drives a stereo display of the video, with various graphic overlays. The system is capable of operating at real-time frame rates in 2 megapixel resolution in stereo 3D. Current capabilities include video tracking of the retina and surgical tools in the images (Fig. 3), together with initial methods for

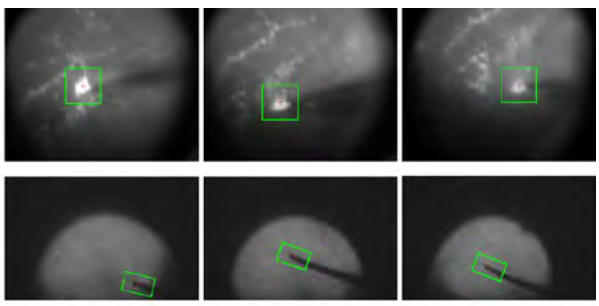

Fig. 3 (Top) Tracking the tip of a scraping tool during an ILM peeling procedure. (Bottom) Tool tracking on wide-angle lens (BIOM lens)

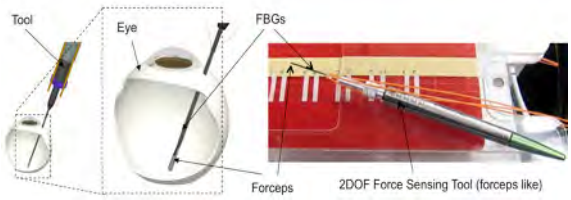

Fig. 4 FBG-based 2DOF force sensing forceps tool. (Left) concept; (Right) implementation

registering preoperative images to the stereo video, as well as methods for adaptively modifying the illumination spectrum and video colorization to reduce light toxicity. There is active research within our group to improve all of these capabilities.

"Smart" Sensing Instruments: We have developed sub-millimetric surgical tools that use optical fiber sensing to significantly extend the surgeon's sensory capabilities by directly sensing tool-to-tissue relationships. Optical fibers have many advantages, including low cost, sterilizability, small size, biocompatibility, and immunity to electromagnetic interference, that make them natural choices for microsurgical instruments. Tools developed so far include microsurgical force sensing tools based on FBG sensors embedded in the tool shafts (Fig. 4) and OCT sensing tools capable of sensing tool-to-tissue proximity, tissue structure beyond the tool, and tissue spectral properties.

Robotic Devices: Currently, our system environment supports two rather different robots: 1) Carnegie-Mellon University's hand-held MICRON device; and 2) the Johns Hopkins University steady-hand "eye robots". Both systems (Fig. 5) are research prototypes and considerable work needs to be done before either is ready for clinical use. Although each has very different dynamic characteristics and low-level control interfaces, there are some basic similarities as well. One of our goals is to develop higher-level functions in a way that both exploits the unique capabilities of each device and also permits functions developed for one platform to be ported to another in a relatively straightforward way, wherever that makes sense.

Surgical Augmentation Environment: One of the significant challenges for a system like ours is developing a coherent framework for managing all the different information streams and devices and making the capabilities developed available to the surgeon in a natural way. We have spent considerable effort to adapt our open-source Surgical Assistant Workstation (SAW) to provide a very flexible environment for combining the capabilities of our individual subsystems to assist the surgeon in performing useful tasks. Examples include: 1) integration of our OCT tools with our robotic devices to constrain tool-to-tissue distance relationships and to produce scanned images; 2) the use of our force sensing tools with our robotic devices to implement force-based virtual fixtures; 3) auditory sensory substitution methods to control tool-tissue forces in membrane peeling with hand-held tools and to warn of tool-to-tissue proximity; 4) visual overlay of OCT image and tool track information onto microscope images. Fig. 6 shows an annotated screen capture of our surgical display from a recent experiment on a phantom eye.

Fig. 5 (Left) CMU MICRON handheld robot; (Right) JHU cooperatively controlled Steady Hand robot

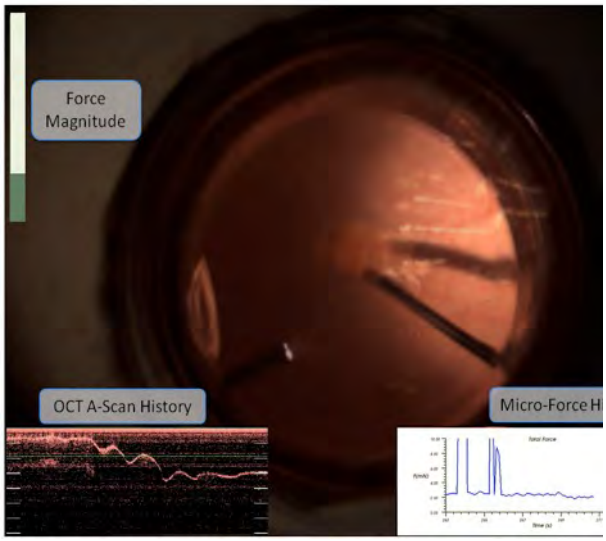

Fig. 6 Typical surgical display screenshot showing real time OCT and Force overlays

ACKNOWLEDGMENS

This work was funded in part by NIH BRP Grant 1 R01 EB 007969 and in part by Johns Hopkins internal funds.

REFERENCES

This abstract is intended as a system overview of recent work. Fuller project descriptions and a bibliography of our relevant publications may be found at http://ciis.lcsr.jhu.edu/dokuwiki/doku.php?id=research.robot_assisted_microsurgery and at http://www.ri.cmu.edu/research_lab_group_detail.html?lab_id=59&menu_id=263.

Novel Endoscopic Platforms for Endoluminal and Notes Surgery

Lee L. Swanstrom

Oregon Health Sciences University, Portland, Oregon, USA

lswanstrom@orclinic.com

The merger of interventional endoscopy and minimal access surgery is a natural progression as we continually push the envelope of minimally invasive surgery. ERCP, biliary stents and EUS have forever changed treatment algorithms and newer procedures like EMR and ESD stand to dramatically change the landscape of GI cancer care. NOTES and advanced endoluminal techniques like full thickness resection and POEM are early in their development but potentially have patient benefits including less pain, quicker recovery and fewer wound complications. A common theme to all these advances is the need for flexible endoscopic access but current endoscopes fall far short of functional practical design. To make these procedures a practical reality there needs to be a rethinking and redesign of current flexible endoscopes.

TECHNOLOGY AND INSTRUMENTATION FOR ADVANCED ENDOSCOPIC PROCEDURES

Like all advances in minimally invasive surgeries, NOTES is highly technology dependent. There are currently many operative platforms and instruments under investigation as enabling technologies for NOTES. The current platforms available for clinical and investigational use are few however. The first IRB approved transgastric cholecystectomy was performed using the EOS (Endosurgical Operating System, USGI Medical, San Clemente, CA). It is a flexible, 16mm, shape-lock platform with two 6mm and two 4mm working channels. The EOS requires the passage of a second flexible endoscope for light source and video with the remaining 3 channels as working channels permitting trimanual coordination. One major limitation of this platform is the requirement of a second scope operator to control the flexible light and video source. USGI has a prototype table-mounted platform under investigation, which provides the independence lost in the initial prototype as it provides a more stable platform that allows a transition from an endoscopic paradigm (surgeon directing scope and the instruments) to a laparoscopic approach (camera person maintaining visualization while the surgeon runs both instruments). (Figure 1)

Boston Scientific, Inc (Natick, MA) has a similar ergonomic operative platform providing a more stable mechanism called the Direct Drive Endoscopic System (DDES). Also table mounted, it has a 6mm channel for passage of light and video source with two 4mm working channels. Its ergonomic instrument handles are mounted on a gliding rod and provide 5 degrees of freedom to the tip. Bench top testing has shown superior visualization and bimanual opposition compared to dual channel or "R" type endoscopes. (Figure 2)

Another prototype of a NOTES "3d generation" operating endoscope is known as the "Endo-Samurai" (Olympus Medical, Tokyo). It is a 15.3mm device with built in light and video source, the first of its kind, and 3 working channels. (Figure 3) The results of our bench top and animal testing using this device were presented at the 3rd international Congress on NOTES in San Francisco. This and all of the current operative platforms carry the significant challenge of maintaining spatial orientation experienced with current endoscopic procedures.

A final new generation endoscope that is currently on the market in the EU is the Anubiscope by Storz. (Figure 4). This is an integrated reusable endoscope with ergonomic instrument designs that allow triangulation and once again replicate the "laparoscopic paradigm" of a stable platform with the camera directed by a camera person and the surgeon controlling the two instruments.

While current 3d generation endoscope designs rely on mechanical drives in order to achieve cost savings, the future of flexible endoscopic operating platforms may require or be augmented by robotic technology. Several companies have recently explored this possibility (Endovia) but none have reached the stage of a commercially viable design.

Fig. 1

Fig. 2

Fig. 3

Fig. 4

SUGGESTED READING

1. Kalloo AN, Singh VK, Jagannath SB, Niiyama H, Hill SL, Vaughn CA, Magee CA, Kantsevoy SV (2004) Flexible transgastric peritoneoscopy: a novel approach to diagnostic and therapeutic interventions. Gastrointest Endosc 60: 114–7
2. Horgan S, Thompson K, Talamini M, Ferreres A, Jacobsen G, Spaun G, Cullen J, Swanstrom L. Clinical experience with a multifunctional, flexible surgery system for endolumenal, single-port, and NOTES procedures. Surg Endosc. 2010 Aug 24. [Epub ahead of print]PMID: 20734085
3. Rieder E, Martinec DV, Cassera MA, Goers TA, Dunst CM, Swanstrom LL. A Triangulating Operating Platform Enhances Bimanual Performance and Reduces Surgical Workload in Single-Incision Laparoscopy. J Am Coll Surg. 2011;212(3):378-384.PMID: 21193330

Insertable Robotic Imaging and Effector Platform

Dennis L. Fowler

Reemtsma Center for Innovation and Outcomes Research, Dept of Surgery, College of Physicans and Surgeons, Columbia University and Simulation Center, New York Presbyterian Hospital/Columbia

ABSTRACT

The laparoscopic revolution changed the way most surgeons approach abdominal surgery. Patients experience significant benefit from less invasive surgical procedures. However, therapeutic laparoscopy, as performed in 2011, still uses primitive tools that are difficult to use and limit the amount of information available to the surgeon during surgery. To overcome some of the obstacles created by laparoscopic technology, we have initiated the development of a platform which, when fully developed, will enhance and enable minimally invasive surgery.

Beginning in 2002, using state government funding, we developed an insertable, remotely controlled stereoscopic camera for use in minimally invasive surgery. The device was designed to deliver the following advantages when compared with standard laparoscopic imaging:

- Increased mobility of the image source within the abdominal cavity
- 3-dimensional image
- One less incision per case
- Intuitive control of the image
- Shorter learning curve for "camera operator"

Multiple prototypes and multiple animal trials were completed. The result was a functional white light based image source that 1) could deliver either monoscopic or stereoscopic images to the surgeon, 2) could be controlled intuitively with a joystick, and 3) did not occupy an incision for the duration of the operation. Once the hardware was tested, we developed software that would allow the camera to function autonomously during a surgical procedure by "tracking" a surgical instrument using visual servoing technology.

Using federal government funding, we then designed and built a prototype of an insertable robot with stereoscopic imaging and two continuum robot arms. The device is designed to enable single site access for intra-abdominal surgery. The imaging technology was similar to that described for the insertable camera technology and functioned autonomously. A surgeon controlled each robotic arm with a Phantom Omni master.

These hardware and early software developments are intermediate steps in the development of useful surgical robots. Although the hardware is an essential component of a surgical robot, the real value in surgical robotic technology will be the addition of intelligent software to create "smart" robots. By combining affordable, miniaturized hardware with intelligent software, we can develop surgical robots that will assist a human surgeon by automating certain tasks. Using modern computational capabilities, and by adding additional sensors to the hardware, the "smart robot" can process the additional sensory information and simultaneously inform the surgeon and autonomously improve the precision and functionality of the robotic device.

GPS for the Body

K.G. Vosburgh[1],J. Jayender[2], R. San José Estépar [1]

[1]Brigham and Women's Hospital,
[2]Massachusetts General Hospital
Harvard Medical School
kirby@bwh.harvard.edu

INTRODUCTION

Interventions in the body increase markedly in difficulty when the instrument body and distal tip cannot be seen from an outside vantage point. Thus most endoscopic applications require long training periods to attain proficiency, and even experts may find themselves disoriented during a procedure.

Fluoroscopy may be used to provide position and orientation views, but this technique is limited to a small number of applications because the displayed contrast of extra-luminal soft tissues is low. Several studies have been conducted using CT or MRI to better navigate instruments and reach selected diagnostic or therapeutic targets. [1,2] These approaches have not been widely adopted due to the cost and complexity of the imaging systems and multidisciplinary teams. Alternatively, the availability of small electromagnetic tracking sensors and position detection systems has enabled the direct, real-time measurement of instrument position. Some commercial products, such as the SuperDimension bronchoscopy navigation system, [3] use these trackers as well as the optical images from the bronchoscope to traverse the bronchial tree.

MATERIALS AND METHODS

We support endoscopic procedures in the torso using pre-procedure 3D models and real time tracking of the endoscope position and orientation, displayed in the context of these models. This provides the operator with a "GPS-like (Global Positioning Satellite) for the patient's body," the ability to navigate and position the instrument inside that specific patient accurately and easily.

While this work is enabled by advanced electromagnetic (EM) tracking hardware, the key technical challenges have been in developing robust, high performance algorithms and software architecture to make tracking systems practical for real time guidance. The overall goals of these studies have been to demonstrate and use systems that may be added onto a conventional endoscopy system in a standard procedure room without radiologic capability. To reduce costs and system complexity, only broadly available commercial hardware units have been used.

Figure 1 presents a block diagram view of such an "image registered" endoscopy system. [4]

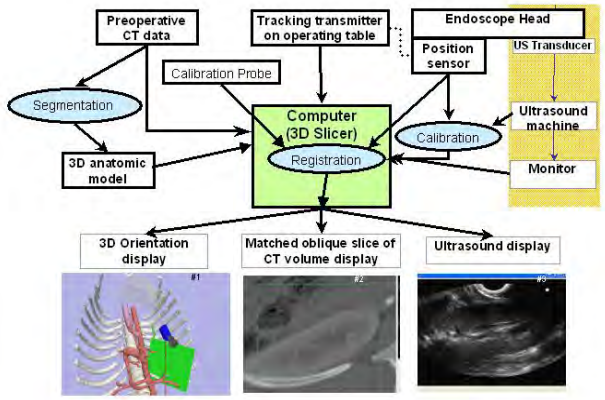

Fig. 1 Electromagnetic (EM) Position Sensors are attached to the head of the endoscope, and a tracker system is used to provide position and orientation signals to the computer. These signals are combined with calibration data and registered to the patient's body and 3D model to create a real-time display to guide the operator.

For all applications, a Windows XP platform, with a 3D Slicer User Interface is coupled to a "flat plate" electromagnetic transmitter/sensor system and supplied by Ascension Technologies Corp. Our technical goals have been met for both endoscopic and laparoscopic systems in porcine model and human subject testing, although some key metrics, such as 0.5 cm targeting resolution, are not achieved routinely. User response and performance enhancement is favourable. The overall system uses only commercially available components, although the PC is augmented with video capture and graphics accelerator cards. The total cost of a "clinical grade" system in a procedure room is under $20,000, and it appears that it will be operated easily by clinical personnel without lengthy training. The system has been designed to use standard MRI and CT DICOM files normally available in the clinical practice, although image segmentation for 3D model construction is still conducted by an experienced operator. The open system architecture permits the use of electromagnetic trackers, and endoscopic/ laparoscopic instruments from a variety of suppliers, and no special requirements are placed on clinical operations to ensure the sterility of the instruments. The system has now received approval for use with human subjects at three clinical sites.

RESULTS

These "GPS for the Body" systems appear to be practical to implement and potentially useful. They

support the physician in two important tasks: instrument navigation and targeting. Fig 2. shows data from a porcine model experiment [4] for a typical navigation task: identifying landmarks in the porcine abdomen in a timed period using either conventional gastroscopic ultrasound or Image Registered Gastroscopic Ultrasound (IRGUS).

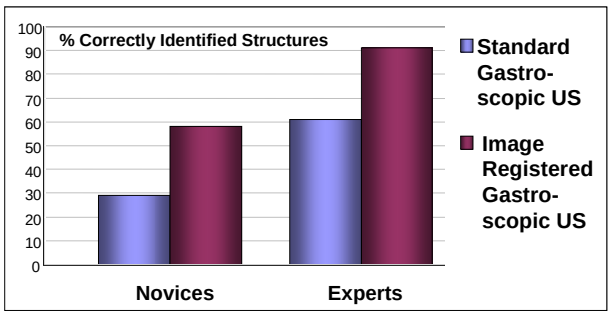

Fig. 2 Measured performance of experts and novices showing the benefits of Image Registration: "GPS for the Body."

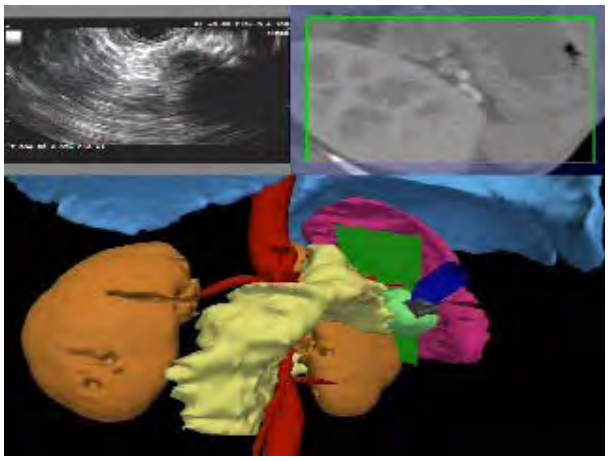

Fig. 3 IRGUS display for a human patient: top left: b-scan ultrasound image. Right: reformatted CT data in US-defined plane. Bottom: 3D CT-based model of patient for navigation and biopsy probe positioning. The pancreas is yellow, the ultrasound image plane is green, and the kidneys are orange. The tip of the endoscope (blue) is tracked by an ATC MedSafe tracker.

The IRGUS display for a human patient case is shown in Figure 3. [5] Five patients who were scheduled to undergo conventional EUS of the pancreas were randomly chosen to undergo their procedure with IRGUS. Localization of pancreatic lesions was accomplished efficiently and accurately, with no complications. Image synchronization and registration was accomplished in real time without procedure delay. Real-time display of CT images in the EUS plane and echoendoscope orientation was the most beneficial characteristics. Operator performance was characterized suing kinematics metrics and validated performance surveys. Similar results were obtained in a single patient study using image registered laparoscopic ultrasound. [6]

These patient specific models may also be used for procedure planning. Fig. 4 shows the utility of the 3D display for planning access to a transplanted kidney through the ureter. The goal is to position a laser probe at a kidney stone; note that the kidney is not superior to the bladder in this patient.

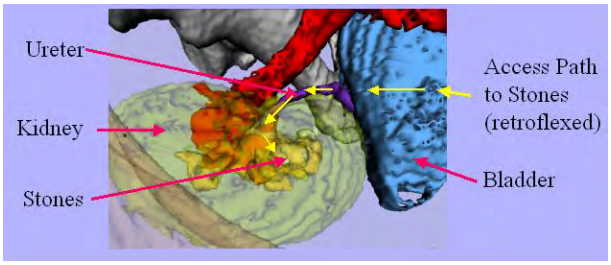

Fig. 4 Example of the use of a 3D model for planning a urologic procedure. This is the planning stage for the insertion of a laser fiber through the ureteroscope to treat the stone. In the next stage, the model will be used for real time guidance so that the urologist enters the ureter at the correct angle to minimize stress.

DISCUSSION

Image Registered "GPS-like" techniques for endoscopy and laparoscopy appear to be feasible and safe in human subjects, and efficient and accurate at identification of probe position and image interpretation. These techniques have the potential to broaden the adoption of intracorporeal US techniques and shorten learning curves. Related studies using these techniques to support improved training for colonoscopy are now in progress. [7]

REFERENCES

[1] Vosburgh KG, Jolesz FA. The concept of image-guided therapy. Acad Radiol 2003;10:176-9

[2] Peters T, Cleary, K. Image-Guided Interventions: Technology and Applications. Springer, 2008.

[3] SuperDimension Inc, Minneapolis, MN, USA.

[4] Vosburgh KG, Stylopoulos N, San José Estépar R, Ellis RE, Samset E, Thompson CC. EUS with CT improves efficiency and structure identification over conventional EUS. Gastrointest Endosc 2007;65:866-70.

[5] Obstein KL, San José Estépar R, Jayender J, Patil VD, Spofford IS, Ryan MB, Lengyel BI, Shams R, Vosburgh KG, Thompson CC. Image Registered Gastroscopic Ultrasound (IRGUS) in human subjects: a pilot study to assess feasibility. Endoscopy 2011;43:394-9.

[6] Ellsmere J, Stoll J, San José Estépar, Vosburgh KG, Tracking laparoscopic ultrasound probe improves surgeon performance: early clinical experience. Society of American Gastrointestinal and Endoscopic Surgeons (SAGES) 2010

[7] Obstein, KL, Patil VD, Jayender J, San José Estépar R, Spofford IS, Lengyel BI, Vosburgh KG, Thompson CC. Evaluation of colonoscopy technical skill levels by use of an objective kinematic-based system Gastrointest. Endosc. 2011;73(2):315-321.

Multimodality Image-Guided Diagnosis, Therapy and Non-Invasive Surgery: Integrated Interventional Imaging Operating System

A. Melzer, R.J. Toomey

Institute for Medical Science and Technology, University of Dundee,

a.melzer@dundee.ac.uk

INTRODUCTION TO IMSAT

The Institute for Medical Science and Technology (IMSaT) is a joint venture of the Universities of Dundee & St Andrews and a member of the Northern Research Partnership's Joint Research Institute for Medical Technologies (with the Universities of Aberdeen and Robert Gordon). IMSaT's remit and core research and development activities focus on the translation of new technologies for non-invasive imaging modalities (MRI, ultrasound and biophotonics) to life science and clinical applications.

IMSaT comprises labs for ultrasound, biophotonics, tissue and cell culture and a fully equipped workshop. Since December 2008 a state-of-the-art 1.5 Tesla MRI scanner connecting to a surgical suite has been operational (Fig. 1). GE has made IMSaT their first European Center of Excellence for MRI-guided Interventions and Surgery. A key clinical goal of IMSaT is to develop integrated multi-modality imaging-guided diagnostic and therapy of early-stage cancer and cardiovascular disease.

Fig. 1 IMSaT, including MRI/surgical suite layout

We organise regular translational seminars in the fields of life sciences, clinical research and medical technologies to foster collaboration and joint projects. International collaborations are very important for medical technology development and thus IMSaT has made contacts to various leading sites in Europe, USA and Asia. Commercialisation is a prerequisite of a sustained clinical impact of medical technologies, as the only successful medical technology is a product which sells well. IMSaT is also currently adopting an ISO-compliant Quality Management System.

ROBOT-GUIDED PROCEDURES

Image guidance is important in many clinical procedures. CT/MR-guided percutaneous interventions have been clinically established with open low-field MR systems and multiplanar real time CTs. Although the image quality of closed-bore MRI scanners is superior, they offer limited access to the patient. The Innomotion robotic system (Fig 2) has been developed in collaboration with Innomedic, GMBH Herxheim as the world's first MRI and CT compatible robotic system with a CE mark. The system demonstrates excellent precision in insertion site location and orientation of the cannula or ablation probe [1]. Current clinical studies on MRI-guided liver, prostate and bone biopsy and sciatic pain treatment (Fig 3)reveal significant improvement of MRI-guided percutaneous interventions. The system will be further developed at IMSaT for use in 1.5/3 Tesla MRI scanners, with specific focus on image-guided interventions in oncology and neurology and MRI-guided surgery. MRI-guided breast biopsy, tumour ablation, abscess drainage may be first clinical studies.

Fig. 2 Innomotion robotic system and MRI scanner

Fig. 3 Innomotion robotic system used for sucessful sciatic/back pain reduction

DIAGNOSTIC AND THERAPEUTIC IMAGING

Ultrasound can not only be used for diagnostic imaging but also to influence cell membrane interactions, to release drugs or to destroy tissue. The application of MRI-guidance to focused ultrasound and other ablation techniques allows precise navigation to the target lesion and monitoring of temperature responses and tissue

destruction. Biophotonics and novel techniques such as Photoporation [2] will play major roles in future diagnostic and therapeutic imaging. There is great potential for the integration of image-based diagnosis and treatment of cancer through technological innovations such as sonography or sonoporation with US [3], nanoparticle-based, contrast-enhanced molecular MR imaging and molecular therapy and nano hyperthermia. Novel targeted drug delivery using nanospheres or lysosomes utilizing heat or electromagnetically activated drug release in the target volume of a tumour opens new opportunities for medical device design. The University of Dundee has invested more than £10m into lab and imaging infrastracture at the Clinical Research Centre (CRC) at NHS Tayside Ninewells Hospital and Medical School and IMSaT. The CRC complements the technology development pipeline for image-guided oncology, with the world's first installation of a 3 Tesla MRI and a PET/CT scanner linked via a multipurpose interventional/ surgical suite.

MR-GUIDED INTERVENTIONS R&D PROGRAMME (IMSAT AND CRC)

MR guided vascular procedures are of significant interest for device and implant development at IMSaT. The following program is supported by FP7, SMART grant, MRC and InSightec corporate research.

MRI-visible stents for peripheral and cardiac implantation and a vena cava filter (Fig. 4) have been realized through the use of resonant circuits integrated with the implant structure [4]. Two types of stents are currently in preclinical trials – a balloon-expanding resonant stent is currently undergoing testing in a trial at Dept of Cardiology, University of Essen, and a self-expanding Nitinol peripheral stent is currently been developed and evaluated with the support of Boston Scientific. The resonant circuit overcomes the shielding of Nitinol stents, increases signal and signal to noise (S/N) and provides a high contrast without contrast agents. Further applications of resonant implants include occluder devices for closure of cardio-septal defects (such as patent foramen ovale, atrial and ventricular septal defects), occlusion of patent Botallo's Duct and sealing of the left atrial appendage.

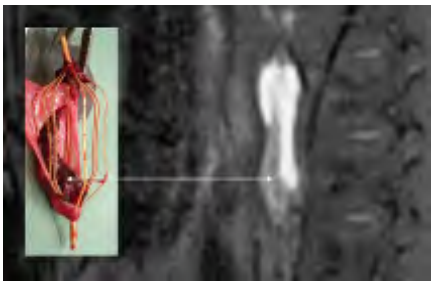

Fig. 4 Resonant vena cava filter with visualised blood clot

IMSaT also develops MR-resonant, percutaneously implantable heart valves and delivery systems [5]. An initial application has been carried out in collaboration with the National Heart, Lung and Blood Institute (National Institutes for Health, Bethesda) (Fig. 5). A self-expanding resonant aortic heart valve was implanted in 80-85 kg female mini pigs under general anaesthesia through a transapical approach. MRI-guided implantation of heart valves can be facilitated with the INNOMOTION robotic system as the delivery system is kept stabile and aligned to the image orientation.

Fig. 5 Resonant heart valve implantation

MRI-compatible guidewires have been developed at our own group and at University of Basel. Resonant markers have been made for catheters and delivery systems and will be further developed at IMSaT in collaboration with microsystems groups at University of Dundee. Based on work such as that of M. Wendt at Case Western Reserve University in Cleveland, tracking techniques can be implemented for image localization using passive resonant markers. Once the visualisation and localization of interventional devices has been optimised for 1.5/3 Tesla, other MRI-guided cardiac procedures can be realized e.g. myocardial ablation, stem cell injection, revascularisation etc.

New medical technologies require thorough testing prior to clinical use, but animal models fail to mimic human anatomy and fresh, frozen and formalin-embalmed human cadavers all present potential hazards (e.g. infection risk and exposure to carcinogens respectively) and difficulties (e.g. short useful period and rigidity respectively). The Thiel embalming has recently been established at the Centre for Anatomy and Human Identification (CAHID) at the University of Dundee, and could provide a realistic solution to this unmet need, but itself requires significant further development - for medical imaging applications respiratory-induced organ movements and pulsatile flow are essential for the provision of realistic test parameters. Our preliminary tests with digital subtraction angiography, fluoroscopy and MR angiography have demonstrated feasibility of vascular access at the femoral arteries with many open arterial sections, including open renal arteries up to the sub-sub segmental level and free flow through the heart. One area where testing with Thiel-embalmed cadavers has begun and will be further developed is in MRI-guided Focused Ultrasound (MRgFUS).

Robot-assisted MRgFUS is the latest achievement at IMSaT and currently implemented with the ExAblate conformal bone system (Insightec, Israel). MRgFUS has been applied on Thiel-embalmed humans for liver, kidney and adrenal gland ablation and targeted drug delivery. Using small powers the focused ultrasound can be locally applied on various tissues, for example kidney (Fig. 6). The tissue is heated up to coagulation temperatures where a thermal map of the heating process is presented. For higher power sonication in Thiel-embalmed cadavers we detected large cavitation activity, which eventually blocks the energy from getting to its destination.

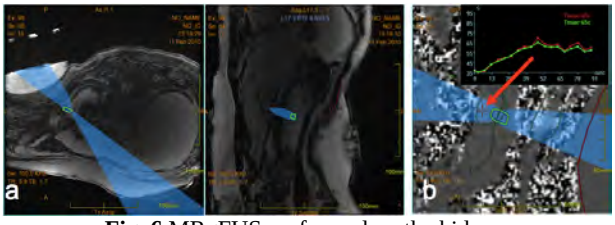

Fig. 6 MRgFUS performed on the kidney

CONCLUSION

IMSaT conducts forward-thinking and cutting-edge research in medical device development, with a focus integration of multiple imaging and interventional techniques and on translation of our work from bench to bedside.

ACKNOWLEDGEMENTS

IMSaT imaging research is funded by the European Commission, MRC, EPSRC, KTP, SMART and InSightec. Ltd. Tirat Carmel; Israel.

REFERENCES

[1] Melzer A, Gutmann B, Remmele T, Wolf R, Lukoscheck, A, Bock M, Bardenheuer H. Fischer H. INNOMOTION for percutaneous image-guided interventions: principles and evaluation of this MR- and CT-compatible robotic system. IEEE EMBM 2008 27(3):66-73.

[2] Paterson L, Agate B, Comrie M, Ferguson R, Lake T, Morris J, Carruthers A, Brown CT, Sibbett W, Bryant P, Gunn-Moore F, Riches A, Dholakia K. Photoporation and cell transfection using a violet diode laser. Opt. Express 2005 13(2):595-600.

[3] Prentice P, Cuschieri A, Dholakia K, Prausnitz M Campbell P. Membrane disruption by optically controlled microbubble cavitation. Nature-Physics 2005 1:107-110

[4] Immel E, Melzer A. Improvement of the MR imaging behavior of vascular implants. Minim Invasive Ther Allied Technol. 2006 15(2):85-92.

[5] Immel E, Gilbert FJ, Melzer A. Experimental MRI visible resonant prosthetic heart valves. Minim Invasive Ther Allied Technol. 2009;18(3):149-55.

The Value of an Instantiation Index for Intra-operative Shape Tracking

Su-Lin Lee[1], Celia Riga[2,3], Lisa Crowie[2], Mo Hamady[2],
Nick Cheshire[2,3], and Guang-Zhong Yang[1]

[1]*The Hamlyn Centre for Robotic Surgery, Imperial College London, UK,*
[2]*Regional Vascular Unit, St Mary's Hospital, Imperial College London, UK,*
[3]*Academic Division of Surgery, Imperial College London, UK*
su-lin.lee@imperial.ac.uk

INTRODUCTION

Intra-operative surgical guidance requires the tracking of tissue deformation, imaging probes and surgical instruments. While the use of intra-operative imaging is increasing, the acquisition of a volumetric scan is limited by temporal constraints. While a shape instantiation has been introduced, it was assumed that the scan plane acquired was the optimal one defined. However, accurate localization of the plane is difficult due to patient motion or when using a handheld imaging probe such as ultrasound.

We introduce the use of an instantiability index to analyze scan planes on a model to determine their robustness to errors in scan plane orientation or ultrasound calibration. By examining the index for a scan plane during perturbation, the sensitivity of the plane can be determined. A stable index indicates a robust scan plane suitable for shape instantiation, i.e. the instantiation is not sensitive to minor changes in the orientation of the plane. A sharp peak in the index would indicate a unique solution, making it more suitable for localization of, for example, an imaging probe. Results are shown on detailed phantom experiments for both real-time 3D shape instantiation and imaging catheter tracking. This paper is a summary of the work submitted to MICCAI 2011.

METHODS

The shape instantiation framework was previously introduced by Lee *et al.* [1]. A statistical shape model is first built from a set of pre-operative shape and an optimal scan plane determined from it. These shapes and their corresponding scan plane contours were fed to a partial least squares regression (PLSR). Intra-operatively collected scan planes can then be input to this PLSR which will predict the entire shape in real-time.

With the use of a preoperative 3D model and a scan plane, the instantiability index is defined as:

$$II = f(R,T) = -\left(\sum_i I_i + (RP + T)\right)$$

where R and T are the rotation and translation of the scan plane (the parameters to be optimized) and P is the intersection of the scan plane and the preoperative model. I_i is the intensity of the image at pixel *i*; the ultrasound images collected were preprocessed before use.

An ALOKA prosound α10 system (Aloka Co. Ltd, Tokyo, Japan) was used to collect data on the Regina phantom [2]. For calibration, a three-point crossed-wires phantom was built. Scans were obtained at 7 different "respiration" positions of the liver. The instantiability index was used to optimize the position of the scan plane for intraoperative anatomical instantiation.

IVUS images were collected of an Elastrat pulsatile silicone phantom of the aortic arch (Elastrat Sarl, Geneva, Switzerland) on a Volcano IVUS system (Volcano, San Diego, CA, USA). Ten IVUS catheter positions were collected along with a corresponding CT roll scan with a Philips Allura Xper CT scanner. The instantiability index was used here to determine the final position of the catheter within the mesh.

Segmentation and model building of the phantoms was performed using Analyze (AnalyzeDirect, Inc, Overland Park, KS, USA). Simulated annealing [3] was used for optimization of the scan plane orientation.

For validation, the ground truth was segmented from CT scans of the phantoms. With the liver phantom, the error was calculated as distance from each point in the instantiated shape to the closest point on the surface of the ground truth. For the vascular phantom, the error was calculated as the distance from the estimated catheter position to the extracted position from the CT scans.

RESULTS

A comparison of the indices for different scan planes for instantiation is shown in Fig. 1. Table 1 shows the errors of the instantiation from the scan planes collected from the 7 different respiratory positions available with the Regina phantom. The optimised scan planes provide better instantiation results.

The setup of the IVUS experiment within the CT scanner and the comparison of the indices for different locations on the vascular phantom are shown in Fig. 2. The positional errors of the optimization of the scan

plane with respect to the IVUS images, allowing for localization of the imaging probe, are shown in Table 2.

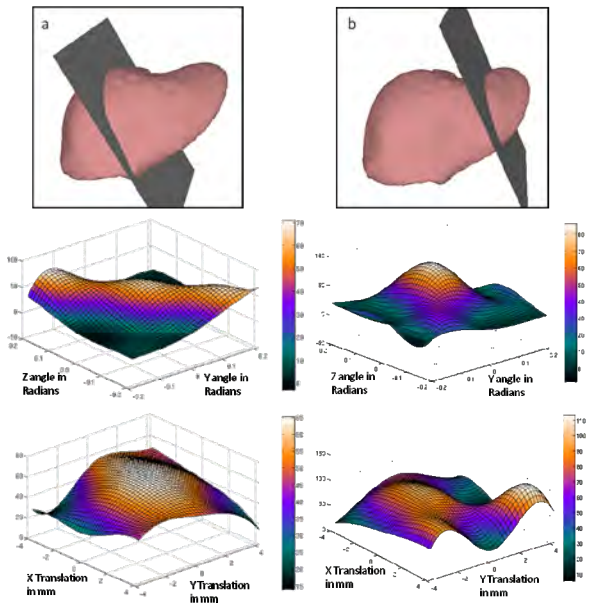

Fig. 1 A comparison of the Instantiability Index at three scan plane locations on the silicone liver phantom. The first (a) scan plane is more suitable for shape instantiation than the second (b) scan plane as the graphs show less sensitivity to rotation and translation of the scan plane.

Table 1 The optimised instantiation mean errors, and standard deviations, and instantiation with the collected data at the original scan plane mean errors to the ground truth. The silicone model is capable of 7 different respiratory positions.

	Original Scan Plane		Optimised Scan Plane	
Respiratory Position	Error in mm	Std Dev in mm	Error in mm	Std Dev in mm
1	4.76	3.86	0.77	0.65
2	1.48	1.20	1.29	0.97
3	3.17	2.31	1.25	0.98
4	6.36	6.01	1.25	0.98
5	15.69	15.14	0.50	0.43
6	8.84	8.42	1.11	0.92
7	4.01	3.44	1.92	1.46

CONCLUSION

To conclude, a new index for shape instantiation has been proposed; its use has been demonstrated for both intraoperative anatomical reconstruction and probe tracking. Examination of the instantiability index can show whether a scan plane is suitable for instantiation or localization. Results on phantom experiments demonstrate the potential of the technique.

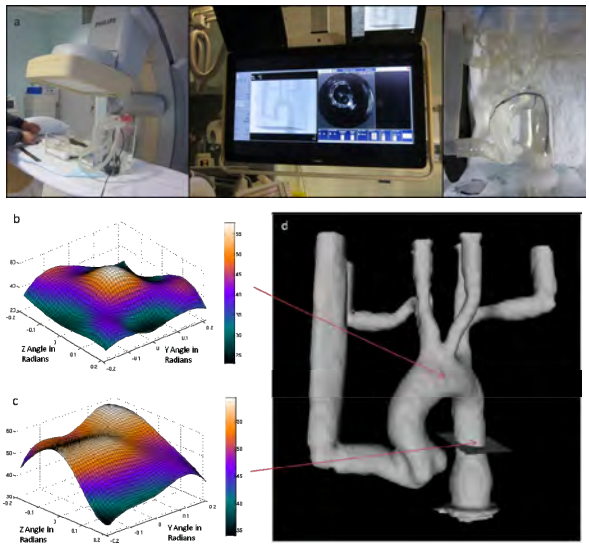

Fig. 2 (a) The setup for data collection of the IVUS system with the Elastrat vascular phantom and (b-c) the instantiability indices at two different positions within the (d) silicone vascular phantom.

Table 2 The position errors in mm of the estimated IVUS transducer position and their associated Instantiability Indices for the 10 different catheter positions in the silicone vascular phantom.

Catheter Position	Error in mm	Instantiability Index
1	3.05	0.97
2	2.32	1.19
3	2.58	1.08
4	6.86	1.10
5	3.20	1.52
6	2.01	1.48
7	1.83	1.27
8	3.70	1.23
9	4.08	1.07
10	1.14	1.49

REFERENCES

[1] S.-L. Lee, A. Chung, M. Lerotic, M. Hawkins, D. Tait, and G.-Z. Yang, "Dynamic Shape Instantiation for Intra-operative Guidance," in *Medical Image Computing and Computer-Assisted Intervention (MICCAI)*. vol. LNCS 6361, T. Jiang, N. Navab, J. Pluim, and M. Viergever, Eds. Beijing, China: Springer Berlin / Heidelberg, 2010, pp. 69-76.

[2] M. Lerotic and S.-L. Lee, "A Multimodal Silicone Phantom for Robotic Surgical Training and Simulation," in *The Hamlyn Symposium on Medical Robotics*, London, UK, 2010.

[3] W. H. Press, S. A. Teukolsky, W. T. Vetterling, and B. P. Flannery, *Numerical Recipes in C*, 2nd ed.: Cambridge University Press, 1992.

A Novel Surgical Robotic Platform Minimizing Access Trauma

T. Ranzani, C. Di Natali, M. Simi, A. Menciassi, P. Dario, P. Valdastri

The BioRobotics Institute, Scuola Superiore Sant'Anna

p.valdastri@sssup.it

INTRODUCTION

Robotic surgery is nowadays common in clinical practice, thanks to the spread of the Intuitive Surgical's Da Vinci platform [1]. The next generation of surgical robots should still guarantee the same dexterity and performances, while reducing access trauma. A promising approach in this direction is represented by robotic platforms specifically developed for laparoendoscopic single site (LESS) surgery [2-4]. Actuation for the several degrees of freedom (DoFs) may be external, by means of cables [2], internal, using on-board motors [3], or hybrid [4]. In any case, the mechanical continuity of the kinematic chain constraints the workspace to the insertion point proximities. Having the single components of the platform, i.e. at least 2 manipulators and one camera, magnetically linked across the abdominal wall as in [5] would greatly enhance both freedom of operation and triangulation. On the other hand, relying just on on-board motor actuation, as in [6], results in limited dexterity and low speed. Larger, thus more powerful, motors can be used at the price of enlarging the access port. The aim of the present paper is to describe a novel concept for LESS robotic surgery, targeting Da Vinci system performances, but to be introduced and deployed by a single 12 mm access port. Thanks to a trans-abdominal magnetic link (TML), obtained by coupling external to internal permanent magnets (EPM and IPM), several DoFs of the internal tools can be actuated outside the patient's body. This reduces the number of DoFs to be actuated by on-board motors, thus minimizing the size of the internal robots. Additionally, thanks to the separation of the kinematic chain, the components of the robotic platform are not constrained to the access point, thus resulting in a wider workspace and in the possibility to reposition the tools during the surgical procedure. This disruptive approach has the potential to completely restore the workspace typical for open surgery, while limiting the access trauma to a single minimal incision.

MATERIALS AND METHODS

The proposed robotic platform is intended for bimanual abdominal surgery, therefore it is composed by at least 2 internal robotic arms and a camera. Once the internal modules have been introduced into the abdomen through a single 12 mm entry point and magnetically docked to the EPM, all the DoFs of the platform, both the external and the internal ones, are teleoperated by the user. Each EPM is independently held by an external robotic arm. As represented in Fig. 1, at least 5 DoFs can be transmitted across the TML, while additional distal DoFs are actuated by on board motors. Each internal module is provided with energy and data transmission by a soft tether, which can also be used for a safe retrieval in case of failure. While some parts of the platform are either commercially available (e.g. the external robotic arm) or already reported in literature (i.e. the camera robot [7] and the distal part of the internal robotic arms [8]), the main open challenge is the TML. This must reliably transmit the externally actuated DoFs to the internal robotic devices, while guaranteeing stable anchoring.

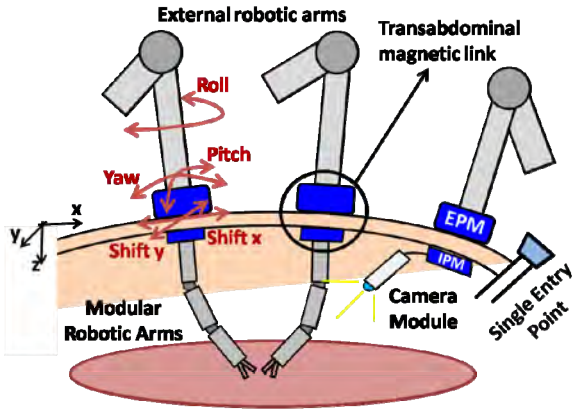

Fig. 1 Concept of the proposed surgical robotic platform. The DoFs transmitted by the TML are represented by the red arrows.

Three different actuation concepts for the TML (i.e. passive link (PL), active magnet rotation (AMR) and active magnet translation (AMT)) were identified and analyzed to find out the most effective actuation strategy. In PL (Fig. 2A), the actuation is provided just exploiting the magnetic coupling between EPM and IPM and taking advantage of the abdomen's elasticity. While roll and shift on x and y are obtained as in PL, the rotation or the translation of a single couple of magnets facing each other across the abdominal wall enables pitch and yaw of the internal joint in the AMR and AMT concepts, respectively (Fig. 2B-C). The AMR exploits a cable transmission and a winding mechanism to transmit forces from the IPM to the modular arm, whereas the AMT actuation takes advantage of rigid links. In order to compare these approaches, standard conditions were defined for magnet arrangement and features. In particular, a cross-shaped arrangement of 5 magnets was adopted for both EPM and IPM. Such a configuration can be deployed into the abdomen through a standard trocar by taking advantage of an umbrella-like opening mechanism.

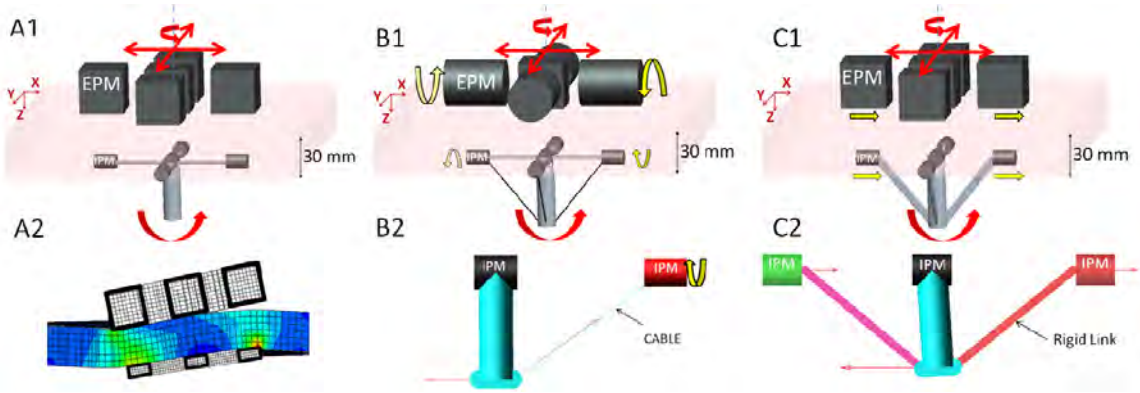

Fig. 2 A1, B1, C1: Schematic representations of PL, AMR and AMT approaches. **A2, B2, C2:** In A2 an ABAQUS FEA simulation of EPM-tissue-IPM interaction during a pitch displacement for the PL approach. In B2 and C2 ADAMS analysis of force/torque transmitted at the joint for the AMR and the AMT approaches, respectively.

Given the symmetric structure of the TML, each concept was modeled and studied along a single plane, perpendicular to the abdomen. TML maximum anchoring force (i.e. normal force during pitch/yaw actuation), maximum pitch/yaw force and range of motion were adopted as benchmarks for this study.
Based on a 30 mm average abdominal tissue thickness upon insufflation [9], maximum forces and torques induced from the EPM to the IPM were predicted. Mathematical estimation of the magnetic field was based on the charge model [10], which was implemented in MatLab (MathWorks). The magnetic interactions were then used to simulate the internal magnetically actuated joint and to find the pitch/yaw force and motion range. The AMR and AMT concepts were modeled using ADAMS (MSC Software Corporation), while for the PL design the abdomen mechanical resistance during pitch/yaw was evaluated with ABAQUS FEA (Simulia). Views of these simulations are represented in Fig. 2-A2, B2, C2. Finally, considering as worst case scenario a 100 mm long manipulator on the distal end of the TML, laying straight on the z axis, the maximum tangential force available at the end effector (EE) was estimated.

RESULTS & DISCUSSION

Numerical results coming from simulations are reported in Tab. 1. The PL approach shows the best performance in terms of anchoring force, while all the other benchmarks suggest the AMR approach as the most promising.

Table 1 Forces and pitch/yaw range for the three actuation concepts.

	Max anchoring force		Max pitch/yaw force		Max tangential force EE		Pitch/ yaw range
	N	Kg	N	Kg	N	Kg	
PL	15	1.53	4	0.40	1.3	0.13	±10°
AMR	14	1.43	8	0.82	2.6	0.27	±80°
AMT	12	1.22	3.4	0.35	1.1	0.11	±20°

In particular, the winding mechanism of AMR enables a much wider range than AMT, since wires are less bulky than rigid links.

Considering both the contact area and the results reported in [11], the tissue in between EPM and IPM gets damaged in case anchoring force exceeds 80 N. The estimated maximum anchoring and tangential forces at the EE for the AMR approach are 14 N and 2.6 N, respectively. Given that forces exerted on the tip of a surgical instruments do not usually exceed 5 N [12], an improvement in tangential loading capabilities is still called for. Next steps will be fabrication of the AMR approach and its integration into a robotic platform.

REFERENCES

[1] Intuitive Surgical website, www.intuitivesurgical.com.
[2] Ding J, et al. Design, Simulation and Evaluation of Kinematic Alternatives for Insertable Robotic Effectors Platforms in Single Port Access Surgery, 2010 IEEE ICRA, Anchorage AK, pp. 1053-1058.
[3] Lehman AC, et al. Dexterous miniature robot for advanced minimally invasive surgery. Surg End. 2010; 25:119-123.
[4] Piccigallo M, et al. Design of a novel bimanual robotic system for single-port laparoscopy, IEEE Trans Mech. 2010 Dec; 15(6): 871-878.
[5] Park S, et al. Trocar-less instrumentation for laparoscopy magnetic positioning of intra-abdominal camera and retractor. Ann Surg. 2007; 245:379–384.
[6] Lehman AC, et al. Natural orifice cholecystectomy using a miniature robot. Surg End. 2009; 23:260-266.
[7] Valdastri P, et al. A magnetic internal mechanism for precise orientation of the camera in wireless endoluminal applications. Endoscopy 2010; 42:481-486.
[8] Harada K, et al. A reconfigurable modular robotic endoluminal surgical system: vision and preliminary results. Robotica 2010; 28:171-183.
[9] Song C, et al. Mechanical properties of the human abdominal wall measured in vivo during insufflation for laparoscopic surgery. Surg End. 2006; 20:987-990.
[10] Furlani E. P. Permanent Magnet and Electromechanical Devices, A. Press, Ed., 2001.
[11] Best L S, et al. Magnetic Anchoring and Guidance System Instrumentation for Laparo-endoscopic Single-site Surgery/Natural Orifice Translumenal Endoscopic Surgery: Lack of Histologic Damage After Prolonged Magnetic Coupling Across the Abdominal Wall. Urology 2011;77: 243-247.
[12] Richards C, et al. Skills evaluation in minimally invasive surgery using force/torque signatures. Surg End. 2000; 14:791–798.

Real-Time 3D Reconstruction of Tissue Surfaces for Robotic MIS

Danail Stoyanov and Guang-Zhong Yang

Hamlyn Centre for Robotic Surgery, Imperial College London
danail.stoyanov@imperial.ac.uk

INTRODUCTION

Recovering 3D structure of soft-tissue surfaces during robotic assisted surgery is an important step for intra-operative surgical guidance and deployment of intelligent instrument control [1]. With the introduction of stereo-laparoscopes as shown in Fig 1, the recovery of metric information using optical techniques has been demonstrated as an effective and practical approach for 3D reconstruction and motion tracking [2,3,4]. However, the recovery of 3D geometry from stereo in real-time during robotic procedures is difficult due to tissue deformation, occlusion due to instrument movement, and complex specular inter-reflections.

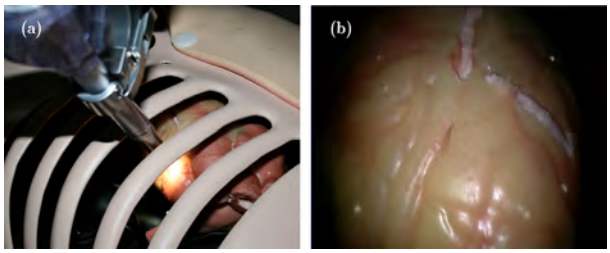

Fig. 1 (a) Stereo-laparoscope of the daVinci surgical system observing a silicone heart phantom model used for validation in this study; (b) image of the phantom from the left camera of the scope.

In recent studies, the computation of structure and motion from stereo-laparoscope images has made marked progress [2,3,4,6]. Most approaches for stereo based reconstruction and tracking use a geometric surface model, which cannot represent complex tissue shapes and discontinuities [3,4]. Furthermore, the robustness of these methods is dictated by the presence of prominent surface texture and, in practice, they are susceptible to view dependent highlights and structural discontinuities between the tissue and the instruments. In this paper, we present a method for recovering 3D tissue shape and tracking tissue deformation by propagating information around a set of salient feature points. To our knowledge, this is the first work to report semi-dense structure recovery combined with morphology tracking. Experiments with *in vivo* video sequence demonstrate the potential clinical value of the method.

MATERIALS AND METHODS

The first step of the proposed method is to recover a sparse set of matches across the stereo-laparoscopic image pair using a feature based technique. We use the method reported in [4] but it is important to note that for the proposed propagation strategy, any matching technique can be used. In our implementation, features across the stereo pair are matched and then tracked in time by minimising the following Lucas-Kanade error criteria:

$$\varepsilon = \sum_{\mathbf{x}} \begin{bmatrix} \left[I\left(W(\mathbf{x};\mathbf{p}+\Delta\mathbf{p})\right) - T(\mathbf{x}) \right]^2 \\ + \left[J\left(W'(\mathbf{x}';\mathbf{p}+\Delta\mathbf{p})\right) - T'(\mathbf{x}') \right]^2 \end{bmatrix} \quad (1)$$

where I and J are the images, W and T represent a warped image template and the original template respectively, and $\mathbf{x}$ and $\mathbf{x}'$ are the pixel coordinates of features and their motion parameterisation using a full 3D re-projection model.

The sparse set of feature matches is sorted subject to the correlation score between templates and stored using a priority queue structure. The algorithm then proceeds to propagate structure around each of the matches with highest correlation scores on a best-first basis by popping the priority queue as reported in [5]. As new matches are determined, they are simply added to the queue as the algorithm iterates until no more matches can be found. Formally, the spatial neighbourhood of a seed match $(\mathbf{x},\mathbf{x}')$ is defined as $N(\mathbf{x},\mathbf{x}')$ and it is used to enforce a 2D disparity gradient limit as a smoothness constraint in space and a motion constraint in time. Spatial neighborhoods around a respective seed match are defined by $N(\mathbf{x}) = \{\mathbf{u}, \mathbf{u}-\mathbf{x} \in [-N,N]^2\}$ and $N(\mathbf{x}') = \{\mathbf{u}', \mathbf{u}'-\mathbf{x}' \in [-N,N]^2\}$ where a candidate pair of pixels is $(\mathbf{u},\mathbf{u}')$. The formulation means that the points considered for propagation are within a spatial window of $(2N+1)\times(2N+1)$ pixels centred at the respective seed locations. The full match propagation neighbourhood is then denoted as:

$$N(\mathbf{x},\mathbf{x}') = \begin{Bmatrix} (\mathbf{u},\mathbf{u}'), \mathbf{u} \in N(\mathbf{x}), \mathbf{u}' \in N(\mathbf{x}'), \\ \left\| (\mathbf{u}-\mathbf{u}') - (\mathbf{x}-\mathbf{x}') \right\| \leq \gamma \end{Bmatrix} \quad (2)$$

This defines all the possible candidate matches around the seed correspondence $(\mathbf{x},\mathbf{x}')$ and the term γ is used to control the smoothness of the disparity map or motion model. Full details of the scheme are provided in [6].

The propagation method can be used at each time instant to recover 3D spatial information and also in temporally consecutive image frames to infer the tissue morphology. In order to improve the computational performance of the method it is possible to exploit modern technology to concurrently calculate multiple

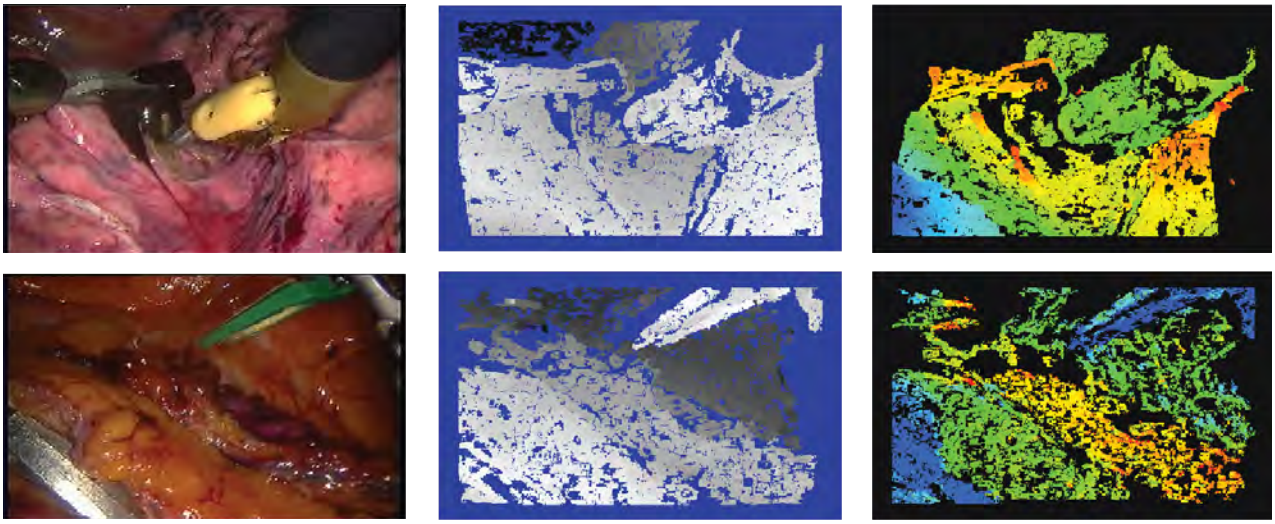

Fig. 2 (a) Examples of *in vivo* robotic assisted MIS images taken with the daVinci® surgical system; (b) the corresponding disparity maps for each image computed with the method proposed in this study, where light colors indicate closer to the camera; (c) motion heat maps where warmed colours indicate larger motion.

correlation searches during propagation in parallel. This can be implemented to exploit the large number of concurrent threads that run on modern graphics hardware or multiple core CPUs. In our implementation, integral images were used to keep the running time invariant to the correlation window size.

RESULTS

In order to achieve real-time performance, the proposed method was implemented using C++ and the NVIDIA® CUDA language for hardware acceleration using the GPU. Currently, the method can operate at approximately 10fps, however, with further optimization we believe it is feasible to achieve 30fps performance. Experimental validation of the proposed method was performed using a phantom heart model with known ground truth obtained using CT. This data had been made available online for the community (http://vip.doc.ic.ac.uk/vision). Results and comparison studies with different techniques are reported fully in [6] and summarised in the table below.

Method	Heart 1 Disparity	Heart 2 Disparity
Proposed	0.89 [± 1.13]	1.22 [± 1.71]
BP	9.95 [± 5.22]	9.59 [± 2.77]
RT	12.58 [± 4.57]	9.32 [± 2.80]
CUDA	10.12 [± 4.21]	9.92 [± 3.43]

To qualitatively evaluate the performance of the proposed method on *in vivo* images, we have used several datasets taken from different surgical procedures using the daVinci® surgical system. The results for the disparity map, the corresponding 3D renditions of reconstructions and the temporal deformation maps are shown in Fig 2. It is evident that the proposed technique effectively captures the 3D geometry of the surgical site.

DISCUSSION

In this article, we have presented a real-time stereo reconstruction and motion tracking framework for robotic assisted MIS. The proposed technique relies on propagating a sparse set of correspondences into a semi-dense 3D structure and morphology map by using a best-first principle growing scheme. The effectiveness of the approach is validated using phantom data with known ground truth and qualitative validation on *in vivo* data has also been carried out. In our future work, we hope to extend the method by incorporating spatio-temporal continuity constraints for enhancing the computation performance of the method and avoiding structural inconsistencies.

REFERENCES

[1] D. Stoyanov, G. Mylonas, A. J. Chung, M. Lerotic and G.-Z. Yang, “Intra-operative Visualisations: Perceptual Fidelity and Human Factors,” *IEEE/OSA Journal of Display Technologies*, vol. 4, pp. 491-501, 2008.

[2] G. Hager, B. Vagvolgyi, and D. Yuh, "Stereoscopic Video Overlay with Deformable Registration," in *MMVR*, 2007.

[3] R. Richa, P. Poignet and C. Liu, "Efficient 3D Tracking for Motion Compensation in Beating Heart Surgery," in *MICCAI*, vol. II, pp. 684-691, 2008.

[4] D. Stoyanov, G. P. Mylonas, F. Deligianni, A. Darzi, and G.-Z. Yang, "Soft-tissue Motion Tracking and Structure Estimation for Robotic Assisted MIS Procedures," in *MICCAI*, pp. 139-146, 2005.

[5] M. Lhuillier and L. Quan, "Robust dense matching using local and global geometric constraints" in *ICPR*, vol. 1, pp. 968-972, 2000.

[6] D. Stoyanov, M. V. Scarzanella, P. Pratt, and G.-Z. Yang, "Real-time Stereo Reconstruction in Robotic Assisted Minimally Invasive Surgery," in *MICCAI*, pp. 275-282, 2010.

A Robotic Needle Interface for Interventional Radiology Training

C. J. Hughes, N. W. John

School of Computer Science, Bangor University, UK
c.j.hughes@bangor.ac.uk

INTRODUCTION

Interventional Radiology (IR) provides a minimally invasive method for accessing vessels and organs as an alternative to traditional open surgery. By manipulating coaxially a catheter and guidewire through the vascular system, a range of pathologies can be treated from within the vessel themselves.

The Seldinger technique [1] focuses on the initial step of gaining access to a vessel, by means of a needle puncture into an artery. After identifying that the needle is within the vessel, by a flow of blood from the hub of the needle, a guidewire is then passed through the needle into the vessel. Both tactile feedback and fluoroscopy (real time x-ray imaging) are used to guide the wire into a suitable position within the vessel. Finally the needle is removed, whilst applying pressure to the vessel to stem the bleeding, and the guidewire is left in place to act as a conduit for the catheter.

In collaboration with other groups in the UK (the CraIVE consortium) we have developed a simulator for training the steps of the Seldinger technique [2]. It uses segmented 3D vascular data from real patients [3] and the measured properties of the instruments [4] in order to provide a physically correct virtual environment.

In order to provide a tactile real world interface into the virtual environment, two hardware devices were used. Firstly a proprietary VSP interface (Vascular Simulation Platform, from Mentice, Sweden) was used to track the position and rotation of the guidewire and catheter coaxially as well as the depth and rotation of the needle, as shown in figure 3. Secondly a 'HapticNeedle' interface (UK Patent Application Number: 1001399.3, European Patent Application Number: PCT/EP2010/ 066489) was developed at Bangor University, in order to allow the trainee to insert and manipulate the orientation of the physical needle. The two devices were coupled together with a guide tube, transferring the instruments from the 'HapticNeedle' into the VSP. The construction of this interface is described in this paper.

MATERIALS AND METHODS

The 'HapticNeedle' is a prototype device designed to allow a real needle to be inserted and reorientated by the trainee. The simulator can then use the position of the needle, in real-time, to update the virtual environment.

A comprehensive task analysis [5] was used to identify the key steps of the Seldinger technique. It is required that the needle is freely manipulatable within the device in order to allow the trainee to choose how to orientate the needle and also to allow the guidewire to be passed into the vessel both antegrade and retrograde. It is also important that subtle tactile responses can be recreated on the needle in order to accurately provide the cues that the trainee must identify, such as the resistance to movement through different tissues, and the patients pulse, which should be felt through the needle, increasingly as the needle approaches the artery.

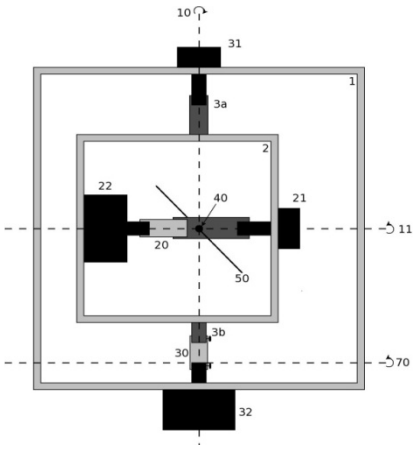

Fig. 1 The Top-down view of the 'HapticNeedle' Interface clearly showing a two frame gimbal which is able to rotate freely around point (40).

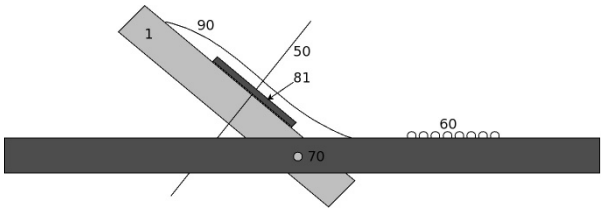

Fig. 2 The side view of the 'HapticNeedle' Interface, showing a possible mounting option within a tabletop and secured in place around pivot point (70).

Other visual feedback was simulated, such as the flow of blood from the needle hub, as this is a vital indicator to the trainee that the needle is correctly in the artery. As part of the training curriculum it was important to be able to record and assess that each step had been completed, and as such sensors were required to ensure that the trainee applied pressure to the artery to stem the flow of blood. Therefore it is required that we track the position of the trainees fingers on the skin surface.

An initial prototype was constructed using a computer mouse roller ball mechanism, with a hole through the centre of the ball to hold the needle. However, without direct links between the needle position and the potentiometors, the needle was prone to slip when applying force to it. The current 'HapticNeedle' device was designed to overcome these problems. As shown in Figures 1 and 2, the

'HapticNeedle' is based around a two frame gimbal, where the larger outer frame is fixed (although an initial angle can be set based upon the position of the virtual patient), and a smaller inner frame can be rotated on a pivot within the outer frame. A second pivot point is created within the inner frame by a lightweight alluminium tube. At the centrepoint an inset tube provides a conduit through which the needle and other instrements can be passed.

Both pivot points are contructed from three main components. A potentiometer forms one end of each and is used to provide a high resolution position for the rotation of each axis. The other end of each pivot point is formed by a servomotor, which can be used to reposition the pivot point, and also apply tactile feedback onto the needle. This makes it possible to provide dynamic cues such as the virtual pulse which causes the hub of the needle to pulsate realistically whilst it is inside the artery. A flexible joint is employed between the servomotor and the pivot in order to give an average resistance between the needle and the servos and allow the needle to be moved against the fixed position. Due to the direct linkage between the servomotors and the potentiometers, a software calibration matches the servo position to the position as measured by the potentiometers.

An array of eight tri-coloured LED's is mounted inline with the direction of the needle, to indicate the blood flow from the needle. By allowing both the colour of the LED's to change and the speed that they are cycled, it is possible to represent different scenarios for the position of the tip of the needle.

Finally a circular membrane potentiometer is mounted around the needle interface, to allow the users finger position to be identified, before being overlaid with a realistic silicone skin. The whole interface is then dressed using surgical drapes to replicate the scene from within the operating room.

RESULTS

As shown in Figure 3, the final prototype provides a complete solution for providing a needle interface for a Seldinger Technique training environment. Several interventional radiologists have been involved in the development of the 'HapticNeedle' and they confirm that our interface provides an accurate representation of the needle in the real world, in terms of translation, rotation and force feedback.

The full simulator from the CraIVE consortium, which includes the 'HapticNeedle' as its main user interface has also been independently validated as part of a transfer of skills training program. Preliminary results based on responses from 28 participants who completed the simulated Seldinger procedure, lend support for the simulator's face validity (82% agree that the simulator would be effective for learning basic skills and 86% believe it would be useful in learning how to use equipment). In addition, preliminary results from 26 radiology registrars who completed four trials on the simulator, showed that on average, participants' performance improved on all metrics.

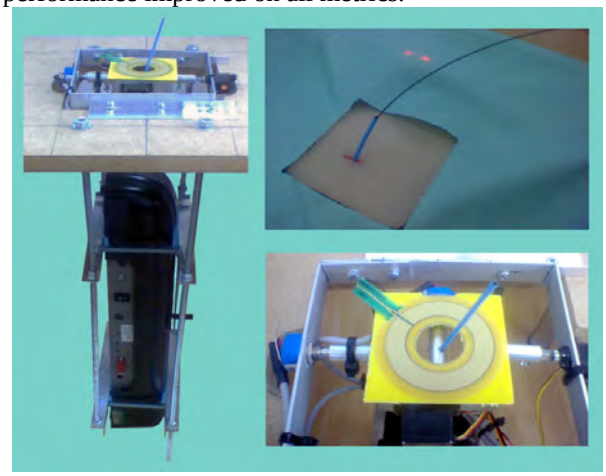

Fig. 3 The 'HapticNeedle' prototype. Left: the 'HapticNeedle' coupled to the VSP. Right/top: The 'HapticNeedle' dressed with artificial silicon skin and medical drapes. Right/bottom: The 'HapticNeedle' including the membrane potentiometer used to measure the location of the trainees fingers.

DISCUSSION

This prototype has been developed as part of a simulator to train the Seldinger technique. This new technology allows the trainee to re-orientate the needle whilst inserting a guidewire into a vessel, a step which is not included in any of the existing commercial simulators. There are also many other applications for this device.

ACKNOWLEDGMENTS

This work has been completed within the scope of the EPSRC funded project (EP/E002587/1) - 'A physics-based virtual environment for training in vascular interventional radiological procedures' in collaboration with Imperial College, London (Vincent Luboz, Fernando Bello), Liverpool Royal Hospital (Derek Gould, J Zhai, T How), Manchester University (Sheena Johnson), Hull University(Caroline Kilkenny, Yan Zhang) and Leeds University (Andy Bulpitt, David Kessel).

REFERENCES

[1] S.I. Seldinger. "Catheter replacement of the needle in percutaneous arteriography; a new technique". Acta radiol. 39(5):368-76, 1953.

[2] Luboz V., Hughes C., Gould D., John N. and Bello F., "Real-time Seldinger Technique Simulation in Complex Vascular Models", International Journal of Computer Assisted Radiology and Surgery, vol.4/6, p 589, 2009.

[3] Y. Song, V. Luboz, et al. "Segmentation of 3D vasculatures for interventional radiology simulation". MMVR 2011.

[4] Odetoyinbo T., Zhai J., Littler P., Luboz V., Bello F., How T., Gould D.A. Instrument modelling in virtual interventional radiology training simulations using direct measurement of instrument properties. Proceedings of the British Society of Interventional Radiology (BSIR), Brighton, November 2009.

[5] Johnson, S. Woolnough, H. Hunt, C. Gould, D. England, A. Crawshaw, M. & Lewandowski, W. "Simulator Training in Interventional Radiology: The Role of Task Analysis." APA Annual Conference, Boston, US, 2008.

Actuated, Flexible and Dynamically Changeable Surface Textures for Medical Instruments

A. Schneider[1], E. Huq[1], T. Parittotokkaporn[2], F. M. Rodriguez y Baena[2]

[1] *Micro and Nanotechnology Centre, STFC - Rutherford Appleton Laboratory, Harwell Oxford, Didcot, UK*

[2] *Mechatronics in Medicine Laboratory, Department. of Mechanical Engineering, Imperial College, London, UK*

andreas.schneider@stfc.ac.uk

INTRODUCTION

Certain medical devices such as deep brain stimulation (DBS) probes need to be implanted with high precision (few millimeters to µm) relative to particular parts of an organ, nerves or blood vessel and, in addition, need to reside at a minute distinct position over a long period. Hence surface modifications of medical devices and implants are desirable which facilitate an increase of friction between device and tissue so that unintentional migration of the device can be reduced. However, for the positioning of the implant during operation, a smooth surface is needed so that it can easily be maneuvered through the tissue until it is in the correct position. Consequently a surgeon would like to have implants with surfaces which can be flexibly and dynamically changed by a simple actuation mechanism during operation. The challenge here is – in particular for minimally invasive surgery – that the actuators require small dimensions (µm-size) for various reasons: a) to fit on small implants, b) to create minimal damage to the surrounding tissue, and c) still to fulfill the purpose of reducing the implant's slippage when fully implanted. Our previous experiments [1] with fixed and static surface structures of a feature size in the range of 10µm to 500µm indicated already some reduction of probe migration in cadaverous pig brain which was subjected to a rotational motion for simulating a brain shift. Using a novel probe design, we demonstrate a dynamically changeable surface texture of similar flexible microstructures and present current results of tests conducted on artificial brain models.

MATERIALS AND METHODS

Test prototypes with actuated, flexible and dynamically changeable surface were fabricated onto platforms which emulates DBS electrode probes. The surface texture can undeniably also be applied to any other form of medical device such as cochlea implants in the inner ear.

The prototypes are intended for tests on artificial brain models (agar gel) to prove the concept that microactuators can alter surface properties and texture on demand so that slippage of the medical implants can be reduce and minimized when required.

A) Probe manufacturing with changeable surface

A variety of novel test probes were built using different substrate materials such as silicon (Si), epoxy-base photoresist, or a medical grade silicone of polydimethylsiloxane (PDMS). The flexible surface microstructures were fabricated from various layers of polyimide and metal. A Ti/Au metal layer was predominately used as stimulation electrode and for the electrical circuit to actuate the surface texture. A standard bi-layer lift-off process with LOR and JSR photo resist was applied for structuring these electrodes, which is a commonly used process in microelectronics or for fabrication of micro-electro-mechanical systems (MEMS) [2]. The surface texture and microactuators were structured by photolithography and dry etching techniques. For prototypes on Si, final probes were diced from the Si wafer in a shape of a needle (17.5 mm long, 9 mm or 1.3 mm wide, and 0.5 mm thick). The top end of each needle has a triangular tip with integrated stimulation electrodes; the bottom end of such needle is flat and contains contact pads for the electrical circuit of the actuators. Test probes based on epoxy-substrates or PDMS structures have similar dimensions and design apart from the thickness of the needle, which was approx. 0.25 mm. These types of probes do not need to be diced because their shape was defined for instance by photo-lithography and subsequently separated together with the surface texture from a Si wafer by wet chemical etching. A typical detail of a probe with texture on epoxy-based material is shown in Fig. 1.

For testing purpose, prototype probes were glued to printed circuit boards (PCB) and the probe's contact pads were wire bonded to the PCB. A connector for a cable to a power supply and controller for the actuator was mounted on the opposite end of the PCB (Fig.2). The surface texture of the probe consists of microstructures, which protrude from the probe surface by up to 150 µm in default setting. When actuated, these structures retract and create a smooth surface. The length of actuators ranges from 200 µm to 400 µm and arrays of such structures are systematically distributed across the surface of the probe. For initial tests on brain models of agar gel, a textured probe on Si substrate with typical actuator size of 200 µm was chosen.

B) Friction / gripping force measurement

An experimental set-up with a variable inclined plane (Fig. 3) is used to test the friction between probes

and agar gel while the texture of the probe is either protruding or flattened by the actuation mechanism. The inclination of the plane was increased so that the probe moves out of the agar gel under its own weight (15g). The rig was elevated using a mechanism of a linear bearing run by the DC motor with a slow angular velocity of 0.55 degree/s to avoid any vibration to the probe. The angle of elevation was recorded until the probe has fully slipped out of the agar gel and the required force was calculated from the degree of angulation and weight accordingly. Experiments were repeated several times and averaged. For calibration purpose, the slip angle was also recorded for the same sample which was not inserted into the agar gel.

RESULTS

The results obtained from a probe with 200µm-long actuators showed that the sample was capable to hold on to the agar gel (tissue) up to a weight force equivalent of 2.34g and 4.70g for a flat and protruded surface texture, respectively. Hence a significant difference of friction was noticed between conditions with deployed texture and actuated flat surface (table 1). Similar but smaller differences were also observed for other samples.

Table 1 The summary results obtained from inclination test of probe with 200-µm textured.

200µm Probe	Angle (˚)	SD (˚)	Force (gram force)
Calibration	18.43	0.68	4.74
Flat surface	28.15	3.78	2.34
Deployed surface	39.03	4.21	4.70

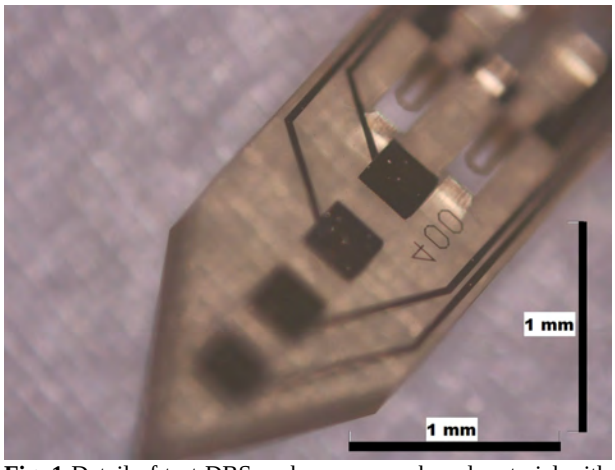

Fig. 1 Detail of test DBS probe on epoxy-based material with pointed top and 4 stimulation electrodes; surface actuators for changeable texture are visible behind those electrodes.

DISCUSSION

This experiment was designed to measure the required force to retract the sample from the brain model (agar gel). The results are promising and indicate that an anchoring effect to surrounding tissue is increased while the flexible texture of the probe is deployed. Because the elastic properties of agar gel are similar to brain tissue, we assume that the actuation mechanism and flexible texture is suitable for DBS probes to reduce probe migration. A flatter texture creates less friction with tissue so that this is well suited for positioning the probe at target location during minimally invasive implantation. However, this assumption requires more repeatable experiments performed with different sizes and geometries of probe actuators and texture.

ACKNOWLEDGEMENT

This article presents independent research commissioned by the National Institute for Health Research (NIHR) under its i4i Invention for Innovation Programme (II-FS-0509-12008). The views expressed are those of the authors and not necessarily those of the NHS, the NIHR or the Department of Health. The authors would like to thank the NIHR for funding this work.

REFERENCES

[1] T. Parittotokkaporn, L. Frasson, A. Schneider, S.E. Huq, B.L. Davies, P. Degenaar, F. M. Rodriguez y Baena, D.G.T. Thomas. Advanced Surface Topographies for Deep Brain Stimulation (DBS) Electrodes: a Possible Means to Reduce Probe Migration. Marseille Neurosurgery 2009, Joint Annual Meeting EANS-SFNC, Marseille, France, March 27 - 31,2009, Session: Functional neurosurgery

[2] http://www.microchem.com/products/pmgi.htm

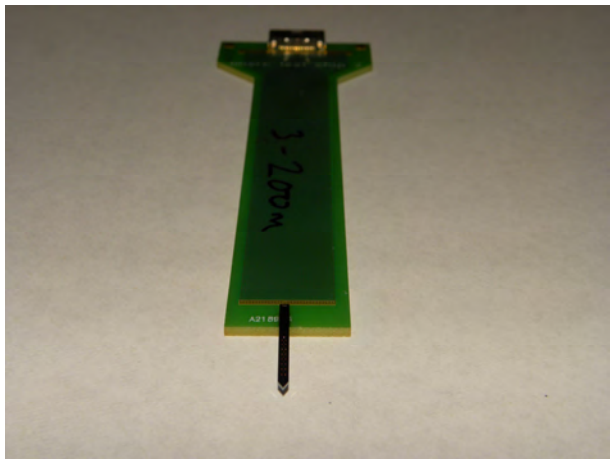

Fig. 2 Test DBS probe with dynamical changeable surface texture mounted onto a PCB with connector at the back.

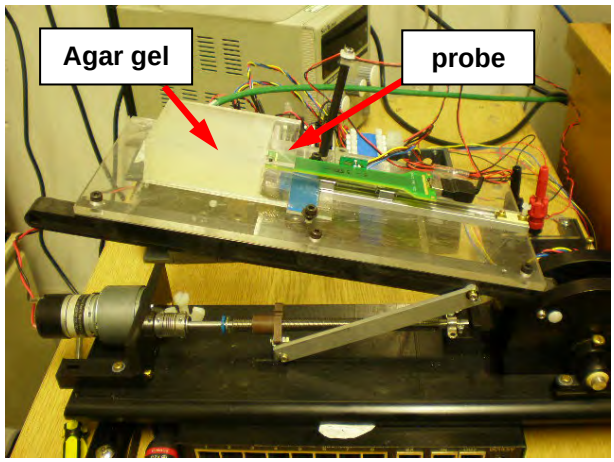

Fig. 3 Test set-up with variable 'inclined plane' using sample from Fig.2.

3D Tissue Deformation Recovery for Minimally Invasive Surgery

Stamatia Giannarou, Guang-Zhong Yang

Hamlyn Center for Robotic Surgery, Imperial College London,
stamatia.giannarou@imperial.ac.uk

INTRODUCTION

In Minimally Invasive Surgery (MIS), the 3D reconstruction of the surgical environment is important for 3D anatomical registration, intra-operative planning and surgical guidance. Dynamic motion stabilization and controlling the motion of surgical instruments by visual servoing are essential in robotically assisted laparoscopic surgery. To this end, reliable tissue deformation recovery is the prerequisite of all these techniques. Methods based on stereo reconstruction [1], Simultaneous Localization and Mapping (SLAM) [2] and Structure From Motion (SFM) [3] have the disadvantage that they cope with deforming environments based either on the assumption that the camera is static or that the tissue is deforming with periodic motion. These assumptions are not always realistic for MIS procedures as they cannot deal with free-form tissue deformation induced by tool-tissue interaction.

The aim of this work is to propose a novel approach to the 3D reconstruction of a deforming surgical environment. The proposed framework extends a content-based data representation scheme [4] which identifies surgical episodes and reflects not only the scene structure but also the underlying semantic and context of the *in vivo* environment. Probabilistic tissue tracking is used to generate motion patterns that represent visual content complexity in order to cluster the scene into independently deforming areas. The camera motion is recovered from the static part of the scene. The only assumption of the proposed approach to recover free-form deformation is that prior to the tool-tissue interaction, the camera navigates in the surgical environment in order to estimate the initial 3D structure of the scene while it is static.

MATERIALS AND METHODS

For reliable content representation, affine-invariant anisotropic regions [5] are tracked over a series of frames. An EKF parameterisation scheme based on the elliptical parameters of the anisotropic regions is used to adaptively estimate the optimal template, enabling the accurate identification and matching of the tracked features.

To eliminate tracking failure due to linking features across temporal discontinuities, temporal segmentation is applied on the video data to derive coherent episodes which represent distinct surgical actions. Episode borders occur when feature tracking fails as this is due to the contrastingly different visual appearance of the changing surgical environment.

Each surgical episode is reconstructed individually. In this work, the 5-point algorithm [6] combined with the Random Sampling Consensus (RANSAC) is applied in two views to estimate the camera motion and identify outliers. The inliers correspond to static scene patches which are successfully reconstructed whereas, features on deforming areas are automatically identified as outliers and their reconstruction accuracy is low. In order to recover an accurate 3D structure of the entire observed environment, deformable areas are localized and their structure is refined.

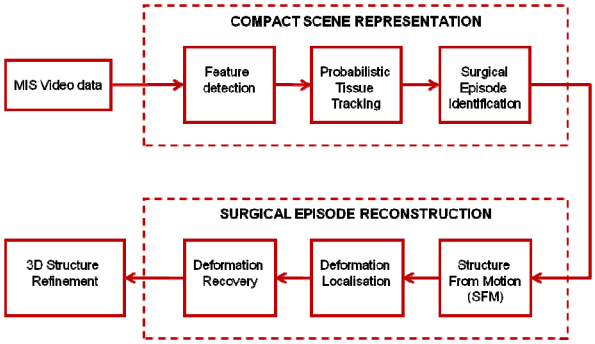

Fig. 1 Schematic representation of the proposed framework for 3D deformation recovery.

For the identification of deforming areas, the motion of each tracked feature is represented as a Gaussian Mixture Model (GMM). The *k*-means algorithm is employed to group the features into clusters. The cluster with the highest number of inliers extracted from the SFM framework corresponds to the static scene part while the remaining clusters represent independently deforming areas.

Once the scene has been divided into static and deforming areas, the initial structure that has been estimated from the SFM framework explained above is refined for each deforming area, individually. The recovery of the deformation of a feature i on an area j can be formulated as an under-determined system:

$$A^i D^j = B^i$$

$$A^i = \begin{bmatrix} W^i_{l\,x} p_{31} - p_{11} & W^i_{l\,x} p_{32} - p_{12} & W^i_{l\,x} p_{33} - p_{13} \\ W^i_{l\,y} p_{31} - p_{21} & W^i_{l\,y} p_{32} - p_{22} & W^i_{l\,y} p_{33} - p_{23} \end{bmatrix}$$

$$B^i = \begin{bmatrix} X^i_{l\,x} - W^i_{l\,x} X^i_{l\,z} \\ X^i_{l\,y} - W^i_{l\,y} X^i_{l\,z} \end{bmatrix}$$

where, D is the deformation at time l, W^i_l is the 2D projection of feature i, $p_{u,v}$ are the elements of the

projection matrix P_l and X_l^i is the 2D projection of the feature for the given camera motion, if the structure had remained static. Since all the points on a deforming area are moving with coherent motion, individual systems of each point are grouped to estimate the area deformation. The above process is repeated for each deforming scene area. The proposed framework for 3D reconstruction of a deforming surgical environment is illustrated in Fig. 1.

Table 1 Deformation Recovery Error for varying noise level and number of outliers.

Noise Level	1	2	3	4	5
Min Error	0.61	1.67	3.12	4.11	8.66
Max Error	1.36	5.27	5.81	8.28	16.3
Outliers	20%	30%	40%	50%	60%
Min Error	3.12	4.96	4.12	6.77	4.17
Max Error	3.23	7.03	5.22	7.37	11.24

RESULTS

The proposed framework had been validated on synthetic and phantom data. The practical value of the method is further examined on *in vivo* MIS data. Synthetic scenes were generated with definable camera motion and deformation, represented as a volume of 100 points in space. The camera was set at 50mm from the volume and the baseline was 10mm. Observation error was added to the image points in the form of Gaussian noise with zero mean and standard deviation ranging from 0 to 5 pixels. The performance of the method was also evaluated for different number of outliers. The above experiments were carried out under different deformation levels ranging from 10mm up to 50mm. The deformation recovery error is estimated as the Euclidean distance from the ground truth. The camera rotational error is estimated as the smallest angle of rotation that can bring the estimate to the true value. The translational error is the deviation of the estimated translation direction from the true value. The deformation recovery results are presented in Table 1.

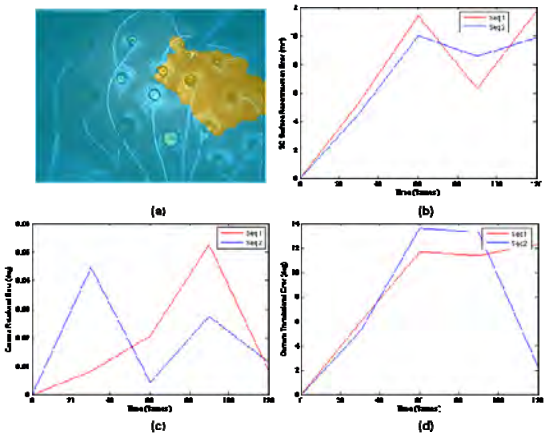

Fig. 2 (a) Deformation localisation (b) Reconstruction error (c) Rotational and (c) translational error.

Phantom data was generated using a liver phantom made of silicon rubber. The *da Vinci* robotic system (Intuitive Surgical Inc., Sunnyvale, CA, USA) was used to capture video data with the camera navigating around the phantom in the presence of tool-tissue interaction. The ground truth data used for comparison was collected using an optical tracking device (Northern Digital Inc., Ontario, Canada). The scene clustering result on phantom data is illustrated in Fig. 2(a). Static areas are highlighted in blue and deforming areas in orange. The deformation recovery error ranges from 8.65mm to 11.60mm and the surface reconstruction and camera motion errors are shown in Fig. (b)-(d).

The practical value of the proposed framework has been verified on *in vivo* data recorded from a robotically assisted MIS procedure, involving significant tissue deformation due to instrument-tissue interaction. Since a ground truth is not available, quantitative evaluation is not possible. The scene structure extracted with the SFM framework prior to the tool-tissue interaction is recovered and refined by incorporating the estimated deformation in the deformed area.

DISCUSSION

A novel approach for the recovery of free-form tissue deformation has been proposed. The advantage against previous approaches is that it does not impose explicit constraints on tissue deformation, allowing realistic free-form deformation recovery. The proposed framework has been tailored for adaptive motion stabilization and visual servoing in robotically assisted laparoscopic surgery. It can also be used to maintain consistent force of imaging probes such as the pCLE on the tissue surface to prevent distortion to the image morphology due to excessive probe pressure. Furthermore, the proposed method could help the diagnosis of diseases such as liver cirrhosis by measuring the modulus of stiffness of the liver during instrument-tissue interaction.

REFERENCES

[1] Richa, R., Bo, A., Poignet, P.: Robust 3d visual tracking for robotic-assisted cardiac interventions. In: Medical Image Computing and Computer-Assisted Intervention. Volume 1. (2010) 267-274

[2] Mountney, P., Yang, G.Z.: Motion compensated slam for image guided surgery. In: Medical Image Computing and Computer-Assisted Intervention. Volume 2. (2010) 496-504

[3] Hu, M., Penney, G., Rueckert, D., Edwards, P., Bello, R., et al, R.C.: Non-rigid reconstruction of the beating heart surface for minimally invasive cardiac surgery. In: Medical Image Computing and Computer-Assisted Intervention. Volume 1. (2009) 34-42

[4] Giannarou, S., Yang, G.Z.: Content-based surgical workflow representation using probabilistic motion modeling. In: International Workshop on Medical Imaging and Augmented Reality. (2010) 314-323

[5] Giannarou, S., Visentini-Scarzanella, M., Yang, G.Z.: Affine-invariant anisotropic detector for soft tissue tracking in minimally invasive surgery. In: IEEE International Symposium on Biomedical Imaging. (2009) 1059-1062

[6] Nister, D.: An efficient solution to the five-point relative pose problem. IEEE Trans. Pattern Anal. Machine Intell. 26(6) (June 2004) 756-770

Preliminary In-vivo Tests with a Magnetic Levitation Camera Robot for Laparoscopic Surgery

M. Simi[1], P. Valdastri[1], N. Di Lorenzo[2], G. Basili[3], A. Menciassi[1], P. Dario[1]

[1]*The BioRobotics Institute, Scuola Superiore Sant'Anna, Pisa, Italy*
[2]*Department of Surgery, University of Tor Vergata, Roma, Italy*
[3]*General Surgery Unit, Pontedera Hospital, Health Unit 5 Pisa, Italy*
m.simi@sssup.it

INTRODUCTION

In the era of laparoscopic surgery, less postoperative pain and early recovery are major goals in order to achieve better patient care and cost-effectiveness. Several studies demonstrated that less postoperative pain is associated with reduction in either size or number of ports, thus many developments have been directed toward the goal of minimal invasive surgery [1, 2]. Two port laparoscopy (TPL) represents a possible technique, for specific procedures and selected patients. Only a tool and a laparoscope respectively are inserted in the body thus strongly reducing surgeon capabilities [3]. In the continuous quest to limit access trauma, Single Port Laparoscopy (SPL) is concretely emerging from research into clinical practice [4]. However, SPL procedures are significantly hampered by limited instrument triangulation capabilities, narrow visual field through conventional laparoscopes, and both internal and external tool collisions that can considerably limit surgeon performance and jeopardize the patient's safety [5]. In order both to preserve surgeon dexterity and capabilities and to enable less invasive surgery, a number of preliminary camera devices have been developed [6-10]. Building on this background and to overcome the main present technical drawbacks, we developed a softly-tethered miniaturized magnetic camera robot with an internal magnetic levitation system (MLS) [11].

Herein we present two preliminary in-vivo surgical procedures performed on porcine models using the MLS cameras, in place of conventional laparoscopes, as enabling and improving technologies for TPL and SPL respectively.

MATERIALS AND METHODS

As described extensively in [12], the small robotic MLS camera can be intra-abdominally anchored and moved by external permanent magnets (EPM) placed on the abdominal skin. Furthermore the innovative embedded mechanism exploits the external magnetic field to guarantee a precise wide-range (0-80°) robotic tilt motion of the camera, activated by a push button interface. A thin flexible cable guarantees robot powering, real time signal transmission and an effective retrieval of the device in case of failure. Thanks to its compact size, the camera is compatible with standard 12 mm trocar, thus the access port can be used both for inserting the robot and a different instrument afterwards, avoiding a dedicated port for a videoendoscope.

The *in-vivo* tests were conducted using two 30-kg female domestic pigs under general anesthesia. The experiments were carried out in an authorized laboratory, with the assistance and collaboration of a specially trained medical team, in accordance with all ethical considerations and regulations related to animal experiments. In TPL procedure two 12 mm trocars were fixed in the porcine abdomen and two camera robots were introduced through each of them (Fig. 1). A cholecystectomy was then performed using two surgical tools (i.e gripper and cauterizing hook) at the same time introduced in the two ports.

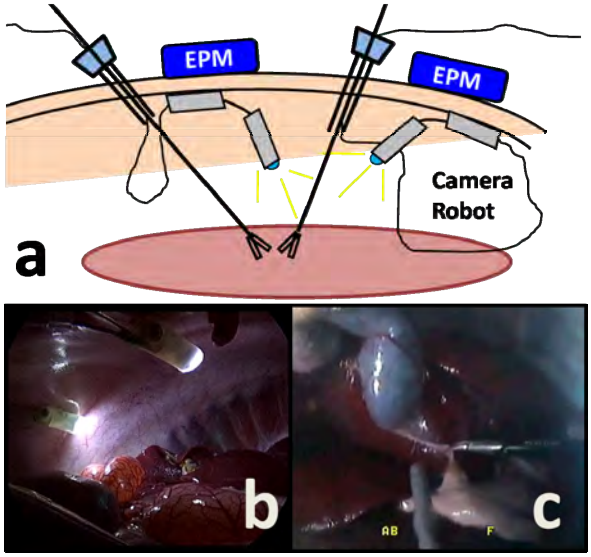

Fig. 1 a) TPL procedure schematic representation.
b) Two camera robot inside abdominal cavity.
c) Camera robot view point during surgical procedure.

In SPL procedure two 5 mm and one 12 mm cannulas were introduced into a SILS™ (Covidien, Norwalk, CT, USA) port fixed in the porcine right flank. A small bowel resection with intracorporeal anastomosis was performed by using all the three cannulas available for introducing articulated instruments while a single camera robot provided visual feedback (Fig. 2).

In both experiments, before camera robots insertion, ethylene oxide sterilization of the device was performed and a hydrophobic coating was sprayed on the camera lenses to prevent moisture accumulation. Then about

500 mm of cable were left inside the inflated abdomen to provide freedom of movement to the cameras. The entire surgical procedures were performed using the image obtained from the MLS cameras externally controlled by a surgeon assistant.

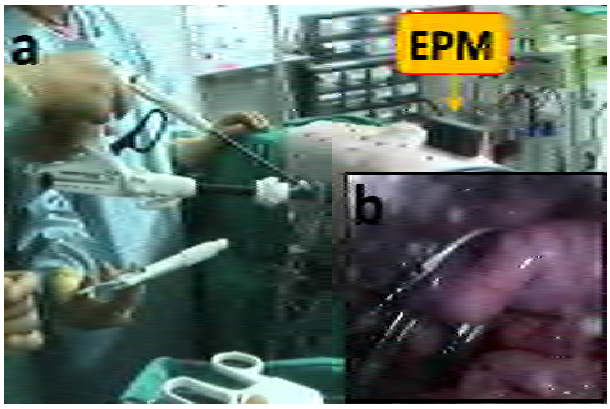

Fig. 2 a) All three port accesses can be used for surgical instruments. **b)** Camera robot view point of the three surgical instruments operating together at the same site.

RESULTS & DISCUSSION

Surgery was successful in both cases (TPL and SPL) in 30 and 50 minutes respectively, without any intraoperative complication. MLS camera robot introduction, magnetic coupling and motion control were trivial and intuitive. The device provides adequate illumination and image quality that was comparable to a traditional video laparoscope. Moreover, the magnetic anchoring and motion provide a larger viewing volume than a traditional laparoscope which is restricted by the fulcrum point of insertion. The MLS enhanced image stability and motion resolution still guaranteeing a tilt wide span ranges, without pushing EPM on the abdomen wall or needing needle fixation [7, 8]. Due to moisture on the camera sometimes jeopardized clear vision, we believe a lens cleaning system, such as the one implemented in flexible endoscopes, may be desirable.

In multiport laparoscopic procedures, use of this innovative approach would reduce the number of external incisions, since a devoted access for the camera would no longer be required, without affecting surgeon dexterity. In particular, considering TPL procedure, the surgeon dexterity and capabilities are clearly improved than traditional technique, by using two surgical tools at the same time instead one laparoscope and one instrument (Fig 1).

Considering the SPL procedure, the MLS camera robot restored instrument triangulation while improving ergonomics as one instrument (i.e conventional laparoscope) was omitted from the port. Since no laparoscope was used, both internal and external collision of the instruments was minimized significantly while only two tools were used. Furthermore, eventually all the ports were used to insert instruments, thus improving and facilitating surgical outcome (Fig. 2). Most importantly, since the camera handle was positioned far from the insertion port, the MLS camera allowed the surgeon assistant to continuously slide and adjust the camera view point without interfering with the surgeon hands.

The two *in-vivo* tests suggest that safe procedures can be performed with MLS cameras both in TPL as in SPL. Multiple camera robots, providing the surgeon with multiple points of view of the surgical arena, represent a great improvement in terms of visual information. Moreover, multiple points of view combined with robotic camera steering may potentially enable three-dimensional reconstruction of the abdominal cavity, to be presented to the surgeon by augmented reality techniques [12]. We strongly believe that insertable and softly tethered devices like MLS camera will be an integral part of future surgical systems, thus improving procedures efficiency, minimizing invasiveness and enhancing surgeon dexterity.

REFERENCES

[1] Leggett PL, et Al, (2000) Minimizing ports to improve laparoscopic cholecystectomy. Surg Endosc 14:32–36

[2] Osborne DA et Al (2006) Laparoscopic cholecystectomy: past, present, and future. Surg Technol Int 15:81–85

[3] Poon CM, et Al, (2003) Two-port vs four-port laparoscopic cholecystectomy: A prospective randomized controlled trial. Surg. Endosc. 17:1624–1627.

[4] Romanelli JR, et Al, (2009) Single-port laparoscopic surgery: an overview. Surg. Endosc. 23(7):1419-1427.

[5] Box G, et Al, (2008) Nomenclature of natural orifice translumenal endoscopic surgery and laparoendoscopic single-site surgery procedures in urology. J Endourol 22(11):2575-2582

[6] Swain P, et Al, (2010) Development and testing of a tethered, independent camera for notes and sigle-site laparoscopic procedures. Surg. Endosc. 24:2013-2021.

[7] Cadeddu J, et Al, (2009) Novel magnetically guided intra-abdominal camera to facilitate laparoendoscopic single-site surgery: initial human experience. Surg. Endosc. 23:1894-1899.

[8] Ohdaira T., et Al. (2009) Usefulness in NOTES of an intra-abdominal antifogging wireless charge-coupled device (CCD) camera with pantograph-type needle unit for placement to the intra-abdominal wall. Surg. Endosc. 24:198-209

[9] Lehman A, et Al, (2008) Surgery with cooperative robots. Computer Aided Surgery. 13:95-105.

[10] Fowler DL, et Al, (2010) Initial trial of a stereoscopic, insertable, remotely controlled camera for minimal access surgery. Surg. Endosc. 24:9-15.

[11] Simi M, et Al, (2011) Magnetic Levitation Camera Robot for Endoscopic Surgery, in Proc. of IEEE International Conference on Robotics and Automation (ICRA) 2011, Shanghai, China, May 2011, pp. 5279-5284.

[12] Lee SL, et Al, (2010) From medical images to minimally invasive intervention: Computer assistance for robotic surgery. Comput Med Imaging Graph 34:33-45.

Collaborative Gaze Channelling for Cooperation within a Shared Tele-Surgery Environment

G.P. Mylonas, L.-W. Sun, K.-W. Kwok, D. R. C. James, F. Orihuela-Espina and G.-Z. Yang

The Hamlyn Centre for Robotic Surgery, Imperial College London
george.mylonas@imperial.ac.uk

INTRODUCTION

With the introduction of a new generation of surgical consoles, like the daVinci Si®, collaborative operation within the same surgical scene has been made possible through the use of two separate master consoles. Whilst retaining all the benefits of single-operator robotic surgery such as enhanced manual dexterity, stereoscopic vision, precision and ergonomic control, additional functionality of collaborative surgery offers several advantages in that it allows several expert surgeons with complementing skills to perform a surgical procedure simultaneously. It also permits the sharing of expertise and knowledge while enabling each surgeon to take responsibility and control of different aspects during the procedure. This is particularly useful during complex tissue manipulation tasks, which may be beyond the capability of bimanual control of a single surgeon and may require active control of more than two robotic arms. Collaborative platforms also permit remote mentoring and assistance, where an expert surgeon can take over a part of the procedure when it is considered too difficult or risky for the non-expert surgeon or trainee.

Although this new paradigm is in direct analogy to traditional MIS practice in terms of their cooperative nature, it suffers from a number of difficulties. These can be mainly attributed to the physical separation between the operators that deprives them from many of the perceptual cues people rely upon during vis-à-vis interaction. Albeit a commonly established lingo and the ability for verbal communication, shared control of the surgical instruments still leads to confusion and hinders efficient and safe interaction between the collaborators. The sole use of utterances such as left/right/in/out can lead to misunderstandings and can be cumbersome and misleading when manipulating complex anatomical scenes. This necessitates the ability to provide the surgeons with some means to share their intention without explicit verbal guidance.

Vis-à-vis interaction normally offers additional contextual information and often involves gestures or other communication media. In [1], Clark demonstrated that pointing at an object in space, leads the conversing participants to shift attention towards that object, with a consequent disambiguation of context and economy of words. However, pointing for referencing is not usually available when both interlocutors‘ hands are busy with tool manipulation.

The recently introduced concept of Gaze-Contingent Perceptual Docking makes use of eye tracking as a means of more effective human-machine interaction, hand-eye coordination and robotic control [2-4]. Eye gaze also represents one of the fundamental cues we rely upon for face-to-face communication. For instance, speakers would normally demonstrate their focus by looking. Studies have also shown that when speakers are describing a scene, they tend to fixate at the objects they mention and in fact up to one second before they name them [5]. Other studies have demonstrated the close coupling between speaker and listener eye movements and its correlation to discourse comprehension over the same visual scene [6]. Based on current experience and the above observations, it is desirable to reveal the visual attention of the collaborating counterparts. The use of eye tracking through the concept of Collaborative Gaze Channelling (CGC) presented here, can achieve this goal.

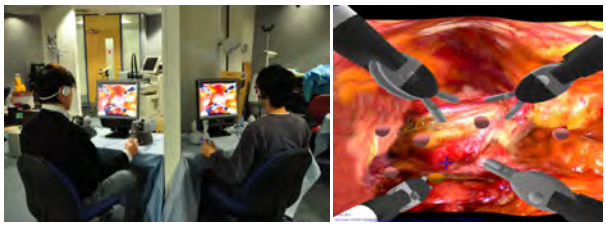

Fig. 1 The setup (left) consists of two surgical consoles displaying an identical surgical scene shown on the right.

MATERIALS AND METHODS

A study involving 40 subjects, demonstrates enhanced collaboration in a shared tele-operated environment by showing improvement on speed, accuracy and reliability during a collaborative task. For studying the effectiveness of CGC and the role that eye–gaze can play, a remote collaborative environment was developed. It consists of two surgical consoles displaying identical views of a shared surgical environment. Each console is equipped with two haptic manipulators that allow the collaborators to control their allocated pair of surgical instruments. For capturing the focus of visual attention, each of the consoles is equipped with a Tobii x50 eye tracker. The fixation point of an operator can be displayed on the collaborator’s screen so both collaborators are aware of the point of attention of their counterparts. The setup can be seen in Fig. 1 on the left. For this study, realistic texture rendering is used to generate a synthetic surgical

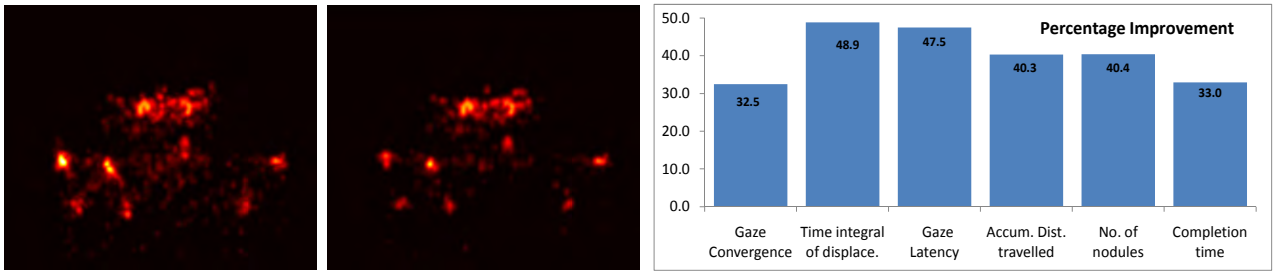

Fig. 2 On the left, hot spot fixation analysis for verbal (left) and CGC (right) tasks for one of the subjects. The graph shows the percentage improvement achieved during the CGC guidance task over the control task.

scene simulating collaborative extraction of seven nodules from soft tissue (Fig. 1 right) according to a predetermined order and within 30 seconds.

Of the two operators, one is the master and the other is the assistant. A nodule can be removed from the surgical scene by the assistant by grasping it and then passing it to one of the master's tools. Communicating to the assistant which nodule is to be extracted is the responsibility of the master and this can be achieved in any of two possible ways. One way engages vocal communication and a predetermined set of utterances such as up/down/left and confirmations such as yes and no. This is considered as the control task. The second way is complemeted by eye tracking, on top of the vocal commands. For this second task, the fixation point of each collaborator is displayed on the counterpart screen. This represents the CGC task. For both tasks the collaborators share an identical surgical view with the master having control of the bottom pair of surgical tools and the assistant of the top pair of tools, as can be seen in Fig. 1 on the right.

The aim of the study is to compare the vocal (control) guidance with the CGC one. For this, a total of 40 subjects have participated to the experiment while a number of variables have been recorded. Each of the two tasks has been performend five times in random order and with a fixed resting period in between. The recorded variables are: *number of nodules* successfully extracted, master and assistant *tool trajectories*, *fixations position* and *duration* and *time* taken to complete the task. Six performance indicators have been evaluated: (1) *Completion time*. (2) *Number of nodules extracted*. (3) *Accumulated distance* travelled by instruments (both those used for extraction of nodules and idle ones). (4) *Gaze displacement*, representing the spatial offset between the master's and assistant's fixations at the moment the master requests removal of a specific nodule. (5) *Gaze convergence*, defined by the area integral of the gaze displacement between the master and the assistant over the time it takes for the two to merge within a defined convergence tolerance. (6) *Gaze latency*, defined as the time between a nodule removal request and the eventual gaze convergence

RESULTS

For all 40 subjects studied, the results show statistically significant improvement (p<0.05) over all six performance indices analysed for the CGC guidance as this can be seen on the graph in Fig. 2. On the left of Fig. 2 a typical hotspot fixation plot for one subject with verbal and CGC guidance respectively can also be shown. On the same figure and with reference to Fig. 1 right, it is evident that in the CGC case, the fixations are well clustered around the nodules. The two clusters on the top that do not demonstrate a significant difference are those corresponding to the tools position where nodule exchange and elimination took place between assistant and master.

DISCUSSION

We have presented a framework based on eye tracking for improved collaborative manipulation of surgical robots. A number of performance indices were introduced to assess operator's performance over a surgical task. Fixation analysis reveals the underlying visual attention and permits more detailed assessment of factors affecting surgical performance. *Gaze convergence* and *latency* have been considered as key performance indices of task quality. Both were significantly improved with the use of CGC by 33% and 48% respectively. This work supports our hypothesis that measurement of visual attention facilitates hand-eye coordination during surgery and in a collaborative environment further enhances coordination of the team.

REFERENCES

[1] Clark HH. Pointing: where language, culture, and cognition meet. In: Associates LE, ed. NJ, USA 2003:243-68

[2] Kwok KW, Sun LW, Vitiello V, James D, Mylonas GP, Yang GZ. Perceptually docked control environment for multiple microbots: application to the gastric wall biopsy. IEEE/RSJ International Conference on Intelligent Robots and Systems 2009; 2009; 2009.

[3] Mylonas GP, Kwok K-W, James DRC, Leff D, Orihuela-Espina F, Darzi A, et al. Gaze-Contingent Motor Channelling, haptic constraints and associated cognitive demand for robotic MIS. Medical Image Analysis.In Press, Corrected Proof.

[4] Yang G-Z, Mylonas GP, Kwok KW, Chung AJ. Perceptual docking for robotic control. Lecture Notes In Computer Science, Proc of the 4th Int workshop on Medical Imaging and Augmented Reality. 2008;5128:21-30

[5] Clark HH, Krych MA. Speaking while monitoring addresses for understanding," in Journal of Memory and Language. J of Memory and Language. 2004;20:62-81.

[6] Richardson DC, Dale R. Looking to understand: The coupling between speakers' and listeners' eye movements and its relationship to discourse comprehension. Cognitive Science. 2005;29:1045-60.

Platform for Magnetic Propulsion and Ultrasound Tracking of Endovascular Devices

C. Di Natali[1], G. Ciuti[1], V. Castelli[1,2], S. Tognarelli[1], E. Sinibaldi[2], P. Dario[1,2], A. Menciassi[1*]

[1]*The BioRobotics Institute, Scuola Superiore Sant'Anna, Pisa, Italy*

[2]*Istituto Italiano di Tecnologia, Center for Micro-BioRobotics@SSSA, Pontedera, Pisa, Italy*

**arianna.menciassi@sssup.it*

INTRODUCTION

Cardiovascular disease is a major worldwide health problem and atherosclerotic plaque build up in the arteries is the main cause of vascular and heart disorders [1]. The most common surgical techniques for vascular problems are angioplasty and bypass grafting performed by endovascular catheters. Typical drawbacks of these procedures are related to the operation under fluoroscopy and to the lack of a real removal of the plaque and obstruction that normally are by-passed or pushed against the vessel wall. Recently, some remote catheter navigation systems have been introduced: they are based on steerable cable activated sheaths for catheters precise steering and coronary interventions (e.g., Hansen system), or on a controlled, permanent magnetic field in which a magnetically equipped catheter can align and bend (e.g., Stereotaxis system). All these platforms are based on catheters, they basically provide just steering and not propulsion abilities, and they cannot be adapted to wireless or softly-wired endovascular devices.

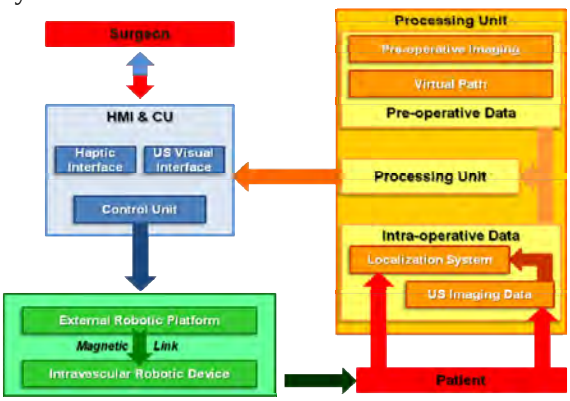

Fig. 1 Traditional CAS architecture adapted to intravascular medical procedures with magnetic dragging and ultrasound servoing control.

By combining the benefits of robotic-aided magnetic navigation and ultrasound (US) imaging, the authors propose an innovative platform based on the traditional computer-assisted surgery (CAS) architecture adapted to intravascular medical procedures. As schematized in Fig. 1, the robotic platform for vascular navigation consists of three main units: 1) the magnetic unit including an external permanent magnet dragging a magnetic endovascular device in the patient body; 2) the control unit interfacing the magnetic unit and the operator; 3) the processing unit merging the pre-operative data (e.g., the diagnostic data about obstruction/plaque location and its features) and the intra-operative data coming from the US localization system, thus implementing an ultrasound-based servoing control.

MATERIALS AND METHODS

With reference to Fig. 1, the magnetic unit is composed by an external permanent magnet (EPM) attached to the end-effector of a 6 degrees of freedom (DoFs) anthropomorphic robotic arm (RV-3SB, Mitsubishi Electric, Japan) and dragging a miniaturized endovascular device. The endovascular device is a capsule with 6 disk-shaped internal permanent magnets (IPM) [2], [3]. Features of the magnetic modules are reported in Tab. I. A second 6 DoFs anthropomorphic robotic arm (RV-6SL, Mitsubishi Electric, Japan) is exploited for holding and moving the US probe (CA430E, Esaote, Italy) for US-based servoing control. The human-machine interface (HMI) consists of an intuitive haptic input device (PHANTOM-Omni, Sensable Technologies Inc., Wilmington, MA). The operator can drive the system by controlling in real-time the motion of the robotic arm equipped with the EPM at the tip. The endovascular capsule prototype has a diameter of 5 mm, it is 10.6 mm in length, and it has a mass of 0.75 g.

Table 1 Features of the Nd-Fe-B magnets (axial)

	L (mm)	D (mm)	m (g)	Br (T)
EPM	25	51	400	1.43
IPM	1.6	3.2	0.08	1.43

L = Length, D = Diameter, m = Mass, Br = Remanence

For testing purposes and for extracting the main parameters governing the procedure of magnetic dragging and US tracking, a home-made test bench has been set-up, as represented in Fig. 2. A pool was fabricated with plexiglass and a straight path was reconstructed inside it by using three different materials: a plexiglass tube, a polyvinyl chloride (PVC) tube, and a porcine vessel. Several trials were performed to control the locomotion of the magnetic endovascular device by using three different water flow rates (2.3

l/min, 3.1 l/min and 3.7 l/min) in flow-wise (FW) and counter-flow-wise (CFW) conditions, thus mimicking a real in-blood operation.

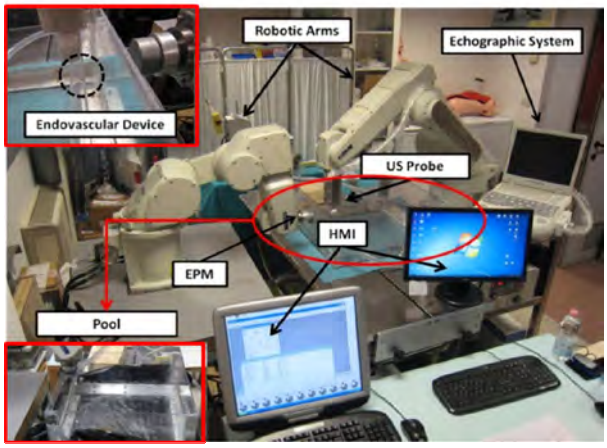

Fig. 2 System architecture of the robotic platform for endoluminal applications.

A first set of trials aimed at determining the EPM-IPM static limit attraction distance (LAD) for a stable link and control. The EPM-IPM distance was increased with an incremental step of 5 mm until the capsule was no longer attracted. A second set of trials were carried out by using both PVC and plexiglass tubes for a proper evaluation of the magnetic dragging efficiency. The endovascular capsule was moved with a constant velocity of the robotic arm of 5 mm/s. Moreover, a third set of trials qualitatively assessed the US robotic tracking in the porcine artery tract: once the US probe is positioned above the artery, an US image-based algorithm guarantees a real-time tracking of the capsule.

RESULTS

By using the previous experimental conditions, the value corresponding to the maximum static LAD between the magnets centers was 143 mm for all the three selected flow rates. The results of the experimental dragging test are reported in Tab. II, both for the PVC and plexiglass tube. The artery tract was not used in order to minimize test bench variability and for the sake of direct visualization.

Table 2 Dynamic LAD at different flow rates

Material / Flow rate (l/min)	PVC		plexiglass	
	LAD_CFW *(mm)*	LAD_FW *(mm)*	LAD_CFW *(mm)*	LAD_FW *(mm)*
2.3	137	202	132	172
3.1	132	242	127	222
3.7	117	252	112	232

For US tracking of the device, a proper algorithm was implemented and validated by using the porcine vessel: the echographic images are reported in Fig. 3.

The average control loop time of the algorithm is about 40 ms mainly sized by the image acquisition frame rate. For the considered procedure, proper gain values were selected in the control implementation for both robotic arms in order to allow a maximum end-effectors speed of 50 mm/s, which is well below the maximum speed (order of 10^2 mm/s) that can be achieved with the aforementioned control loop time.

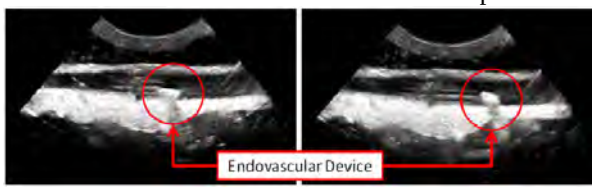

Fig. 3 Echographic images of the device in the porcine artery.

DISCUSSION

An innovative platform for intravascular applications was set-up and assessed in terms of magnetic dragging and US localization of a miniaturized endoluminal capsule. The experimental outcomes are consistent with a simple analytical model (here omitted, for brevity), that analyzes the magnetic capsule dragging in a tubular environment. By means of this model, different working conditions can be considered to select the proper functioning parameters, such as flow rate, friction coefficient, or magnetic properties. Moreover, the magnetic compression on the vessel can be assessed, in order to also consider safety margins in the presence of diseased tissue portions. Future efforts will include quantitative assessment of tissue-capsule interaction by histological analysis. With the above described set-up, we have assessed the possibility of an effective magnetic dragging in well defined conditions and we have validated the tracking of the capsule by US. In order to apply the same protocol in a physiological pathway, the EVE endovascular evaluator (Fain Biomedical, Japan) will be used. The implementation of an autonomous robotic servoing control by means of pre-operative multimodal images will be the next step of this activity. Additional efforts will be devoted to provide the control algorithm with respiratory and cardiac motion compensation strategy [4].

REFERENCES

[1] Naghavi M, Falk E, Hecht HS, Jamieson MJ, *et al.* From vulnerable plaque to vulnerable patient: executive summary of the screening for heart attack prevention and education task force report. Am J Cardiol. 2006;98(2):2H-15H.

[2] Ciuti G, Valdastri P, Menciassi A, Dario P. Robotic magnetic steering and locomotion of capsule endoscope for diagnostic and surgical endoluminal procedures. Robotica. 2009;156:48-58.

[3] Ciuti G, Donlin R, Valdastri P, Arezzo A, Menciassi A, *et al.* Preliminary validation of a novel robotic-controlled platform for capsule endoscopy. Endoscopy. 2010;42:148-152.

[4] Liu J, Spincemaille P, Codella NCF, Nguyen TD, Prince MR, Wang Y. Respiratory and cardiac self-gated free-breathing cardiac CINE imaging with multiecho 3D hybrid radial SSFP acquisition. Magnetic Resonance in Medicine. 2010;63:1230-1237.

New Control Device for Computer-Assisted Laser Phonomicrosurgery

G. Dagnino[1], L.S. Mattos[1], G. Becattini[1], M. Dellepiane[2], D.G. Caldwell[1]

[1]*Advanced Robotics Dept., Italian Institute of Technology, Genoa, Italy*

[2]*ENT Dept., University of Genoa, Italy*

giulio.dagnino@iit.it

INTRODUCTION

Laser phonomicrosurgery is a demanding surgical technique which involves the use of a CO_2 surgical laser to perform meticulous operations on the vocal folds requiring significant psychomotor skills [1], [2]. Scalability, operative distance, and the anatomically small nature of the vocal folds all combine to create numerous surgical challenges. Currently the dominant user interface for remotely aiming a CO_2 surgical laser is the manual micromanipulator coupled with surgical microscope [3] (see Fig. 1). This device allows accurate laser aiming but is prone to error resulting from inexperience and ergonomic factors [2]. Very small, precise changes in the joystick position of manual micromanipulator are necessary to accurately alter the surgical laser aiming point. Clinicians who work with the classic mechanical micromanipulator, have to be skilled and experienced. All of these issues [2], [4] lead to conclude that some form of robotic assistance will prove beneficial to the clinician practicing laser phonomicrosurgery in terms of safety, efficiency, patients outcome, surgery time, surgeon training and, consequently, health care costs.

In this direction, the Italian Institute of Technology (IIT) has developed a novel robotic system for assistive laser phonomicrosurgery (Fig. 1) in order to improve precision, safety and ergonomics [5].

The main idea of the present work is to test several subjects using the system to aim the laser beam with two different control devices: the mechanical micromanipulator, and a Microsoft Xbox 360 controller.

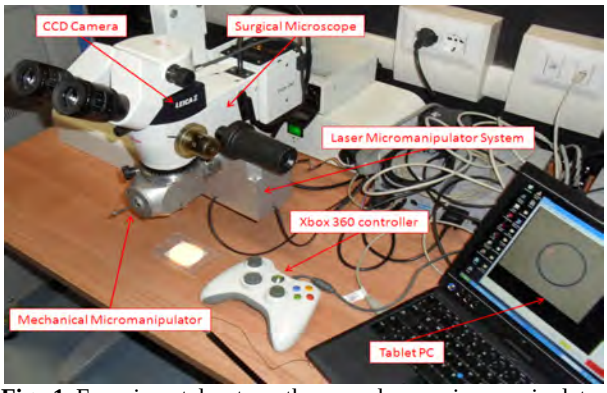

Fig. 1 Experimental setup: the new laser micromanipulator system is attached to surgical microscope. A real-time video from microscope camera is shown on laptop screen. Mechanical micromanipulator and Xbox 360 controller are shown.

MATERIALS AND METHODS

A robot prototype for aiming laser beam has been developed by IIT as shown in Fig. 1 and described in [5]. The basic hardware setup used in our experiments is made up of: one low-power red LASER (Cameo 1260, Global Laser, UK, class 2, 1mW); two stage controllers (C-867.160 PI-Line® Controller, 1 axis) connected to PC via USB and to ultrasonic motors via dedicated socket; two linear stages (single axis) used to aim the laser beam by means of scanning mirrors (one for x-axis and one for y-axis movement); one mechanical manipulator; one Microsoft Xbox 360 controller; one Tablet PC (DELL Latitude XT2, tablet PC), one surgical microscope with CCD camera (Leica M651), and the IIT's software graphical user interface (GUI), which allows the user to control the laser on surgical field by means of various controllers such as mouse, pen on tablet PC, mouse and Xbox 360 controller.

We performed 10 experiments with 10 different subjects with different skills and experience with teleoperation, micromanipulation, microscope and videogaming. Three of them were ENT surgeons. We asked subjects to complete a task consisting on aiming the laser beam along a given path with different control devices (i.e. mechanical micromanipulator and Xbox 360 controller) and view mode (i.e. through the microscope or through PC display). The target path used for the experiments consisted of a circle with 8.5 mm in diameter printed on a piece of white paper with a 0.5 mm line width. This target was set under the surgical microscope, which was set to a 16x magnification. The aiming laser spot was relatively large, measuring around 1 mm.

After a familiarization phase with the setup (about 1 minute) subjects performed the task ten times each with different control devices, 5 times clockwise and 5 counter-clockwise: 10 times with mechanical micromanipulator and microscope view (MM); 10 times with mechanical micromanipulator and pc display view (MD); 10 times with Xbox 360 controller and microscope (XBM); 10 times with Xbox 360 controller and display (XBD).

During the execution of the trials we recorded the videos of the performances which were later analyzed to obtain performance metrics related to control system and view mode in terms of root mean square error (RMSE) on the trajectory following task and time employed to complete the task (TECT).

At the end of the experiment we submitted a

questionnaire to the user in order to collect data about the rating of the system and in particular of control devices, view modalities and GUI.

Data from trials under manual control and evaluation questionnaires were used to evaluate the best control device, learning on the system, precision and safety.

RESULTS

The experimental results from these tests are summarized in Fig. 2, which shows both the overall average path following RMSE and TECT around the circular path. These values were computed over data from all experiments with all subjects, and prove the Xbox 360 controller enables a more precise (thus safer) system operation, with average path following RMSE almost 30% smaller than that obtained with the traditional surgical system, and 52% smaller when view is through PC display.

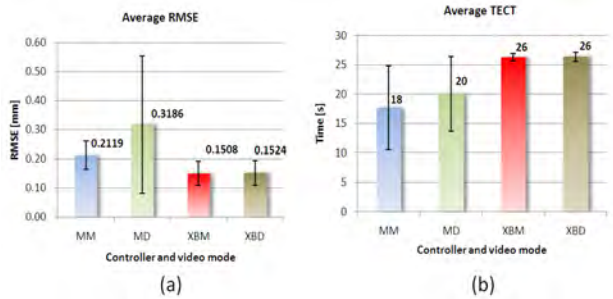

Fig. 2 (a) Overall average path following RMSE and (b) TECT around the circular path.

Furthermore, a learning trend analysis shows that the trend lines of average RMSE and TECT decreasing over the trials performed by the users (both with mechanical micromanipulator and Xbox 360 controller), meaning that the users themselves become familiar with the system and more precise each trial. It is worth to notice that the slopes of Xbox 360 controller RMSE trend lines are steeper than mechanical micromanipulator ones, meaning that they could further improve if more training is performed by the users. The Xbox 360 TECT trend lines are approximately constant: that is because of, in these experiments, the maximum aiming velocity is constant and fixed to 1 mm/s while the mechanical micromanipulator one is very dependent on the individual subject capability. However, if required by a particular surgical scenario, Xbox 360 maximum aiming velocity could be adapted in real-time.

Fig. 3 shows plot comparing trajectories achieved with micromanipulator (a) and Xbox 360 controller (b).

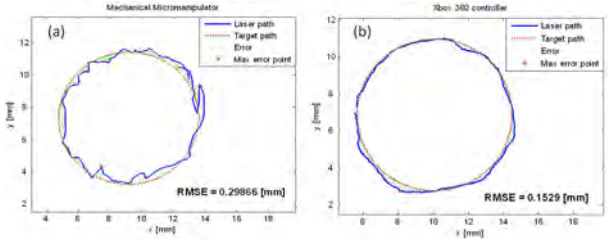

Fig. 3 Graphs of laser path over target path: (a) mechanical micromanipulator and (b) Xbox 360 controller trajectories.

Data collected during the experiments agree with the data from the evaluation questionnaires. All users said that Xbox 360 controller is their favorite control device and found it easy to use, controllable, very precise and more ergonomic. Nine out of ten users found PC display view better than microscope view because the microscope is not ergonomic and is very tiring for the eyes. Nonetheless, experimental data say that average RMSE increases when pc display is used: this is probably due to background skills of users. Indeed users who are very good videogamers and/or had a good familiarization with the system (four users), also had a better result with display vision mode than with microscope.

DISCUSSION

This study is part of the development of a novel medical robotic system to improve precision, ergonomics, controllability and safety in phonomicrosurgeries. Here, a new control device (the Xbox 360 controller) was introduced to aim the laser beam with higher precision and accuracy than classic mechanical micromanipulator. This new setup was investigated through a series of experiments with 10 different subjects in terms of RMSE on the trajectory following task and TECT. These experiments showed a reduction of almost 30% on the RMSE when using the new system versus the traditional setup and a reduction of 52% when view is through PC display. The new system resulted to be easy to use and very ergonomic. All users appreciated the new control device as evidenced by both questionnaires and experimental data (learning curve).

These results will be used to guide further development of the IIT's medical robotic system for laser phonomicrosurgeries. In the future we plan to introduce and test new control devices through another extensive set of experiments to evaluate the quality, the overall safety of the system, and the impact of the new system on the acquisition of phonomicrosurgery skills by novice surgeons. These experiments will be conducted on real laser phonomicrosurgery settings, using a CO_2 surgical laser and pig larynxes as model.

REFERENCES

[1] S. M. Zeitels. Atlas of phonomicrosurgery and other endolaryngeal procedures for benign and malignant disease. San Diego, Calif.: Singular, 2001.

[2] J. F. Giallo. A Medical Robotic System for Laser Phonomicrosurgery. *PhD Dissertation, North Carolina State University*, 2008.

[3] M. Remacle, V. Oswal. Principles and practice of lasers in otolaryngology and head and neck surgery. Kugler Publications, The Hague, The Netherlands, 2002.

[4] S. Chawla, A. S. Carney. Organ preservation surgery for laryngeal cancer. Head & Neck Oncology 2009, 1:12.

[5] L. S. Mattos, D. G. Caldwell, M. Dellepiane, E. Grant. Design and control of a robotic system for assistive laser phonomicrosurgery. *32nd Annual International Conference of the IEEE Engineering in Medicine and Biology Society*, EMBC 2010, September 2010.

Design of a Hybrid Joint Module for a Flexible Access Platform for MIS

D.P. Noonan, V. Vitiello, J. Shang, C.J. Payne, A. Darzi, G.-Z. Yang

The Hamlyn Centre for Robotic Surgery, Imperial College London
dnoonan@imperial.ac.uk

INTRODUCTION

The main advantages of minimally invasive surgery (MIS) are related to reduced tissue scars and surgical trauma, less pain and faster recovery due to the use of long, slender instruments introduced through small incisions. However, there are still significant drawbacks associated with conventional MIS instruments including the fulcrum effect, poor ergonomics and a loss of wrist articulation [1]. The ability to reach areas outside of the direct line of sight from the entry point is therefore one of the main design requirements for novel MIS instrumentation. In addition, the integration of flexibility to allow conformance to curved instrument pathways has to be achieved whilst keeping a small device diameter and ensuring intuitive control. In this work, we present a modular joint design that can potentially fulfill these requirements. As described in detail in the next section, the joint module (Fig. 1) can provide one or two revolute degrees-of-freedom (DoF) which can be arranged in different configurations to form a flexible access robotic platform [2].

Among the articulated systems for MIS, the CardioARM [3] has a diameter of 10mm and a flexible element 300mm in length, which consists of a series of cylindrical links coupled by spherical joints. The system has the ability to maintain an arbitrary 3-D shape or to become completely flexible when needed. However, the joints are not independently addressable. The modular instrument for minimally invasive coronary artery bypass grafting by Salle *et al* [4], features five independently addressable revolute joints with embedded position control and motor-actuation. A SMA actuated gripper can also be attached to each 1-DOF module; however, the system provides no internal instrument channels. The 'hyper-finger' [5] is designed for intra-abdominal interventions and is comprised of identical master and slave manipulators, each featuring a total of 9 DoF arranged as four links serially connected by universal joints and a gripper. The three-armed robot for laryngeal surgery presented in [6] features shape memory alloy (SMA) actuated 'snake-like' distal dexterity units. Neither of the latter two systems provides internal channels for instruments.

A drawback of the above cited systems, excluding [4], is the use of long transmission elements passing through the body of the device to connect with the external primary actuators. In spite of advantages such as high force transmission and small cross sectional area, the large theatre footprint of the remote actuators can disrupt the surgical workflow, and the presence of non-linearities and transmission inefficiencies increases the modeling and control complexity of these devices.

MATERIALS AND METHODS

In contrast to previous designs, the proposed joint module features an embedded hybrid 'pre-tensioned tendon-micromotor' actuation scheme, as can be seen in Fig. 1. Rotation of the motor (4mm brushless DC motor (SBL-04, Namiki Precision Jewel Ltd)) drives a capstan around which the tendon is wrapped. The tendon passes from the capstan to a link which is rotated as the tendon is pulled in or reeled out. The 2-DoF joint has an outer diameter of 12.5mm, a length of 35mm, a weight of 10.1g and three internal channels of diameter 3.5mm, 3mm and 1.8mm respectively. The transmission element from one end can be removed to create a 1-DoF unit if required.

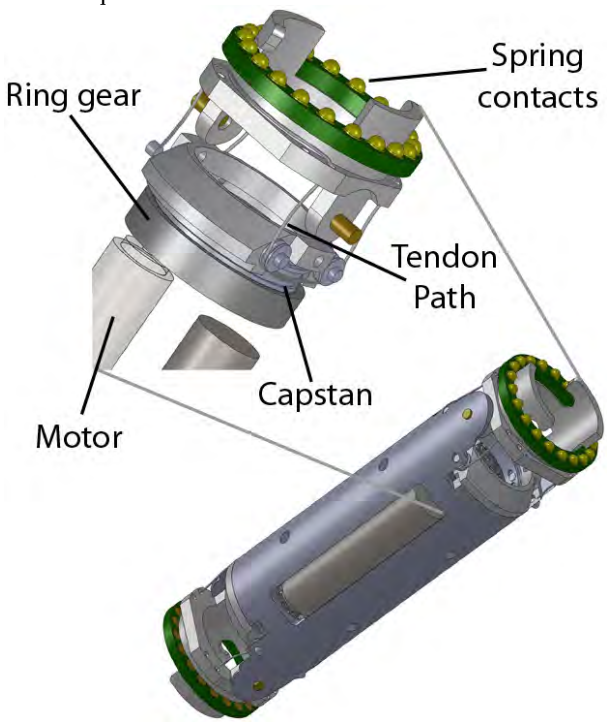

Fig. 1 CAD schematic of the joint module featuring two orthogonal degrees of freedom at each end. The joint segment accommodates three internal channels (1×3.5mm, 1×3m, 1×1.8mm) and a hybrid "micromotor-tendon" transmission system for actuation. The module can also be integrated as a single DoF module with one of the DoFs removed. A close up view of the transmission mechanism is also provided with key components marked

Each embedded motor can output a torque of up to 5.7mNm via a 337:1 planetary gearbox and is connected to a 3-phase sensorless drive circuit (SSD04, Namiki) in

a remote control box. This torque value is further amplified by the transmission stage. Power and signal lines for up to seven motors can be passed between adjacent joint units through a custom interconnect board (Fig. 1) and flexible 4-core wires which pass through the 1.8mm channel. Position feedback is provided by a miniature potentiometer (3203X103P, Tyco Electronics) mounted on each joint axle.

RESULTS

To assess the mechanical repeatability of the design, a closed loop position controller was implemented on 2-DoF joint (configured as a universal joint). The base of the joint was clamped and the tip servoed to nine different positions within its workspace. The positions corresponded to the 0°, ±22.5° and ±45° angular positions on each joint axis. An optical tracking system (Optotrak Certus, Northern Digital Inc) was used to track the 3D position of the tip. The joint was servoed to each of the nine positions three times in a random order. This results in 27 data points, which are shown in Fig. 2. The nine positions can be clearly identified as clusters in the plot. The average standard deviation in tip position in *X*, *Y* and *Z* were 0.38mm, 0.22mm and 0.48mm respectively.

DISCUSSION AND CONCLUSION

A modular, hybrid joint design for MIS has been presented. It features three internal channels for passage of third party instrumentation, ±45° range of motion, modularity and trocar port compatibility. The use of embedded actuation eliminates the need for external actuators. A 7-DoF Flexible Access Platform has been developed by integrating three 1-DoF and two 2-DoF modules and successfully deployed during laboratory and *in vivo* trials [2]. A demonstration of the system workspace in an abdominal simulator and an example of its dexterity in-vivo are shown in Fig. 3. In addition, positional feedback has been used for kinematic control purposes in a laboratory setting using a 5-DOF prototype [7].

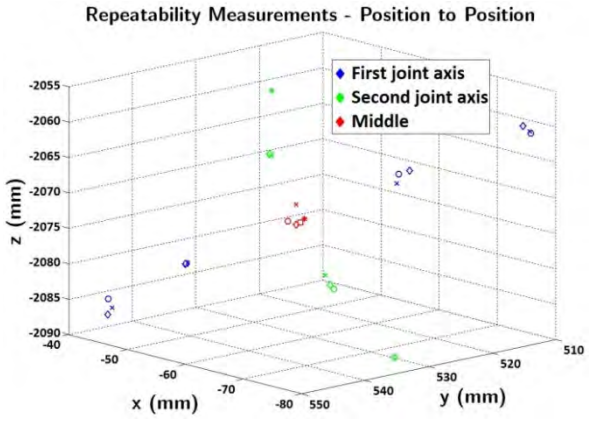

Fig. 2 Position-to-position repeatability analysis when servoing the universal joint randomly between nine different positions within the joint workspace. Clusters represent the nine positions the tip was servoed to and each individual point represents a 3D position of the tip.

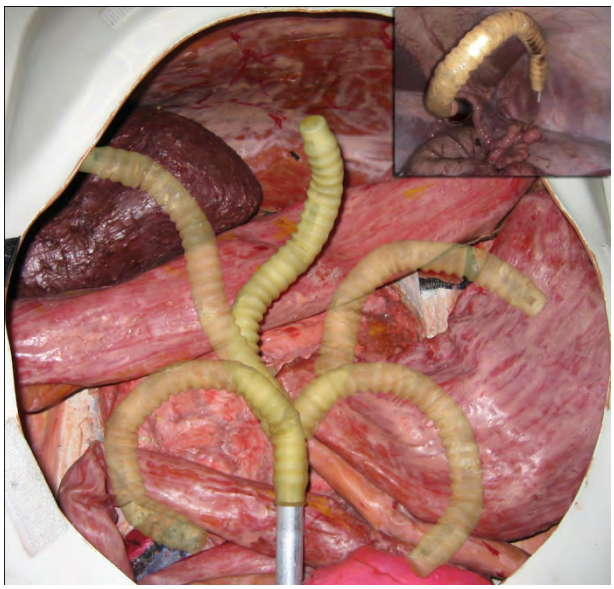

Fig. 3 Demonstration of the flexibility provided by the platform when five joint modules are used to create a 7-DoF device. The dexterity of the device when operating in-vivo is also demonstrated.

ACKNOWLEDGEMENTS

This work was supported by i-Snake™, a Strategic Translational Award from the Wellcome Trust [GR083689].

REFERENCES

[1] Fuchs KH (2002) Minimally invasive surgery. Endoscopy 34(2):154-159.

[2] Shang J, Noonan D, Payne CJ et al. (2011) An Articulated Universal Joint Based Flexible Access Robot for Minimally Invasive Surgery. In: IEEE Int Conf Robot Autom, Shanghai, China.

[3] Ota T, Degani A, Schwartzman D, et al. (2009) A Highly Articulated Robotic Surgical System for Minimally Invasive Surgery. Ann Thorac Surg 87(4):1253-1256.

[4] Salle D, Bidaud P, Morel G (2004) Optimal design of high dexterity modular MIS instrument for coronary artery bypass grafting. In: IEEE Int Conf Robot Autom, New Orleans, LA, 2:1276-1281.

[5] Ikuta K, Sasaki K, Yamamoto K et al. (2002) Remote Microsurgery System for Deep and Narrow Space - Development of New Surgical Procedure and Micro-robotic Tool. In: Dohi T and Kikins R (eds) Med Image Comput Comput Assist Interv - MICCAI 2002 (Lecture Notes in Computer Science, Springer, Berlin, 2488:163-172.

[6] Simaan N, Xu K, Wei W (2009) Design and Integration of a Telerobotic System for Minimally Invasive Surgery of the Throat. Int J Robot Res 28(9):1134-1153.

[7] Vitiello V, Kwok KW, Payne CJ et al. (2011) DOF Minimization for Optimized Shape Conformance under Active Constraints for a Hyper-redundant Flexible Robot. In: Jannin P, Navab N, Taylor R and Yang G-Z (eds) Inf Process Comput Assist Interv - IPCAI 2011 (Lecture Notes in Computer Science), Springer, Berlin.

The First National Examination of the Trends and Outcomes of Robotic Surgery in the US

J.E. Anderson[1], D.C. Chang[2], M.A. Talamini[2]

[1]*University of California, San Diego*

[2]*Department of Surgery, University of California, San Diego*

jaa002@ucsd.edu

INTRODUCTION

Robotically assisted minimally invasive surgery began around 2003, but distinct ICD-9 procedure codes for robotic surgery were not in place in the United States until October 2008. This study compares robotic versus non-robotic surgery in a nationally representative population database in the US.

MATERIALS AND METHODS

Retrospective analysis of the US Nationwide Inpatient Sample (NIS) database was performed from October 2008 to December 2008, the only currently available time period of the dataset that includes robotic procedure codes. The NIS is the largest all-payer inpatient database in the United States, sampling from approximately 20% of all U.S. community hospitals. In 2008, the NIS contained discharge data from 1,056 hospitals located in 42 states. It includes over 100 clinical and nonclinical data from each hospital stay, including primary and secondary diagnoses, primary and secondary procedures, admission and discharge status, patient demographics, expected payment source, total charges, length of stay, and hospital characteristics (including teaching hospital status).[1]

The top 20 robotic procedures by frequency were identified by ICD-9 procedure codes, to include patients with a robotics procedure coded in any of the procedure records. The top three procedures performed robotically were radical prostatectomy (n=2,346), laparoscopic total abdominal hysterectomy (n=427), and laparoscopic assisted vaginal hysterectomy (n=282). Then, patients with any of these 20 procedures as their primary procedure were identified and grouped into categories, including prostate, gynecology, nephrology, gastrointestinal, cardiac, and orthopedic. Procedures were also identified as being performed laparoscopically or not. Patients with multiple procedures of interest, or less than age 18, were excluded. Multivariate analyses examined length of stay and total hospital charges, controlling for robotic procedures, age, race, gender, Charlson co-morbidity index, and teaching hospital status. Statistical analysis was performed in Stata 11.0. Statistical significance was defined as $P < 0.05$.

RESULTS

A total of 78,811 patients were identified. The mean age was 58 (median 59), with 66.4% women. By race, there were 76.2% whites, 10.8% blacks, 7.7% Hispanic, 1.7% Asian or Pacific Islander, 0.5% Native American, and 3.2% other. The Charlson index is a measure of co-morbidities, based on the presence of absence of a number of diagnoses in the patient and combined together in a weighted formula.[2] The ICD-9 diagnosis codes for these conditions were derived using the method by Romano and collagues.[3] Patients with 3+ co-morbidities made up 7.8% of the patient population. Less than half (47.0%) of all procedures were performed at teaching hospitals.

On unadjusted analysis, mean hospital charges were less in robotic versus non-robotic cases ($37,707 versus $42,620, p<0.001) (Table 1). Among procedures already performed laparoscopically, however, the robotic procedures were associated with increased total charges on unadjusted analysis ($36,387 versus $34,713, p=0.002). And on adjusted analysis, robotic cases were associated with an increase in total charges of $2,428 (p<0.001, Figure 1). On subset analyses, the adjusted difference in total charges increased in all laparoscopic procedures ($7,181, p<0.001) as well as in procedures mostly performed laparoscopically, specifically gynecological ($7,349, p<0.001) and gastrointestinal procedures ($16,086, p<0.001).

The unadjusted length of stay decreased by 0.5 days in procedures performed robotically, while the adjusted length of stay decreased by 0.6 days (p<0.001). On adjusted subset analyses, procedures that were already performed laparoscopically had no significant change in length of stay when performed robotically, whereas robotics decreased open procedures by 0.5 days (p=0.028, Figure 2). This greater decrease in length of stay for open procedures was also evident in subset analysis by procedure type. Those procedures performed mostly open had greater decreases in length of stay when performed robotically (prostate, -0.3 days, p<0.001; gynecological, -1.1 days, p<0.001; nephrology, -1.3 days, p=0.006).

DISCUSSION

In this first-ever national analysis of robotic surgery in the US, the data suggest that the additional operating room expense of robotic surgery is compensated for by decreased length of stay in procedures where robotics enables a laparoscopic approach, but not in those already performed laparoscopically.

REFERENCES

[1] Agency for Healthcare Research and Quality. Overview of the Nationwide Inpatient Sample (NIS). http://www.hcup-us.ahrq.gov/nisoverview.jsp Accessed March 2, 2011.

[2] Charlson ME, Pompei P, Alex KL, MacKenzie CR. A new method of classifying prognostic comorbidity in longitudinal studies: development and validation. J Chronic Dis 1987;40:373-383.

[3] Romano PS, Roos LL, Jollis JG. Adapting a clinical comorbidity index for use with ICD-9-CM administrative data: differing perspectives. J Clin Epidemiology 1993;46:1075-1079; discussion 1081-1090.

Table 1 Unadjusted differences in total charges and length of stay for robotic compared to non-robotic procedures

	Total (n=78,811)	Non-robotic (n=75,685)	Robotic (n=3,126)	P-Value
Total charges, mean				
All procedures	$42,421	$42,620	$37,707	<0.001
Laparoscopic procedures	$35,112	$34,713	$36,387	0.002
Prostate	$35,157	$34,899	$35,545	0.286
Gynecologic	$26,207	$26,050	$33,500	<0.001
Nephrology	$54,104	$54,019	$56,348	0.617
Gastrointestinal	$41,570	$41,465	$53,671	0.006
Cardiac	$132,712	$132,916	$120,291	0.453
Orthopedic (knee replacement)	$46,120	$46,118	$52,198	0.365
Length of stay, mean number of days				
All procedures	3.3	3.4	1.9	<0.001
Laparoscopic procedures	2.0	2.0	1.8	<0.001
Prostate	1.9	2.1	1.7	<0.001
Gynecologic	2.7	2.7	1.5	<0.001
Nephrology	5.5	5.5	4.5	0.028
Gastrointestinal	2.5	2.5	2.5	0.903
Cardiac	9.5	9.6	6.2	0.004
Orthopedic (knee replacement)	3.4	3.4	2.6	0.085

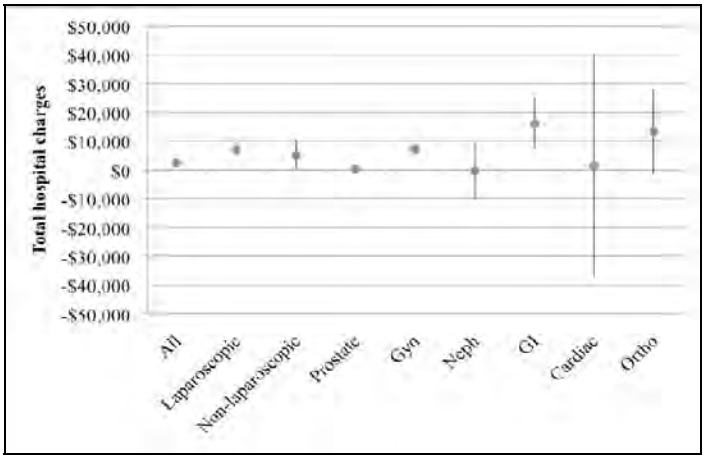

Fig. 1 Adjusted differences in total charges for robotic compared to non-robotic procedures

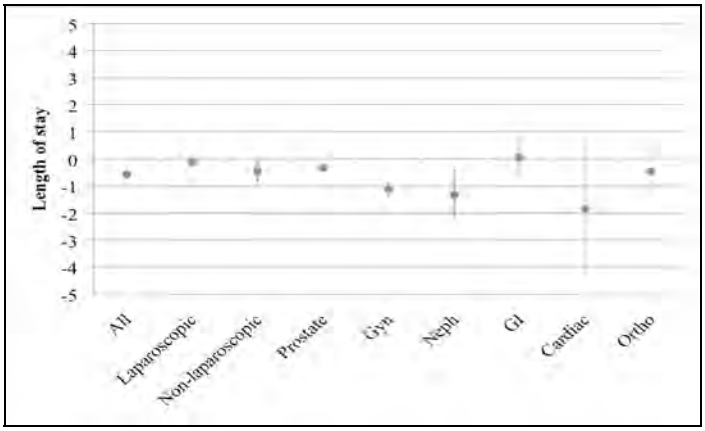

Fig. 2 Adjusted difference in length of stay for robotic compared to non-robotic procedures

Tool Vibration Feedback May Help Expert Robotic Surgeons Apply Less Force During Manipulation Tasks

William McMahan, Karlin Bark, Jamie Gewirtz, Dorsey Standish, Paul D. Martin, Jacquelyn A. Kunkel, Magalie Lilavois, Alexei Wedmid, David I. Lee, and Katherine J. Kuchenbecker

University of Pennsylvania, Philadelphia, Pennsylvania, USA

wmcmahan@seas.upenn.edu, kuchenbe@seas.upenn.edu

INTRODUCTION

Teleoperated robotic surgery systems can provide naturalistic hand-to-tool motion mappings and high-definition stereoscopic visuals; however, surgeons [1-2] and engineers [3-4] recognize that the lack of touch feedback provided to the operator remains a major limitation of these devices. Without effective haptic cues, the surgeon must rely on vision to guide their interactions with the surgical environment, a practice that may lead to increased cognitive load, error incidence, and tissue trauma. Although various haptic interfaces have been developed for robotic minimally invasive surgery, researchers have only recently begun to evaluate the influence of haptic feedback on task performance. Here, we present results from a set of in vitro tasks done by Dr. David I. Lee, an expert urologic surgeon who has performed over 2500 da Vinci procedures on human patients. The aim of the study was to explore the potential clinical impact of VerroTouch, a haptic and auditory tool vibration feedback system recently developed by our group [5].

MATERIALS AND METHODS

This IRB-approved study included three in vitro manipulation tasks: peg transfer, passing a suture needle through holes in a vertical plastic sheet, and suturing a laceration in simulated tissue. Subjects used an Intuitive da Vinci S robot to perform each task under four sensory feedback conditions: visual only (V), visual with audio (VA), visual with haptic (VH), and visual with audio and haptic (VAH), where visual signifies the da Vinci's stereoscopic camera. Audio and haptic indicate the two modes of tool vibration feedback available from VerroTouch. The presentation order of the feedback conditions was randomized by subject. Dr. Lee experienced the conditions in the following order: VA, VH, VAH, V. Subjects were instructed to complete the tasks quickly, accurately, and with minimal force.

The da Vinci robot used in this study was augmented with the tool vibration feedback system described in [5]. It consists of basic modules that can be quickly attached to a surgical robot without permanent modifications. As shown in Fig. 1, a low-cost three-axis accelerometer is mounted on each patient-side manipulator just below the interchangeable tool mounting point. This location within the robot's sterile drapes eliminates the need for sensor sterilization, a common hurdle for haptic feedback in medical robotics. The measured acceleration signals are band-pass filtered from 80 to 1000 Hz and amplified to drive the outputs. Stereo speakers mounted to the sides of the surgeon console provide auditory feedback, and voice coil actuators mounted near the surgeon's hands generate vibrotactile haptic feedback. High-frequency accelerations experienced by the left or right tools are displayed to the surgeon via the corresponding speaker and actuator. The vibrations provided by this system are similar to what a surgeon could hear and feel if they were directly manipulating the instruments, though low-frequency forces and torques are not transmitted.

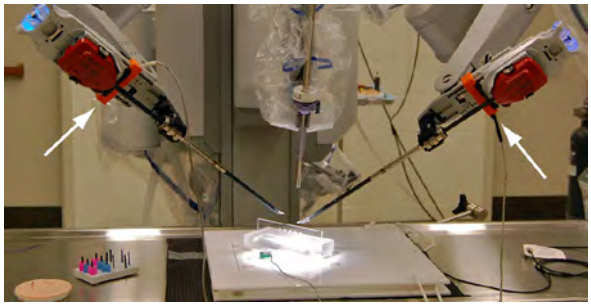

Fig. 1 A da Vinci S robot augmented with tool vibration sensors (arrows). Task materials are mounted to the white board, which is instrumented with a force sensor.

A time history of the tool accelerations and contact forces that occurred was recorded during each trial. Forces were measured by mounting the task materials to a white acrylic board that was instrumented with an ATI Mini40 force-torque sensor, as seen in Fig. 1. To reduce data dimensionality, we calculated the root-mean-square (RMS) of the magnitude of the three-dimensional force vector when either instrument exerted a measurable force on the task materials.

RESULTS

In addition to the expert subject discussed here, the study included five attending surgeons and six surgical residents of varying specialty, none of which had prior exposure to VerroTouch. Only three of these surgeons had significant clinical experience with robotic surgery (from 150 to 800 operations). Results from these other eleven subjects are reported in a separate publication [6]. Fig. 2 shows how the RMS forces applied by Dr. Lee compare to the range of forces applied by the other

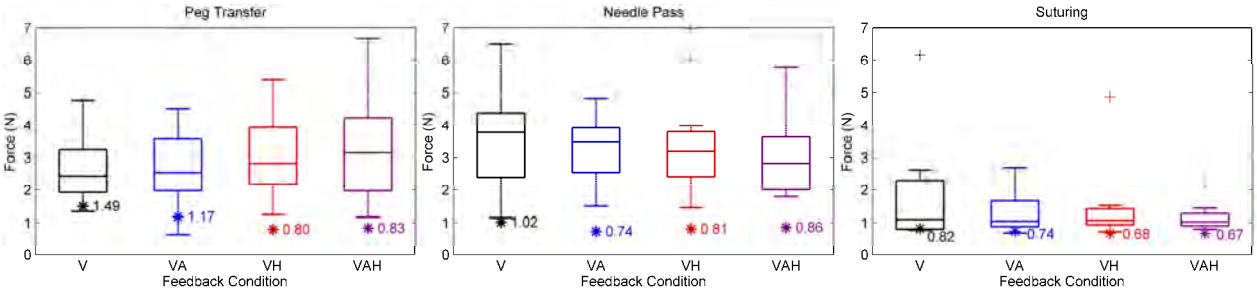

Fig. 2 Box plots of the RMS forces applied to the task materials by the eleven surgeons who participated in the study from [6]. The expert surgeon's performance, not included in the box plots, is overlaid with an asterisk.

subjects for each task and feedback condition. Additionally, Dr. Lee was among the quicker subjects to complete each trial, and often the quickest. His data have no discernible relationship between completion time and feedback condition.

We performed a within-subject analysis of variance of Dr. Lee's RMS force data, where the factors examined were auditory feedback (provided or absent), haptic feedback (provided or absent), and task (peg transfer, needle pass, or suturing). Taking $\alpha = 0.05$, this analysis shows that the presence of haptic feedback of tool vibrations ($F(1, 11) = 5.18$, $p = 0.057$, $\eta^2 = 0.24$) and task identity ($F(2, 11) = 4.34$, $p = 0.060$, $\eta^2 = 0.40$) approach significance, while audio feedback does not ($F(1, 11) = 1.07$, $p = 0.336$). The trend for haptic feedback did not hold for the population of less experienced subjects who participated in the study [6].

DISCUSSION

It is natural to expect that more experienced surgeons handle task materials efficiently and delicately. Our study quantifies efficiency and delicacy via task completion time and the RMS force applied to the task materials. The efficiency and delicacy of Dr. Lee's manipulations are evident when comparing his times and forces with those of less experienced surgeons. For many conditions, he achieved both the fastest time and the lowest forces. These findings suggest that one may be able to evaluate robotic surgery skill or experience by measuring the force a surgeon applies to in vitro task materials. We are in the process of analyzing the recorded tool accelerations to determine whether they may also be a potential candidate for assessing skill.

An analysis of variance of the force data suggests that the haptic tool vibration feedback provided by VerroTouch enabled Dr. Lee to apply less force to the task materials while still completing tasks quickly. Since the visual only (V) feedback condition was presented last, the performance improvement cannot be attributed to practicing the tasks. Given this subject's prior exposure to VerroTouch (approximately three hours total), this result suggests that surgeons can learn to use tool vibration feedback to interact more delicately with their environment.

While this trend was not generally replicated in the study reported in [6], the eleven other participants were naive to VerroTouch, and the majority had no experience with robotic surgery. We hypothesize that giving these subjects more time to practice with VerroTouch and the da Vinci would enable them to learn to use the haptic tool vibration feedback to operate more delicately. These subjects also expressed a significant positive preference for the inclusion of tool vibration feedback [6], indicating that they believe it would be useful in a real operative setting.

In summary, analysis of an expert's RMS force data from in vitro tasks suggests that haptic tool vibration feedback may help experienced users reduce the forces they apply during manipulation tasks. Furthermore, we believe RMS force may be a useful metric for evaluating an individual's skill at robotic surgery.

ACKNOWLEDGMENTS

This project is funded, in part, under grants with the Pennsylvania Department of Health and the NSF.

REFERENCES

[1] G. T. Sung and I. S. Gill, "Robotic laparoscopic surgery: a comparison of the da Vinci and Zeus systems," *Urology*, vol. 58, no. 6, pp. 893-898, 2001.

[2] O. Meireles and S. Horgan, "Applications of surgical robotics in general surgery," in J. Rosen et al. (eds.), *Surgical Robotics*, ch. 33, pp. 791-812. Springer, 2011.

[3] A. M. Okamura, L. N. Verner, T. Yamamoto, J. C. Gwilliam, and P. G. Griffiths, "Force feedback and sensory substitution for robot-asisted surgery," in J. Rosen et al. (eds.), *Surgical Robotics*, ch. 18, pp. 419-448. Springer, 2011.

[4] M. O. Culjat, J. W. Bisley, C.-H. King, C. Wottawa, R. E. Fan, E. P. Dutson, and W. S. Grundfest, "Tactile feedback in surgical robotics," in J. Rosen et al. (eds.), *Surgical Robotics*, ch. 19, pp. 449-468. Springer, 2011.

[5] K. J. Kuchenbecker, J. Gewirtz, W. McMahan, D. Standish, P. Martin, J. Bohren, P. J. Mendoza, and D. I. Lee, "VerroTouch: high-frequency acceleration feedback for telerobotic surgery," In A. M. L. Kappers et al. (eds.), *Proc. EuroHaptics, Part I*, vol. 6191 of LNCS, pp. 189-196. Springer, July 2010.

[6] W. McMahan, J. Gewirtz, D. Standish, P. D. Martin, J. A. Kunkel, M. Lilavois, A. Wedmid, D. I. Lee, and K. J. Kuchenbecker, "Tool Contact Acceleration Feedback for Telerobotic Surgery," accepted for publication in *IEEE Transactions on Haptics, Special Issue on Haptics in Medicine and Clinical Skill Acquisition*, vol. 4, 2011.

The Impact and Extent of Nerve Preservation on Potency Outcomes Following Robot- Assisted Radical Prostatectomy – A Propensity Matched Analysis

Ananthakrishnan Sivaraman, Vipul R. Patel, Sanket Chauhan, Kenneth Palmer, Oscar Schatloff, Bernardo Rocco

Global Robotic Institute, Florida Hospital Celebration Health, University of Central Florida School of Medicine, Orlando, FL, USA

PURPOSE

To discern the impact and extent of nerve preservation on the potency rates following robot- assisted radical prostatectomy (RARP).

MATERIALS AND METHODS

From January 2008 through October 2010 a total of 1972 RARP were performed by a single surgeon who graded the extent of nerve sparingas non nerve sparing, partial and full. Partials were subdivided into the percentage of nerve bundle preserved (> 75%, > 50% and < 50%,< 25%) on each side. Patients were further categorized into 3 groups: Bilateral full nerve sparing (BFNS); Unilateral full nerve sparing, contralateral partial nerve sparing(FNS/PNS) and Bilateral partial nerve sparing(BPNS). From a cohort of 968 preoperatively potent men (SHIM>21) having atleast one year of follow up, 371 had BNS; 72 FNS/PNS and 34 had bilateral PNS. Only patients with > 50% nerve preservation were included in the analysis. A propensity analysis with optimal matching algorithm was used to match the BFNS vs FNS/PNS and BFNS vs BPNS.(1)(2)

RESULTS

The mean followup months was22.6 (range 12.1 to 33.6), FNS/PNS group was 21.9 months (range 12.1 to 33.4) and the BPNS group was 21.3(range 12.0 to 33) . Potency rates of BFNS and FNS/PNS group were 93.1% vs 79.3%. This difference approached statistical significance (p= .057). Continence and BCR rates were comparable between the two groups. Composite trifecta rates between BNS and FNS/PNS was 89.7% vs 74.1% (p = .030). The potency rates between the BNS and BPNS groups was 90.9 vs 66.7% (p = .033)and the time to potency was 5.6months vs 10.8months. Composite trifecta rates between BNS and BPNS groups was 81.8% vs 54.5% (p=.017). BCR and continence rates were similar among the groups. The positive surgical margin rate was not different among the three groups.

CONCLUSION

Nerve preservation without compromising oncological safety should be the goal of RARP. This study has demonstrated that the extent of nerve preservation clearly impacts on both the quality as well the time to return of sexual function following RARPFurther, incremental nerve preservation leads to an incremental return of potency.

REFERENCES

[1] Moskovic DJ, Alphs H, Nelson CJ, Rabbani F, Eastham J, Touijer K, et al. Subjective characterization of nerve sparing predicts recovery of erectile function after radical prostatectomy: defining the utility of a nerve sparing grading system. J Sex Med. 2011 Jan;8(1):255-260.

[2] Levinson AW, Pavlovich CP, Ward NT, Link RE, Mettee LZ, Su L. Association of surgeon subjective characterization of nerve sparing quality with potency following laparoscopic radical prostatectomy. J. Urol. 2008 Apr;179(4):1510-1514.

Table 1 Comparison of Outcomes in Bilateral and Partial Full Nerve Sparing in Propensity-Matched Groups

Variables	Propensity Matched Patients				*p* Value
	Bilateral Full Nerve Sparing		Partial Full Nerve Sparing		
Total patients	58	(100.0)*	58	(100.0)	
Follow-up (months) Mean ± SD	22.6 ± 6.2		21. 9 ± 6.0		0.456
Time to continence (months) Mean ± SD	2.6 ± 4.1		2.9 ± 4.6		0.687
Time to potency (months) Mean ± SD	4.9 ± 6.2		7.1 ± 9.2		0.129
Time to biochemical recurrence (months) Mean ± SD	22.2 ± 6.7		20.9 ± 6.9		0.333
Composite Trifecta	52	(89.7)	43	(74.1)	0.030
Continence	56	(96.6)	54	(93.1)	0.679
Potency	54	(93.1)	46	(79.3)	0.057
Biochemical recurrence	2	(3.4)	2	(3.4)	1.000

Table 2 Comparison of Outcomes in Bilateral Full and Bilateral Partial Nerve Sparing in Propensity-Matched Groups

Variables	Propensity Matched Patients		*p* Value
	Bilateral Full Nerve Sparing	Bilateral Partial Nerve Sparing	
Total patients	33 (100.0)*	33 (100.0)	
Follow-up (months) Mean ± SD	21.2 ± 5.7	21.3 ± 6.7	0.956
Time to continence (months) Mean ± SD	3.0 ± 3.9	2.4 ± 3.9	0.558
Time to potency (months) Mean ± SD	5.6 ± 6.4	10.8 ± 9.8	0.013
Time to biochemical recurrence (months) Mean ± SD	20.9 ± 6.2	19.5 ± 7.7	0.427
Composite Trifecta	27 (81.8)	18 (54.5)	0.017
Continence	31 (93.9)	31 (93.9)	1.000
Potency	30 (90.9)	22 (66.7)	0.033
Biochemical recurrence	1 (3.0)	2 (6.1)	1.000

*Numbers in parentheses are percentages

Neuroergonomic Assessment of Collaborative Gaze Control for Robotic Surgery: a functional Near Infrared Spectroscopy (fNIRS) Study

D.R.C. James[1,2], D.R. Leff[1,2], F. Orihuela-Espina[1], K.-W. Kwok[1], L.W. Sun[1], T. Athanasiou[2], A.W. Darzi[1,2], G.-Z. Yang[1]

[1]*Hamlyn Centre for Robotic Surgery, Imperial College, London*

[2]*Department of Surgery and Cancer, Imperial College, London*
d.james@imperial.ac.uk

INTRODUCTION

Collaboration within surgery is essential - whether between trainer and trainee, a surgeon and their assistant or between colleagues from different specialties. It is imperative that communication is optimized allowing intent to be conveyed effectively. Collaborative Gaze Control (CGC) is a system that captures the gaze behaviour of the lead surgeon and displays their fixation point on the monitor of the trainee as a cross. Thus guidance can be delivered visually obviating the need for verbal direction. This system is likely to become all the more relevant as progressively more complex procedures are undertaken with minimally invasive or robotic assistance necessitating surgeon cooperation.

It is critical that novel technology is scrutinized not only for performance effects, but also as to how it impacts on those using it. This ensures that new instrumentation does not cognitively overload the surgeon rendering them unable to deal with unanticipated events such as unexpected bleeding. Neuroergonomics is the study of the brain and behaviour at work [1,2] and enables determination of the cortical substrate for task execution and how this may be modulated by assistive technology.

Visual search may be divided into *'bottom-up'* where search is guided by target saliency; and *'top-down'* necessitating voluntary gaze direction more reliant on cortical input beyond the visual cortex [3]. Thus with CGC it is likely that visual cortical activity will be reduced as the search strategy is modulated.

In this study, a simulated robotic surgical task is undertaken under verbal and CGC guidance. It is hypothesized that with CGC, visual search will be modulated leading to reduced cortical activity and performance enhancement.

MATERIALS AND METHODS

20 subjects (1 female) with a mean age of 28.9 +/- 1.5 (years +/- SD) were recruited from Imperial College. Task setup is illustrated in Fig. 1 and necessitated the subject (*'trainee'*) undertaking a simulated robotic surgical task under the direction of the expert (*'trainer'*). Haptic manipulators were used to control

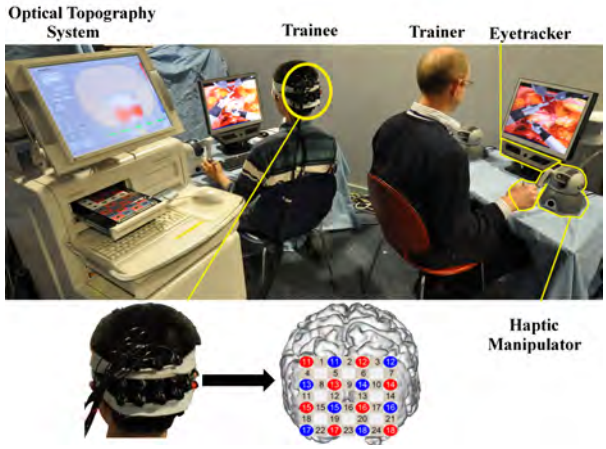

Fig. 1 Task setup. Trainer (right) and trainee (left) control virtual instruments with 2 haptic manipulators each (Phantom Omni, SensAble Tech., USA). Gaze behaviour is extracted with a portable eyetracker (x 50 eyetracker, Tobii Tech., Sweden) beneath the task monitors. A 24 channel optical topography system (ETG-4000, Hitachi Medical Corp., Japan) detects relative changes in oxy- and deoxyhaemoglobin (HbO_2 and HHb) over the visuoparietal cortices (subplot).

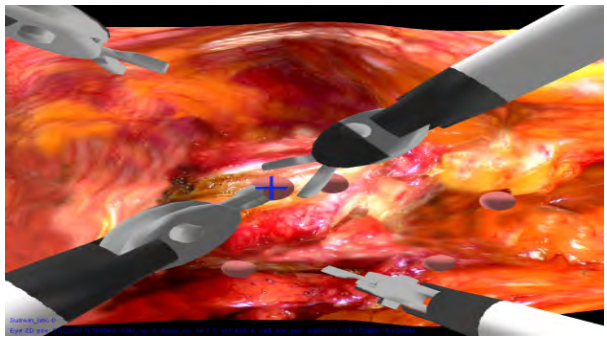

Fig. 2 Task image with trainee's graspers (inferiorly) passing the nodule to the trainer's instrument (superior aspect of screen). Trainer fixation point can be appreciated (blue cross).

robotic graspers in a virtual scene with the aim of biopsying nodules and transferring them to the trainer's instruments (visible within the same field of view) as shown in Fig. 2. Seven nodules were visible however the target lesion was only displayed to the trainer and its location had to be communicated to the trainee. This was undertaken either verbally (control) or with visual (CGC) guidance. With CGC, trainer fixation point (detected with eyetracker) was displayed on the trainee's monitor as a blue cross (Fig. 2).

All subjects undertook the task under both conditions (order randomised). Performance was determined as the number of successful biopsies taken and instrument pathlength. Cortical activity was assessed as number of activating channels (increase in HbO_2 and decrease in HHb, Wilcoxon rank sign, α=0.05). A task-evoked cortical network was generated and was used to derive econometric data of network connections, cost, efficiency and cognitive burden [2]. Gaze latency was determined as the time taken for the trainee to fixate on the same target as the expert. Group related differences in dependent variables were determined with a random effects model with group as the independent variable.

Table 1 Results of performance, cortical activity and econometrics of cortical network (mean+/-SD).

	Control	*CGC*	*p*
Biopsy number	5.9 +/- 1.6	7.2+/-2.0	<0.001
Pathlength (m)	0.6 +/- 0.1	0.3+/-0.1	<0.001
Gaze latency (s)	1.6 +/- 0.4	0.9+/-0.2	<0.001
ΔHbO_2 (mMolxcm)	2.8 +/- 12.5	1.5+/-10.9	<0.001
ΔHHb (mMolxcm)	-0.9 +/- 5.6	-1.1+/-5.1	0.188
No. connections	97.6+/-119.3	81.6+/-97.3	<0.001
Normalised cost (a.u.)	0.5 +/- 1.0	0.3+/-0.6	<0.001
Cognitive Burden (a.u.)	0.4 +/- 1.1	0.3+/-0.6	<0.001
Global Efficiency (a.u.)	0.13 +/- 0.32	0.09+/-0.27	<0.001

RESULTS

Results (Table 1) indicate that performance was enhanced with CGC both in terms of number of successful biopsies and with regard to instrument pathlength, which was diminished compared to control. The magnitude change of HbO_2 was less with CGC and, as displayed in Fig. 3, a spatially diminished area of activity was seen. The ensuing cortical network from a representative subject is displayed in Fig. 4. It can be appreciated that with CGC, fewer connections are present. With regard to the econometric data, performing with CGC lead to significantly fewer

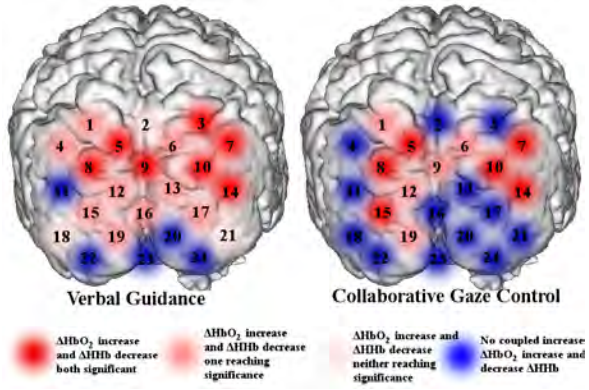

Fig. 3 Group-averaged activation map for control (left) and CGC (right) guidance. Degree of activation is described (figure legend). A greater number of channels is seen to activate under the control condition.

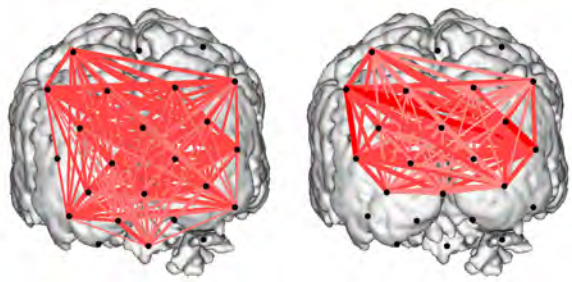

Fig. 4 Cortical networks from a representative subject for control (left) and CGC guidance (right). Channel locations (black circles) are overlain onto a reference MRI. Connections are depicted as red lines with strength indicated by thickness of line.

cortical connections. The efficiency of this network was higher under the control condition; however, network cost and the task-induced cognitive burden were lower with CGC.

DISCUSSION AND CONCLUSIONS

This study has demonstrated that operating under CGC guidance leads to enhanced performance in a simulated robotic surgical task. This improvement is likely to be underpinned by a modulation in search strategy from a *'top-down'* search under verbal guidance, which is reliant on greater cortical activity, to a *'bottom-up'* search with CGC. The latter leads to decreased cortical activity, a reduction in gaze latency and superior performance. Task-induced cognitive burden was lower under CGC guidance which indicates a greater network economy [2]. The findings of this study indicate that operating under CGC guidance is likely to be *'easier'* for the surgeon and thus may free up cortical resources in order to devote to other aspects of the task such as the overall stages of the procedure or to deal with unexpected events. In the current study instrument pathlength is lower under CGC guidance implying greater economy of movement which is possibly due to the surgeon being able to focus more on undertaking the task as guidance had been seamlessly delivered.

The strength of this study lies firstly with the potential that CGC has as a means of surgical guidance; and secondly in the relevance of the neuroergonomic assessment of surgical tasks. In this instance, the latter indicates that CGC enhances performance without impairing the surgeon's cognition.

REFERENCES

[1] James DR, Orihuela-Espina F, et al. The ergonomics of natural orifice translumenal endoscopic surgery (NOTES) navigation in terms of performance, stress and cognitive behavior. Surgery 2011 Apr; 149(4): 525-33.

[2] James DR, Orihuela-Espina F, et al. Cognitive burden estimation for Visuomotor learning with fNIRS. LNCS 2010; 13(Pt 3): 319-26.

[3] van der Stigchel S, Belopolsky AV, et al. The limits of top-down control of visual attention. Acta Psychologica 2009 132(3): 201-12.

SIMBiopsies: An Augmented Reality Training SIMulator for Needle Biopsies

M. S. Narayanan[1], X. Zhou[1], S. Garimella[2], W. Waz[2], F. Mendel[3], V. Krovi[1]
[1]*MAE Department, SUNY at Buffalo, NY, USA,*
[2]*Pediatric Nephrology, SUNY at Buffalo, NY, USA,*
[3]*School of Medicine and Biomedical Sciences, SUNY at Buffalo, NY, USA*
vkrovi@buffalo.edu

INTRODUCTION

Tissue biopsies, the procurement of small tissue samples, remain the gold standard for assessing the health of internal organs such as kidney, liver, and bone. Extracted tissues are used to find abnormal cells (e.g. cancers), investigate symptoms (e.g. ulcers, hepatitis, kidney disease or endometriosis), or inflammation [1]. The anatomical location of the tissue dictates the selection of the biopsy instrument (e.g., curette, punch, needle, endoscope), additional visualization modalities (e.g. CT/MR, ultrasound, fluoroscope), and in turn the biopsy setting (e.g. outpatient clinic, operating-room).

Typically clinicians learn to do biopsies by observing more experienced personnel actually performing them. Then the student clinicians are 'talked through it' by the supervising clinician as the student performs the procedure *on a live patient needing that particular biopsy*. Students are shown the anatomical landmarks (visual clues) that guide placement of the biopsy, and urged to 'feel' the different tissues as the needle encounters or passes through them. In rare instances, novice clinicians are subjectively evaluated for such things as dexterity, speed, coordination and skill by an experienced examiner before the student is allowed to perform the procedure unassisted [2]. But, only few programs have such examinations because of, among other things, the time and expense involved and the unpredictable availability of subjects (patients) needing the particular biopsy. Consequently, training of these common, important, but potentially risky procedures are not uniformly taught or often repeated. The result is inadequately or poorly trained practitioners, who then go on to poorly train others [3].

In this work, we will focus on needle biopsies, wherein long needles are inserted through cutaneous tissues and body wall to obtain samples of lung, liver, prostate, kidney, etc. Several of the more intricate biopsies such as those of the kidney, prostate, or liver are difficult because of the risk of injury to other organs. These procedures require considerable training in **both cognitive and sensorimotor skills** to successfully execute. The sheer number of biopsies performed and the variety of clinical specialties performing these procedures argue compellingly for a more comprehensive, quantitative, computer-based training, testing, and certification regimen for resident training. Within the medical education community, there is also growing awareness of the need for a quantitative skill-based assessment of residents to justify credentialing and hence the need for such virtual trainers [4].

However, such biopsy simulators are still in their infancy due to limitations in visual and haptic technologies, lack of suitable assessment metrics, and, most importantly, lack of accreditation/validation/ certification of these methodologies. Our motivation to create and deploy such a simulator arises from several reasons, including: (i) inadequate conventional training due to various economic and logistical issues; (ii) marked differences in learning among trainees using current training techniques; (iii) evidence directly linking trainee improvement to duration, regularity, realism and diversity of training sessions; (iv) a growing need for procedural training that closely couples cognitive with sensorimotor training, and (v) improved understanding and technological progress in kinesthetic human-computer interactions that make feasible low-cost implementation of such a simulator. Thus, in this work we propose to develop and validate an Augmented Reality Training SIMulator for Needle Biopsies (AR-SIMBiopsies) that replicates both the look (graphics) and feel (haptics) of an actual biopsy triaining.

THE SIMBIOPSIES TRAINING SIMULATOR

In this work, we addressed the creation of an **immersive Augmented Reality SIMBiopsies Training Simulator Kiosk** (refer **Fig. 1**) for capturing **quantitative assessment** of motions and forces (of novitiates and experts) as they perform selected biopsies. SIMBiopsies is intended to allow systematic gradation of training and can serve both as an educational tool for beginners and a practice tool to increase expertise as well as for planning and training complicated 3D needle biopsy procedures in the future.

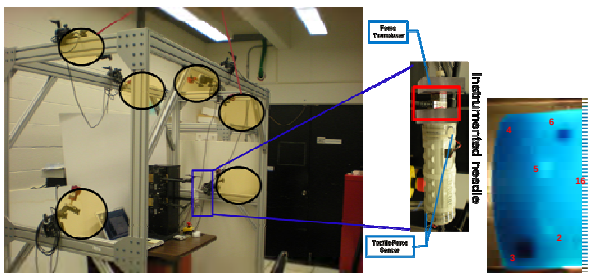

Fig. 1 SIMBiopsy Trainer– coupling instrumented haptic devices with MoCap cameras to quantitatively assess sensorimotor performance during biopsy training on the Blue Phantom™.

We intentionally selected an established biopsy phantom (the Blue Phantom™) for both the virtual and

physical studies to facilitate comparative studies of skill. The augmented reality (AR) environment allows users to be presented with realistic sensorimotor stimuli during the commission of a biopsy with seamless quantitative measurement of their responses within a carefully-controlled environment. The key element of this system is the high-fidelity haptic device [5] attached to biopsy needle which is retrofitted with force-transducers and motion capture markers. Both the cameras and haptic device are interfaced with a multirate real-time (200 Hz- 2000 Hz) data-acquisition environment. Varying grades of visual assist for accurate targeting of sites in percutaneous procedures (such as CT or ultrasound scans) will be evaluated for biopsy training [6] as a part of our future work.

Haptigrams (motions and force profiles) of users are captured while operating the AR-SIMBiopsies simulator in two modes:

(1) **Physical Interaction Mode**: The trainee can use the needle to perform biopsies directly on the physical Blue Phantom™ phantom as shown in **Fig. 2** (a). The ability to transparently monitor user-performance (without having to computationally simulate the haptic response) is a benfit but this approach is expensive in terms of consumption of biopsy-phantoms.

(2) **Haptics/VR Simulation Mode**: In this mode, the users operate using the needle (haptic device probe) on the virtual phantom with haptic feedback as shown in **Fig. 2** (b). Virtually reproducing the realistic 'feel' (haptics) of the biopsy needle passing through different materials offers promising and cost-effective means to safely and methodically train clinicians to perform various biopsy training.

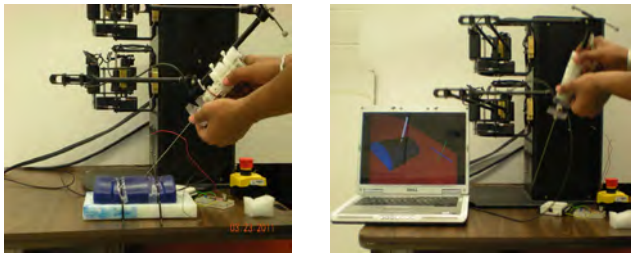

(a) (b)

Fig. 2 AR-SIMBiopsies Trainer (a) Physical Interaction Mode (b) Haptics/ VR Simulation Mode

The haptic models for use in the virtual phantom system (for Mode 2 above) were developed by an empirical material testing approach on the physical Blue Phantom™. A 6-DOF robotic manipulator [7] equipped with a 6 DOF force/ torque sensor (**Fig. 3**) was used to systematically obtain force-displacement data as shown in **Fig. 3**.

DISCUSSION

The AR-SIMBiopsies trainer was developed and is being deployed for conducting a series of needle biopsy studies. The principal benefits of using such a trainer include: (i) creation and deployment of an application-specific environment/tool; (ii) validation of the applicability and viability of the environment; and (iii) exposure of the current and next generation of medical professionals to these computer-aided methods.

The flexibility to operate the trainer under two modes allowed us to conduct a series of subject studies on both virtual and physical phantoms. The following comparative studies are being analyzed: (i) quality of haptic feedback model versus the physical phantom study (ii) comparison of trainees as well as experts using the hand and needle motions and forces as primary metrics (iii) monitoring skill acquisition and performance levels of trainees in physical simulation mode after a period of training in haptics mode.

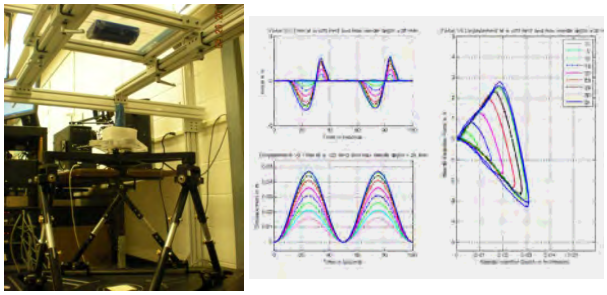

Fig. 3 Force-Displacement curves for material characterization of the Blue Phantom™ obtained by systematic parametric sweeps using a 6-DOF robotic system.

At a minimum, we anticipate that it can help train students in many of the cognitive-, procedural- and sensorimotor-aspects to attain competency (certification) to begin performing these procedures on live patients. However, efforts are also underway to extend the capability of this system to establish secondary (specialized) metrics for skill evaluation, quantitatively (objectively) compare the performance of students with an 'expert' and provide assessment (feedback) for improving proficiency.

REFERENCES

[1] Mrug, M., and Bissler, J. J., 2010, "Simulation of real-time ultrasound-guided renal biopsy," Kidney International, 78, pp. 705-707.

[2] Shah, J., Mackay, S., Vale, J., and Darzi, A., 2001, "Simulation in urology--a role for virtual reality?," BJU international, 88(7), pp. 661-665.

[3] Gaies, M. G., Landrigan, C. P., Hafler, J. P. and Sandora, T. J., "Assessing procedural skills training in pediatric residency programs."

[4] Wignalla, G.R., Denstedta, J.D., Premingerb, G.M., et al., 2008, "Surgical Simulation: A Urological Perspective," The Journal of Urology, 179(5), pp. 1690-1699.

[5] Lee, L.-F., Narayanan, M. S., Mendel, F. C., et al., 2010, "Kinematics Analysis of In-Parallel 5 DOF Haptic Device," IEEE/ ASME International Conference on Advanced Intelligent MechatronicsMontreal, Quebec, Canada.

[6] Thainual, P. U.-., Ioradachita, I., and Fichtinger, G., 2008, "The Perk Station: Design of a Percutaneous Internvention Training Suite," 2008 International Conference of the Society for Medical Innvoation and Technology (SMIT) Vienna, Austria.

[7] Narayanan, M. S., Chakravarty, S., Shah, H., and Krovi, V. N., 2010, "Kinematic- Static- and Workspace Analysis of a 6- P-U-S Parallel Manipulator," 2010 ASME International Design Engineering Techincal Conference Montreal, Quebec, Canada.

A Virtual Reality Simulator for Shoulder Arthroscopy – Face and Construct Validity

Roger J Emery[1], Sofia Bayona[2], Chinmay Gupte[1], Fernando Bello[1]

[1]*Department of Surgery & Cancer, Imperial College London*

[2]*Department of Computer Architecture and Technology, Computing Sciences, and Artificial Intelligence, Universidad Rey Juan Carlos, Madrid*

r.emery@imperial.ac.uk

INTRODUCTION

Virtual Reality surgical simulators offer great possibilities in surgical education. They allow the training of psychomotor skills and are learner centred. Trainees can practice in a non-threatening environment and learn from errors without involving any risk to the patient.

Despite these known advantages, there are challenges to the widespread use of simulators and simulation-based environments. One of them is the need for further research to validate them rigorously [1], so that enough evidence can be provided about their effectiveness and the transfer of skills from the simulated environment to the operating theatre.

This paper presents a study to evaluate a virtual reality simulator for shoulder arthroscopy. Specifically, we address two particular types of validity: face validity (the extent to which the simulator resembles reality), and construct validity (ability to objectively differentiate between subjects with varying levels of arthroscopic experience).

MATERIALS AND METHODS

An experiment with 53 subjects (ranging from inexperienced medical students to consultants) was carried out with the virtual reality arthroscopy simulator *insightArthroVR*® [2] to evaluate its face and construct validity.

Subjects were grouped into ***novices*** (no arthroscopic experience as the main surgeon), ***intermediates*** (less than 50 arthroscopy procedures as the main surgeon), and ***experts*** (50 or more arthroscopy procedures as the main surgeon). Participants had to perform 3 simulated shoulder arthroscopic procedures and then answer a questionnaire.

The arthroscopic simulator consists of a platform composed by two haptic devices that provide force feedback (Sensable PHANTOM Omni [3]). A simulated arthroscope (an optical instrument inserted through a small incision that allows doctors to view the interior of a joint) and the instruments are inserted into a simulated shoulder through the portals. They are handled like in real arthroscopy and a monitor shows the arthroscopic view according to the simulated arthroscope's movements (see Fig 1).

Fig. 1 Virtual reality simulator *insightArthroVR*® Courtesy of GMV.

Each subject performed three simulated procedures (specifically designed for this study) in the following order:

- **Procedure 1:** ***A shoulder diagnostic arthroscopy within the gleno-humeral cavity***. In this procedure, the arthroscope is inserted through the posterior portal.
- **Procedure 2:** ***A sub-acromial examination.*** In this procedure, the arthroscope is inserted through a lateral portal and the probe through an anterior inferior portal.
- **Procedure 3:** ***A palpation of a posterior Bankart lesion.*** In this procedure, the arthroscope needs to be inserted through an anterior portal whereas the probe is inserted through the posterior portal.

The simulator registered objective metrics:

- ***Completion time:*** the time (in seconds) subjects took in completing the procedure
- ***Camera path***: Length (in mm) of the path covered with the arthroscope
- ***Camera roughness***: Roughness handling the arthroscope
- ***Probe path***: Length of the path covered with the probe
- ***Probe roughness***: Roughness handling the probe.

In order to test the face validity of the simulator, we designed a questionnaire (using a five-point rating Likert-type scale) that gathered information about subjects' previous clinical and arthroscopic experience, and asked about their experience using the simulator, the usefulness of the simulator, and their view on the objective metrics provided by the simulator.

The statistical package SPSS was used for data analysis. After all data was collected, we analysed the subjective opinion on the simulator, and performed non-parametric tests to compare the rank of the means of the metrics that the simulator registered during each exercise for the different expertise groups.

RESULTS

The data collected through the questionnaire shows that the simulator has good face validity. Next we summarize some of the most relevant data:

- 84.9% of the participants agreed (or strongly agreed) that the simulator provides an ***insight into the skills*** required in arthroscopy
- Every subject (100%) agreed or strongly agreed that ***the whole experience with the simulator was enjoyable***.
- 96.2% think (either agree or strongly agree) that the simulator is ***useful for training surgical skills*** (mean 4.42, σ=0.58).
- One participant (1.9%) disagreed with the suggestion that the ***simulator should be an optional tool available to all students who want to use it***.
- 92.4% of the participants think (either agree of strongly agree) that ***the simulator is useful for learning new surgical skills***.
- Nobody disagreed with the statement that ***the objective metrics provided by the simulator are useful***.
- 71.7% agreed that the simulator is ***useful for assessing arthroscopic skills.***

Regarding the simulated procedures and the performance metrics automatically registered, results prove that the simulator was able to distinguish subjects depending on their level of arthroscopic experience. In Fig 2 we can see for ***Procedure 1,*** the values of ***Camera path*** metric (in mm) for the different experience groups.

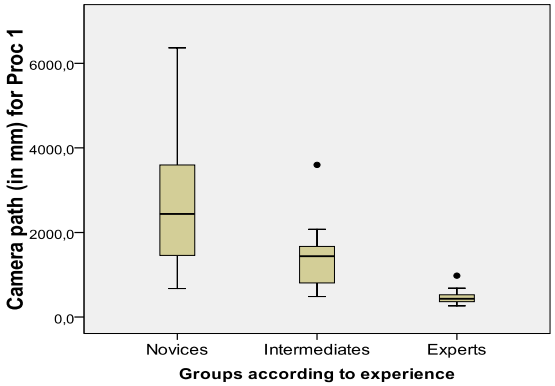

Fig. 2 Values obtained in *Proc 1* for *Camera path* (in mm) for each experience group. We can observe how experts are able to perform the procedure with more economy of movement, covering less distance with the arthroscope.

We performed a Kruskal-Wallis rank mean comparison between the experience groups for each metric and procedure. The detailed analysis for each specific metric and procedure is shown on Table 1.

Table 1 Results for construct validity. The values represent the variance of the ranks in each metric mean among the experience groups (*p-value* is shown in brackets). The asterisk indicates a *p-value* < 0.05, implying significant differences in the metric mean rank according to experience.

Metric	Proc 1	Proc 2	Proc 3
Completion time	23.5 (0.000*)	19.5 (0.000*)	6.7 (0.035*)
Camera path	25.7 (0.000*)	15.2 (0.001*)	3.8 (0.149)
Camera roughness	12.7 (0.002*)	3.2 (0.197)	1.6 (0.440)
Probe path	Not applicable	7.7 (0.022*)	2.6 (0.279)
Probe roughness	Not applicable	3.1 (0.216)	0.6 (0.723)

DISCUSSION

The simulator was considered useful for training surgical skills and, according to the great majority of our participants, it should be an optional tool available to all students who want to use it. Additionally, the objective metrics automatically registered by the simulator were considered useful by the participants, and they considered the simulator as a useful tool for assessing arthroscopic skills.

For the three simulated procedures designed for our study, the simulator was able to distinguish between different levels of experience. The simulator proved construct validity for most of the objective metrics registered (***completion time***, ***camera path***, ***camera roughness***, and ***probe path***). This opens new possibilities about using VR simulators as an additional tool for the assessment of arthroscopic surgeons.

Further research needs to be done to evaluate other types of validity and the learning effect of this VR simulator, and new studies should be carried out to determine if the skills acquired with the simulator are transferable to the operating theatre. Nevertheless, results are promising, and most of our participants already value the simulator as a useful tool for learning, training, and assessing arthroscopic surgical skills.

REFERENCES

[1] Bayona S, Fernández JM, Bayona P, Pastor L. A new assessment methodology for virtual reality surgical simulators. Computer Animation and Virtual Worlds, 2009;20(1):39-52.
[2] GMV Innovating Solutions, 2011. http://www.gmv.com
[3] Sensable Technologies. OpenHaptics toolkit. 2011. www.sensable.com

Critical Analysis of Robot-Assisted Laparoscopic Dismembered Pyeloplasty for Ureteropelvic Junction Obstruction: A Multi-Institutional Experience

Ananthakrishnan Sivaraman[1], Vipul R. Patel[1], Raymond J. Leveillee[3], Manoj B. Patel[1], Sanket Chauhan[1], Charles R. Moore[3], Oscar Schatloff[1], Rafael F. Coelho[1], Kenneth J. Palmer[2], Vincent G. Bird[3], and Ravi Munver[2]

[1]Global Robotics Institute, Florida Hospital, Celebration, FL

[2]Hackensack University Medical Center, Hackensack, NJ

[3]University of Miami School of Medicine, Miami, FL

BACKGROUND

Historically, the standard treatment for ureteropelvic junction obstruction (UPJO) has been open pyeloplasty. Over the past 15 years, the laparoscopic approach has shown substantial efficacy, challenging the traditional open approach. The introduction of robotic assistance into laparoscopy has enabled more laparoscopically naïve surgeons to attempt a minimally invasive approach to dismembered pyeloplasty.

OBJECTIVE

To report a six year multi-institutional experience with robot-assisted laparoscopic pyeloplasty (RLP) for the repair of UPJO.

MATERIALS AND METHODS

Between June 2002 and October 2008, a total of 168 adult patients, from 3 institutions underwent RLP for UPJO. After IRB approval, a retrospective analysis of prospectively collected data was performed. Demographic, preoperative, operative and postoperative endpoints for primary and secondary repair of UPJO. Success was defined as a t1/2 of less than 20min on diuretic renogram and symptom resolution.

RESULTS

Of 168 patients, 147 (87.5%) had primary repairs and 21 (12.5%) had secondary repairs. Of the secondary repairs, 57% had a crossing vessel etiology. Mean operative time was 134.9 min, estimated blood loss was 49 ml, and length of stay was 1.5 days. Mean follow up was 22 months. Overall, 97.6% of patients had a successful outcome with a 6.6% overall complication rate. Pain resolution was assessed by subjective patient reports.

CONCLUSIONS

To our knowledge, this review represents the largest multi-institutional experience of RLP with intermediate - term follow-up. RLP is a safe, efficacious and viable option for either primary or secondary repair of UPJO with reproducible outcomes, a high success rate and a low incidence of complications.

REFERENCES

[1] Patel V. Robotic-assisted laparoscopic dismembered pyeloplasty. Urology. 2005 Jul;66(1):45-9.

[2] Moon DA, El-Shazly MA, Chang CM, Gianduzzo TR, Eden CG. Laparoscopicpyeloplasty: evolution of a new gold standard. Urology. 2006 May;67(5):932-6.

TABLE 1: Patient demographics

	Overall	Primary Repair	Secondary Repair
Number of Patients (N)	168	147 (87.5%)	21 (12.5%)
Mean Age (years)	37.6 (19-71)	37.8	36.0
Sex (Female/Male)	94/74	82/65	12/9
Body Mass Index (kg/m²)	25.6 (17.2-43.5)	25.5	26.7
Side (Right/Left)	96/72	88/59	8/13
Intrinsic Etiology	93/168 (55.4%)	84/147 (57%)	9/21 (43%)
Crossing Vessel Etiology	75/168 (44.6%)	63/147 (43%)	12/21 (57%)

TABLE 2: Etiology of secondary pyeloplasty repairs	
Procedure	**No.**
Previous Open Pyeloplasty	7
Previous Laparoscopic Pyeloplasty	1
Previous Laser Endopyelotomy	9
Previous Electrosurgical Cutting Balloon Endopyelotomy	3
Previous Open Pyeloplasty and Laser Endopyelotomy	1

TABLE 3: Operative and postoperative outcomes of RLP			
	Overall	**Primary Repair**	**Secondary Repair**
Mean OR Time (Minutes)#	134.9 (110-342)	125.9	190.4
Mean Estimated Blood Loss*	48.7 (20-200)	42.9	86.2
Mean Length of Stay (days)	1.48 (1-7)	1.45	1.7
Success Rate	164/168(97.6%)	140/143 (97.9%)	20/21 (95.2%)
T half-life Improvement	96.9%	96.5%	100%
Renal Function Improvement	72.7%	73.3%	67%

No satistically significant differences were found

p = 0.109

* p = .083

TABLE 4: Complications - Clavien system			
	Overall	**Primary Repair**	**Secondary Repair**
Complications	11/168 (6.6%)	8/147	3/21
Clavien Grade 2			
Blood Transfusion	3	2	1
Ileus	4	3	1
Post-Op UTI/Pyelonephritis	1	1	0
Urine Leak	3	2	1
Clavien Grade 3b			
Need for second procedure	6	4	2
		Retrograde Laser Endopyelotomy for stricture (2 cases) Retrograde Balloon Endopyelotomy and Ureteroscopy for stone extraction (1 case) Re-stenting for clot retention in renal pelvis (1 case)	Retrograde Laser Endopyelotomy for stricture (1 case) Re-stenting for clot retention in renal pelvis (1 case)

Nerve Sparing Procedure Improves Early Return of Continence After Robotic-Assisted Radical Prostatectomy

Ananthakrishnan Sivaraman,Young Hwii Ko, Rair Jose Valero Carrion, Sanket Chauhan, Oscar Schatloff, Rafael F. Coelho, Kenneth J. Palmer, Jun Cheon, Vipul R. Patel

Global Robotics Institute, Florida Hospital Celebration Health, Celebration, Florida, USA

OBJECTIVES

Early recovery of urinary continence after radical prostatectomy remains a challenge despite several technical modifications. The purpose of this study was to identify the preoperative or intraoperative factors responsible for early return of continence (within 3 months) after robot-assisted radical prostatectomy (RARP) in data from a high volume center.

PATIENTS AND METHODS

From January 2008 to June 2010, the data of 1299 patients who underwent RARP by a single experienced surgeon were collected prospectively and analyzed retrospectively. Patient was categorized according to whether he regained his continence within 3 months or not, and then the variables were compared. Continent status and the time of recovery were assessed with a self-administrated validated questionnaire (Expanded Prostate Cancer Index Composite). Continence was defined as the use of no absorbent pads or no leakage of urine. To identify independent factors for continence after adjusting baseline characteristics, univariate and multivariate Cox regression analysis were used.

RESULTS

Within 3 months after the surgery, 86.3% of the patients (1121/1299) recovered their continence. When divided two group based on continence status, patient who had not regained continence were significantly older (mean [interquartile range]; 62.8 [10] vs. 59.7 [10] years old), and had longer operative time (77.8 [15] vs. 75.4 [10] minutes), prolonged catheterization period (5.4 [2] vs 5.2 [2] days), increased estimated blood loss (118.4[50 vs. 112.8 [0]], and higher proportion of the a median lobe (25.3% vs 17.9%) and non nerve-sparing (NNS; 18.1% vs. 7.6%) as compared to continent counterpart. Univariate Cox regression revealed that age, gland size, American Urological Association (AUA) symptom score, preoperative preoperative Sexual Health Inventory for men (SHIM) score, operative time, catheter indwelling period, the presence of median lobe, and difference distribution of patient in NS status were associated with continence status in 3 months. Multivariate analysis indicated that only age ($p<0.001$, odds ratio=0.982, 95% confidential interval [CI] = 0.973 – 0.990) and performing NS procedure were independent predictors. After adjusting for potential covariates, the odds ratio (95% CI) was 1.603 (1.222 – 2.101, $p=0.002$) for partial NS (PNS), and and 1.419 (1.079 – 1.888, $p=0.012$) for bilateral NS (BNS) relative to the NNS group. The median (95% CI) time to recovery of continence was also prolonged in older patients and NNS group (both $p<0.001$, by log-rank test); it were 6 weeks (5.723 – 6.277), 5 weeks (4.730 – 5.270), 4 weeks (3.645 – 4.355) for each age stratification (over 65 years, 55-65, and below 55 years old, respectively); it were 6 weeks (5.117 – 6.883), 4 weeks (3.601 – 4.399), and 5 weeks (4.702 – 5.298) in the NNS, PNS, and BNS group, respectively. When comparing PNS and BNS, no statistic difference was observed ($p=0.249$).

CONCLUSIONS

This analysis indicates that the age and the NS status are independent predictor of early recovery of continence. The likelihood of postoperative urinary control and the time required for the continence recovery was significantly higher and shorter in younger patients and when a NS procedure was performed.

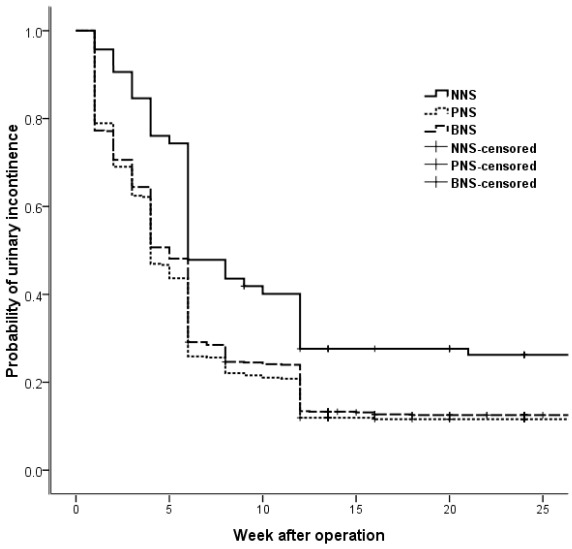

Fig. 1 Kaplan-Meier curve for each nerve-sparing subgroup. Log-rank test indicate statistic significant between each subgroup ($p<0.001$). Between partial nerve-sparing and bilateral nerve-sparing, there was no statistic significance ($p=0.249$).

REFERENCES

[1] Sandhu JS, Eastham JA. Factors predicting early return of continence after radical prostatectomy. Curr Urol Rep. 2010 May;11(3):191-7.

[2] Jonler M, Madsen FA, Rhodes RP, et al. A prospective study of quanrification of urinary incontinence and quility of life in patients undergoing radical retropubic prostatectomy Urology 1996;48:430-40

Validation of a Virtual Reality Temporal Bone Simulator

A. Arora[1], S. Khemani[2], J. Budge[1], A. Singh[2], A. Darzi[3], N. Bhatti[4], N. Tolley[1]

[1]*Dept. Otolaryngology, St Mary's Hospital, Imperial College Healthcare NHS Trust*

[2]*Dept. Otolaryngology, Northwick Park Hospital, North West London NHS Trust*

[3]*Dept. Biosurgery and Surgical Technology, St Mary's Hospital, Imperial College Healthcare NHS Trust*

[4]*Dept. Otolaryngology, John Hopkins Hospital, Baltimore*

asitarora@doctors.org.uk

INTRODUCTION

Obtaining the surgical proficiency to perform lateral skull base surgery using cadaveric temporal bones or real cases provides variable skill acquisition which lacks objective feedback. Operating time constraints and patient safety are also key issues. [1]

The VOXELMAN TempoSurg is the first commercial temporal bone simulator. Its usefulness as a training tool has not been evaluated. The objective was to evaluate face, content and construct validity of the VOXELMAN simulator for temporal bone dissection.

MATERIALS AND METHODS

Six Virtual Reality (VR) Temporal Bone study days were conducted across 3 sites, 60 Otolaryngology trainees and 25 consultants were recruited to one of 3 groups; experienced, intermediate or novice based on operative experience. Following a standardised familiarisation session, subjects performed a VR temporal bone dissection followed by a structured task; delineation of the sigmoid sinus.

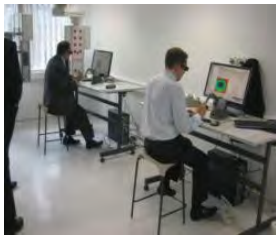

Fig. 1 Familiarisation tasks being completed.

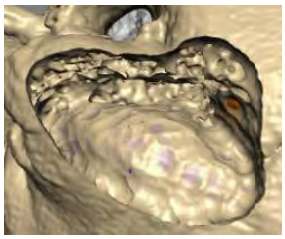

Fig. 2 Example of a completed structured task.

Subjects used a 5 point Likert scale to evaluate the simulator over 3 domains; realism, training capacity and global rating. Data was analysed using the Statistical Package for the Social Sciences (SPSS) v10.1. The minimum threshold for acceptability was a score > 4. Objective performance and error data were recorded for the structured task. Time taken, injury to structures, volume of bone removed, drilling efficiency (volume of bone/time) and drilling technique were compared between the 3 groups (Kruskall-Wallis test).

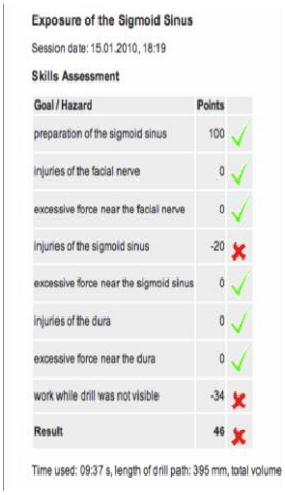

Exposure of the Sigmoid Sinus

Session date: 15.01.2010, 18:19

Skills Assessment

Goal / Hazard	Points	
preparation of the sigmoid sinus	100	✓
injuries of the facial nerve	0	✓
excessive force near the facial nerve	0	✓
injuries of the sigmoid sinus	-20	✗
excessive force near the sigmoid sinus	0	✓
injuries of the dura	0	✓
excessive force near the dura	0	✓
work while drill was not visible	-34	✗
Result	46	✗

Time used: 09:37 s, length of drill path: 395 mm, total volume

Fig. 3 Example of the Automated Performance Metrics generated by the VOXELMAN simulator.

RESULTS

Demographics: Seventy one participants (84%) were UK and fourteensubjects US based. The experienced group (n=25) had each performed at least 150 mastoid operations and were qualified on average for 13.4 years (range 2-30 years). The intermediate group (n=15) had each performed at least 10 mastoid operations. Their mean ENT experience was 4.9 years (range 3.4–8 years). The novice group (n=45) had a mean ENT experience of 5 months (range 0-2 years) with no experience of mastoid surgery as the primary surgeon.

Face Validity: Realism was assessed for appearance of the drill and anatomical structures, drill handling characteristics, depth perception and graphics (Fig 4).

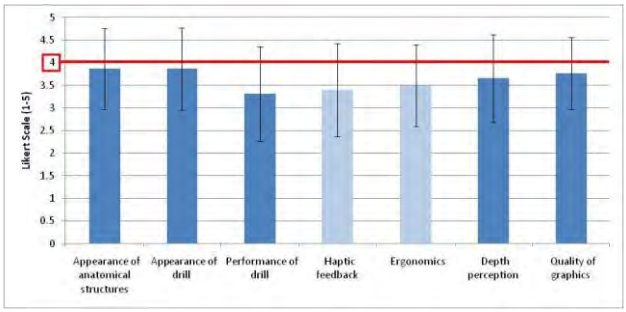

Fig. 4 Graph showing face validation measures as judged by participants.

Content Validity: The level to which the simulator covers the subject matter of temporal bone dissection was assessed for; surgical anatomy and planning, drill navigation and technique, hand-eye coordination and overall usefulness as a training tool (Fig 5).

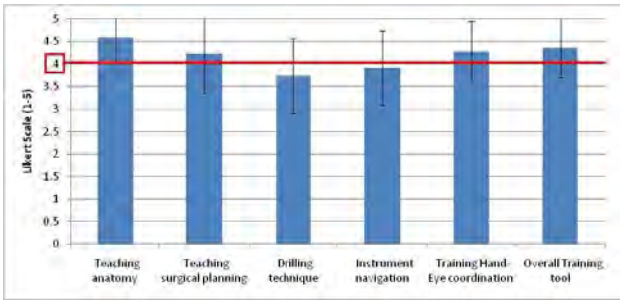

Fig. 5 Graph showing content validation measures as judged by participants.

Global Rating: There was consensus regarding overall usefulness of a VR integrated training curriculum. Trainees were more likely to recommend the simulator to a colleague than the experienced group (p=0.01) Transferability of VR to OR skills was undecided (Fig 6).

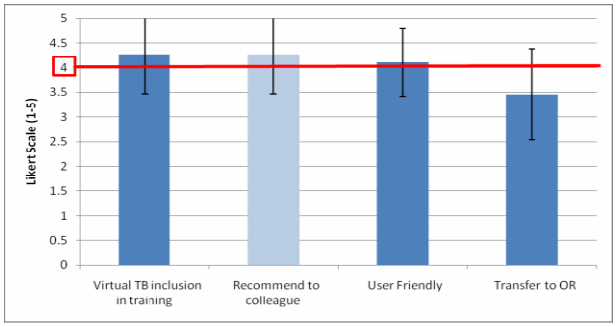

Fig. 6 Graph showing global rating measures as judged by participants.

Construct Validity: Experts outperformed novices in: total time taken (p<0.001), bone volume removed (p<0.001), drilling efficiency (V/T) (p<0.001), drilling with bur obscured (p<0.001), number of injuries (p<0.001) and force applied near vital structures (p=0.001). The intermediate group injured the sigmoid sinus on more occasions than the experts (p=0.008) and were less efficient (p=0.005) (Fig 7).

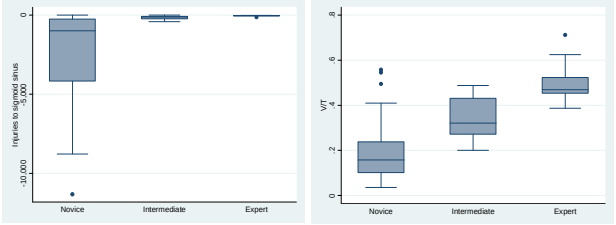

Injuries Efficiency

Fig. 7 Graphs showing construct validation data.

DISCUSSION

Changing work practice, a reduction in training hours and patient safety have all contributed to a paradigm shift in surgical training.[2] Advantages of integrated simulation training include standardised models which permit unlimited practice and objective skills assessment. Validated simulation training programmes expedite the acquisition of anatomical knowledge, psychomotor skills and can improve operating room performance.[3]

Otolaryngology trainees have traditionally used cadaveric temporal bones to understand the complex 3D anatomy and develop the necessary drilling skills. Laboratory maintenance costs, biohazard risks, lack of pathology and reduced availability are inherent limitations.[1] Following EAES guidelines, prior to incorporation within a training programme, simulator validation is required.

This is the 1st such study with the VOXELMAN temporal bone simulator. Realism was rated as suboptimal in all domains although appearance of anatomical structures and drill approached acceptability. One handedness, limited depth perception and suboptimal bone appearance near vital structures were the most frequently cited limitations. The experienced group rated drill ergonomics and haptic feedback worse than the referent group (p=0.01, p=0.04). Content validation was evident across most domains suggesting that the simulator doesn't necessarily need to be a higher level fidelity system in order to be an effective training tool. The principal advantages are for temporal bone anatomy, surgical planning and hand eye co- ordination. It was considered a valuable training adjunct particularly for junior trainees with no experience of cadaveric temporal bone dissection. Construct validation was demonstrated for several performance measures. There were significant differences between all three groups with respect to the number of injuries to the sigmoid sinus and efficiency of drilling. Novices were more likely to perform the procedure with the tip of the drill obscured.

The results suggest that temporal bone simulation represents a potential solution to the challenge of delivering effective otology training. Establishing the reliability and validity of VR simulation is the first step in developing a proficiency based VR integrated curriculum. Further benchmarking and learning curve studies are required before it is established as a useful adjunct to the existing training methods.

REFERENCES

[1] George AP, De R. Review of temporal bone dissection teaching: how it was, is and will be. JLO 2010;124:119-25.

[2] Reznick RK, MacRae H. Teaching surgical skills – changes in the wind. N Engl J Med 2006;355:2664–9.

[3] Seymour NE. VR to OR: A Review of the Evidence that Virtual Reality Simulation Improves Operating Room Performance. World J Surg (2008) 32:182–188.

A Research Platform for Active Constraints in Robotic Neurosurgery

S. Bowyer, F. Rodriguez y Baena

Department of Mechanical Engineering, Imperial College London, UK
f.rodriguez@imperial.ac.uk

INTRODUCTION

Active constraints (also referred to as *virtual fixtures*) are software functions used in the control of human-robot cooperative systems which anisotropically regulate robot motion in order to augment the user's ability. Active constraints have previously been used in various telemanipulation tasks as well as in medical devices such as the Acrobot system for knee replacement surgery [1]. Imperial College London is part of a European consortium working on the *Active Constraints Technologies for Ill-defined or Volatile Environments* (ACTIVE) project. The consortium aims to develop an integrated system for robotic neurosurgery which utilises two tool-holding manipulators (Fig 1.). The motion of the tools during the operation will be prescribed by two control algorithms: *hands-on* – where the surgeon manually guides the end-effectors (admittance control) and *teleoperation* – where the surgeon uses a remote, haptic master station (impedance control).

Fig. 1 The ACTIVE robotic system concept showing two manipulators being positioned by the surgeon under hands-on control. Also visible are the haptic master station, surgeon interface and workspace monitoring cameras [2].

Both the hands-on and teleoperation control paradigms will utilise active constraints to assist the surgeon by:

- Preventing the surgical implements from penetrating eloquent and delicate brain regions.
- Encouraging conformance to an optimum surgical plan.
- Limiting motion properties such as insertion force and speed.

The Mechatronics in Medicine Lab at Imperial College London is responsible for the development of the active constraint controller which provides the assistance described above. The primary challenge for active constraints in this project is that the system is to be used in surgery upon epileptic patients where patient fits can cause fast and irregular motion of the brain and therefore the constraints require updating at a very high frequency. Further to this, the brain will be deformed by the surgical implements during the procedure and therefore the constraints must also accommodate for this change. An example of the constraint complexity involved in this system is shown in Fig 2.

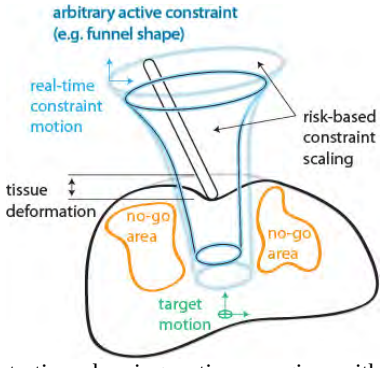

Fig. 2 Illustration showing a tissue region with two no-go areas which must be avoided and a moving target with funnel shaped guidance constraint which is scaled based on the deformation and motion.

Another research group at Imperial College London (the Tribology Lab, Department of Mechanical Engineering) are responsible for creating a reduced-order, deformable, brain model which will be updated intra-operatively as part of the ACTIVE system. This model will be used by the active constraint controller to specify and update the geometry of the constraints based on the recognition of regions which are unsafe to pass through as well as an optimal surgical plan.

MATERIALS AND METHODS

The initial research into active constraints at Imperial College will be carried out using a 6 degree-of-freedom, Staubli TX-90, industrial robot and CS8C controller. The robot can be controlled using a high-level scripted programming language called VAL-3 [3], but this language provides very limited functionality for velocity control and the control loop is restricted to 250Hz. Due to the fast and erratic variation in brain tissue in ACTIVE both accurate and high frequency velocity control is required and therefore this control method was deemed unsuitable.

Staubli also provide a C library of low-level interface (LLI) functions [4] which allows greater control of the robot joints and also provides a facility for altering the control loop frequency up to 1000Hz. To use the LLI a downloadable VXWORKS program module must be placed onto the robot controller which includes the LLI library. This program module is loaded by the VXWORKS kernel on the controller during the boot process and is used to initialise and direct a synchronous, real-time, control loop which sends commands to the robot at the required frequency.

For the hands-on control required for ACTIVE the surgeon's desired motion will be interpreted by a force/torque sensor mounted between the robot's end-effector and the surgical tool. For the research apparatus a six-axis ATI Gamma transducer [5] is used. To ensure modularity of the system the force/torque sensor is connected, via TCP/IP, to the robot controller so that any the external computer implementing active constraints only requires a single TCP/IP connection to the robot. The complete system is shown in Fig. 3.

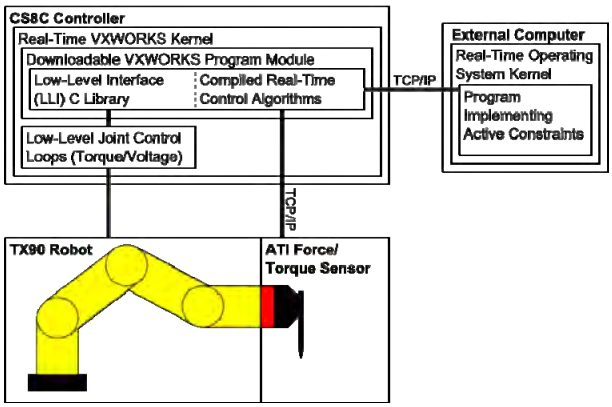

Fig. 3 System diagram of the research platform.

It can be seen in fig. 3 that the active constraints will be implemented on a separate computer that communicates with the synchronous control algorithm on the robot controller. There are two primary reasons for this segregation: (1) the controller architecture is limited and the processor and memory are not suitable for the complex algorithms which will be required for fully dynamic constraints and (2) separating the two components can improve the modularity and hardware independence of the algorithms developed. The two communicating algorithms are shown in fig. 4 for the hands-on control paradigm. It can be seen that by separating the two loops, the active constraints can operate purely based on the tool's Cartesian position and requires no knowledge of the robot's kinematics. This abstraction is useful for integration into the ACTIVE project as different robots will be used and the control for these robots will be created out by another ACTIVE partner.

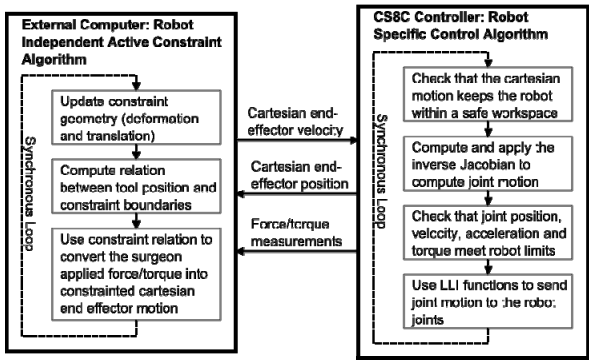

Fig. 4 Algorithm interaction between the controller and the external computer for hands-on control of the robot.

RESULTS

At this stage the robot specific control algorithm which runs on the robot controller has been built and tested. The Cartesian motion check is implemented using a modified version of the preferential-motion admittance controller described in [6]. Using this constraint technique with a Cartesian velocity of 100 $mm.s^{-1}$, the controller can prevent the end-effector from leaving the safe workspace. The Jacobian is computed using the efficient, closed-form, method described in [7]. Using these algorithms and the other safety checks the robot controller is currently able to operate at 500 Hz.

DISCUSSION

Testing thus far has shown that the modular controller can efficiently and safely control the velocity of the robot at a much higher frequency than the standard robot programming language will allow. The next stage in the development platform will be to decide upon a communication protocol between the two synchronous loops. Then once the platform is complete the external control loop will be used to research and improve on the many active constraint methods defined in the literature.

ACKNOWLEDGEMENTS

The support of EU Grant FP7-ICT-2009-6-270460 is gratefully acknowledged.

REFERENCES

[1] Jakopec M, Harris SJ, Rodriguez y Baena F, Gomes P, Cobb J, Davies BL. "The first clinical application of a "hands-on" robotic knee surgery system". Comp Aid Surg. 2001 6:329-339.
[2] ACTIVE Project 2011, www.active-fp7.eu.
[3] Staubli, Pfaffikon, Switzerland. www.staubli.com.
[4] Pertin F, des Truves J-MB "Real time robot controller abstraction layer", in proc. Int. Symp. on Robots (ISR), Paris, France, March 2004.
[5] ATI Industrial Automation, NC, USA. www.ati-ia.com.
[6] Marayong P, Li M, Okamura AM, Hager GD "Spatial motion constraints:theory and demonstrations for robot guidance using virtual fixtures", in proc. Int. Conf. on Robotics and Automation, Sept 2003.
[7] Paul RP, Zhang H "Computationally efficient kinematics for manipulators with spherical wrists based on the homogeneous transformation representation", in Int. Journal of Robotics Research, 5(2):32-44, 1986.

Optimization of Rapidly-exploring Random Trees (RRT)-based Path Planning for a Neurosurgical Steerable Probe

C. Caborni[1], S. Y. Ko[2], E. De Momi[1], G. Ferrigno[1], F. Rodriguez y Baena[2]

[1]*Department of Biomedical Engineering, Politecnico di Milano, Italy,*

[2]*Department of Mechanical Engineering, Imperial College London, UK*
f.rodriguez@imperial.ac.uk

INTRODUCTION

Image-guided percutaneous interventions have become the standard in many procedures, such as biopsies, aspiration, or tissue ablations. Needle-based operations provide several obvious advantages over traditional surgery, including less blood loss, reduced trauma and faster patient recovery. Classic rigid needles may be unable to reach targets with straight paths. Several prototypes of flexible/bendable needles have been developed: a bevel-tip needle, a stiff needle using external torque, a set of pre-bent concentric tubes and a multi-segment programmable bevel-tip flexible probe, codenamed STING [1]. Different approaches, originally developed for the path planning of mobile robots, have been implemented to find a feasible path for the aforementioned needles, including potential fields, deterministic sampling-based search such as A*, level-set-based methods such as Fast Marching, and probabilistic sampling based search, such as Rapidly-exploring Random Trees (RRTs) and Stochastic Motion Roadmaps [2]. However, potential fields methods tend to fall into local minima and require great computation, A* cannot generate smooth paths, and some probabilistic and deterministic methods cannot deal with the non-holonomicity of the flexible needles.

This work presents a path planning algorithm for flexible probes, especially, for the neurosurgical flexible probe STING [1]. Since STING can produce a limited range of curvatures, the maximum curvature needs to be constrained explicitly during the path planning phase. Fast Marching and RRTs were identified to be able to produce the curvature-constrained smooth path. However, Fast Marching's theoretical maximum curvature's bound is too conservative to use in real application [2]. By contrast, RRT methods can constrain the curvature of the resultant path precisely while computing the smooth path quickly. Due to its sampling-based characteristics, however, it produces a semi-optimal solution. In this work, the optimization of RRT-based path planner has been proposed and discussed.

MATERIALS AND METHODS

In order to implement a risk-based trajectory planning, the main structure of the brain has been classified into six categories according to the level of risk associated with the insertion of the probe into each structure. The labels are "Avoid", "Dangerous", "Warning", "Careful", "Common" and "Accessible" and each of these is represented by a different corresponding grey value on the image, ranging from the white for impenetrable areas to the black for accessible areas. "Avoid" and "Dangerous" areas and optional user-defined restricted regions such as patient-specific constraints are defined as *no-go* areas to avoid. The no-go areas are dilated by a control margin that considers the outer radius of the probe and the uncertainty of the probe control.

RRT is a data structure suitable for probabilistic sampling-based search. The general RRT-based algorithm [3] works as follows. First, the tree is initialized by the initial configuration q_{init}, i.e. the entry position and orientation of the probe tip; then a random point p_{rand} is sampled over the space. A goal bias strategy is adopted in the sampling procedure because it speeds up the search and improves the path's convergence to the goal. The goal bias strategy is the method to select the goal position as the random candidate position occasionally (e.g. 20% in this work). Since a reachable-guided RRT ensures the minimum radius constraint on the final path, it has been adopted in this work. Therefore, when p_{rand} is sampled, it is checked if this point is reachable (i.e. tangentially connectable to p_{rand} with an arc of bounded curvature $\rho<1/r_{min}$) from at least one of the configurations (x, y, θ) already stored in the tree. The probe tip's position is constrained to be inside a region defined locally by:

$$y_r \geq \sqrt{2r_{\min}|x_r| - x_r^2},$$

where r_{min} is the minimum radius feasible by the steerable probe and (x_r, y_r) is the position of p_{rand} converted into the local coordinate frames of the configurations (i.e. nodes) already stored in the tree. Among those configurations to which the sampled position is reachable, the closest configuration q_{near} is selected and connected by an arc C.

The exact arc's parameters C: (l, r, φ) are computed, where l is the arc length, r the arc radius and φ is the angle subtended by the arc. If the collision checking routine verifies that the arc is valid, i.e. it does not cross any no-go area, the new configuration and the new arc are added to the tree as a node and an edge. These procedures repeat and the tree iteratively expands its branches into the workspace randomly until it reaches the target position as shown in Fig. 1(a). The path is found by tracking the tree back from the goal to the start q_{init}. Therefore, a final path is composed of a set of lines or arcs, each of which is parameterized as a triplet (l, r,

φ). The final path is then converted into a set of configurations (x, y, θ) with a sampling interval (e.g. 1mm in this work), where (x, y) are the coordinates and θ the orientation of the probe's tip with respect to the insertion position, which is set to the reference frame. Due to the probabilistic nature of the algorithm, the resultant path is a semi-optimal solution and is different at each trial. A parallel growth of trees has been proposed and implemented, where multiple RRTs grow independently [2]. Among the feasible paths obtained from different RRTs, the best one is chosen based on the following predefined cost function:

$$Cost_i = \alpha \cdot \frac{\lambda_i}{\max(\lambda)} - \beta \cdot \frac{\psi_i}{\max(\psi)} + \gamma \cdot \frac{\Delta_i}{\max(\Delta)}$$

Where $Cost_i$ refers to the ith-path, λ_i indicates the length of the path, ψ_i the minimum distance from no-go areas, and Δ_i the accumulated risk along the trajectory. It is possible to adjust these objectives using the weights α, β and γ, which vary from 0 to 1, and whose sum is 1.

Finally, the path planner has been integrated with the steerable flexible probe with a realistic minimum radius of curvature of 250 mm [2].

RESULTS

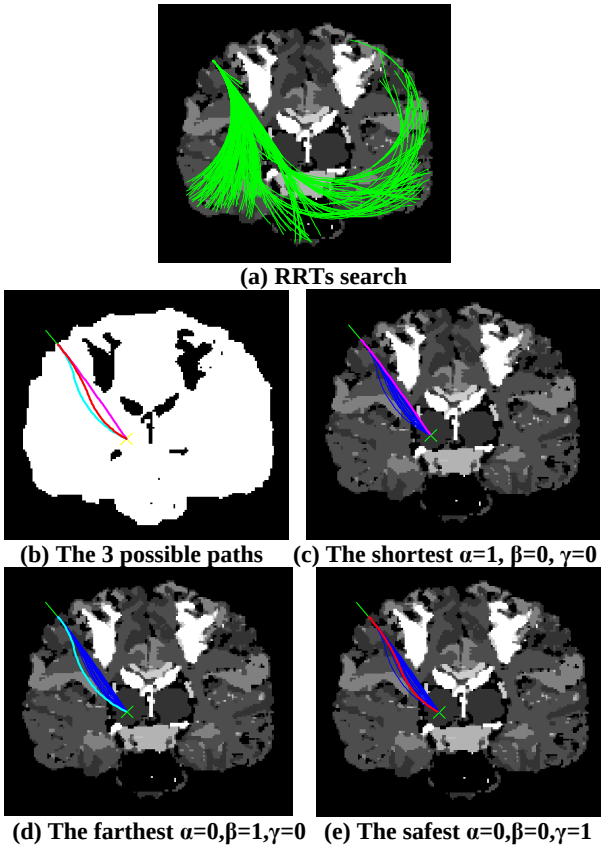

(a) RRTs search

(b) The 3 possible paths **(c) The shortest α=1, β=0, γ=0**

(d) The farthest α=0,β=1,γ=0 **(e) The safest α=0,β=0,γ=1**

Fig. 1 Resulting paths obtained by the proposed path planner on a coronal section of a risk brain map. A 3x3 medium filter has been applied to the brain risk map to remove the small dots with high risk. (a) the final RRTs on coronal brain map; (b) the final three trajectories with three different weights; the black area represents the no-go region while the white area is the explorable region; (c) the shortest path; (d) the path farthest from the no-go areas; (e) the path with minimum risk.

The algorithm has been implemented using MATLAB 7.6.0 (®2008a), ran on an Intel® Core™2 Duo CPU T5870 @ 2.00GHz processor.

Fig. 1 shows the results of the proposed path planner being applied to a grey scale risk map (134×153 pixels) of a coronal section of the brain, where 20 parallel random trees are utilized while the maximum number of search iterations is set to 6000, the goal bias to 0.2, r_{min} to 40 mm, and the control margin to 4.5 mm. The entry configuration and the target position are set to (29 mm, 30 mm, 50˚) and (65 mm, 80 mm), where 1 pixel value was assumed to be 1 mm. Fig.1(a) shows all resulting RRT trees with green lines on the brain risk map. In Fig. 1(b), the black regions represent no-go areas after their dilation and the paths with three extreme weight selections are also displayed in different colours. The minimum, maximum, root-mean-square, and average computation times of 100 trials measured as t_{min}= 20 sec, t_{max}=42 sec, t_{rms}=27.92 sec, and t_{mean}=27.45 sec [2]. Performing experiments with the STING prototype and the bespoke feedback controller [4], the measured real displacement in gelatine sample showed reasonable results with errors e_{mean}=1.15 mm, e_{rms}=1.31 mm, e_{std}=0.63 mm, e_{max}<2 mm [2].

DISCUSSION

The RRTs algorithm's convergence time depends on the complexity of the environment and on the randomness of the search. Despite the semi-optimality of the output and the elapsed time to produce a feasible trajectory, the proposed path planner performs well in complex brain risk maps, while considering the mechanical and kinematic constraints of the probe. In addition, the surgeon will be able to evaluate and select the most feasible trajectory using the weight variables.

To reduce the computation time, and thus to be able to extend the algorithm in three dimensional space, optimizing the code to reduce the computation time and/or implementing it using a pre-compiled language such as C++ seems necessary.

ACKNOWLEDGEMENT

This work was supported by the EU-FP7 Project ROBOCAST (FP7-ICT-215190).

REFERENCES

[1] L. Frasson et al. "STING: a soft-tissue intervention and neurosurgical guide to access deep brain lesions through curved trajectories," IMechE Part H: Journal of Engineering in Medicine, vol.224, pp 775-788, 2010.

[2] Chiara Caborni, "Curvilinear Path Planning for a Steerable Flexible Neuro-surgical Probe," Master thesis, Politecnico di Milano, A.A. 2010-11.

[3] S. Patil and R. Alterovitz, "Interactive Motion Planning for Steerable Needles in 3D Environments with Obstacles," IEEE BioRob, Tokyo, Japan, 2010, pp. 893-899.

[4] S. Y. Ko et al. "Two-dimensional needle steering with a programmable bevel inspired by nature: Modeling preliminaries," IEEE/RSJ IROS, Taipei, Taiwan, 2010, pp. 2319-2324.

Haptic Gesturing as Human-Machine Interface in Minimally Invasive Robotic Surgery

C. Staub, S. Can, A. Knoll

Robotics and Embedded Systems, Technische Universität München,Germany

Corresponding author: staub@in.tum.de

INTRODUCTION

Tele-operated master-slave systems have created new opportunities in assisting surgeons during complex interventions. In addition to sophisticated input devices, tremor filtering, force feedback, and a stereoscopic view, researchers have drawn their attention to higher level functionality. Intelligent and automated camera tracking, knot-tying and partially autonomous executed tasks, as well as augmented reality applications are prominent examples. In contrast, the available number of input options to control these functions is limited, not last more because of the traditional design of master consoles. For instance, the high immersiveness of master consoles makes it hard to distinguish more than 4 to 5 pedals with the feet. Since autonomous functions are to be primarily actions to shorten operation time, new input modalities have to be time-saving alternatives to convectional human-machine interaction. If triggering a system function takes more time than its actual execution, the benefit of autonomy in medical robotics is diminished significantly. “Hands free” camera control has been introduced quickly after the AESOP camera holder was introduced to the market. Voice activated control and visual tracking of the surgeon’s head movement replaced foot pedals and hand controller [1]. Vision-based control often comes with the burdon of additional tracking markers, which have to be borne by the doctor. A promising alternative might be to execute suitable system functions by means of gaze contingent control. Mylonas et al. investigated the integration of an eye tracking system into the daVinci master console [2], with application to e.g., depth recovery, virtual fixtures, and instrument control.

Fig. 1 Master console with haptic input devices, stereoscopic screen, and slave system in the background

We have implemented a gesture-based user interface, whereas the haptic input devices of the master console are used to trigger actions. Intuitive and customizable gestures are learned by the system once, linked by the surgeon to the preferred command, and recalled during operation as the gesture is presented to the system. In particular, the aspect of time consumption is interesting, since, in contrast to many conventional input modalities, full control of the surgical instrument can be kept during system interaction and the time-consuming resembling of the original robot posture is avoided.

MATERIALS AND METHODS

The setup of our robotic system for minimally invasive surgery consists of a master console, where the surgeon is located at, and a robotic slave part. The surgical workstation is equipped with two PHANToM™ haptic in-/output devices, a stereoscopic monitor and several foot pedals that can be programmed individually for system interaction (cp. Fig. 1). The slave part of the system is composed of four ceiling mounted robots, carrying EndoWrist™ surgical instruments from Intuitive, Inc. The instruments have been modified to measure occurring forces at the instrument tip via strain-gauge sensors. In order to recognize a set of four pre-defined surgical gestures, a discrete Hidden Markov Model (HMM) with left-right topology is used. The gestures have been chosen after an initial interview and reflect movements that subjects found to be intuitive for the autonomous actions “knot-tying”, “suturing”, “retract 3rd arm”, and “measure distance”. The HMM was trained on a basis of 15 individual executions of each gesture. Observations for building the HMM are derived from the vectors of the time-series representing the instrument trajectory. The trajectory data was sampled with a frequency of 10Hz and stored in a data base, comprising the Cartesian position of the end effector, corresponding forces, the state of the forceps (open/closed), and a time stamp. In a preprocessing step, the raw trajectory data is resampled position equidistant. This smoothes variation in the execution speeds and removes outliers, which arise due to the human tremor. The used features either deal with a single instrument (left *l* and right *r*), or refer to the interaction of both. The following features have been used: (1) change of the instrument trajectory (*l*/*r*) over

time, (2) directional change of one instrument w.r.t. the second instrument (3), velocity of an instrument (*l/r*), (4) distance between the two instruments, (5) temporal change of the distance between two instruments. To simplify the evaluation for untrained subjects, the state of the gripper was neglected at this time. If environmental interaction is assumed during a gesture, the readings of the force sensors can also be included.

RESULTS

The evaluation study was conducted with 24 medical students (*M=24yrs., SD=3yrs.*), half of whom had surgical experience. The gesture input described above, was tested against menu input. A plausible two-tiered menu design was chosen: on the first screen of the menu, a general "surgical action" option had to be selected out of 4 possibilities. The second screen then offered the 4 surgical actions plus one arbitrary dummy menu entry, whereas the appropriate action had to be selected and confirmed with the foot pedal. Since none of the subjects were familiar with a robotic surgery system, participants had training time to become acquainted with the system and where asked to trigger all actions with both gesture and menu input mode. The time that it took people to activate the asked action as well as the success rate in triggering the correct action was measured.

The usability of both input modes was assessed with the AttrakDiff2 [3], a well-tested questionnaire measuring four different aspects of usability on Likert-type scales. Each of these scales was found to show high reliability with Cronbach's $\alpha > 0.70$. A factorial ANOVA found a large and statistically significant effect of input mode on input time ($F(1,22)=38.44$; $p<.001$; $\eta=.64$). The estimated marginal means indicate that, on average, it took significantly less time to trigger the surgical action via gesture input (*M=4.45sec., SD=0.86sec.*) compared to activation via menu input (*M=7.41sec., SD= 2.06sec.*). There was also a significant main effect of gesture ($F(2.04,44.79)=23.79$; $p<.001$, $\eta=.52$), but no significant interaction effect ($F(3,66)=2.18$, $p=.10$). Together, these results suggest that while some surgical actions (e.g. arm retraction) took longer to activate than others (e.g. suturing), input times were consistently shorter with gesture input than with menu input (cp. Fig. 2). A look at the input errors suggest that, while it took less time to input a command for a surgical action via gesture, this mode is slightly more error prone with 10.42% of gesture inputs classified as false compared to 5.21% of false inputs via the menu (out of 96 commands). Finally, an ANOVA of the usability scores indicates a significant main effect of input mode ($F(1,23)=23.74$, $p<.001$; $\eta=.51$), whereby significantly higher mean usability ratings were given for gesture input (*M=5.40, SD=0.87*) than for menu input (*M=4.21; SD=0.85*).

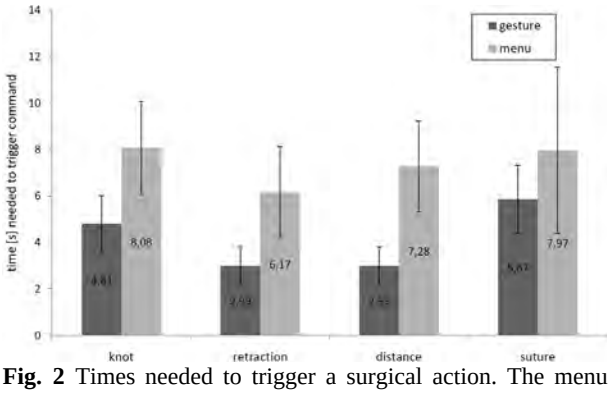

Fig. 2 Times needed to trigger a surgical action. The menu interaction time does not comprise the time needed to resemble the posture of the robots afterwards.

DISCUSSION

The results show that gesture-based input is faster and receives higher usability ratings compared to the tested menu-mockup, even though this input method is still slightly more error prone. Although the effect of learning on input success has not been explicitly investigated in this study, it seems likely that, despite the rigorous training protocol implemented in this experiment, participants were more practiced in menu-based input than in gesture-based input. Hence, one might assume that the likelihood to commit an error with gesture input would decrease with further practice. Nevertheless, further studies are required to determine the factors that mitigate the effectiveness of gesture-based input. For example, obviously, the superior effectiveness of gesture-based input over the traditional menu input strongly depends on the complexity of the menu, as well as the input mechanisms (e.g. foot pedals vs. mouse-type interaction). Whether or not gesture-based input is equally effective for other setup needs to be tested in future studies. Similarly, the usability ratings should be interpreted with caution. Three of the four scales on the usability questionnaire would favor technology that would be considered novel and exciting. The pragmatic qualities of gesture-based input, such as its ability to integrate into the surgical workflow, need to be tested in long-term user studies.

REFERENCES

[1] J.-B. Gómez, A. Ceballos, F. Prieto, and T. Redarce, "Mouth gesture and voice command based robot command interface", Proceedings of the IEEE International Conference on Robotics and Automation, *2009, pp. 333–338.*

[2] G. Mylonas, A. Darzi, and G.-Z. Yang, "Gaze contingent depth recovery and motion stabilisation for minimally invasive robotic surgery", Proceedings of the International Workshop on Medical Imaging and Augmented Reality. *Springer Berlin / Heidelberg, 2004, pp. 311–319.*

[3] M. Hassenzahl, M. Burmester, and F. Koller. "Attrakdiff: Ein Fragebogen zur Messung wahrgenommener hedonischer und pragmatischer Qualität", Mensch & Computer 2003: Interaktion in Bewegung, 2003, pp. 187–196.

Virtual Natural Orifice Transluminal Endoscopic Surgery Simulator

Przemyslaw Korzeniowski[1], Vincent Luboz[1], Alejandro Granados[1], Danial Sheikh[1], Sudip K Sarker[2], Fernando Bello[1]

[1] *Biosurgery and Surgical Technology, Department of Surgery and Cancer, Imperial College London – St Mary's Hospital, London, UK*

[2] *Department of General, Colorectal, Endoscopic and Minimally Invasive Surgery, Whittington Hospital, London, UK*

f.bello@imperial.ac.uk

INTRODUCTION

Natural Orifice Transluminal Endoscopic Surgery (NOTES) is an emerging surgical technique considered as a possible next stage in minimal access surgery. It uses flexible endoscopes inserted through natural orifices leaving only internal scars. Potential barriers to the use of NOTES in clinical practice include technical challenges such as reliable methods to close the insertion site, and optimization of the instrument interface. The development of adequate training facilities is recognized as one of the key challenges to the widespread adoption of NOTES [1]. At present, practical training is only possible in animals, with just two alternative training mannequins appearing in the literature: NOSse or Natural Orifice Simulated Surgical Environment [2], and ELITE or Endoscopic-laparoscopic Interdisciplinary Training Entity [3]. Whilst these models offer a viable, less expensive and more humane alternative to training, their degree of anatomical variability is limited, suffer from wear and tear, and do not have inbuilt capabilities for feedback and performance measurement. Virtual Reality (VR) simulators have already been shown to improve both operative and endoscopic skills [4]. They also have the potential to offer unlimited variability, and can compute objective, quantitative measures of performance for formative and summative feedback. This project aims at creating such VR training simulator prototype.

MATERIALS AND METHODS

The core of the environment is programmed in Visual C++ and interfaced to the FLTK library (Fast Light Tool Kit, www.fltk.org/) for the user interface, and to the VTK library (Visual Tool Kit, www.vtk.org) for the graphics. The SOFA framework (www.sofa-framework.org) is used as a library to handle collision detection and tissue deformation. The NOTES endoscope can be manipulated with the keyboard or with a joypad (one stick controls the instrument, whilst the other one drives the endoscope tip angle).

The chosen endoscope is composed of a main shaft, a camera, a light source, and two actuators. The main shaft consists of a long flexible body and a shorter bendable tip, to allow the user to stir the direction of the endoscope during navigation. The two actuators are limited to grasping tools for this study. Both endoscope and actuators are modeled based on the mass-spring model described in [5]. During the collision response phase, four forces (external, spring, 2D bending and 3D bending) are applied on the instrument and allow interactions with the surrounding tissues. Fig. 1 illustrates the current simulated flexible endoscope, instruments and camera view.

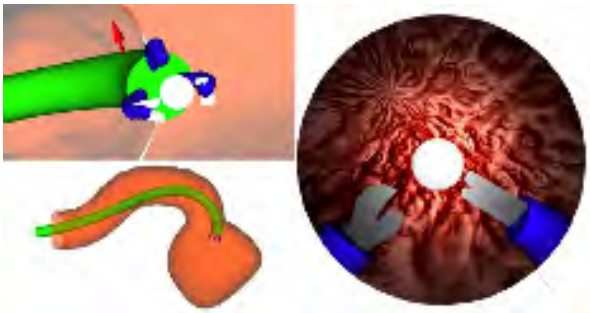

Fig. 1 Top left: actuators about to grasp a white sphere. Bottom left: external view. Right: endoscope view.

The oesophagus, stomach and spleen were modeled from an idealized dataset and given realistic biomechanical properties using SOFA's Mass Tensor Model. Fixed Plane Constraints were added to recreate the organs' natural positioning and interactions in the abdominal cavity. To facilitate real time computation of the interactions between the instruments and the organs, two different meshes were used for each organ: a visualisation mesh, with plenty of detail for enhanced graphics, and a collision mesh, with fewer triangles for faster collision computation. Fig. 2 illustrates the insertion of the endoscope inside the oesophagus towards the stomach, pushing the stomach wall towards the underlying spleen.

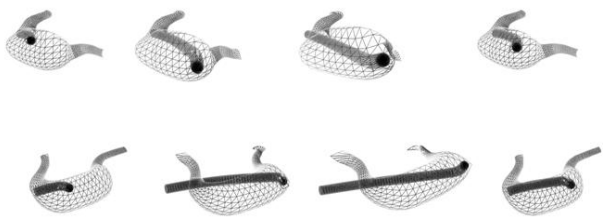

Fig. 2 Interactions between the virtual endoscope and the stomach at different positions.

Whilst this may not be a realistic scenario in surgery, it demonstrates the performance of the collision detection, deformation and relaxation.

RESULTS

An initial evaluation of the endoscope behaviour was carried out by inserting a real flexible endoscope in a silicon rubber vascular phantom. We used a vascular phantom because no upper gastro-intestinal phantom was available in our laboratory. Nevertheless, it is relevant for our study because of the diameter and length of the main vessel (an aorta deformed by an aneurysm), which is similar to that of the oesophagus and the beginning of the stomach. We then compared the behaviour of a real endoscope in the real phantom to the virtual endoscope in the reconstruction of the phantom in our simulator. Fig. 3 shows that the shape of the virtual endoscope visually matches the shape of the real endoscope in the phantom, and that both have similar collision points.

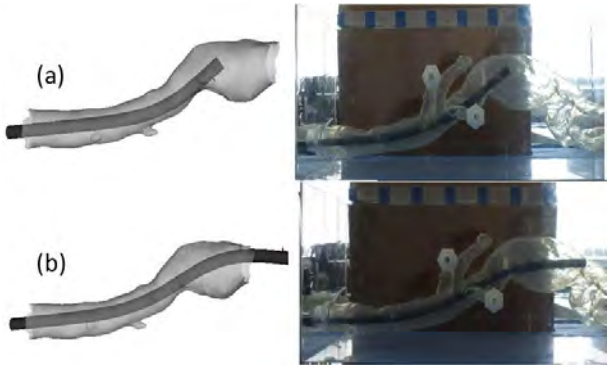

Fig. 3 Comparison of the virtual environment (left) with the real flexible endoscope in a silicon rubber phantom (right) at (a) a shallow insertion and (b) a deeper insertion.

With respect to the soft tissue deformation and instrument behavior, subjective feedback obtained through informal interviewing of a consultant surgeon in General, Colorectal, Endoscopic and Minimally Invasive Surgery versed in the techniques and instruments of NOTES, stated that the behavior of the endoscope is realistic. Its overall parameters such as size and flexibility are correct. The endoscope moves and bends in an accurate way. The actuators work and interact properly between them, with the soft tissue surface and during soft tissue grasping (Fig. 1). The visual feedback is also correct in terms of camera view angle, light amount and triangulation. On the tissue deformation side, the expert stated that the tissues are too elastic and look thicker in real life, but that the deformation and relaxation speed is realistic.

In terms of performance, the simulation was tested on two different computers: a Dell Optiplex 980 (Intel Core i5 at 3.20GHz, 8GB of RAM, nVidia GeForce GT 330 graphic card, Windows7) and an Apple MacBook Pro (Intel Core i5 at 2.40GHz, 4GB of RAM, nVidia GeForce GT 330M graphic card, Windows7). When a large amount of deformations is recorded and only the three last particles of the endoscope are taken into account for collision detection, the simulator runs at 20 frames per second on the Dell desktop and at 25fps on the MacBook Pro. When no deformation is simulated and all the endoscope particles are taken into account, the simulator runs at 40 frames per second on the Dell desktop and at 45fps on the MacBook Pro.

DISCUSSION AND CONCLUSIONS

This paper presents a first attempt at developing a prototype VR simulator for NOTES surgery. The ultimate goal is to support learning how to use the complex flexible endoscope and actuators, as well as to control the interactions with the soft tissues. Both endoscope and actuators are represented by a mass-spring model, defining their behaviour using four forces and four corresponding coefficients: external, spring, 2D and 3D bending. Tuning these coefficients allows adapting the behavior of each instrument to different types of flexible actuators and improving the realism of the simulation. The interactions with the soft tissues are handled using the SOFA framework, which permits modeling realistic tissue deformations thanks to the mass tensor model used to simulate the behavior of the stomach and the spleen. Changing the properties of the soft tissues (Young modulus and Poisson ration) allows simulating different organ properties and will enable improving our soft tissue behavior, and adapting our simulator to different organs, and therefore different NOTES interventions.

Future improvements include more realistic and efficient organ deformation, as well as the use of a specialized haptic device mimicking a real-life endoscope manipulator handle, to enable the simulator to be used as a more efficient training tool. We also aim to extend the simulator to support more types of actuators including cutting and suturing devices, which are key steps in NOTES surgery, improve the graphical aspect of the simulation by adding textures to the organs in the VTK graphical environment, and conduct further quantitative evaluation.

REFERENCES

[1] www.noscar.org/resources last accessed Mar 2011.
[2] Clark J, Sodergren M *et. al.* (2009). The natural orifice simulated surgical environment (NOSsE): exploring the challenges of NOTES without the animal model. J Laparoendosc Adv Surg Tech A.;19(2):211-4.
[3] Gillen S, Wilhelm D, Meining A, Fiolka A, Doundoulakis E et. al. (2009).The "ELITE" model: construct validation of a new training system for natural orifice transluminal endoscopic surgery (NOTES). Endoscopy;41(5):395-9.
[4] Buzink SN et. al. (2007). Acquiring basic endoscopy skills by training on the GI Mentor II. Surg Endoscopy; 21:1996–2003.
[5] V. Luboz., R. Blazewski, D Gould and F Bello (2009). Real-time Guidewire Simulation in Complex VascularModels, Visual Computer, 25(9), 827-834, 2009.

A Hand-held Force Control Instrument for Probe-Based Confocal Laser Endomicroscopy

W. T. Latt, R. C. Newton, M. Visentini-Scarzanella, C. J. Payne,
D. P. Noonan, J. Shang, and G.-Z. Yang
Hamlyn Centre for Robotic Surgery, Imperial College London
w.tun-latt@imperial.ac.uk

INTRODUCTION

Probe-based confocal laser endomicroscopy (pCLE) is a new 'optical biopsy' technology that provides high resolution in vivo images; target tissues include the gastrointestinal tract [1], peritoneal cavity and lung. Regardless of whether the probe is navigated to the target through an endoscope operating channel or using a hand-held device, the acquisition of pCLE videos, stills and mosaics for subsequent interpretation requires perpendicular probe apposition with steady probe contact against the tissue. Small variations in contact force of biophotonic probes have been shown to alter the image and data acquired[2][3]. However, maintaining consistent pCLE tissue contact is difficult with an endoscope due to (depending on target organ) cardiorespiratory movement, bowel deformation and peristalsis. With a hand-held device there is more dexterity but erroneous movement of the operator's hand to consider. Therefore, a hand-held instrument that helps control the contact force is required. Several force control systems or devices have been developed for various medical applications [4][5][6]. However, they were not designed for use with pCLE probes. Therefore, to equip clinicians with a versatile platform for pCLE examination, a hand-held instrument is designed and developed which compensates for contact force variations due to tissue motion and erroneous motion of the hand.

MATERIALS AND METHODS

The main components of the instrument include a linear voice coil actuator (VCA) which has an integrated position sensor (LAS13-18-00A, BEI Technoligies, Inc.), a donut load cell (LC8100-200-5, Omega Engineering, Inc.), and a 2.5mm diameter pCLE probe (Cellvizio Gastroflex 'Z-probe', Mauna Kea Technologies, Paris, France). Fig. 1 shows the instrument in comparison with a standard ruler and a hand. The length of the whole instrument is 175 mm, and the weight is 200 grams. The controller used to control the contact force is CDS-3310 from Galil Motion Control, Inc. A PID control scheme is used, with the contact force provided by the donut load cell providing the feedback signal. The donut load cell, which allows passage of the pCLE probe from the proximal-end to the tissue at the distal-end, is placed at the distal-end, and is connected to the shaft of the VCA via a hollow shaft. A voice coil type of actuator is chosen due to its fast response, sufficient stroke length, and adequate force for this application. The instrument body, and other connecting parts such as the instrument handle are fabricated using a rapid-prototyping machine (Objet EDEN350).

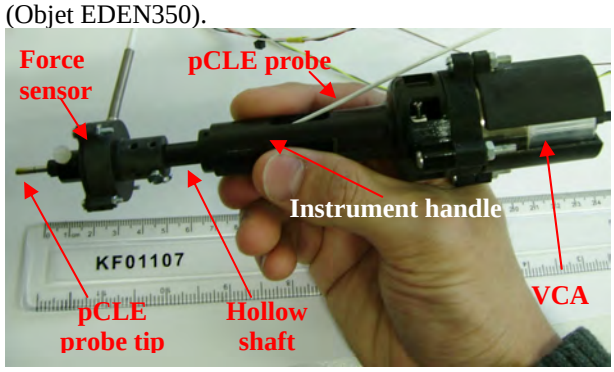

Fig. 1 The hand-held force control instrument and the main components involved

RESULTS

Force control performance and image consistency using the force control is evaluated in bench tests and hand-held tests using full thickness porcine bowel. Three trials are performed in both types of tests. The experiment setup for the tests is shown in Fig. 2.

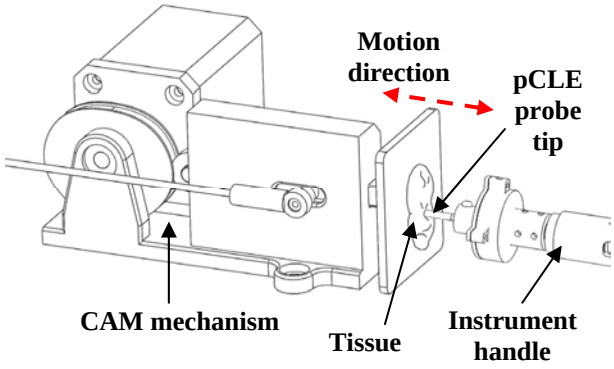

Fig. 2 Experiment setup showing the relative positioning of the instrument and tissue during laboratory validation

In bench tests, the instrument is clamped using a vice, while in hand-held tests, the instrument is held by the hand. In both tests, the instrument is positioned in such a way that the probe tip is perpendicularly in contact with the tissue. To simulate tissue motion caused by respiration, a motorized CAM mechanism is used. Peak-to-peak amplitude and frequency of tissue motion caused by the CAM mechanism are 3 mm, and 0.37Hz (~22 bpm) respectively. Force control

performance in a hand-held test is shown in Fig. 3. In the figure, durations marked with "***Control ON***" represents force variations with force control while "***Control OFF***" without force control. pCLE images were acquired at 12 Hz during the tests. Images obtained in a hand-held test are shown in Fig. 4. In this figure, images in (a) are acquired without the force control, whilst in (b) are with the control. For quantification of consistency of the images, features (mucosal crypts within the tissue) in the images are detected and tracked over the duration while the instrument force control is switched on. Mean changes in centroid locations of the tracked regions, and changes in distances among centroids of the tracked regions are quantified and shown in **TABLE 1**.

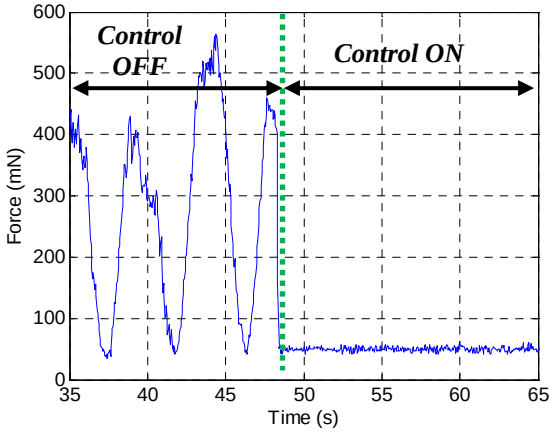

Fig. 3 Force variation during a hand-held test with ex-vivo tissue attached to the cam

(a)Hand-held test images obtained without force control

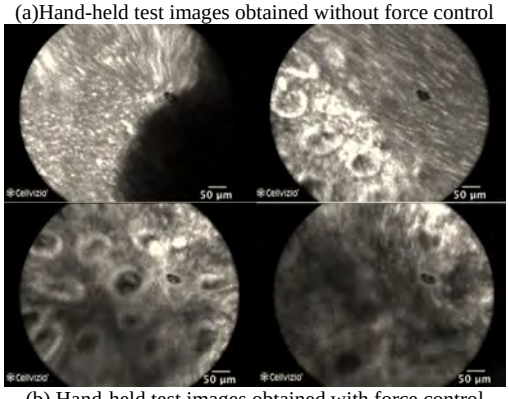

(b) Hand-held test images obtained with force control

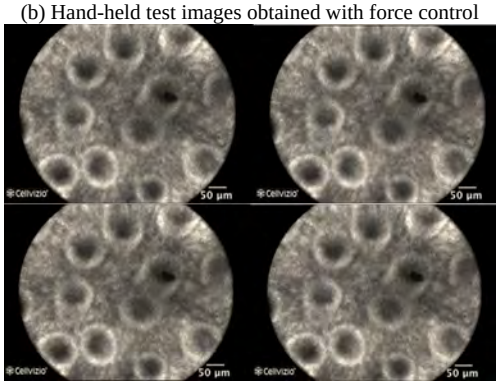

Fig. 4 Hand-held test tissue images obtained (a) without force control, and (b) with force control

Table 1 Root Mean Square of changes in centroid locations, and changes in distances among centroids of the tracked regions

Test type	Changes in centroid locations (μm)	Changes in centroid distances (μm)
Bench test	2.42±0.45	2.62±1.72
Hand-held test	7.66±5.5	2.85±1.44

DISCUSSION

Effective use of pCLE requires sensitive force control to obtain consistent images. The proposed instrument has shown to perform well in maintining a desired contact force. Peak-to-peak amplitude of the contact force variation without force control is approximately 400 mN. This reduces to approximately 4 mN rms when the instrument force control is switched on. It has been observed that force variation is slightly higher in hand-held tests than in bench tests. This is due to the added disturbance created by erroneous motion of the operator‘s hand in hand-held tests. Substantial nonhomogenity can be seen in the images acquired from a single area of tissue when the force controller is switched off. The results derived show clearly that the instrument can provide consistent images. It should be noted that average translational movement of centroids of the crypts is slightly greater in hand-held tests than in bench tests. Again, this is perhaps due to erroneous motion of the hand laterally. It is nevertheless negiligible since it is only approxmately 4% of the whole field of view of the probe.

Future work includes design and development of a more compact and lighter version of the instrument, and evaluating how different contact forces affect the morphology of tissues in both ex-vivo and in animal trials using the instrument.

REFERENCES

[1] M. B. Wallace, and P. Fockens, “Probe-based confocal laser endomicroscopy”, Gastroenterology 2009; 136:1509-13.

[2] L. Thiberville, M. Salaun, S. Lachkar, S. Dominique, S. Moreno-Swirc, C. Vever-Bizet, *et al.*, “Human in vivo fluorescence microimaging of the alveolar ducts and sacs during bronchoscopy,” Eur Respir J 2009; 33:974-85.

[3] Y. Ti, and W. C. Lin, “Effects of probe contact pressure on in vivo optical spectroscopy,” Opt Express 2008; 16:4250-62.

[4] G. Duchemin, E. Dombre, F. Pierrot, and P. Poignet, “Robotized Skin Harvesting,” 8th Int. Symp. on Experimental Robotics, ISER'02, Sant'Angello d'Ischia, Italy, July 8-11, 2002.

[5] J. Stoll and P. Dupont, “Force control for grasping soft tissue,” IEEE International Conference on Robotics and Automation, Orlando, Florida, May 2006.

[6] S. G. Yuen, D. P. Perrin, N. V. Vasilyev, P. J. del Nido, and R. D. Howe, “Force tracking with feed-forward motion estimation for beating heart surgery,” IEEE Transactions on Robotics, Vol. 26, No. 5, Oct 2010.

Electromagnetic Noise Measurement of the Motor Assisted Robotic Stereotaxy System (MARS)

M. Heinig[1], O. Christ[2], V. Tronnier[3], U.G. Hofmann[2], A. Schlaefer[1], A. Schweikard[1]

[1]*Institute for Robotics and Cognitive Systems, University of Luebeck*
[2]*Institute for Signal Processing, University of Luebeck*
[3]*Clinic for Neurosurgery, University Clinics Schleswig-Holstein, Campus Luebeck*
heinig@rob.uni-luebeck.de

INTRODUCTION

Stereotactic intervention is a standard way to treat neuropsychiatric degenerative diseases. Deep brain stimulation (DBS) presents an effective tool to treat Parkinson's disease (PD) and other movement disorders as well as psychiatric diseases [1]. Besides PD, DBS can be used to treat chronic pain or mental decline [2]. Accurate positioning of stimulating probes in the patient's brain is crucial to the outcome of the interventions [3]. The use of high-accuracy robotic aids is beneficial and many systems have been introduced since the late 1980's. An overview can be found in [4].

During the surgical intervention, an electrode is inserted into the brain. The neuronal firing at the electrode's tip is continuously monitored using a microelectrode recording (MER) system. The signal is displayed to the surgeon via loudspeakers. Every brain region has its specific firing patterns, expressed through frequency and amplitude [5]. Skilled surgeons can determine the current position of the electrode based on the firing pattern they hear. Once the target position is reached, the area is stimulated by the electrode.

One problem that arises when using robotic aids is the electromagnetic noise induced by the motors and controllers of the robot. This noise can interfere undesirably with microelectrode recordings and stimulations.

The Motor Assisted Robotic Stereotaxy system (MARS) is a newly developed robot for stereotactic interventions [6]. It was specially designed to show low electromagnetic noise. This is achieved by using low-noise brushless DC motors and controllers, consequent shielding of current-carrying cables and careful mechanical and electric design. In this work, we present the results of electronic noise measurements and we discuss the impact of the noise on the MER system.

MATERIALS AND METHODS

The MARS robot can be transported on a modified instrument table and is attachable to operating tables via quick-release mountings (Fig. 1). Its kinematic design is derived from the Zamorano-Duchovny (ZD) stereotactic frame (inomed Medizintechnik GmbH). The MARS robot is actuated by five DC servo motors. A motorized micro-drive unit to forward the electrode in the brain is attached to its end effector. The controllers are located in a box underneath the ground plate, the power electronics are mounted to the instrument table (Fig. 1, top right). Both, motors and electronics cause an alternating electromagnetic field that may interfere with the microelectrodes.

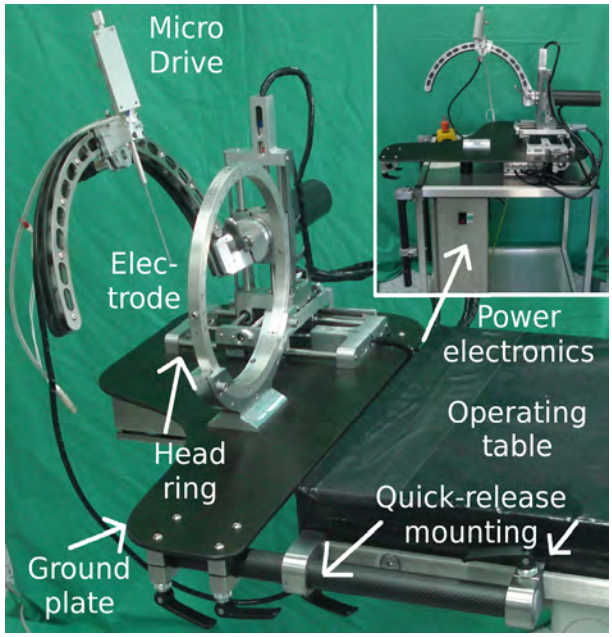

Fig. 1 MARS robot attached to an operating table with micro-drive unit and electrode. Top right: Instrument table with MARS robot and power electronics.

We used the experimental setup depicted in Fig. 2 to determine the influence of the generated electromagnetic noise. A commercially available microelectrode recording system (ISIS MER), in combination with a micro-macro electrode - both inomed Medizintechnik GmbH - was used to measure the noise. The robot was controlled via PC.

The electrode was attached to the micro-drive unit, which in turn is mounted on the robot's end-effector. To simulate brain tissue's conductivity, the tip of the electrode was immersed in physiological saline. The saline was positioned on the ground plate of the MARS, where the head ring is usually attached – the same position the patient's head would be in a real operation.

A set of five measurements will be discussed in the following (Table 1). The description of the measurement is given in the first column of the table.

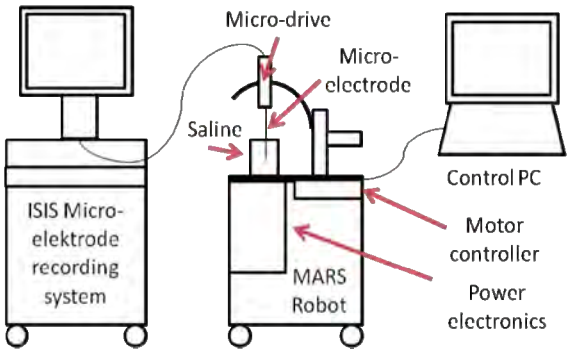

Fig. 2 Schematic of the experimental setup; left: ISIS MER (Microelectrode Recording) system; center: the MARS robot with saline solution, microelectrode and micro-drive; right: MARS control PC.

Next, the mean value and standard deviation of the measured noise in mV is presented. The two last columns give the maximal measured voltage and the minimal measure, respectively (also in mV). Measurement time was in the range of 30 - 140 s, with a sampling frequency of 25 kHz.

First, the background noise generated by electronic equipment in the room not involved in the experiment was determined. Therefore, the robot's AC/DC power converters, its controllers and motors, as well as the control computer were not connected to power. Next, the AC/DC converter and the control PC were connected to power. The controllers and motors were activated. Then, a second noise measurement was conducted. In the third measurement, all five motors of the MARS robot were activated, and the robot was moving during the data acquisition.

As the micro-drive unit is closest to the microelectrodes, its influence was determined separately. Note that the motors of the MARS robot were activated, and that the robot was not moving during the measurements. The micro-drive, however, was moving at a constant speed. In the last measurement, the micro-drive's motor as well as the MARS robot's motors were activated but not moving. Stimulation pulses from the ISIS MER system were delivered to the saline via the microelectrode (4mA). This measurement was done to determine the influence of the micro-electrode's currents on the motors, encoders and controllers of the MARS robot during stimulation. No notable influence was observed.

RESULTS

The results of Table 1 show, that the MARS robot has no substantial influence on the micro-electrode recordings. We determined a slightly higher mean value and standard deviation in comparison with the background noise measurement.

The minimal and maximal values are lower for the last three measurements in comparison with the first two. So far, no explanation is available for this behavior.

Depending on the brain-area, patient and electrode the signal amplitude is approximately 0.1 mV with a firing rate of up to 80 Hz [5]. The maximal measured peak-to-peak amplitude in our measurements is below 0.04 mV.

Table 1 Electromagnetic noise measurements of the MARS robot.

Description	Mean (mV)	Std. (mV)	Max. (mV)	Min. (mV)
Background	-0.000360	0.0038	0.0211	-0.0197
AC/DC	-0.000399	0.0039	0.0212	-0.0203
Movement	-0.000416	0.0039	0.0175	-0.0183
Micro-drive	-0.000422	0.0039	0.0179	-0.0196
Stimulation	-0.000415	0.0039	0.0176	-0.0184

Analysis of the histogram data show normally distributed noise. The applied Fourier transformation shows no distinguishable peaks in the frequency spectrum. Hence the measured noise can be classified as Gaussian normal distributed white noise.

To conclude, no measurable periodic noise is generated by the MARS robot or the micro-drive unit.

DISCUSSION

The presented data shows, that the MARS robot has no measureable influence on the microelectrode recordings. The measured noise level does not differ substantially from the background noise and its amplitude is neglectable for the microelectrode recordings. For the background as well as for the actual measurements we classified the noise as Gaussian normally distributed white noise.

The fact that no periodic noise is induced by the MARS robot is highly beneficial for the navigation inside the brain based on changes of the neural firing frequency. The amplitude of the noise is well below the expected signal's amplitude. Therefore we conclude that the system in its current form can be used in clinical trials.

REFERENCES

[1] J. Bronstein, M. Tagliati, R. Alterman, A. Lozano, J. Volkmann, A. Stefani, F. Horak, M. Okun, K. Foote, P. Krack et al. Deep Brain Stimulation for Parkinson Disease: An Expert Consensus and Review of Key Issues, Archives of Neurology, 68:165, 2011.

[2] T. Loddenkemper, A. Pan, S. Neme, K. Baker, A. Rezai, D. Dinner, E. Montgomery Jr, and H. Lueders, Deep brain stimulation in epilepsy, Journal of Clinical Neurophysiology, vol. 18, no. 6, p. 514, 2001.

[3] A. L. Benabid, Deep brain stimulation for Parkinson's disease, Current Opinion in Neurobiology, vol. 13, no. 6, pp. 696 – 706, 2003.

[4] C. Karas and A. Chiocca, Neurosurgical robotics: a review of brain and spine applications, Journal of Robotic Surgery, no. 1, pp. 39–43, Feb. 2007.

[5] C. Moll, A. Struppler and A. Engel,. Intraoperative Mikroelektrodenableitung in den Basalganglien des Menschen. Neuroforum 1: 11-20, 2005.

[6] M. Heinig, M.F. Govela, F. Gasca, C. Dold, U.G. Hofmann, V. Tronnier, A. Schlaefer and A. Schweikard, MARS Motor Assisted Robotic Stereotaxy System. 5th International IEEE/EMBS Conference on Neural Engineering, 2011 (accepted for publication).

Natural Orifice Transluminal Endoscopic Surgery (NOTES): A Randomized Control Trial Using the ELITE Simulator to Evaluate Training in Endoscopy and Laparoscopy - a Role for Robotic Assistance?

J. Nehme[1], M.H. Sodergren[1], C. Sugden[1], R. Aggarwal[1], S. Gillen[2], H. Feussner[2], G.-Z. Yang[1], A. Darzi[1]

[1]Dept of Surgery and Cancer, Imperial College, London, United Kingdom

[2]Dept of Surgery, Klinikum rechts der Isar, Technische Universität Munich, Germany

INTRODUCTION

Natural orifice transluminal endoscopic surgery (NOTES) further blurs the boundaries between therapeutic endoscopy and surgery, utilizing a flexible endoscopic platform, surgical knowledge and technique. The aim of this study was to evaluate whether training novices in either a laparoscopic or endoscopic simulator curriculum would enhance their performance in a NOTES simulator task.

MATERIALS AND METHODS

This study was a randomized parallel group study conducted at Imperial College London. A total of 30 third year undergratuates at Imperial College were recruited. Eligible participants completed a registration questionnaire, which recorded cohort characteristics. Exclusion criteria included pevious simulator experience or pior handling laparoscopic/endoscopic instruments.

Subjects were randomized to 3 groups (Figure 1) with each group consisting of 10 participants:

Group 1: Control group (*n=10*). Participants in this group did not receive any training.

Group 2: Endoscopy group (*n=10*). Participants received training on a validated endoscopy curriculum, using the Olympus endoscopy simulator.

Group 3: Laparoscopy group ((*n=10*). Participants recieved training on a validated laparoscopy curriculum, using the MIST-VR (minimal invasive surgical trainer virtual reality) (1).

The ELITE (Endoscopic-Laparoscopic Interdisciplinary training Entity) model is a full size replica human female torso. It contains a modular organ package. Face and construct validity testing has previously been established (2). The ELITE was assembled with an Olympus gastroscope (GIF XQ-240, Olympus Japan) and a Stortz endoscopy stack. The NOTES simulated task was developed and assessed by two independent investigators with experience in clinical NOTES. The task consisted of a total of 7 steps. Steps were incorporated into a complete task procedure and were designed to represent real surgical techniques. The task begins and ends within the stomach.

The steps in sequential order included:

1) Entry through pre-prepared gastric incision into peritoneal cavity

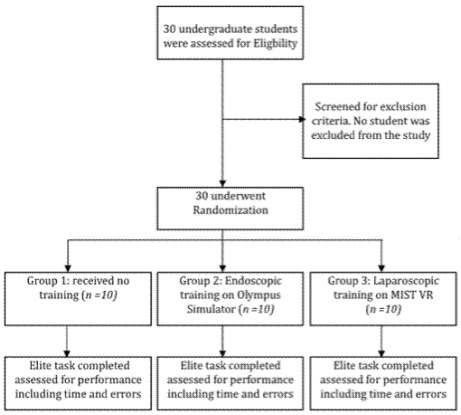

Fig. 1 Flow chart showing randomization and methodology: 3 groups of participants each consisting of 10. All participants completed NOTES task.

2) Navigation and identification of appendix
3) Diathermy of the base of the appendix. This involved feeding needle knife (RX Needle Knife XL, Ref 4584, Boston Scientific, IN, USA) through the instrument channel to touch the base of appendix.
4) Retroflexing endoscope to navigate to and identify gallbladder
5) Clipping cystic artery. This involved feeding endoscopic clip applicator (Resolution clip, Ref 2261, Boston Scientific, MA, USA) through the endoscopic channel and capturing the vessel.
6) Dissection of gallbladder from liver bed. This involved using needle-knife (RX Needle Knife XL, Ref 4584, Boston Scientific, IN, USA) to touch plane between gallbladder and liver.
7) Exit peritoneal cavity into stomach.

A 5 minute multimedia presentation was used to show participants the NOTES task. Performance metrics and errors (inappropriate contact of an instrument with non target organ) were described.

The primary endpoint of performance was assessed by time taken to complete individual steps, overall task time and number of errors.. Two independent observers blinded to participant group recorded subject performance.

Data analysis was completed using SPSS v18.0 (Chicago, USA). Statistical comparison off all groups was achieved using the Kruskall-Wallis test and

between respective groups using the Mann-Whitney U Test. Statistical significance was taken to be a p value < 0.05.

RESULTS

Of the 30 participants 16 were female and 14 male. The mean age was 21. As can be seen from Table 1 there was a significant difference in the times taken to complete steps 1,3,5,6,7,8. There was a tendency for the endoscopy group to perform the task in a shorter time than the laparoscopy group whom in turn were generally faster than the control group.

Table 1 Median times in seconds and Interquartile ranges (IQR) for control, endoscopy and laparoscopy groups.

Task	Group 1: Control (Median time [s]) (IQR)	Group 2: Endoscopy (Median time [s]) (IQR)	Group 3: MIST VR (Median time [s]) (IQR)	P
Access Peritoneal cavity	78 (160)	27 (16)	48.5 (36)	0.04
Navigate to Appendix	87.5 (244)	88.5 (70)	97 (128)	0.77
Diathermy Appendix	173 (151)	103.5 (53)	146.5 (117)	0.04
Navigate to Gallbladder	169.5 (302)	76 (109)	150.5 (160)	0.08
Clip Cystic Artery	641.5 (966)	444.5 (337)	1260.5 (1389)	0.005
Diathermy Gallbladder	256 (393)	102.5 (52)	84.5 (160)	0.014
Pass into stomach	22.5 (19)	15.5 (9)	20 (9)	0.047
Total Time	1645.5 (988)	863 (260)	2074 (1238)	0.001

Control vs Laparoscopy: The laparoscopy group took significantly less time to apply diathermy to the base of the gallbladder than the control (84.5 s vs 256 s) (p= 0.034). There was no other statistically significant differences in times to complete steps between the laparoscopy and control groups. There was no significant differences in error rates between these groups.

Control vs Endoscopy: The endoscopy group was significantly faster at accessing the peritoneal cavity through the gastric incision (27 s vs 78 s) (p=0.015), applying diathermy to the base of the appendix (103.5 s vs 173 s) (p=0.014), and navigating to the gallbladder (76 s vs 169.5 s) (p=0.049). Endoscopy participants took less time than the control to complete the entire NOTES procedure (all 7 steps) (863 s vs 1645.5 s; p<0.001).

The endoscopy group achieved significantly fewer errors at the gallbladder (p=0.02). Finally the total errors were significantly lower for the endoscopy group versus control (p= 0.003).

Laparoscopy vs Endoscopy: Participants in the endoscopy group required significantly less time to maneuver the endoscope out of stomach (27 s vs 48.5 s) (p= 0.001). Endoscopy subjects were also significantly faster at clipping the cystic artery (444.5 s vs 1260.5 s) (p=0.002). Furthermore, the endoscopy group was also significantly faster at completing the NOTES task (all 7 steps) (863 s vs 2074 s) (p<0.001). Finally, the endoscopic group had significantly lower errors at the gallbladder (p=0.01) and total errors than the laparoscopic participants (p= 0.01).

DISCUSSION

The results of this randomized control trial indicate that training novices on an endoscopic simulator curriculum to a determined proficiency level increases performance level compared to 1) no training and 2) laparoscopy training, in a simulated NOTES task.

Significant differences in task time and error rates were found between the endoscopy and the control group. In addition, comparison between endoscopy and laparoscopy trained groups found that endoscopic participants were significantly faster and incurred fewer errors. The laparoscopy group was significantly faster at applying diathermy to the base of the gallbladder.

As outlined in the NOSCAR white paper, training is an important obstacle confronting safe clinical introduction of NOTES (3). Our understanding of training requirements in surgery has undergone a number of significant changes in recent years. This follows the transition from open to laparoscopic surgery where the absence of structured validated training programs was associated with increase in patient morbidity and complications (4). Currently clinical NOTES is performed predominately by surgeons in a multidisciplinary setting. The learning curve and the corresponding skills required to achieve proficiency in NOTES has not yet been defined.

This study highlights the importance of endoscopic training for a simulated NOTES task which involves both navigation and resection / operative maneuvers. Laparoscopic training is also useful for operative steps such as diathermy to base of the gall bladder. All groups had difficulty to maintain retroflexion and clip the cystic artery. Until we have standardized curriculums, NOTES training should incorporate simulation in advanced endoscopy and laparoscopy. It is especially important for surgeons who perform NOTES to be trained in advanced endoscopy. If this is not the case the operative team should include an interventional endoscopist with complementary skill-sets to ensure patient safety and oprimum operative performance. This study also emphasises the limitations of the flexible endoscope as a NOTES platform and raises clear opportunities for computer-assisted robotic solutions to decrease the learning curve and further minimise patient danger.

REFERENCES

[1] Aggarwal, R. *et al.* A competency-based virtual reality training curriculum for the acquisition of laparoscopic psychomotor skill.

[2] Fiolka A, *et al*. ELITE—the ex vivo training unit for NOTES: development and validation. Minim Invasive Ther Allied Technol. 2010; 19(5):281-6.

[3] Al-Akash, M. *et al.* N.O.T.E.S.: the progression of a novel and emerging technique. Surg Oncol. 2009; 18 (2):111-9.

[4] Moore, M.J.& Bennett C.L. The learning curve for laparoscopic cholecystectomy. The Southern Surgeons Club, Am J Surg. 1995: 170; 55–59.

Stealth Calibration Eye Tracking Algorithm for Minimally Invasive Surgery

Kenko Fujii, George Mylonas, Guang-Zhong Yang

The Hamlyn Centre for Robotic Surgery, Imperial College London
kfujii09@imperial.ac.uk

INTRODUCTION

Advancements in robotic surgical platforms such as the daVinci® have overcome many of the limitations of conventional MIS, in particular the lack of 3D vision, the fulcrum affect and restricted degrees of freedom during instrument manipulation [1]. However the master-slave nature of such robotic platforms has also caused a lack of direct sensory and haptic feedback to enable natural visuomotor control. To alleviate some of these problems, the concept of Gaze Contingent Perceptual Docking has been introduced to enhance the control of the surgeon with the aid of gaze-fixation information [2]. This permits, for example, gaze-contingent instrument guidance and motion stabilization [3]. However eye trackers today have a number of practical limitations, namely the necessity for the surgeon to actively participate in a repetitive calibration procedure when initializing the eye tracker, the user dependent performance variability as well as the degradation of gaze accuracy over long periods of use. Clinical use of the current eye trackers may require recalibration during operation, thus disturbing surgical workflow and more critically compromising patient safety. Hence the above usability limitations are hindering its routine adoption. Therefore, to enable clinical use of gaze-contingent applications for delivery of better surgical outcomes to patients, it is necessary to overcome these usability limitations, many of which stem from the eye tracker's calibration procedure.

The work presented here focuses on delivering an algorithm that can discretely calibrate and continuously maintain accurate gaze-fixation information, thus not only forgoing the need for the surgeon to undergo a repetitive calibration procedure but also withdrawing the necessity for a recalibration during an operation.

MATERIALS AND METHODS

The discrete or stealth calibration eye tracking algorithm consists of four components as illustrated in Fig. 1;

- A regression mapping projects the uncalibrated gaze coordinates streaming from the eye tracker to the computer screen coordinates;
- Incorporation of a fixation identification algorithm to remove saccadic noise from the raw eye tracking data. Temporal information of fixations can in turn aid in identifying salient cues which help extraction of calibration control points;
- Calibration control points, a set pair of gaze coordinates and the respective screen location coordinates, are estimated, extracted and placed into memory;
- A number of calibration control points are then selected from the stored collection to update the regression mapping.

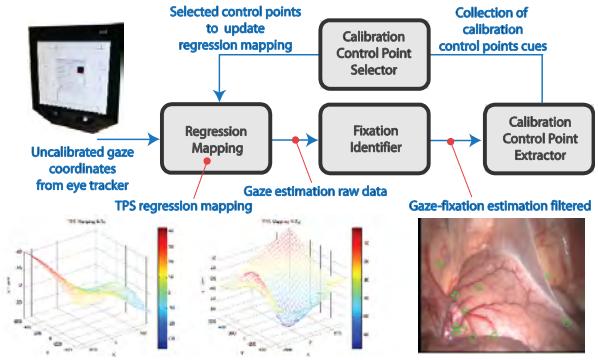

Fig. 1 Stealth calibration eye tracking algorithm. The algorithm consists of four components; a regression mapping, fixation identification block, a calibration control point cue extractor and a calibration control point selector.

For the regression mapping, a thin-plate spline (TPS) was adapted where two splines were used to map both the x and y coordinates of the raw gaze coordinates to the corresponding screen plane coordinates. The use of the TPS was based on its elegant characteristics to interpolate surfaces over scattered data, but also due to its performance when empirically tested against a commonly used parametric calibration and the Tobii® system's calibration over 12 subjects (see Table 1).

Table 1 The average error and standard deviation taking into account all 12 subjects. The TPS shows superior performance.

	Avg. Eye Tracking Error All Subjects (Degrees)	Std Dev All Subjects (Degrees)
TPS	0.48	0.33
Parametric	0.57	0.46
Tobii	0.93	0.56

A dispersion-threshold fixation identification algorithm based on [4] was used with a dispersion threshold of 1° of visual angle and the fixation duration as 100ms. This type of fixation identification algorithm was adapted due to its accuracy and robustness of identifying fixations.

Our preliminary experiments investigate a method appropriate for the calibration control point extraction part of the stealth calibration algorithm. It has been

documented that abruptly appearing new objects to a scene can capture the human visual attention [5]. In order to assess whether abruptly appearing objects can give rise to calibration points, an experiment was conducted on 10 subjects. A set of 6 natural scene images was presented to the subject each for 7 seconds long. Subjects were asked to memorize the scenes for a test at the end of the experiment. In 4 out of 6 of the presented images, a newly appearing object was introduced. The objects introduced were chosen to blend in with the scene of that image. The object was displayed 4.2 seconds after the image was revealed and was presented for 2.8 seconds. Subjects were not informed about appearing objects to assess the effect of an unexpected object appearing during the experiment. During the experiment, 2 image scenes without any abruptly appearing objects were also displayed in order to prevent the user from thinking that the task of the experiment was to look out for newly appearing objects. The experimental setup used a Tobii 1750 eye tracker with eye tracking data recorded in the background at 50Hz. All subjects' eye tracking data was analyzed offline.

RESULTS

Fig. 2 shows the difference in visual angle between the subject's gaze and the location of each respective newly appearing object for all 10 subjects around the time interval of the onset of the newly appearing object i.e. 4.2 seconds. As can be seen from the graphs, the newly appearing objects are attracting the subject's gaze where the visual angle difference between the subject's gaze and the object decreases soon after it appears at 4.2 seconds. There is a delay of approximately 1 second for 2 subjects to notice the new object in the first image scene. This delay might be explained by the visually crowded scene, in which a newly appearing object had less effect in attracting the subject's attention.

DISCUSSION

In this paper we have proposed a new eye tracking calibration algorithm that will discretely calibrate the eye tracker. The aim of the algorithm is to enable the continuous use of gaze contingent surgical applications without having to undergo a calibration procedure, thus enabling clinical use of gaze contingent applications. The algorithm is still in its early stages yet realization of a calibration free eye tracking technique will enhance the surgeon's control modality through the enabled use of gaze-contingent applications, which will become a critical part in the future of robotic surgical platforms.

The results from the experiment showed that abruptly appearing objects were effective in capturing attention. One aspect that needs looking into is the subject's latency to noticing the newly appearing objects. Further investigation of utilizing abrupt visual onsets stimuli to discretely obtain calibration points in a surgical scenario will be conducted. Additionally, it would be necessary to look into the surgical workflow to understand when visual stimuli could be used to discretely calibrate the eye tracker, as flashing abrupt visual stimuli whilst conducting surgery is unrealistic. We also plant to look into other means of obtaining calibration points such as through utilizing the close interrelation between eye-instrument coordination where the instrument tip location can be used as a reference guide to where the surgeon is looking, for example during operation of a cutting instrument [6]. Once calibration points are accumulated, selection of a good set of calibration points can be conducted through the use of the RANSAC algorithm or iterative closest point algorithm.

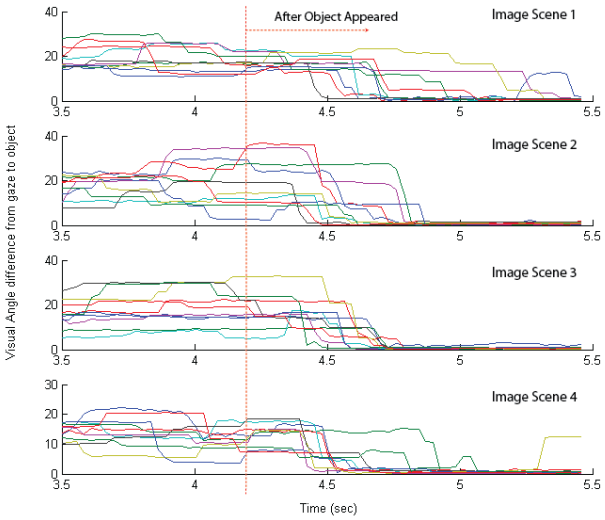

Fig. 2 Graph showing the visual angle difference between the gaze and the newly appeared object location. As can be seen from the chart, the majority of subject's gaze moves rapidly towards the location of the newly appearing object.

REFERENCES

[1] Sung GT, Gill IS. Robotic laparoscopic surgery: a comparison of the DA Vinci and Zeus systems. Urology. 2001 Dec;58(6):893-8.

[2] Yang G-Z, Mylonas G, Kwok K-W, Chung A. Perceptual Docking for Robotic Control. In: Dohi T, Sakuma I, Liao H, editors. Medical Imaging and Augmented Reality: Springer Berlin / Heidelberg; 2008. p. 21-30.

[3] Mylonas GP, Kwok KW, Darzi A, Yang GZ. Gaze-Contingent Motor Channelling and Haptic Constraints for Minimally Invasive Robotic Surgery. Med Image Comput Comput Assist Interv 2008.5242:676-83.

[4] Salvucci DD, Goldberg JH. Identifying fixations and saccades in eye-tracking protocols. Eye tracking research & applications. 355028: ACM; 2000. p. 71-8.

[5] Jonides J, Yantis S. Uniqueness of abrupt visual onset in capturing attention. Percept Psychophys. 1988 Apr;43(4):346-54.

[6] Leong JJH, Atallah L, Mylonas GP, Leff DR, Emery RJ, Darzi AW, et al. Investigation of partial directed coherence for hand-eye coordination in laparoscopic training. Medical Imaging and Augmented Reality, Proceedings. 2008;5128:270-8, 441.

Evaluate your Robot Accuracy

M. Masjedi, K. Davda, S. Harris, A. Altuntas, J. Cobb

Department of Orthopedics, Charing Cross Hospital, Imperial College London,

m.masjedi@ic.ac.uk

INTRODUCTION

In recent years, robots have become common place in industry due to their high accuracy and repeatability. As imaging and robotic technology advance, there is real potential to use these capabilities in the field of surgery, from planning to performing the procedure. However, the accuracy of robots are affected by both software, such as the registration algorithm used, or the hardware, for example the precision of the linkage system.

The Acrobot Sculptor is an example of such a robot, used in orthopaedic surgery. It can assist with bone resection and prosthesis implantation, with current application for uni-compartmental knee replacement [1]. However, the repeatability and accuracy of this robot in clinical settings yet to be determined. With the use of commercial software, Acrobot Modeller, the Acrobot Sculptor utilises patient data from segmented low radiation dose CT scanning, generating 3D surface reconstruction of the specified bones. This data is loaded onto the Acrobot Planner software to create the pre-operative plan. Here, the user is asked to select specified bony landmarks to create a local frame of reference that allows anatomical and hence surgical parameters to be generated. The surgeon is free to alter the plan as required. The Acrobot Sculptor has a cutting burr attached to its three degrees of freedom (DoF) arm which can sculpt the bone based on this plan. A tracking arm is fixed to the bone so that the system is aware of the 3D position of that bone relative to the robot at all times. Following attachment of the bone to the tracking arm, the intra-operative procedure requires registration of points on the bone surfaces using a 2mm ball burr.

Assuming the CT data are valid, potential sources of error from this system that can influence the outcome of surgery include:

1) Acrobot modeller software: this has not been validated and may produce an inaccurate surface model
2) Inaccuracy in the position of the sculpting or tracking arm in different arm angles
3) Inaccuracy in the registration algorithms to match the CT data to the bone
4) Errors may arise from poor fixation of bones to tracking arm, or inaccuracies in the surgical tool and performance.

In this study we have set up various steps to determine the accuracy and repeatability of the Acrobot Sculptor. We believe is also applicable to a wide range of other available similar products.

MATERIALS AND METHODS

In order to evaluate the accuracy of Acrobot sculptor, the following steps were taken:

The initial step was to determine the accuracy of segmentation procedure. There are numerous techniques available to create the surface from the CT images. It is possible to use these 3D images in order to diagnose gross pathology even when surface geometry and orientation has not been determined. However, in robotic procedures, accuracy of these surfaces has direct influence on the outcome of surgery. Using a single femoral bone specimen, we compared the accuracy of segmentation of Acrobot Modeller to other validated software available commercially. These are Mimics (Materialise®) and Robin 3D®. These surfaces were then co registered together using 3-matics software and the differences in size and shape were analysed.

The second step in determining the reliability and reproducibility of the Acrobot Sculpture was by placing a set of points on the femur sawbone that was CT scanned and segmented using an indelible marker. A total of 45 random points were selected on areas of the femoral sawbone model, with features of medial gonarthosis [1]. Four different observers then registered these points using the Acrobot Sculptor, with the RMS and maximum error recorded for each. To check the effect of different tracking and sculpting arm positions (for registration), the same procedure was repeated by changing the fixation of the femur, in order to mimic the surgical operations for various patient sizes or surgeon preferences.

Finally, in order to ensure this registration procedure was accurate, we chose an unrelated and unbiased product to act as a control and test the findings of Acrobot. This step involved using a CAD (3-matic, Materialise) program to determine reproducibility and reliability. A total of eight points were selected and marked across the femur on readily identifiable bone land marks such as medial and lateral epicondyles (Figure 1-a). The 2mm ball cutter arm of the Acrobot Sculptor was used to register and record the position of these points. The same points were then selected visually by 4 observers on a CAD model of the femur using the segmented CT data. For each trial the points selected by the observers was registered to those selected by user of the Acrobot Sculptor arm by minimisation of root mean square difference using a custom written algorithm in Matlab (Mathworks).

RESULTS

The results from segmentation using different software showed an almost identical outcome. The measurements were performed in 3-matic software and the difference was far less than 1mm at all points (Figure 1b).

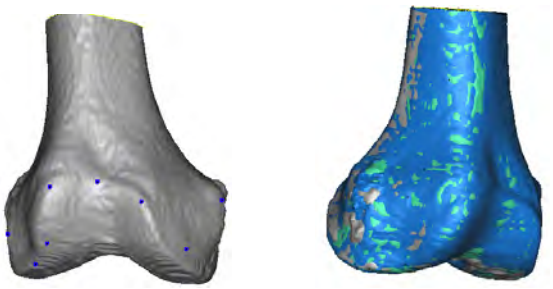

Fig. 1 a) Eights points were marked on the identifiable land marks on the distal femur, **b)** superimposing the segmented femur using three different software systems.

The results from the second step are shown in Table 1, where, overall RMS error was found to be small in all cases. For the third step, (comparing CAD model and data taken from robot) the RMS error were found to have overall average of 2±0.48mm.

Table 1 Registration of femur using 45 points.

Observer	Attempt	RMS Error (mm)	Max Error (mm)
1	1	0.5	1.6
1	2	0.5	1.8
2	1	0.5	1.5
3	1	0.5	1.5
3	2	0.5	1.5
Mean		0.5	1.58 ± 0.13
Second Trial - changing the femoral position			
1	1	0.6	1.9
2	1	0.4	1.2
2	2	0.5	1.4
3	1	0.5	1.6
3	2	0.6	1.8
4	1	0.6	1.3
Mean		0.53 ± 0.08	1.53 ± 0.28

DISCUSSION

Robot assisted surgery could potentially help decrease surgeon error and lead to improved functional outcome by providing a greater level of accuracy and precision during orthopaedic surgery. The robot gives the surgeon more control in terms of the position and alignment of the implant compared to conventional bone resection jigs. The accompanying software can also assist in the pre-operative planning of surgery, as well as intra-operative execution by providing on screen cues that assist the surgeon in bone resection and implant orientation. Improved accuracy is likely to lead to better clinical outcome, with functional benefits to the patient and improved implant survivorship. In this study we looked at the possible sources of error in using one particular robot system. We examined the accuracy of segmentation and the registration using a bone specimen representative of an arthritic knee joint.

There is a lack of data in the literature regarding image-guided robotic surgery, hence we performed only a comparative study. The possible difference across software may also arise from using different Hounsfield units to discriminate bone affecting segmented data, however this is operator error and not software. In this study, we used an extended Hounsfield scale to 16000 units, minimising metal artefact interference. Other studies using CT must be evaluated for the quality of CT produced as metal artefact may significantly compromise segmentation quality.

Overall, the registration data was found to be accurate. The best registration was performed with the person who had the most experience using this robot. The Acrobot Sculptor uses a mechanical digitizer to register the surface. The tip of the cutter (ball point) is used as a probe, which has 2mm diameter. Therefore at all times due to radius of the ball, the captured data are displaced from the true surface. Therefore, it is important to hold the probe normal to the surface at all time when acquiring data for better registration procedures. Hence, training in registration technique is vital to its accuracy.

As mentioned earlier in the introduction, other sources of errors could arise from fixing the patient to the tracking arm. The tracking arm ensures the relationship between bone and cutter are known during the surgery. It is therefore very important to design fixtures that are robust and rigid to minimise loosening (i.e. no movement between the tracking device and the anatomy should be allowed) as this would result in an incorrect relationship between bone and arm. Furthermore, if the anatomy deforms after screwing the fixtures due to over loading the segment, this can possibly cause errors and needs to be evaluated for each robot. In Acrobot the tracking arm is quite light and therefore we assumed this source of error is not significant.

REFERENCES

[1] Cobb, J., et al., *Hands-on robotic unicompartmental knee replacement: a prospective, randomised controlled study of the acrobot system.* J Bone Joint Surg Br, 2006. **88**(2): p. 188-97.

[2] Simon, D., et al. *Accuracy Validation in Image-Guided Orthopaedic Surgery*. in *Proc. 2nd Int. Symp. Med. Robot. Comput. Assist. Surg.,*. 1995. Baltimore, MD

Design of a Miniature Multispectral Structured Lighting Probe for Endoscopic Use

N. T. Clancy[1,2], D. Stoyanov[1], G.-Z. Yang[1] and D. S. Elson[1,2]

[1]*Hamlyn Centre for Robotic Surgery, Imperial College London*

[2]*Department of Surgery and Cancer, Imperial College London*

n.clancy@imperial.ac.uk

INTRODUCTION

For the next generation of surgical robots such as the hyper-redundant snake robot [1], there is a need for accurate mapping of 3D tissue morphology and deformation in order to provide effective intra-operative guidance and adaptive motion stabilisation. An integrated 3D imaging system would also improve visualisation and allow for registration of multi-modality and pre-operative images with the 'live' optical view [2], for instance forming part of an augmented reality system [3]. To this end, structured lighting can be used to reconstruct the 3D shape of tissue by projecting a pre-defined pattern onto the surface. With a calibrated projector-camera arrangement, the location of specific projected points in 3D space can be calculated by triangulation of the projected and reflected rays. However, to make this system robust, the projected features must be uniquely-identifiable to cope with high pattern density or occlusions [4].

This paper describes an optical fibre probe that uses a supercontinuum laser to spectrally encode a pattern of dots. A segmentation algorithm has been developed that allows unique identification of each dot on the basis of its RGB values, regardless of background colour. The small footprint of the probe (< 2 mm) means that it could be used in the instrument channel of flexible surgical robots, acting as part of the on-board imaging and navigation system. This could help to continue the development of MIS procedures such as robotic-assisted natural orifice translumenal endoscopic surgery (NOTES), currently hampered by limited visualisation and feedback to the surgeon.

MATERIALS AND METHODS

The schematic of the fibre probe is shown in Fig. 1 (a). The main component is a spot-to-line converter (FiberTech Optica, Inc., Canada), consisting of 127 fibres (50 μm core) with an average centre-to-centre separation of 68 ± 3 μm. An equilateral prism was used to disperse light from a 4 W supercontinuum laser (Fianium Ltd., United Kingdom), which was then focussed onto the array end of the fibre probe using an achromatic lens. Each fibre corresponded to a unique colour with a narrow bandwidth (2-5 nm FWHM) and a central wavelength separation of ~2.5 nm between neighbouring fibres at the linear array input. The black regions of the pattern seen in Fig 1 (a) are the result of redundant fibres at the array end. The probe has an outer diameter of 1.7 mm, making it possible to use it with existing endoscopic instruments (Fig. 1 (b)).

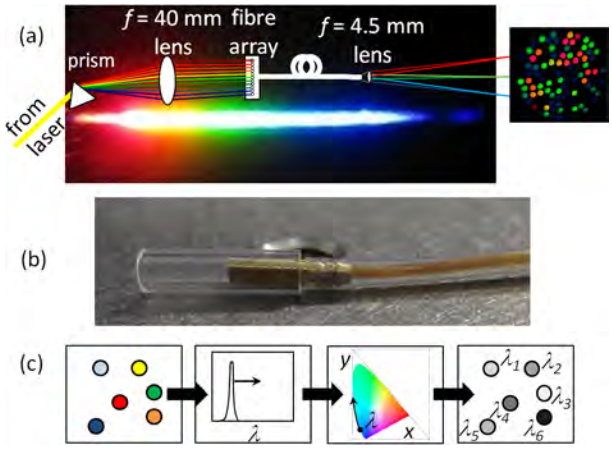

Fig. 1 (a) The collimated output of the supercontinuum laser is dispersed using the prism and focussed onto the probe's linear array end by an achromatic doublet. Background: magnified view of spectrum focussed on fibre array. (b) Photograph of probe with glass ferrule to hold imaging lens. (c) The RGB values for each pixel are converted to wavelength using a look-up table of *xy* coordinates and values.

The RGB values returned by the camera for each pixel may be converted to the CIE 1931 *xyY* colour space, which maps a colour's relative levels of red, green and blue wavelengths to an area encompassed by the sensitivity range of the human eye (tristimulus values) [5, 6]. Since pure wavelengths map to the locus bounding the visible colours in the *xy* plane of this colour space, as shown in Fig. 1 (c), it is possible to deduce the wavelength of a particular pixel from its *xy* coordinates.

A look-up table of *xy* coordinates was generated using published tristimulus data [7] and the measured spectral profile of a sample of spots. Calculated pixel *xy* values are matched to values in the table so that each pixel is converted from RGB to 'λ-space'. The segmentation is performed by first finding clusters of pixels with a similar wavelength value (± 1 nm). Cycling through this 'thresholded λ-space' makes it possible to pick out individual spots by wavelength and return the coordinates of their centroids.

RESULTS

The spot pattern was projected onto a white screen as shown in Fig. 1 (a) and a close-up view of two of those

spots is shown in Fig. 2 with the histograms of each after the λ-space conversion. Spot i and Spot ii can be clearly separated, having sharp well-defined peaks. Each distribution is slightly broadened by the effect of pixels on the periphery of a spot, where low intensity means that RGB values are close to the CCD background noise level. A small peak due to the edge of a neighbouring spot in the region of interest containing Spot ii is visible at approximately 545 nm.

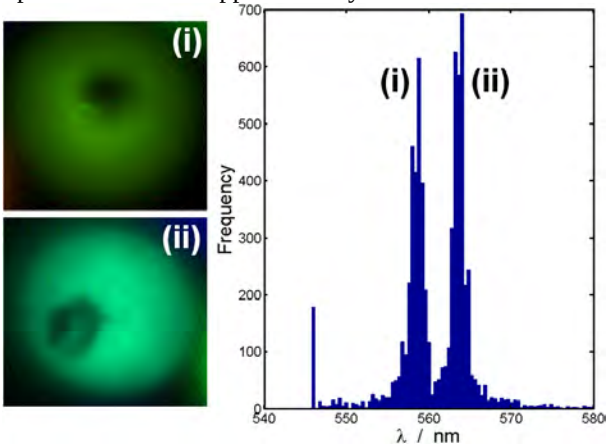

Fig. 2 Close-up of individual projected spots and the histogram of their calculated wavelength values.

The effect of background colour was investigated by measuring the variation in the calculated wavelength of each spot on different-coloured screens (red, green and blue). It was found to be significant (± 10 nm) only in pixels on spot edges, such as those in the tails of the histograms in Fig. 2, where CCD noise becomes dominant.

This insensitivity to background colour is one of the strengths of this technique. Due to the narrow spectral profile, the reflected spectrum of each spot is not modified appreciably and only a variation in intensity from one background to another will be seen. This will be particularly important in the case of tissue during surgery where large differences in surface reflectivity may occur within a small area.

Although the initial set-up described here is a benchtop one, future work will involve full miniaturisation of the probe. The aspheric imaging lens will be replaced by a gradient index (GRIN) lens, which can be manufactured to a diameter to match the 1.7 mm probe tip.

DISCUSSION

The prototype structured lighting probe described is highly-flexible and sufficiently bright for use in endoscopic and robotic-assisted surgical procedures. Due to the use of a supercontinuum laser as a light source, the spectrum of each projected feature has a narrow profile and is located on the spectrum locus on the CIE 1931 xy chromaticity diagram. Wavelength-based identification and discrimination of specific dots is possible regardless of background colour using only the RGB output from the camera, which is compatible with the colour cameras used in surgery.

With regard to the use of the laser *in vivo*, focussing of its entire non-dispersed output to a fine point on the tissue may cause thermal damage. However, in this probe the output is dispersed across the 127 fibres in the bundle and magnified onto the tissue so that the power density per spot is below the level needed (several hundred mW) for damaging non-linear effects.

With a miniature lens fitted to the distal tip, the probe will be able to fit in the instrument channel of a flexible robot or endoscope and used to demonstrate tissue surface identification *in vivo*. Since the projected spot brightness is less than that of standard surgical light sources such as the xenon arc lamp, the probe could be left on continuously. A shutter synchronised with the imaging camera could then be used to block the white light for a fixed percentage of frames per second, thus acquiring structural information without disturbing the surgeon's normal view.

ACKNOWLEDGEMENTS

Funding for this project was provided by the UK EPSRC and Technology Strategy Board grants EP/E06342X/1 and DT/E011101/1.

REFERENCES

[1] Clark J, Södergren M, Noonan D, Shang J, Payne C, James D, Teare J, Athanasiou T, Darzi A, Yang G-Z. A novel articulated robotic laparoscope for single incision and natural orifice surgical applications; preliminary usability trials in a live porcine model. Scientific Session of the Society of American Gastrointestinal and Endoscopic Surgeons (SAGES). National Harbor, Maryland, USA: Surgical Endoscopy, Springer Science + Business Media, LLC, 2010: S690-S1.

[2] Penney GP, Barratt DC, Chan CSK, Slomczykowski M, Carter TJ, Edwards PJ, Hawkes DJ. Cadaver validation of intensity-based ultrasound to CT registration. Med Image Anal. 2006: 10(3): 385-95.

[3] Edwards PJ, King AP, Hawkes DJ, Fleig O, Maurer CRJ, Hill DL, Fenlon MR, de Cunha DA, Gaston RP, Chandra S, Mannss J, Strong AJ, Gleeson MJ, Cox TC. Stereo augmented reality in the surgical microscope. Stud Health Technol Inform. 1999: 62: 102-8.

[4] Batlle J, Mouaddib E, Salvi J. Recent progress in coded structured light as a technique to solve the correspondence problem: a survey. Pattern Recogn. 1998: 31(7): 963-82.

[5] Lindbloom B. RGB/XYZ Matrices. http://www.brucelindbloom.com/. Accessed December 15th, 2010.

[6] Smith VC, Pokorny J. Color matching and color discrimination. In: Shevell SK, ed. The Science of Color. 2nd ed. Oxford: Elsevier, 2003.

[7] Smith T, Guild J. The C.I.E. colorimetric standards and their use. Trans Opt Soc. 1931: 33(3): 73-134.

Eye-Tracking Analysis for Patient-Specific Training and Simulation

Johannes Totz, Guang-Zhong Yang

The Hamlyn Centre for Robotic Surgery, Imperial College London
{jtotz, gzy}@imperial.ac.uk

INTRODUCTION

Minimally invasive surgery requires a high degree of dexterity and spatial awareness. Natural Orifice Transluminal Endoscopy (NOTES) pushes this demand even further and issues related to specialised instrument design, disorientation during navigation and effective closure methods are key research topics within the surgical and engineering communities (Fig. 1). Virtual reality simulators can help reduce that risk by providing realistic scenarios for training. Their effectiveness relies on high fidelity representation of the tissue, organ and instrument interaction. Deriving patient-specific scenarios directly from surgical scenes and pre-operative imaging data opens the opportunity to generate realistic datasets from examinations. For example, projecting video images onto CT-derived triangle meshes produces photo-realistic tissue appearance. But misregistration, imaging artefacts and changing illumination conditions can affect the visual fidelity negatively, leading to obvious seams on the virtual tissue surface. Using texture blending [1], these seams can be hidden by smoothing colour differences while preserving small-scale details.

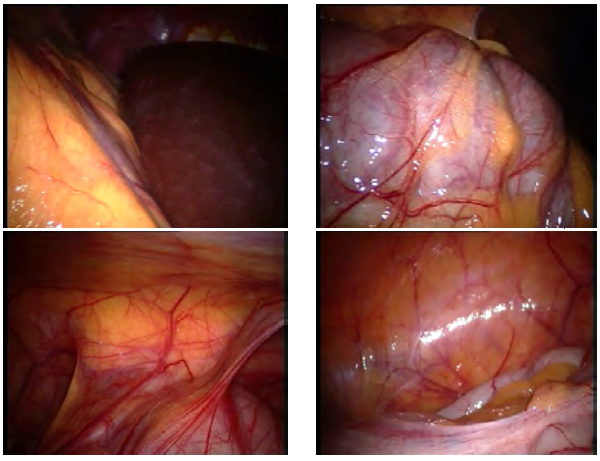

Fig. 1 Disorientation in NOTES. Small changes in position inside the body can lead to a very different video image, potentially disorienting the operator, thus effective training using high-fidelity simulators is essential.

In a previous study [1], different texture blending methods have been investigated, scoring them according to user-preference. Texture artefacts are not the only factors relevant to perceived realism; in fact specular highlight is by far the most important aspect [2]. Therefore, lighting is specifically not simulated or analysed as it would mask texture artefacts and participants were not asked to rate "realism" in [1] but instead rate according to presence of "artefacts". While [1] was performed in the context of virtual bronchoscopy the method and study results generalise to other scenarios as well.

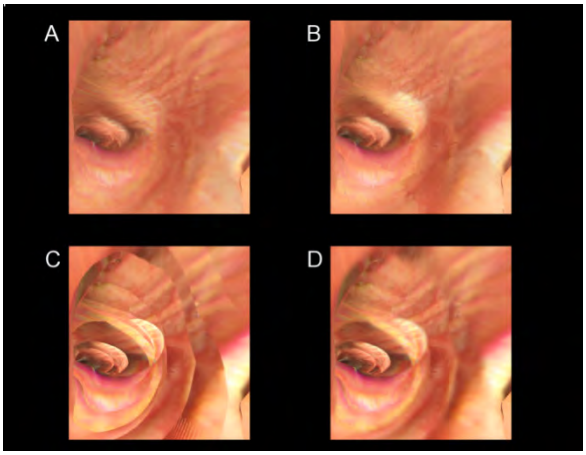

Fig. 2 Example of one slide presented to subjects in [1]. Each image shows a simulated endoscopic view generated by a different texture blending method.

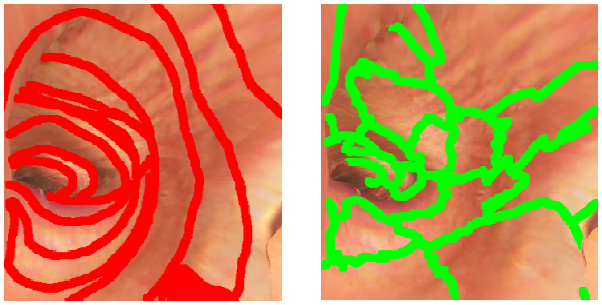

Fig. 3 Artefacts labels on sub-pictures of each slide; red is video-frame boundary, green is texture-domain boundary.

MATERIALS AND METHODS

In [1] visualisations of a texture-mapped bronchus where generated with four different texture blending methods. These four methods are: 1) no blending at all, referred to as "simplestitch", 2) simple feathering of video frames, referred to as "alphablend", 3) multi-band blending with texture-domain overlap and 4) without overlap, referred to as "noparamoverlap". The gaze of 13 participants was recorded and is analysed in this paper to gain insight into why any particular texture blending method was preferred. Fig. 2 shows one of the ten slides used during the study, showing different blending methods. On each slide, each possible artefact was labelled (Fig. 3): video-frame boundaries and texture-domain boundaries. The former result from parts of the organ being observed at different points in time with possibly changing illumination, while the latter are

due to partitioning the organ surface of arbitrary topology into disc-homeomorphic patches. Each artefact is only a few pixels wide and its label was therefore dilated to cover about 1.5 degrees of visual angle. The number of fixations falling on each artefact or background was counted as fixations per method c and as fixations per artefact f. Counts were normalised by total fixations: $p_m = c_m / \sum_n^{Methods} c_n$, similarly for p_f, to account for inter-subject variation. In addition, p was further normalised by its on-screen area.

RESULTS

Fig. 4 shows the average number of fixations for each slide. As can be seen, these vary widely, both inter-slide as well as inter-subject. The error bars indicate the minimum and maximum number of fixations that any participant spent on a slide. The number of fixations spent specifically on artefacts is shown in Fig. 5, with the average percentage of fixations on artefacts per slide, indicating that for some slides background is more important (e.g. slide02 at ~35% artefacts) and for others artefacts do play an important role (e.g. slide04 at ~70%). On average, participants spent about 50% of their fixations on artefacts compared to background. Both artefacts seem to be equally important to subjects as both texture-domain- and video-frame artefacts score about the same amount of fixations. Fig. 6 is in agreement with [1] in that the simple-stitch method is scored lowest and easily disregarded as having the worst artefacts. Multi-band blending with overlap is minimally ahead of feathering/alpha-blending, followed by multi-band blending without overlap. Interesting is the sudden drop in fixations for multi-band blending without overlap (yellow bars in Fig. 6) in the second half of the experiment. Normalising fixations for inter-subject variations yields Fig. 7. Apparent here is that none of the artefacts seem to grab the attention of the participants: the score for each method is a ratio of fixations compared to background. Even for slide07 and slide08, which exhibit a peak at video-frame artefacts with feathering, this ratio is still below 1.0, meaning they are not any more important than background. The only conclusion to draw here is that subjects can make their decision without explicitly looking at artefacts.

DISCUSSION

Studying the actual effects on perception is important to make sure that methods that strive to improve visual quality actually do so. Texture blending has been shown to improve visual quality in [1] but analysing what causes this perceived improvement was still open, which this paper addresses. The gaze analysis does not allow the conclusion that either artefact is more important to participants. In fact, it appears that participants can make decisions without explicitly looking at artefacts due to peripheral vision. The sudden drop of fixations on multi-band-blending without overlap is surprising. It could indicate a learning effect: by the second half of the experiment subjects have figured out how to disregard this method quickly (it has received low scores in [1]).Nevertheless, the eye tracking data allows the analysis of factors affecting visual fidelity in surgical simulation, which offers an objective way of assessing the effectiveness of different rendering approaches.

REFERENCES

[1] J. Totz, A.J. Chung, G.Z. Yang, “Patient-specific Texture Blending on Surfaces of Arbitrary Topology”, Proceedings of AMI-ARCS, 2009, 78-85

[2] M. Elhelw, M. Nicalaou, A.J. Chung, G.Z. Yang, M.S. Atkins, “A Gaze-Based Study for Investigating the Perception of Visual Realism in Simulated Scenes”, ACM Transactions on Applied Perception, 2008, 5, 1-20

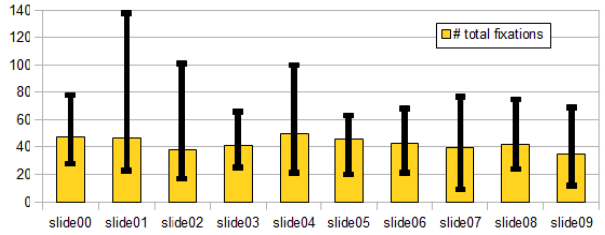

Fig. 4 Average number of fixations per slide. Error bars indicate min/max over all subjects showing large inter-subject variation.

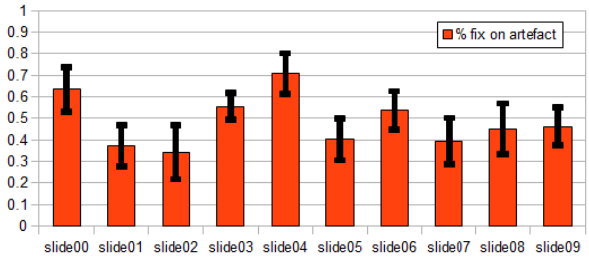

Fig. 5 Average per-slide fixations on artefacts. Error bars indicate standard deviation between subjects.

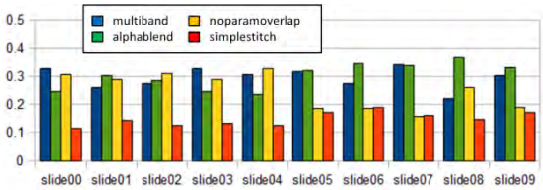

Fig. 6 Percentage of fixation spent on each texture-blending method.

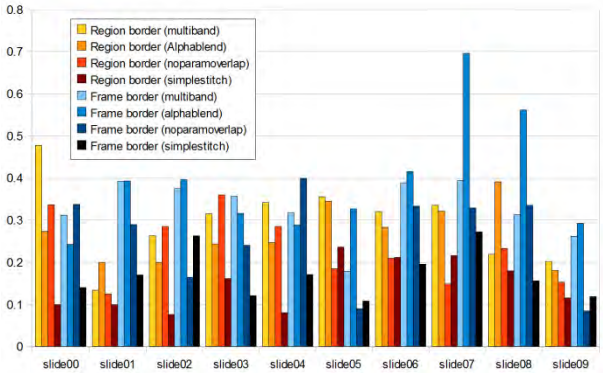

Fig. 7 Scores for each method per slide per artefact.

A Robotic Assistant for Trans-Oral Surgery: The Robotic Endo-Laryngeal Flexible (Robo-ELF) Scope

Kevin Olds[1], Alexander Hilel[2], Elizabeth Cha[1], Martin Curry[2], Lee Akst[2], Jeremy Richmon[1], Russell Taylor[1]

[1]*Engineering Research Center for Computer Integrated Surgery, Johns Hopkins University*

[2]*Department of Otolaryngology – Head and Neck Surgery, Johns Hopkins Hospital*

rht@jhu.edu

INTRODUCTION

This paper describes the development of a simple, clinically usable robot for manipulating flexible endoscopes for laryngeal surgery. Transoral endoscopic surgery aims to reduce the risk of complications such as scarring and infection by utilizing natural orifices when accessing surgical targets. However, despite the many advantages of this approach, it also presents significant challenges, particularly poor sensory feedback, reduced visibility, limited working area, and increased hand tremor due to long instruments.[1]

Robotic surgery systems such as Intuitive Surgical's da Vinci have sought to remedy these problems in other surgical venues, but these solutions do not transfer well to laryngeal surgery. The da Vinci was designed primarily for robotic laparoscopic surgery, in which instrument position and orientation simulate the normal hand position of a surgeon, with widely-spaced large diameter instruments. The result is a large, bulky robot which can be difficult to work around, and can cause additional problems with intubation for general anesthesia when instruments limit access to the airway.[2]

In transoral laryngeal surgery, this approach has further limitations, since access through the airway requires nearly parallel instrument shafts, which the da Vinci cannot achieve. To partially compensate for these shortcomings, such systems often require highly modified surgical techniques and specialized clinical equipment, resulting in the need for extensive additional training for surgeons and prohibitively high startup and maintenance costs.[3]

Outside of robotic systems, the current state of the art in laryngeal surgery makes heavy use of rigid endoscopes. Flexible scopes are frequently used in the clinic for diagnostic and an increasing breadth of therapeutic procedures. Current clinical endoscopes are very advanced, offering HD video, working ports, high range of motion tips, and full sterilizability. However, the way endoscopes are currently used has many drawbacks. In a typical procedure, one surgeon holds and actuates the endoscope, which requires both hands, while another uses instruments such as forceps and a laser to manipulate and ablate tissue. This leads to a crowded working environment with two surgeons crowded around the patient. We also found that coordination between the two surgeons can be difficult and supporting and actuating the endoscope for long periods of time can result in fatigue and inaccuracy.

MATERIALS AND METHODS

We propose a relatively simple, small, inexpensive robot that takes full advantage of existing clinical equipment with the goal of using this technology in the operating room on anesthetized patients. We focused on developing a robot to hold and actuate an unmodified clinical endoscope, allowing one surgeon to control the scope with one hand using a SpaceNavigator 3D mouse, and operate with the other hand, or to position the scope using the robot, then operate bimanually. We used the Pentax VNL-1570STK flexible laryngoscope in these experiments, but the system is designed so that any similar clinical endoscope could be used with minimal modification. We found that surgeons generally use three degrees of freedom when manipulating flexible endoscopes: bending of the scope's tip using the scope handle, rotation of the scope about its axis, and translation of the scope along the axis of the airway. To aid in positioning the scope, and scope removal in case of emergency, we also added two passive lockable degrees of freedom (Fig. 1). Both active and passive joints are sealed with corrosion resistant sealed bearings, o-rings or bellows, allowing the robot to remain fully watertight even when in motion. The electrical connection to the robot is achieved using a Soriau corrosion resistant waterproof electrical

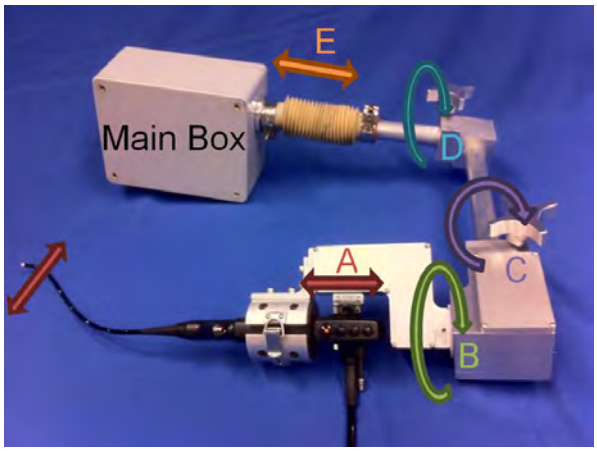

Fig. 1 A) Active scope tip manipulator B) Active axial rotation of the scope C) Passive lockable joints to adjust scope entry angle D) Passive lockable joint to adjust scope height E) Active in-out translation

connector. All compartment covers are sealed with o-rings.

In order to minimize weight over the patient, we designed the system so that the largest motors, for the scope translation and rotation degrees of freedom, are located in the main box. To transmit power from the main box to the scope rotation joint, a cable-pulley mechanism was used. We used 12 V servo motors with planetary gearheads and integrated magnetic encoders for all active degrees of freedom. We also installed potentiometers on each active degree of freedom for added safety and more precise control.

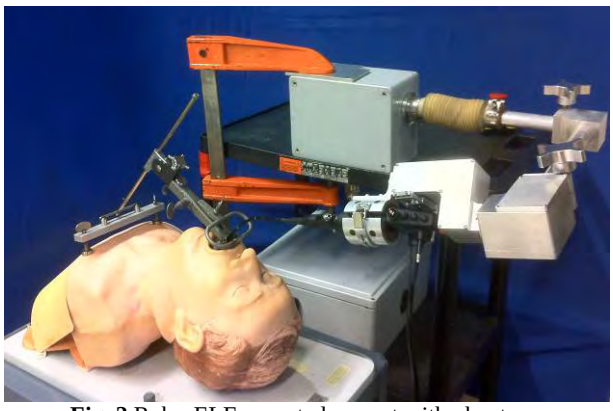

Fig. 2 Robo-ELF mounted on cart with phantom.

The robot grips the scope with custom molded urethane rubber inserts, and uses a quick release latch to hold the scope in place. The scope shaft is highly flexible, so we added a malleable wire scope shaft support to stiffen it for more precise control. The entire robot is built with Johns Hopkins Hospital clinical engineering specifications in mind, including waterproof seals, operating room safe materials, proper electrical grounding with fusing, and an isolated power supply with no voltages greater than 12V. The robot is operable in wet environments and is awaiting a final clinical engineering inspection.

Our surgeon co-authors (Drs. Akst, Hillel, and Richmon) have tested the system using two fresh human male cadavers. We suspended each cadaver with a Steiner laryngoscope to allow visualization of the endolarynx, in a configuration similar to Fig 2. First, we performed standard microlaryngoscopy using 0, 30, and 70 degree rigid scopes, taking representative photographs of the endolarynx with each scope for comparison. We then evaluated the Robo-ELF with the following three tasks: 1) comparable field of view; 2) visualization of challenging anatomical areas with precise biopsy sampling; and 3) bimanual surgery with the Robo-ELF in a fixed position.

RESULTS

Using the passive degrees of freedom, we easily positioned the Robo-ELF through the Steiner laryngoscope. All three active degrees of freedom performed reliably, with smooth, consistent, reproducible motion. The velocity of the movement was reliably transmitted through motion of the 3D mouse, with no erratic artifacts and virtually no learning curve. The Robo-ELF provided a higher resolution image with superior field of view compared to the three rigid endoscopes. In addition, we were able to navigate the flexible tip around the arytenoids into the piriform sinuses, and through the vocal cords into the subglottis, overcoming the line of site limitations of rigid scopes. Though we were able to visualize the intended biopsy sites in both cadavers, the first cadaver's larynx was anteriorly positioned, so despite obtaining a clear view of the subglottis and anterior commissure with the Robo-ELF in a flexed position, the straight laryngoscopic forceps were unable to reach. Finally, after positioning the Robo-ELF above the vocal cords there was still ample room to use two instruments to perform bimanual endolaryngeal surgery.

DISCUSSION

We have shown that a relatively small, inexpensive three degree of freedom robot can be used to precisely control an unmodified clinical endoscope with virtually no learning curve. The Robo-ELF has demonstrated significant advantages over existing robotic surgery systems, and un-actuated rigid and flexible endoscopes in the field of laryngeal surgery. The flexible endoscope also has a working channel through which a therapeutic laser could be introduced, further taking advantage of standard clinical equipment.

The technologic advantages of this approach are substantial. This robot is inexpensive compared with other microscopic and robotic techniques, at approximately $30,000. On top of this platform, we also plan to integrate more sophisticated software features, including automated scope stabilization, 3D reconstruction from multiple monoscopic scope images, automated point-and-click navigation, video registration with pre-operative imaging data, and virtual fixtures. It could also be utilized with other technology, such as image-overlay, ultrasound, optical coherence tomography, and be manufactured with two chips for 3-D vision. Furthermore, it could be adapted to a variety of procedures including bronchoscopy, upper and lower gastrointestinal endoscopy and sinus surgery. Eventually there is potential for microvascular surgery at the base of the skull, as well as single port gastrointestinal and thoracic access surgery.

REFERENCES

[1] Plinkert, P., Lowenheim, H. Trends and perspectives in minimally invasive surgery in otorhinolaryngology-head and neck surgery. *Laryngoscope* 107, 1483-1489, 1997.

[2] Lee H, Yun M, Bahk J, Park H, Jeon Y, Lee S. Rupture of endotracheal tube cuff during robot-assisted endoscopic thyroidectomy. *Korean Journal of Anesthesiology*. 2010 December 59(6): 416-419.

[3] McLeod, I.K., Mair, E.A., Melder, P.C. Potential applications of the da Vinci minimally invasive surgical robotic system in otolaryngology. *Ear Nose Throat J* 84, 483-487, 2005.

A Whole Body Statistical Shape Model for Robotic Surgery Planning

Su-Lin Lee[1], Jennifer Keegan[2], and Guang-Zhong Yang[1]

[1]*The Hamlyn Centre for Robotic Surgery, Imperial College London*

[2]*Royal Brompton Hospital, London*
su-lin.lee@imperial.ac.uk

INTRODUCTION

The increase in minimally invasive robotic therapies and image guided interventions requires images and models on a subject specific basis for surgical planning and guidance. The use of a preoperative model allows for the planning of procedures; this includes the determination of optimal port positions for workspace efficiency and collision avoidance, as well as setting the initial pose of the robot [1]. Currently, planning is performed on either an idealized model or one derived from a patient specific scan. We have previously built 3D models from magnetic resonance (MR) images [2] but the scan and the subsequent model building are time consuming. A reduction in this time would make the use of 3D models for port position planning for robotic surgery more feasible.

In this paper, we present a statistical shape model for the whole body, built from 10 male and 10 female subjects of varying size and height. This model would allow for the understanding of the shape space of this population set and preplan port positioning. In addition, robotic instrument design can benefit from such a model; a study of workspace coverage based on meshes across the population would aid in the development of new tools.

METHODS

MR imaging data of the whole body was acquired from 20 subjects (10 male and 10 female, BMI range of 19.5-27.5). The images were acquired using a balanced steady state free precession (trueFISP) protocol (TR = 382ms, TE = 1.79ms, slice thickness = 10mm, in-plane resolution = 1.6mm×1.6mm) in a 1.5T Siemens Avanto MR scanner. Ethical approval for the work was obtained from the St Mary's Committee.

For whole body scanning, the images were acquired section by section, moving the scanner bed after each acquisition to allow the volume of interest to be in the middle of the scanner. 30cm imaging volumes were acquired, covering the entire length of the subjects' bodies. The entire scan for one subject took an average of approximately 45 minutes.

The surface contours of the body were semi-automatically segmented with an in-house program based on active contours [3]. The segments were then aligned semi-automatically and meshed using the marching cubes algorithm [4]. Post-processing of the meshes was performed in MeshLab [2]. As the hands and feet of the subjects could not be consistently segmented, these were removed from the surface meshes.

There are instances in which a subject-specific mesh cannot be generated and to overcome this issue, a statistical shape model was built using all the subjects obtained in the study. This allows for the examination of the entire range of possible body shapes allowable by the training set. Correspondence was achieved through the use of manual landmarks placed on the bodies and the alignment using these markers, based on the work by Allen *et al.* [5]. Principal components analysis (PCA) was then applied to the training set of shapes [6].

A port position analysis was performed on the statistical shape model. Two port positions and insertion angles were chosen for a coronary artery bypass procedure [7] and were planned on the mean shape. The variation of the insertion points were then examined across the extreme shapes.

RESULTS

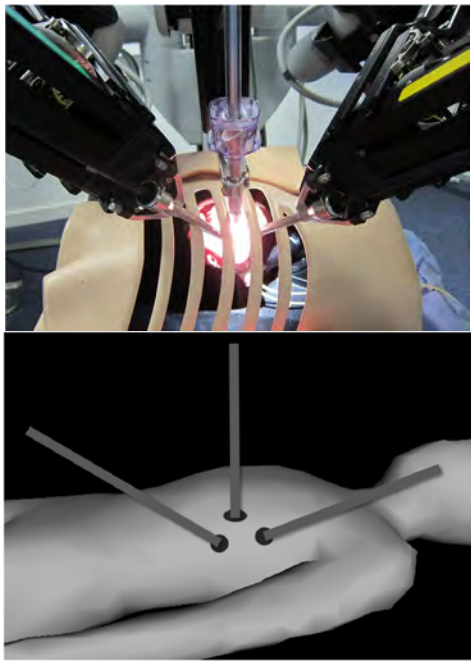

Fig. 1 (top) The da Vinci robotic surgical system with its robotic arms for port insertion. (bottom) The positioning of the endoscope and robotic arms can be preplanned with a preoperative model of the patient.

Nine of the twenty subjects, five female and four male, are shown in Fig. 2. The mean shape and the first mode of variation in the model are also displayed, indicating a need for customized port positions. The first mode showed the height of the subjects, from the tallest male to the shortest female. The second mode also showed some of the height variation. The range of the size of the subjects was captured in the third mode of variation.

Fig. 3 shows the variation of the port positions and workspace analysis across the statistical shape model. An incorrect model used for planning can create large differences in the final port positions as well as covering different parts of the anatomy.

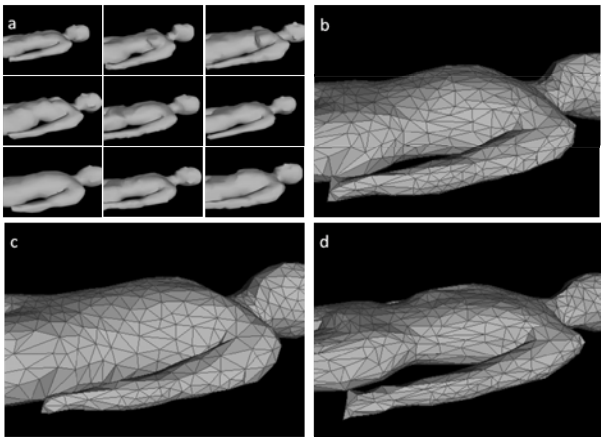

Fig. 2 The statistical shape model (a) nine example torsos in the training set, (b) the mean shape, (c) the third mode of variation with -3σ (fattest) and (d) with $+3\sigma$ (thinnest).

DISCUSSION

The method provides a dimensionality reduction for the training set, allowing for any shape allowable to be reproduced with a linear combination of a limited number of the modes of variation. Each of the original shapes can also be reproduced. A next step to take would be to look at the mapping of the intra-abdominal volumes for the model.

It is shown that the results derived from this initial statistical shape model can be used to aid in port insertion and tool design for minimally invasive robotic surgery.

Acknowledgements: This project was supported by the EPSRC (EP/E057837/1) and by the NIHR Cardiovascular Biomedical Research Unit of Royal Brompton and Harefield NHS Foundation Trust and Imperial College London.

REFERENCES

[1] Adhami, L., Cost-Maniere, E.: Optimal Planning for Minimally Invasive Surgical Robots. IEEE Transactions on Robotics and Automation 19 (2003) 854-863

[2] Lee, S.-L., Lerotic, M., Sani, A., Zhao, Y., Keegan, J., Hao, Y., et al.: Articulated Postures for Subject-Specific RF Simulation. Body Sensor Networks (BSN), 2010 International Conference on, (2010) 96-101

[3] Kass, M., Witkins, A., Terzopoulos, D.: Snake: active contour models. Internationl Journal of Computer Vision 1 (1988) 321-331

[4] Lorensen, W.E., Cline, H.E.: Marching cubes: A high resolution 3D surface construction algorithm. SIGGRAPH Computer Graphics 21 (1987) 163-169

[5] Allen, B., Curless, B., Popovi, Z.: The space of human body shapes: reconstruction and parameterization from range scans. ACM SIGGRAPH 2003 Papers, San Diego, California, (2003)

[6] Cootes, T.F., Taylor, C.J., Cooper, D.H., Graham, J.: Active shape models - their training and application. Computer Vision and Image Understanding 61 (1995) 38-59

[7] Cannon, J.W., Stoll, J.A., Selha, S.D., Dupont, P.E., Howe, R.D., Torchiana, D.F.: Port placement planning in robot-assisted coronary artery bypass. Robotics and Automation, IEEE Transactions on 19 (2003) 912-917

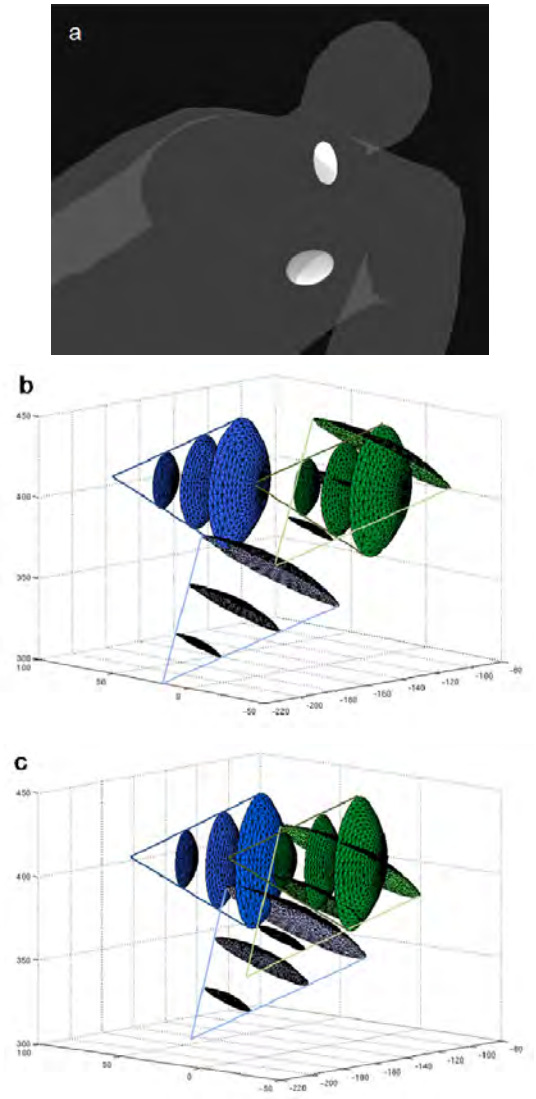

Fig. 3 (a) An analysis of port position variation across the statistical shape model. The mean and standard deviation of the positions across the shapes are shown via the spheres. (b) and (c) showing the workspace analyses of the first and third modes, respectively. The negative extreme is shown in blue while the positive is in green; light and dark are the right and left port positions, respectively.

Real-time Optical Imaging of Bladder Cancer using Fluorescence Lifetime Imaging Endoscopy

A. Kar[1], G.T. Kennedy[2], S. Coda[2], D. Cohen[1], A. Shamsuddin[1], J.A. Vale[1], C. Dunsby[2], D.S. Elson[3], E.K. Mayer[1], P.M.W. French[2]

[1]*Department of Surgery and Cancer, Imperial College London, UK*

[2]*Photonics Group, Department of Physics, Imperial College London, UK*

[3]*Hamlyn Centre for Robotic Surgery, Imperial College London, UK*

ashok.kar@imperial.ac.uk

INTRODUCTION

Bladder cancer is the fourth commonest cancer affecting men; early detection and subsequent treatment in patients with superficial tumours confers an overall 90% survival rate. Current endoscopic techniques rely on the clinician taking biopsies using white light cystoscopy from areas of abnormal tissue for histological diagnosis of suspected bladder cancer, enabling further treatment and management. Significantly white light cystoscopy can miss lesions not visible to the naked eye, and has poor overall sensitivity (56-68%) [1].

Recently, photodynamic detection (PDD) of bladder cancer has been shown in large case series to improve detection of small papillary tumours, carcinoma in situ (CIS) and satellite lesions from previously resected tumours [2]. PDD identifies intensely 'red' fluorescent areas of abnormal tissue under blue light cystoscopy due to the photosensitising agent, hexaminolevulinate (Hexvix®), instilled into the bladder prior to cystoscopy. However PDD is not sensitive at differentiating between inflamed and cancerous tissue, offering low specificity (41.4-98.5%) and giving a high false positive rate, limiting its clinical uptake [3].

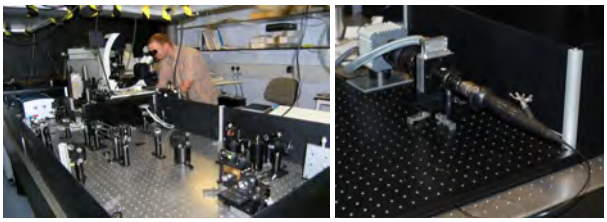

a **b**

Fig. 1 a Leica SP5 confocal FLIM microscope and **b** FLIM widefield ureteroscope (Karl Storz GmbH, Germany)

Fluorescent lifetime imaging (FLIM) endoscopy is a novel technique that measures the characteristic decay of molecules (fluorophores) rather than solely the fluorescent intensity [4]. The fluorescence lifetime of tissue autofluorescence in cancerous and normal tissue has been shown to be different in animal models [5] and has been attributed to changes in cellular respiration and the metabolic state of cells involving endogenous molecules such as Flavins and NADH.

PDD of bladder cancer relies on the administration of Hexvix®, an ester of 5-Aminolevulinic Acid (5-ALA), to induce the accumulation of protoporphyrin IX (PPIX), a fluorescent by-product involved in the haem cycle, which has been shown to build up in rapidly proliferating and therefore neoplastic cells [6]

Although FLIM has been applied to the identification of skin cancer [7], there is little reported in the literature of its use in bladder cancer [8,9]. It is proposed that there are differences in the fluorescence lifetimes signatures between various bladder tissue states, and this is tested in a clinical pilot study. Showing that FLIM can differentiate between normal, inflamed and cancerous *ex vivo* human bladder tissue samples, and validating the molecules contributing to differences in the fluorescence lifetime, will aid in developing a novel endoscopic system to give a real-time optical tissue diagnosis during cystoscopy.

MATERIALS AND METHODS

Patients undergoing rigid bladder cystoscopy at St Mary's Hospital, London were consented for the use of excess tissue in medical research. All cold-cut' bladder tissue biopsies in these experiments were obtained in accordance with Outer West London Research Ethics Committee approval number 08/H0719/37. The *ex vivo* bladder tissue biopsies were kept in physiological Hartmann's solution warmed to 37^0C and transported immediately after resection to the Photonics Group of the Department of Physics, Imperial College London. FLIM was performed within 90 minutes of biopsy and the true histological diagnoses from biopsied areas of tissue were later confirmed.

Fluorescence from the bladder tissue was excited by a frequency-doubled Mai Tai Ti:Sapphire laser (Spectra-Physics) at 405 nm and fluorescence lifetime were measured using time-correlated single photon counting (TCSPC) on a conventional confocal FLIM microscope system (Figure 1a). Instrumental response functions were obtained by imaging a drop of Erythrosin B solution (10-40µM), which has a single exponential decay with a lifetime of 89ps [10]. Image acquisition and data processing were performed using commercially available software, SPC-Image (Becker & Hickl GmbH, Germany). Fluorescence emission spectra for bladder tissue samples were also measured to assist

in determining the molecules involved in producing the fluorescence decay signatures, and these were compared to spectra obtained from pure solutions of flavins and PPIX. Fluorescence lifetimes were further measured using time-gated imaging through a Storz Widefield ureteroscope (Figure 1b).

RESULTS

Preliminary results show a shortening of the fluorescence lifetime between normal and cancerous tissue when using the confocal FLIM system (Figure 2) and also the widefield FLIM ureteroscope (Figure 3). The FLIM optical diagnosis was compared to routine histology. Emission spectra showed a single peak at ~550nm consistent with the fluorescence of flavins [11].

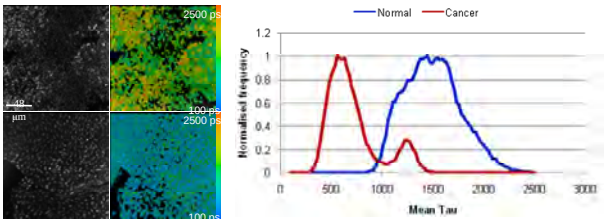

a **b** **c**

Fig. 2 a Matched intensity and **b** FLIM images of *ex vivo* bladder biopsies. **c** Lifetime distribution histograms calculated from the FLIM data.

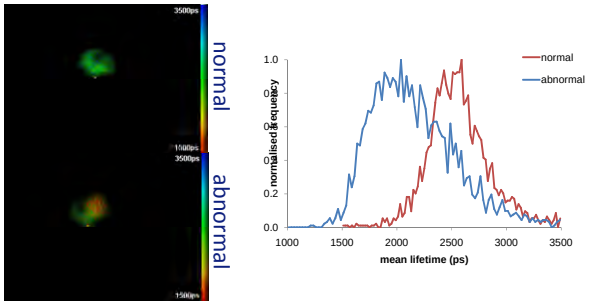

a **b**

Fig. 3 a FLIM images of *ex vivo* bladder biopsies and **b** lifetime distribution histograms calculated from FLIM data.

Similar results of a shortened fluorescence lifetime in cancerous bladder tissue when compared to normal, were obtained when bladder biopsies were instilled with *ex vivo* Hexvix® at therapeutic concentration (8mM). Emission spectra showed a single peak again ~550nm. PPIX was shown in control experiments to have a peak emission spectra ~630nm.

DISCUSSION

Our preliminary data suggest that FLIM endoscopy of tissue autofluorescence is able to differentiate between normal and cancerous tissue, confirmed on histological diagnosis, with a consistently shorter overall lifetime for biopsies of bladder cancer. Our emission spectra suggest that this may be due to the different lifetimes of flavins when bladder tissue is excited at 405nm.

PPIX is another fluorophore which may contribute to different fluorescent lifetimes between various tissue types and further work to characterise biopsies obtained during PDD using blue light cystoscopy, is needed in conjunction with further *ex vivo* Hexvix® instillation studies.

Characterisation of bladder biopsies using FLIM endoscopy in *ex vivo* tissue is necessary before a novel ureteroscopic system can be used for patients undergoing routine cystoscopy *in vivo* to provide real time optical tissue diagnosis. Our work suggests that FLIM offers a novel technological solution to the challenge of accurate diagnosis of bladder cancer.

ACKNOWLEDGEMENTS

This project is funded by an NIHR Invention for Innovation Award [II-3A-0409-10044]. We are grateful for support from the NIHR Biomedical Research Centre Funding Scheme.

This work was completed as part of the Northwest Thames Academic Foundation Programme in Surgery (London Deanery).

REFERENCES

[1] Jocham D, et al. Photodynamic diagnosis in urology: state-of-the-art. Eur Urol. 2008 Jun;53(6):1138-48

[2] Witjes JA, et al. Hexaminolevulinate-guided fluorescence cystoscopy in the diagnosis and follow-up of patients with non-muscle-invasive bladder cancer: review of the evidence and recommendations. Eur Urol. 2010 Apr;57(4):607-14.

[3] Cauberg EC, et al. A new generation of optical diagnostics for bladder cancer: technology, diagnostic accuracy, and future applications. Eur Urol. 2009 Aug;56(2):287-96.

[4] McGinty J, et al. Wide-field fluorescence lifetime imaging of cancer. Biomed Opt Express. 2010 Aug 19;1(2):627-640.

[5] Skala, M, et al. In vivo Multiphoton Fluorescence Lifetime Imaging of Free and Protein-bound NADH in Normal and Pre-cancerous Epithelia. Optical Society of America: Biomedical Topical Meeting, 2006.

[6] Kennedy JC, et al. Photodynamic therapy with endogenous protoporphyrin IX: basic principles and present clinical experience. Journal of Photochemistry and Photobiology, B: Biology, 6 (1990) 143-148

[7] Galletly NP, et al. Fluorescence lifetime imaging distinguishes basal cell carcinoma from surrounding uninvolved skin. Br J Dermatol, 2008. 159(1): p. 152-61.

[8] Cicchi R, et al. Time- and Spectral-resolved two-photon imaging of healthy bladder mucosa and carcinoma in situ. Opt Express. 2010 Feb 15;18(4):3840-9.

[9] Mizeret J, et al. Endoscopic Tissue Characterization by Frequency-domain Fluorescence Lifetime Imaging (FD-FLIM). *Lasers in Medical Science* 1997, 12:209-217

[10] Boens, N., et al., *Fluorescence lifetime standards for time and frequency domain fluorescence spectroscopy.* Anal Chem, 2007. 79(5): p. 2137-49

[11]Wagnières GA, et al. In vivo fluorescence spectroscopy and imaging for oncological applications. Photochem Photobiol. 1998 Nov;68(5):603-32.

Control of an Articulated Endoscopic Camera by Head Motion using the Ear-worn Activity Recognition (e-AR) Sensor

V. Vitiello, B. Lo, G.-Z. Yang

The Hamlyn Centre for Robotic Surgery, Imperial College London
vvitiell@imperial.ac.uk

INTRODUCTION

Minimally Invasive Surgery (MIS) is constantly evolving to allow for safer interventions and shorter recovery. With the integration of robotic technologies, further improvements are made towards flexible access surgical platforms [1]. These can provide navigation along curved anatomical pathways and deliver bimanual dexterity to the operative site through a single port access. Nonetheless, the complexity of the current instruments requires multiple operators to work together. Furthermore, limited field-of-view coupled with misaligned visual-motor axes can cause significant problems due to disorientation. These necessitate the integration of mechatronic articulation in the endoscopic camera, which can be controlled in an ergonomic and intuitive way. Recently, Gaze-Contingent control has been proven to be effective for robotic interface [2]. Head motion control has also been proposed in [3] to position the tip of a motorized endoscope during thoracic surgery. The main drawback of the technique is the need to wear a specialized motion sensor using a headband and a head mounted display (HMD) to ensure that the image is co-registered. The use of such devices can make the surgeons feel restricted and separated from their environment. In this work, a lightweight ear-worn sensor [4] is used to detect the orientation of the surgeon's head and directly control the motion of an articulated endoscopic snake robot.

MATERIALS AND METHODS

As shown in Fig. 1, the system consists of four main components: the ear-worn sensor, a local processing unit, a laptop and the flexible surgical platform. The platform comprises two flexible arms and a 3 degrees of freedom (DoF) articulated endoscope actuated by embedded micro-motors (Namiki Precision Jewel Co. Ltd.) which are arranged as one proximal revolute joint (yaw rotation) and one distal universal joint (intersecting pitch and yaw axis). However, since the motion of the head can only be detected in one plane with this sensor, only the proximal yaw and distal pitch rotations are used to position the endoscopic camera.

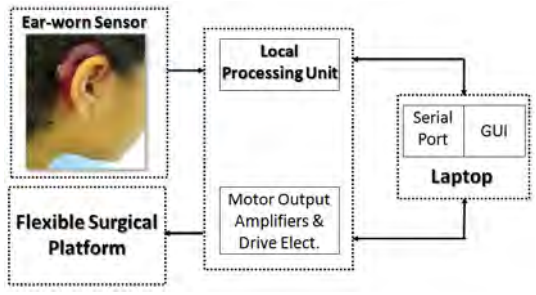

Fig. 1 System components for head motion control.

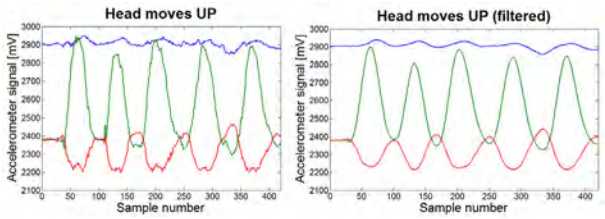

Fig. 2 Signal extracted from the e-AR sensor accelerometer before (left) and after (right) median filtering. Head displacement is detected along right/left (blue line), forward/ backward (green line) and up/down (red line) directions.

The ear-worn activity recognition (e-AR) sensor features a BSN node [5], a built-in battery and a 3-axis accelerometer. The measured angular accelerations are digitalized by the BSN node into three signals in the range of 0-3.5V, where higher outputs correspond to higher accelerations. As shown in Fig. 2, each signal represents the head motion in a different direction, namely right/left (blue line), forward/backward (green line) and up/down (red line). The BSN node also provides a wireless link to send the data to a local processing unit where the signal is processed. Fig. 2 shows the output of the e-AR sensor before (left) and after (right) the application of a median filter with a moving window of size 10 samples. Once the noise is filtered out, the orientation of the head is determined by comparing the signals along the different directions to their baseline values, which are obtained when the head is at rest in the position shown in Fig. 4(a).

The information about the head direction of motion is then sent through a USB connection from the local processing unit to the serial port of the laptop using 5 letters: C (centre), U (up), D (down), R (right), L (left). The desired motion of the articulated endoscope is finally realized by reading the serial port and actuating the corresponding motors via a linear amplifier stage and the Namiki SSD04 3-phase brushless drive electronics.

Table 1 Mean and standard deviation values of completion time and distance from the desired path over 5 subjects for three increasingly complex paths.

	Time [sec]		**Distance [degrees]**	
	Mean	*Std Dev*	*Mean*	*Std Dev*
1st path	62.7	10.6	0.0782	0.0587
2nd path	91	22.5	0.0813	0.0346
3rd path	39.7	13	0.3280	0.0602

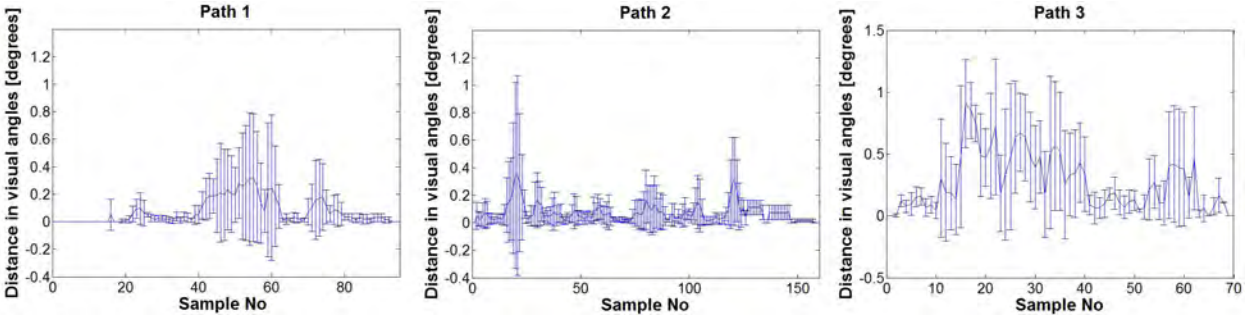

Fig. 3 Plot of the mean and standard deviation values of the distance between the desired path and the actual cursor position in terms of visual angles computed over the five subjects for each point of the three paths.

RESULTS

An experimental task was designed to assess the intuitiveness and precision of the proposed control. Five subjects were asked to follow increasingly complex paths on a screen by moving a cursor using head movements. Two parameters were measured during the experiment: completion time and distance between the desired path and the actual cursor position in terms of visual angles. The resulting mean and standard deviation values for each path over the five subjects are reported in Table 1. Fig. 3 shows the trend of mean and standard deviation values of the distance between the desired path and actual cursor position computed over the five subjects along each of the three paths. The path increasing complexity is clearly reflected in both the graphs and the values in Table 1, where path following accuracy is significantly worse for the third path than for the first two. However, the completion time is longer for the second path because it is constituted by a higher number of points, as shown in Fig. 3.

Fig. 4 shows four snapshots taken during a subject test in a laboratory setting when the articulated endoscope was positioned at extreme workspace positions and the corresponding head orientation. The range of motion of the first DoF is between -45° and +45° along the right/left direction, while the second spans from 0° to 90° downwards. A flexible neck connects the articulated endoscope to a rigid shaft so that it can be elevated from the plane of motion of the flexible arms (removed from figure) once it is passed through the trocar port and the operative site is reached.

The above results demonstrate the ergonomics and efficacy of the e-AR sensor control. Moreover, although positioning accuracy is affected by the complexity of the followed trajectory, a maximum distance of less than 1.5 degrees of visual angle can be considered adequate for the specific application.

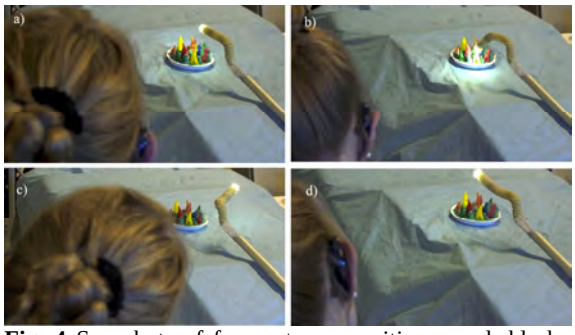

Fig. 4 Snapshots of four extreme positions reachable by the articulated endoscopic camera and corresponding head orientations: a) centre, b) down, c) right, d) left.

DISCUSSION

In this paper, we have proposed an intuitive and ergonomic control modality to position an articulated endoscope using head movements. The e-AR sensor used to detect the orientation of the head is lightweight and wearable, and can seamlessly integrate in the surgical setup with a very small footprint. The overall set-up time of the system is minimal as the calibration of the sensor only requires a short pause at baseline position. In contrast to [3], there is no need for the surgeon to wear a HMD as the endoscopic image remains in the field of view of the user when the head is tilted (see Fig. 4(b,c,d)). The use of a serial-link mechanism to position the camera also eliminates kinematic errors and disorientation issues associated with the unknown tip orientation of standard flexible endoscopes.

REFERENCES

[1] Karimyan V, Sodergren M, Clark J et al. (2009) Navigation systems and platforms in natural orifice translumenal endoscopic surgery (NOTES). Int J Surg 7(4):297-304.

[2] Noonan DP, Mylonas GP, Shang J et al. (2010) Gaze Contingent Control for an Articulated Mechatronic Laparoscope. In: IEEE/RAS-EMBS Int Conf on Biomed Robot Biomechatron - BioRob, 759-764.

[3] Reilink R, de Bruin G, Franken M et al. (2010) Endoscopic camera control by head movements for thoracic surgery. In: IEEE/RAS-EMBS Int Conf on Biomed Robot Biomechatron - BioRob, 510-515.

[4] Atallah L, Lo B, Ali R et al. (2009) Real-Time Activity Classification Using Ambient and Wearable Sensors. IEEE Trans Inf Technol Biomed 13(6):1031-1039.

[5] Lo B, Yang G-Z (2005) Architecture for Body Sensor Networks. In: Perspectives in Pervasive Computing, 23-28.

Robotic-assisted Parathyroidectomy: a Prospective Case Control Study

A. Arora[1], G. Garas[1], J. Budge[1], F. Palazzo[1], R. Dhawan[1], J. Cox[1], A. Darzi[2], N. Tolley[1]

[1]Department of Endocrine and Thyroid Surgery, Imperial College Healthcare NHS Trust
[2]Department of Biosurgery and Surgical Technology, Imperial College London

asitarora@doctors.org.uk

INTRODUCTION

Robotic assisted surgery has been performed in several surgical specialties to address the limitations associated with conventional endoscopic techniques. Its application in endocrine surgery has recently been reported in thyroid and parathyroid surgery [1]. The objective of this study was to prospectively evaluate RAP compared to minimally-invasive parathyroidectomy (MIP) in the treatment of primary hyperparathyroidism (pHPT).

MATERIALS AND METHODS

An ethically approved non-randomized prospective case control study was performed between May 2009 and May 2011. Thirty patients with pHPT were recruited. Triple modality concordant localisation was a pre-requisite for study inclusion. Fifteen patients underwent RAP by the same surgeon (NST). The remaining patients underwent MIP. Intra-operative outcome measures included procedure time and blood loss. Post-operative measures included biochemical and histopathological assessment. Patient-reported outcome measures (PROMs) using validated assessment tools included subjective assessment of pain and scar cosmesis using visual analogue scores (0-100), Voice Disability Index 2 and EQ-5D quality of life assessment performed at 1 day, 2 weeks, 3 months, 6 months and 1 year post-operatively. Mean length of follow-up was 10 months (range 3-24 months).

RESULTS

The parathyroid adenoma was successfully excised in all cases. There was one RAP conversion due to difficult access. The recurrent laryngeal nerve (RLN) was identified and preserved in all cases. Subjective voice assessment demonstrated no post-operative voice change and normal vocal cord mobility was confirmed by fibreoptic laryngoscopy performed on the 1st post-operative day. The mean operative times for RAP and MIP were 129min and 66min respectively. There was no significant difference in mean blood loss between the 2 groups (10ml RAP vs 12ml MIP).

Normalization of adjusted serum calcium levels occurred in 29/30 cases within 2 weeks of surgery. The mean post-operative timeframe for biochemical assessment was 8 months (range, 2 weeks to 24 months). In the remaining patient, further surgical exploration identified four gland hyperplasia not detected by the initial localization studies.

The mean length of the extra-cervical incision used in RAP was 3.5cm compared to 3.2cm in the control group. The mean VAS for scar cosmesis was superior in the robotic cohort from 2 weeks (84% vs. 64%, $p<0.01$). At 1 year, this further increased to 94% compared to 62% in the control group ($p<0.01$). Initial post-operative pain was similar for both groups in the first 2 weeks (Fig. 2). All EQ-5D parameters significantly improved in both groups following surgery.

Fig. 1 Scar cosmesis 9 months after robotic-assisted parathyroidectomy.

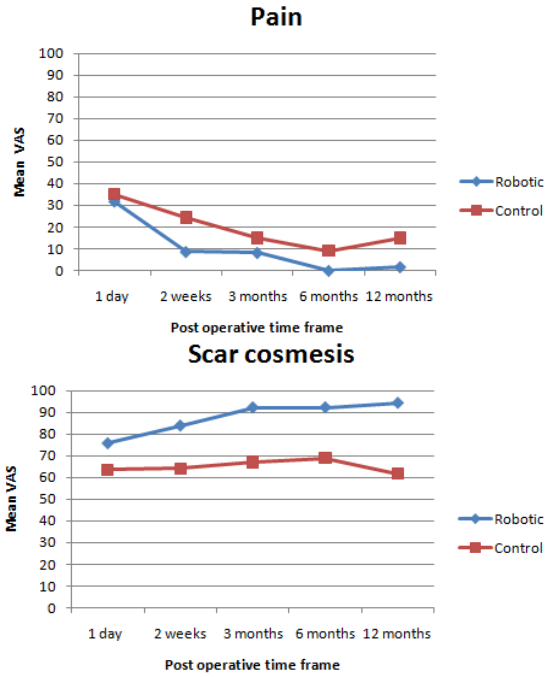

Fig. 2 PROMS for pain (100: worst imaginable pain) and scar cosmesis (100: best cosmetic outcome).

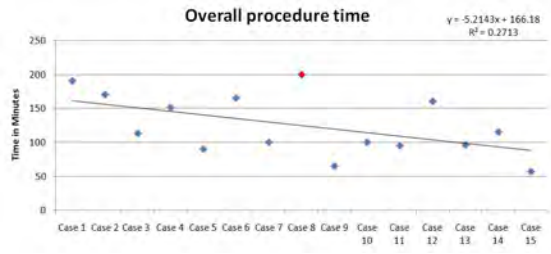

Fig. 3 Learning curve for RAP.

DISCUSSION

Targeted parathyroidectomy is the treatment of choice in at least 65% of patients with pHPT. Cure and complication rates are equivalent to four gland exploration [2]. Parathyroid adenomas are usually small, benign and accurately localised with ultrasound and sestamibi studies.

Several targeted approaches have been described. In this study, a mini incision focused lateral approach was performed in the control group (n=15). RAP using the da Vinci surgical system was performed in the remaining group (n=15). The peri-operative management of both cohorts was standardized and there was no significant difference between the 2 groups regarding mean BMI, age, size and location of parathyroid adenoma or mean follow up.

Scars in easily visible parts of the body such as the anterior neck have detrimental effects on body image [3]. RAP avoids a neck scar by using an infra-clavicular incision (Fig. 1). Limited subcutaneous dissection in RAP appears to translate to postoperative pain and analgesic requirements similar to MIP (Fig. 2). All patients were discharged within 24 hours of surgery.

Mean operative time for RAP was 129 minutes; almost twice that of the control group. A linear regression model was used to evaluate the robotic learning curve based on the total time taken to perform 15 consecutive RAPs (Fig. 3). A calculated line of best fit demonstrates progressive reduction in overall operating time from 3 hours, 10 minutes to 57 minutes ($R^2 = 0.24$ $p< 0.01$). Factors affecting operative time include body habitus, adenoma size and location. There was 1 robotic conversion to open. This occurred due to suboptimal surgical access. The patient's body mass index was 34. In another patient, the post-operative calcium and PTH remained elevated due to four gland hyperplasia not detected by the initial localisation studies. This is a recognised complication of localisation studies and a targeted approach [4].

The primary advantage of the RAP technique is that it permits precise dissection without CO_2 insufflation and avoids a neck incision [2]. This translates to improved patient satisfaction with scar cosmesis. The improvement in quality of life is well established. This study demonstrates that RAP is a feasible alternative to established targeted techniques. The cost-effectiveness of the robotic approach compared to conventional targeted parathyroidectomy warrant further evaluation. This along with the clinical efficacy of RAP and its associated advantages over MIP would be best assessed via a large randomized control trial.

REFERENCES

[1] Arora, A., Cunningham, A., Chawdhary, G., Vicini, C., Weinstein, G. S., Darzi, A., and Tolley, N. Clinical applications of Telerobotic ENT-Head and Neck surgery. *Int. J. Surg.* 2011 Jan 27 [Epub ahead of print].

[2] Henry, J. F. Minimally invasive thyroid and parathyroid surgery is not a question of length of the incision. *Langenbecks Arch. Surg.* **393**:621-626, 2008.

[3] Lawrence, J. W., Fauerbach, J. A., Heinberg, L. Visible vs hidden scars and their relation to body esteem. *J. Burn Care Rehabil.* **25**:25-32, 2004.

[4] Miccoli, P., Berti, P., Materazzi, G., Massi, M., Picone, A., and Minuto, M. N. Results of video-assisted parathyroidectomy: single institution's six-year experience. *World J. Surg.* **28**:1216-1218, 2004.

Image-Guided Robotic Partial Nephrectomy: Benefits and Challenges

Philip Pratt[1], Erik Mayer[2], Justin Vale[2], Daniel Cohen[2],
Eddie Edwards[2], Ara Darzi[2], Guang-Zhong Yang[1]

[1]Hamlyn Centre for Robotic Surgery, Imperial College London
[2]Department of Surgery and Cancer, Imperial College London
p.pratt@imperial.ac.uk

INTRODUCTION

Robotic Partial Nephrectomy (RPN) is presently the fastest-growing robotic surgical procedure, and in comparison to traditional techniques, it offers reduced tissue trauma and likelihood of post-operative infection, whilst hastening recovery time and improving cosmesis. It is also an ideal candidate for image guidance technology since soft-tissue deformation, whilst still present, is localised and less problematic compared to other surgical procedures [1,2,3]. This work describes the implementation and ongoing development of an image guidance system that aims to address some of the remaining challenges in this area.

MATERIALS AND METHODS

Using the 3-arm da Vinci system (Intuitive Surgical), a transperitoneal approach is made to the target kidney. Initially the renal vessels are identified and dissected in preparation for clamping at the appropriate time. Following tumour identification, removal of fatty tissue and kidney mobilisation, the excision boundary is marked with hot shears. The renal vessels are then clamped, initiating a short period of warm ischaemia during which the lesion is resected. The floor of the remaining 'defect' is oversewn, to help achieve haemostasis and prevent urinary leak, then packed with Floseal and bolsters.

Specific image guidance usage has been identified during this procedure, as follows:

- Localisation of tumour and relevant anatomy;
- Marking of excision boundary (of particular importance for completely endophytic lesions which are not directly visible);
- Fast and accurate localisation of renal artery/vein and their respective branches; and
- Ensuring an adequate margin of healthy tissue is resected with the tumour.

The system architecture is based on the NVIDIA Quadro Digital Video Pipeline [4]. This hardware setup offers unprecedented performance in terms of high-resolution video capture, image processing, scene rendering and low-latency data throughput.

Uniquely, capture is direct to GPU memory, and it features some 240 parallel processing cores for which the following real-time CUDA [5] kernels and OpenGL shaders have been developed: image undistortion and rectification, temporal and stereo feature tracking, inverse realism [6], TLED finite element simulation [7], ray-traced composite and isosurface volumetric rendering, and various alpha-blending methods for overlay generation.

In this application, registration is performed using a simple two-stage, semi-automated scheme. A single feature in the left captured image is located and stereo correspondence is established either manually or automatically through parallel template matching. The same feature is located on the surface of mesh geometry, created from segmented preoperative images [8], by means of ray intersections 'picked' through the rendering viewport. The two 3D points are aligned by applying a 3-DOF model translation, effectively 'pinning' the model at one point to the source image. Subsequently, the remaining rotational degrees of freedom are adjusted manually using a highly intuitive rolling ball [9] interface.

RESULTS

Results are presented from both retrospective and live cases. For the former, figure 1 illustrates volumetric and mesh-based rendering of segmented preoperative images, and shows how it is possible to paint a window onto surfaces in the surgical scene, such that target anatomy (tumour, renal vein branch) is revealed underneath using inverse realism.

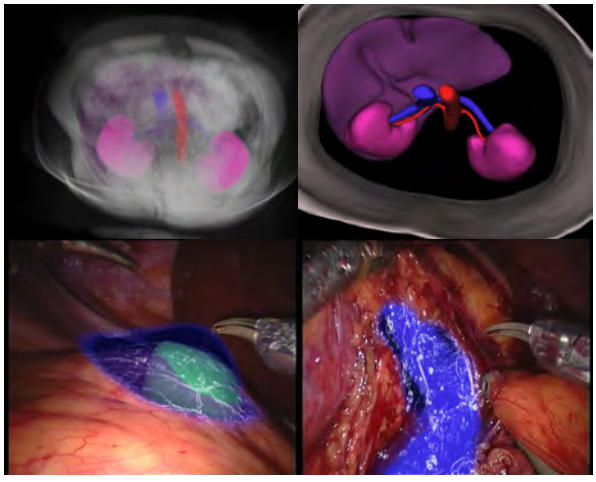

Fig. 1 Images from retrospective guidance footage

Figure 2 illustrates how an excision boundary can be painted on the surface geometry in a preoperative fashion, then rendered as an overlay prior to marking with hot shears. It also shows how a dilated mesh is used to represent the chosen margin of healthy tissue surrounding the lesion, and subsequent comparison against excised tissue.

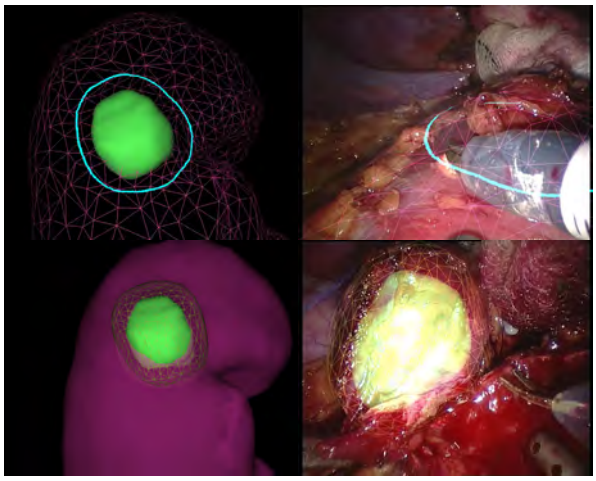

Fig. 2 Additional retrospective guidance footage

In contrast, figure 3 shows still images from guidance footage generated in a contemporaneous manner during a RPN procedure. In this instance, models were built from preoperatively acquired CT data. The intersection of the rendered axes represents the origin of the manual rolling ball rotation.

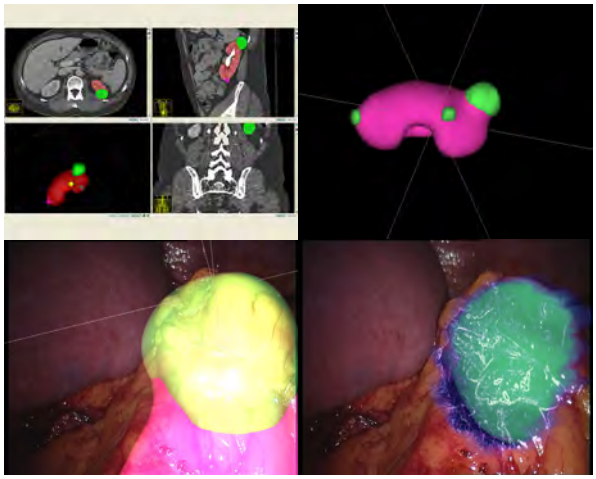

Fig. 3 Preoperative segmentation and images from guidance footage recorded during surgery

DISCUSSION

The system presented offers relatively straightforward, yet immediately valuable opportunities for image guidance at certain key points during RPN procedures. More importantly, it serves as a practical foundation for future development and research into novel registration and tissue deformation modeling techniques. The following enhancements are subject to planning and ongoing development:

- Provision of a comprehensive validation framework to assess overlay accuracy;
- Integration of 6-DOF endoscope and probe tracking, hand-eye and probe calibration, to facilitate live 3D overlay [10] of intraoperative ultrasound images;
- Hybrid dynamic spatial registration techniques which seek to combine ultrasound, optically-based reconstruction and manual adjustment approaches; and
- Integration of existing image-constrained biomechanical modeling techniques [11] to account for soft tissue deformation during the procedure and tool-tissue interaction.

Furthermore, as image quality and resolution obtainable from preoperative scans increase, more accurate models of the vasculature and collecting system in the region of the renal pelvis can be built, helping ensure that warm ischaemia time is kept to a minimum.

ACKNOWLEDGEMENTS

The authors are grateful for support from the NIHR Biomedical Research Centre funding scheme.

REFERENCES

[1] L. Su, B. Vagvolgyi, R. Agarwal, C. Reiley, R. Taylor and G. Hager. Augmented Reality during Robot-assisted Laparoscopic Partial Nephrectomy: Toward Real-time 3D-CT to Stereoscopic Video Registration. Urology 73 (4), 2009: 896-900

[2] D. Teber, S. Guven, T. Simpfendörfer, M. Baumhauer, E. Güven, F. Yencilek, A. Gözen and J. Rassweiler. Augmented Reality: A New Tool to Improve Surgical Accuracy during Laparoscopic Partial Nephrectomy? Preliminary In Vitro and In Vivo Results. European Urology 56, 2009: 332-338

[3] P. Stolka, M. Keil, G. Sakas, E. McVeigh, M. Allaf, R. Taylor and E. Boctor. A 3D-Elastography-Guided System for Laparoscopic Partial Nephrectomies. In Proc. SPIE 7625, 76251I-1, 2010.

[4] http://www.nvidia.com/object/quadro_dvp.html

[5] D. Kirk and W. Hwu. Programming Massively Parallel Processors: A Hands-on Approach. Morgan Kaufmann, 2010.

[6] M. Lerotic, A. Chung, G. Mylonas and G.-Z. Yang. *pq*-space based non-photorealistic rendering for augmented reality. In MICCAI 2007, Part II, LNCS 4792: 102-109.

[7] K. Miller, G. Joldes, D. Lance and A. Wittek. Total Lagrangian explicit dynamics finite element algorithm for computing soft tissue deformation. Communications in Numerical Methods in Engineering 23, 2007: 121-134.

[8] P. Yushkevich, J. Piven, H. Cody Hazlett, R. Gimpel Smith, S. Ho, J. Gee and G. Gerig. User-guided 3D active contour segmentation of anatomical structures. Neuroimage 31 (3), 2006: 1116-1128.

[9] A. Hanson. The Rolling Ball. Graphics Gems III. Academic Press Professional, Inc., 1992: 51-60

[10] C. Cheung, C. Wedlake, J. Moore, S. Paulter and T. Peters. Fused Video and Ultrasound for Minimally Invasive Partial Nephrectomy: A Phantom Study. In MICCAI 2010, Part III, LNCS 6363: 408-415

[11] P. Pratt, D. Stoyanov, M. Visentini-Scarzanella and G.-Z. Yang. Dynamic Guidance for Robotic Surgery using Image-constrained Biomechanical Models. In MICCAI 2010, Part I, LNCS 6361: 77-85.

Active vs. Passive DoF Release during Robot Assisted Knee Anterior Posterior Drawer Tests

R. Takeda, F. M. Rodriguez y Baena, A.A. Amis

Department of Mechanical Engineering, Imperial College, London

r.takeda@imperial.ac.uk

INTRODUCTION

The disease involving the degradation of the joint cartilage, Osteoarthritis (OA) is a common cause of chronic pain and it has been challenge for medical engineers to find solutions and treatments. One stage in finding treatments for OA is to quantify the mechanics of a joint.

In the past various systems have been used to conduct biomechanical testing on the knee joint. An Instron material testing machine was used to analyze the load on the posterior cruciate ligament in the knee during anterior-posterior (AP) drawer [1]. Another example is the use of robotic manipulator in combination with a universal force sensor to create a trajectory for moving a knee joint at a specified load and rate [1]. In both cases, accuracy and repeatability of the systems were crucial for comparing intact or surgically altered knee joint states.

In this work, a robotic knee joint biomechanical testing system was developed, and experiments were conducted to investigate the force measurements of the ligaments during AP drawer tests. Though works in the past have investigated the loads of the ligaments, it has not been assessed whether releasing degrees of freedom (DoF) during AP drawer tests affects the load measurements. This report aims at verifying this by two methods; the first method by mechanically releasing DoFs by means of a free joint fixture (passive), the second by implementing a compliance control algorithm to the robot for generating a force adaptive trajectory (active). Since the active DoF release is controlled by the robot, it can also quantify the amount of DoF release by means of position data. Experiments were conducted on an ovine knee joint specimen and force tendencies between active and passive DoF release were compared.

MATERIALS AND METHODS

The knee joint biomechanical testing systems, basically consists of a 6 DoF industrial robotic manipulator (TX90, Stäubli Ltd), robot controller (CS8C, Stäubli Ltd), 6 axis load/torque sensor (Gamma, ATI Industrial Automation), femur clamp and a tibia clamp fixture (Fig. 1). The robot has a maximum load of 20kg and repeatability of 0.03mm, while the force sensor range is 400N in the Z axis and 130N for the X and Y axis (Fig. 2). Both femur and tibia clamp fixtures were self-developed and the tibia clamp allowed free movement on 3 axes by means of ball bearings.

An ovine knee specimen with the muscular structure surgically removed was prepared. Both the tibia and femur bones were placed in a cylindrical steel pot and fixed with bone cement and screws. The knee specimen was positioned at a 90 degrees flexion extension angle by attaching the femur to the end effector of the robot and the tibia to a clamp fixture attached to the floor. The anterior-posterior (AP) direction was defined in parallel with the Z axis, the medial-lateral (ML) direction with Y axis and the proximal-distal (PD) direction with the X axis of the global coordinate system.

As shown in Fig. 2, the Z axis is always constrained due to the AP drawer test movements however the X and or Y axes can be released or constrained either by:

- **Passive DoF Release**
  Loosening bolts on the tibia clamp results in DoF release in the directions of X, Y or X and Y simultaneously.
- **Active DoF Release**
  Compliance force feedback control can be implemented to release DoF in the directions of X, Y or X and Y simultaneously. The robot will try to reduce the forces in the axes where the control is implemented by changing the position of the end effector.

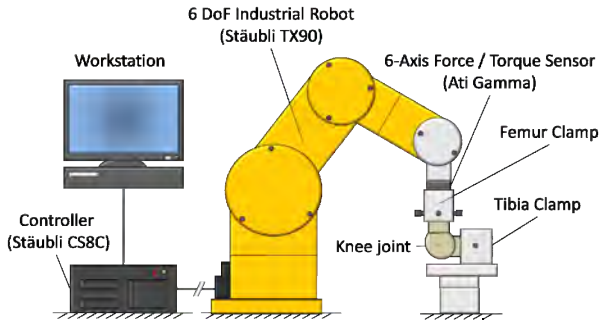

Fig. 1 Components of the developed robotics knee joint bioimechanical testing system.

Force and position data at the end effector of the robot was sampled at 250Hz and recorded via TCP/IP connection to a workstation. The compliance control algorithm for active DoF release was implemented to a real time robot controller using a multi-task capable VAL3 language.

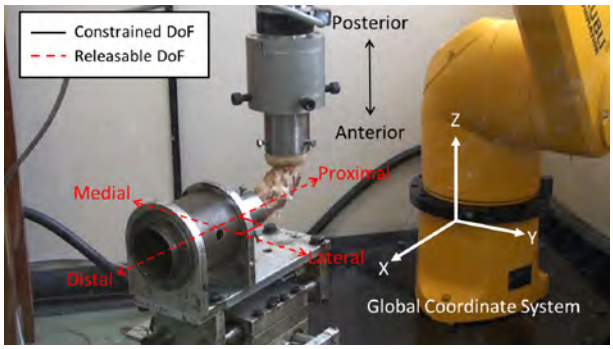

Fig. 2 The experimental setup with ovine knee joint specimen. The constrained axis (black) for conducting AP drawer motion is aligned with the Z axis of the global coordinate system, while the remaing two axes (AL, PD) are aligned with the X and Y.

RESULTS

Figure 3, 4 and 5 represents the force measurements for the PD, ML and AP direction. The vertical axis represents measured force in newtons, horizontal axis represents DoF release conditions; no DoF release (No DoF), X axis or SI direction release (X), Y axis or ML direction release (Y) and the combination of both X and Y released simultaneously (XY). The white bar represents force measurements during No DoF while dark colored bars represents the active release, and light colored bars represents passive release for the X, Y and XY conditions respectively. The data shows the average force measured for ten AP drawer test trials for each condition.

DISCUSSION

From the results obtained from Fig. 3, 4 and 5 it can be said that releasing any degrees of freedom actively or passively, leads to a decrease in force measured in all axes. In addition, the active method showed slightly more force for X and XY release while less for that of Y in the SI and AP direction. However, the force measurement tendencies are similar for active and passive DoF release in all three axes.

This system is still in the pilot stages, therefore more specimens will have to be measured to give a more accurate assessment of the active DoF release method presented here. In addition, the compliance control algorithm of the active DoF release implemented on the robot is not completely optimized and therefore in some condition show higher forces than the passive DoF release. This can also dealt with by modifying the control parameters with more trials on specimens.

The active DoF release is more advantageous than the passive method as it can actually quantify the amount of DoF release by means of position. This will be a crucial element for evaluating and testing the effectiveness of knee joints implants in the future.

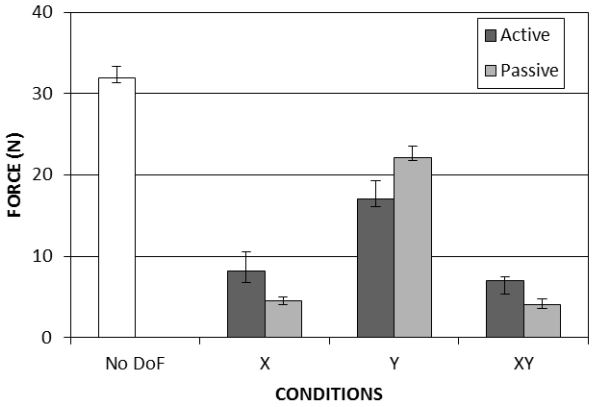

Fig. 3 Forces in the X axis, or PD, direction during AP drawer tests.

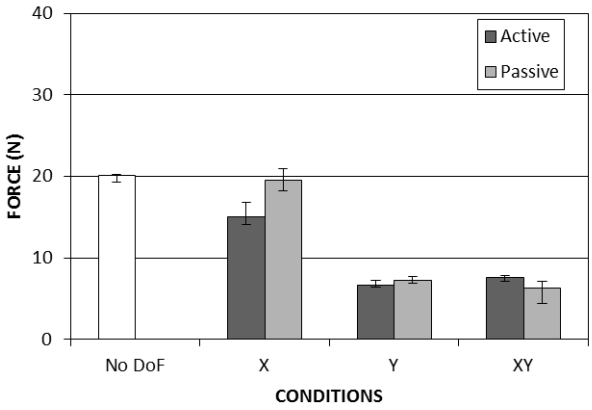

Fig. 4 Forces in the Y axis, or ML, direction during AP drawer tests.

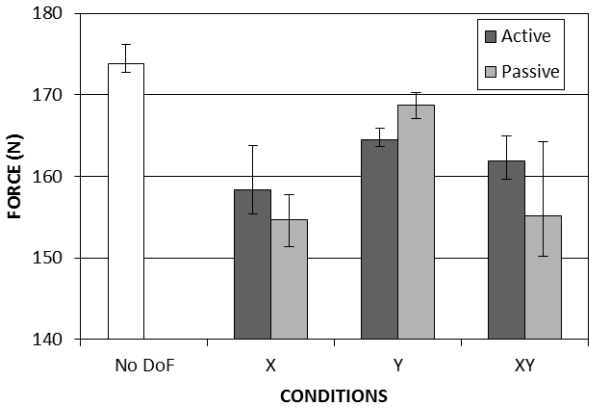

Fig. 5 Forces in the Z axis, or AP, direction during AP drawer tests.

REFERENCES

[1] Race A., Amis A.A. Loading of the two bundles of the posterior cruciate ligament: An analysis of bundle function in A-P drawer. Journal of Biomechanics. 1995 July: 29(7):873-879.

[2] Rudy T.W., Livesay G.A. Woo S. L-Y, Fu F.H. A combined robotic/universal force sensor approach to determine in situ forces of knee ligaments. Journal of Biomechanics. 1996 Oct;29(10):1357-1360.

Robotic Assisted Transvaginal Tubal Ligation using a Novel Hyper-redundant Snake Robot Platform

J. Clark, D. Noonan, M. Sodergren, C. Payne, J. Shang, V. Vitiello, T. Athanasiou, J. Teare, P. Mason, A.Darzi, G.-Z.Yang

The Hamlyn Centre for Surgical Robotics, Imperial College London

INTRODUCTION

Surgery for permanent contraception in women is common worldwide. In the USA alone 650,000 tubal ligation procedures are undertaken per year[1]. Currently the surgery is approached through both the open technique; a 3cm incision in the suprapubic region, and the laparoscopic technique; a 2 port technique one through the umbilicus and one further 10mm port to one side. However,since the operation is often elective and requested by the patient the unsightly abdominal scar or risk of damage to the umbilicus, as may be the case with the conventional laparoscopic approach, may prevent patients opting for this contraceptive option. Presenting an alternative which leaves no visible trace may present women with a greater degree of control over their own choice for contraception.

Natural Orifice Surgery is still in its infancy and although the transvaginal approach is considered a safe access route, significant challenges still remain. These are predominantly as a result of the current flexible endoscopic technology. While an endoscope provides the ability to undertake the curved pathways required to access all areas of the peritoneum including retroflexion into the pelvis, its inherent flexibility along its entire length results in significant difficulty to coordinate the control of both the device and instrumentation when attempting intervention [2]. The introduction of a hyper-redundant robotic platform may overcome some of those challenges and promote the robotic assisted approach as one which is safe and effective.

MATERIALS AND METHODS

The Flexible Robotic Platform

The device is a 12.5mm diameter, multi-articulated robotic endoscope. Its joints enable the robot to be controllably flexible throughout the 185mm length of the articulating segment. This provides a total of seven degrees of freedom serially arranged into two universal joint with two axes of movementand three single axis joints. Forward drive and rotation provides two additional degrees of freedom.

A 3.0mm central channel, transmitted through the entire length of the device and exiting at the tip, provides a route to pass and interchange standard flexible endoscopic instruments and flexible sensing tools [3]. The instrumentation can be passed through the entire device irrespective of the individual joint configurations. A second 3mm channel is used to pass a camera for visualisation (MedigusIntroSpico 115) and power lines for a distal tip mounted Light Emitting Diode (LED) unit for illumination.

The Robotic Assisted Tubal Ligation

The procedure was performed in a live porcine model under United Kingdom approved Home Office License (number 80/2297). A 75kg female pig was used for the purposes of the trial. Due to differences in the pelvic and more specifically the uterine anatomy between the pig and the human, the uterine horns were used to represent the target fallopian tubes. The fallopian tubes in the pig model are shorter and predominantly redundant therefore do not adequately reflect the suitability of the proposed operation in the human nor adequately demonstrate the capabilities of the robot. For the purposes of the trial a single tube was targeted for feasibility. Prior to the procedure urinary catheterisation was undertaken and the bladder deflated.

The Technique

Under direct vision a 10mm transumbilical port was inserted and pneumoperitoneum was established to maintain a pressure of 12mmHg. The transvaginal incision was subsequently made in the posterior fornix and a 15mm, 150mm bariatric port (Applied Medical, CA. US) which had been customised in-house to a length of 400mm to overcome the lengthy porcine pelvic anatomy, was inserted through the colpotomy and into the peritoneal cavity. The placement of the port was confirmed by the use of a 10mm laparoscope inserted transabdominally. This additionally enabled external visualisation of the robot to be undertaken during the task for recording purposes only.

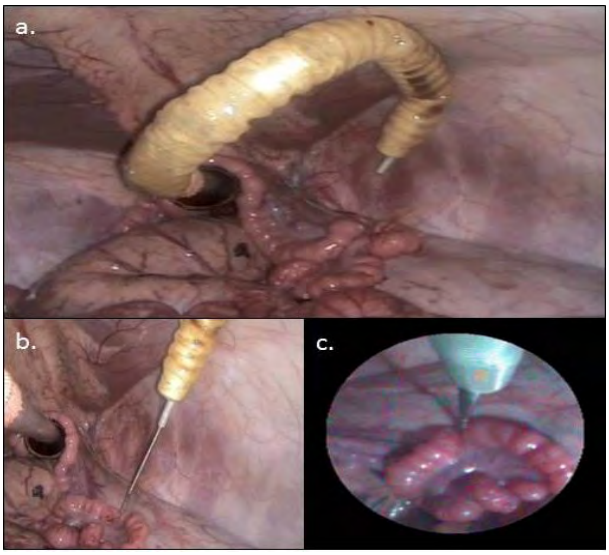

Fig. 1 Robotic assisted transvaginal tubal ligation. a) The robot retroflexed in the pelvis with b) endoscopic clip passed (*view from an external laparoscope*). c) Clipping the tube as viewed from the onboard camera.

The robot was inserted into the port and driven forward, retroflexed and rotated to target the right uterine horn. Once the tissue was visualised, guided by the on-board camera, the instrumental section of the procedure was undertaken. Two endoscopic clips (Boston Scientific, MA. US) were passed separately through the robot whilst in the retroflexed position and activated to lie side by side on the uterine horn. Once security of placement of the clips was confirmed through the elevation of the section using flexible endoscopic graspers, a needle endoscopic diathermy knife was inserted and, using the distal articulating segment of the robot, divided the horn between the 2 clips.

RESULTS

The procedure was completed successfully without any complications, although an initial clip, inserted through the device to clip the horn, was activated before being applied to the tissue and as such required subsequent retrieval by the robot using the flexible endoscopic graspers impacting on overall procedure time. Division of the tube was confirmed prior to removal of the robot from the pelvis. The clip and ligation of one tube from the point of access to the removal of the robot took 47 minutes. No bowel or unrelated injury occurred as a result of the introduction of the robot and the procedure was performed without blood loss.

DISCUSSION

In its current form Flexible access surgery which includes NOTES continues to be unable to present a clinically viable alternative to the laparoscopic approach which, aside from the challenges surrounding safe access and security of closure, predominantly relate to the ergonomic challenges of using the flexible endoscope.

Natural orifice surgery offers a fresh avenue for the exploration and development of novel “focused” robotic surgical platforms which can be utilized for very specific periods during procedures when the benefits of the computer interface may enhance diagnostic and therapeutic intervention. The robotic multi-articulated endoscopic device presented here already meets many of the more significant challenges facing NOTES by providing a stable operating platform, single operator remote control, and a negligible footprint within the operating theatre. Furthermore, it also frees up one hand enabling either, operator control of the flexible instruments down the central channel of the device further reducing the number of assistants within the crowded workspace in theatre.

Adjunctive software to the device will enable automated movements, such as retroflexion, as well as path following and path constraints using pre-operative imaging to navigate safely within the abdominal cavity [4].

The potential for such a device goes beyond the gynaecological with the ability for image guidance and stability, interventions such as cell based therapies or local high dose chemotherapeutic drug delivery can be delivered with precision. Real time histology provided through the use of confocal endomicroscopy [5] becomes an effective sensing tool only because of the automated fine precise motion which can be provided through the use of an articulated robotic platform such as this.

REFERENCES

[1] Chan LM, Westhoff CL. Tubal sterilization trends in the United States. Fertil Steril;94:1-6.

[2] Kondo W, Noda RW, Branco AW, et al. Transvaginal endoscopic tubal sterilization. J Laparoendosc Adv Surg Tech A 2009;19:59-61.

[3] J. Shang, D.P. Noonan, C. Payne, et al. An Articulated Universal Joint Based Flexible Access Robot for Minimally Invasive Surgery. (Submission to IEEE International Conference for Robotics and Automation 2010).

[4] K.W. Kwok, G.P. Mylonas, L.W. Sunet al, Dynamic Active Constraints for Hyper-Redundant Flexible Robot, Medical Image Computing and Computer-Assisted Intervention (MICCAI 2009), LNCS, Springer Heidelberg, Vol.5761, 2009, pp.410-417.

[5] Noonan DP, Payne CJ, Shang J, et al. Force adaptive multi-spectral imaging with an articulated robotic endoscope. Med Image Comput Comput Assist Interv;13:245-52.

Initial Experience with a Randomised Controlled Trial of Open, Robotic, and Laparoscopic (CORAL) Radical Cystectomy: An Interim Report

A. Patel[1], F. Ismail[1], T. S. O'Brien[1], P. Rimington[2], P. Dasgupta[1], M. S. Khan[1]

[1] Department of Urology, Guy's and St Thomas' NHS FoundationTrust

[2]Department of Urology, Eastbourne General Hospital, Eastbourne,

amit.patel@gstt.nhs.uk

INTRODUCTION

Open radical cystectomy (ORC) is the gold standard treatment of muscle invasive and high risk bladder cancer. ORC is associated with significant morbidity (20-50%) [1-2] and hospital stay averaging 18.7days[3] in the United Kingdom. Minimally invasive radical cystectomy has been demonstrated to be feasible and associated with less blood loss (EBL), reduced operative pain, earlier return of bowel function and quicker recovery[4-5]. We present the interim results of a randomized control trial comparing open (ORC), laparoscopic (LC) and robotic assisted radical cystectomy (RALC) (CORAL).

MATERIALS AND METHODS

From March 2009 to March 2011, 33 patients have been recruited to this three arm trial who agreed to take part in the trial and were suitable to undergo radical cystectomy by either of the three techniques. Patients with bleeding diathesis, history of pelvic radiotherapy, extensive abdominal/pelvic surgery were excluded from the study. Of those who have undergone surgery 13 had open, 9 robotic assisted and 11 laparoscopic cystectomy. Extra-corporal urinary diversion was performed in patients randomized to minimally invasive arms. Postoperative management was standardized and managed by a single bladder cancer team at our institution.

A prospective database of operative times, EBL, transfusion, length of stay and inpatient, 30 and 90 day complications were recorded using the modified Clavien system.

RESULTS

The patient demographics are shown in table 1. Patients were evenly matched for age, sex, body mass index(BMI) and ASA grade. There were no deaths. There were 2 conversions: 1 from RARC to ORC and 1 from LRC to RARC.

Table 1

Characteristics	***ORC***	***RALC***	***LC***	Total
Patients, n	13	9	11	33
Sex, n				
Male	12	7	10	29
Female	1	2	1	4
Median (range)				
Age, years	66(54-79)	64(52-71)	67(42-80)	
BMI	27(22-33)	25(20-31)	27(24-32)	
ASA	2(1-3)	2(1-3)	2(1-3)	

Table 2

	ORC	***RALC***	***LRC***
Operating time mean(range)	283 (240-375)	376 (290-465)	308 (240-420)
Estimated blood loss, mean(range) mls	750 (500-1200)	456 (100-1200)	465 (50-1000)
Hospital stay, mean(range) days	12.6 (9-21)	8.7 (5-17)	8.6 (5-14)
Lymph node yield, mean(range)	21.9 (7-37)	12.3 (4-23)	16 (7-23)
Overall complication	54%	33%	27%
Significant complication	8%	22%	18%

Results following ORC, RALC and LC are shown in table 2. The significant complication in ORC was an abdominal collection requiring radiological drainage. During a RALC 1 patient suffered a rectal injury and 1 patient returned to theatre for post operative haemorrhage. During a LC 1 patient suffered an obturator nerve injury and post operatively 1 patient required radiological drainage of an abdominal collection.

CONCLUSIONS

RALC and LC appear to be evenly matched in outcomes from surgery in terms of length of stay, complications rates and estimated blood loss. These findings would correlate to a recently reported prospective non-randomised study comparing post operative complications in ORC (31%) versus RALC (17%) by NG et al.[6] ORC has relatively greater lymph node yield and shorter operative time as compared to minimally invasive RC. The lymph node yield findings for the minimally invasive approaches are low as compared to two comprehensive studies on this matter[6,7] however our interim results have not shown any statistically significant differences between the different surgical approaches as yet. Our study is on-going and hope to present further results in the future.

REFERENCES

[1] B.R. Konety, V. Allareddy, H. Herr. Complications after radical cystectomy: analysis of population-based data. Urology 68 (2006) (58 - 64)

[2] V. Novotny, O.W. Hakenberg, D. Wiessner, et al.. Perioperative complications of radical cystectomy in a contemporary series. Eur Urol 51 (2007) (397 – 402)

[3] M.C. Nuttall, J. van der Meulen, G. McIntosh, D. Gillatt, M. Emberton. Changes in patient characteristics and outcomes for radical cystectomy in England. BJU Int 95 (2005) (513 - 516)

[4] G.-P. Haber, J.R. Colombo Jr., M. Aron, O. Ukimura, I.S. Gill. Laparoscopic radical cystectomy and urinary diversion: status in 2006. Eur Urol Suppl 5 (2006) (950 - 955)

[5] J.B. Basillote, C. Abdelshehid, T.E. Ahlering, A.M. Shanberg. Laparoscopic assisted radical cystectomy with ileal neobladder: a comparison with the open approach. J Urol 172 (2004) (489 - 493)

[6] Ng CK, Kauffman EC, Lee M-M, et al. A comparison of postoperative complications in open versus robotic cystectomy. Eur Urol 2010;57:274–82.

[7] Nix J, Smith A, Kurpad R, Nielsen ME, Wallen EM, Pruthi RS.Prospective randomized controlled trial of robotic versus open radical cystectomy for bladder cancer: perioperative and pathologic nresults. Eur Urol 2010;57:196–201.

Video Motion Analysis for Approaching Objective Assessment of Catheter-based Endovascular Interventions

C.V. Shah[1], C.V. Riga[1,2], D. Stoyanov[3], G.-Z. Yang[3], N.J.W. Cheshire[1,2], C.D. Bicknell[1,2]

[1]*Academic Division of Surgery, Department of Surgery & Cancer, Imperial College London*

[2]*Regional Vascular & Endovascular Unit, Imperial College London*

[3]*Hamlyn Centre for Robotic Surgery, Imperial College London*

chiragh.shah07@imperial.ac.uk

INTRODUCTION

Endovascular surgery is a rapidly evolving field, driven largely by advances in technology, and hence technique. Endovascular treatment options are being applied to all areas of vascular disease, and a range of clinical specialists are interested in offering services such as carotid artery stenting (CAS). With increasing uptake and complexity of cases undertaken, there is a need to address endovascular technical skills assessment.

Technical proficiency is an essential component of surgical competence. With patient safety of paramount importance, there is currently a drive for objective appraisal of technical skill within surgery [1], and a number of approaches to assessment now exist [2]. However, objective evaluation of endovascular skill is limited, with a few areas being studied [3]. Motion analysis is one area that has been relatively unexplored in endovascular procedures.

Hand, instrument, and virtual reality motion analysis has been demonstrated by a number of groups using electromagnetic, mechanical and optical systems [4], of which a few have been validated as part of assessment models for open and laparoscopic procedures [5-11]. This study proposes a system for motion analysis in endovascular interventions by taking advantage of real-time fluoroscopic moving images. Using video motion tracking software, it is possible to track catheter tip movement within video-recorded fluoroscopy of catheter-based endovascular procedures (Fig. 1). The system, while possibly being used for assessing operator performance, has the added prospect of differentiating technologies in both live and simulated cases. The technique provides frame-by-frame two-dimensional (2D) Cartesian coordinates, which can be further manipulated to provide objective descriptive statistics for dexterity analysis.

This study aims to demonstrate the potential application and clinical value of video tracking based 2D catheter motion monitoring and subsequent assessment through analysis of video-recorded *in vitro* simulated interventions.

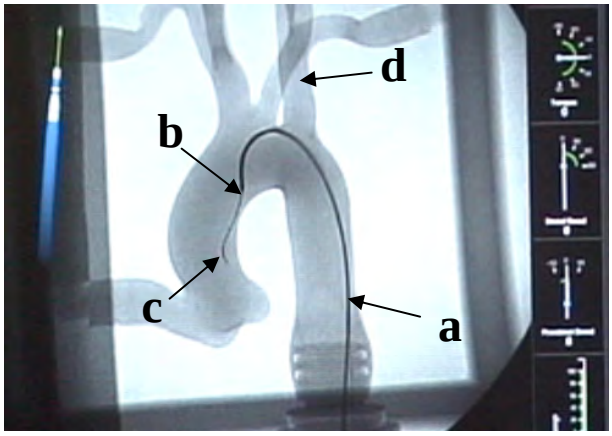

Fig. 1 Example of an aortic arch catheterisation procedure of a phantom model illustrating (a) conventional catheter; (b) catheter tip; (c) guide-wire; (d) aortic arch and target vessels for cannulation.

MATERIALS AND METHODS

Procedures had been video-recorded for previous studies. A computed tomography (CT)-reconstructed pulsatile-flow aortic arch phantom was utilised to simulate target vessel cannulation by conventional and robotic endovascular catheters. Operators of varying levels of skill/experience were asked to cannulate all vessels using both of the catheter technologies. Fluoroscopic images were video-recorded using a standard video camera observing the operator console for assessment by video motion tracking software.

The goal of the proposed tracking framework is to determine the 2D image movement of the catheter tip (Fig. 1b) such that the motion can be analysed for skills evaluation and comparison. This is performed semi-automatically with the user selecting the tip of the catheter and the video tracking software estimating its motion in subsequent frames through template matching. The matching algorithm is simply based on the zero mean normalised cross correlation (ZNCC) of an image template around the catheter tip. The motion model of the template is currently only a translation in the image plane.

This is only a preliminary study and more advanced techniques are available for guide-wire and catheter tip tracking though they are particularly targeted at navigation systems [12,13]. In this work, we do not

require fully automated tracking as the analysis and evaluation of skills is performed retrospectively. Translational measurements would be calibrated against known CT dimensions of models.

RESULTS

Video sequences of the individual procedures were processed through the software to provide coordinates of the catheter tip on a frame-by-frame basis. These were used to provide an image of the catheter tip path.

Some examples of catheter tip tracked paths of left common carotid artery (LCCA) cannulations have been superimposed over their fluoroscopic images to visually illustrate the data provided by the software as shown in Fig. 2. It is apparent that the data can potentially offer valuable information about the varying technical skill levels of different subjects, and therefore demonstrate potential value in utilising the technique for the purposes of training and assessment.

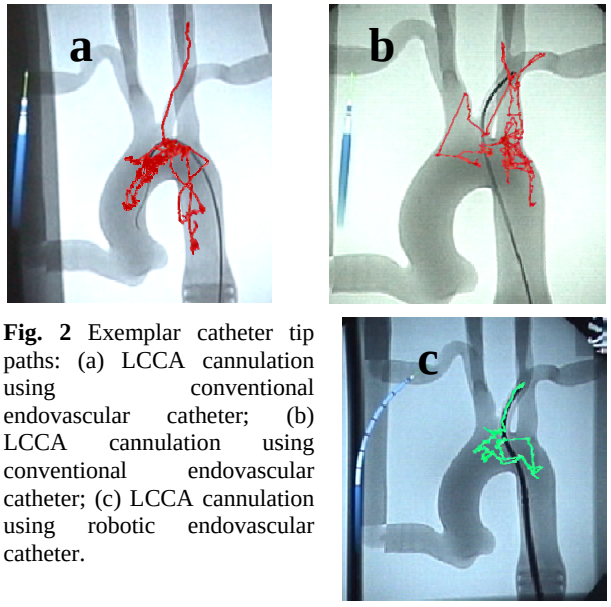

Fig. 2 Exemplar catheter tip paths: (a) LCCA cannulation using conventional endovascular catheter; (b) LCCA cannulation using conventional endovascular catheter; (c) LCCA cannulation using robotic endovascular catheter.

DISCUSSION

In this study, we have presented a method for automated catheter tip tracking for enabling enhanced trajectory analysis and further evaluation of robotic and manual catheter operating skills. The software provides an accurate means by which to quantify movements during endovascular procedures. This data can then be further analysed to demonstrate potential construct and concurrent validity in the parameter of catheter tip path length amongst operators of varying skill/experience. To demonstrate precision of path length measurements, the software would be first run repeatedly against standardised animations.

This form of motion tracking has the potential to offer data for a number of parameters concerned with dexterity through the analysis of raw frame-by-fame coordinate data, and hence its use can be directed at both the assessment of operators as well as catheter technologies. Used in conjunction with other tools measuring other aspects of technical skill, this technique can form part of an assessment program.

As part of our ongoing and future work we are investigating methods for improving the tracking scheme to provide further information about the shape and position of the catheter. In addition, by incorporating measures based on the known geometry of the phantom environments, we believe more advanced evaluation strategies will become apparent.

REFERENCES

[1] Darzi A, Smith S, Taffinder N. Assessing operative skill. Needs to become more objective. *BMJ (Clinical research ed.)* 1999 Apr 3;318(7188): pp. 887-888.

[2] Moorthy K, Munz Y, Sarker SK, Darzi A. Objective assessment of technical skills in surgery. *BMJ (Clinical research ed.)* 2003 Nov 1;327(7422): pp. 1032-1037.

[3] Neequaye SK, Aggarwal R, Van Herzeele I, Darzi A, Cheshire NJ. Endovascular skills training and assessment. *Journal of vascular surgery : official publication, the Society for Vascular Surgery [and] International Society for Cardiovascular Surgery, North American Chapter* 2007 Nov;46(5): pp. 1055-1064.

[4] Chmarra MK, Grimbergen CA, Dankelman J. Systems for tracking minimally invasive surgical instruments. *Minimally invasive therapy & allied technologies : MITAT : official journal of the Society for Minimally Invasive Therapy* 2007;16(6): pp. 328-340.

[5] Datta V, Mackay S, Mandalia M, Darzi A. The use of electromagnetic motion tracking analysis to objectively measure open surgical skill in the laboratory-based model. *Journal of the American College of Surgeons* 2001 Nov;193(5): pp. 479-485.

[6] Datta V, Chang A, Mackay S, Darzi A. The relationship between motion analysis and surgical technical assessments. *American Journal of Surgery* 2002 Jul;184(1): pp. 70-73.

[7] Bann SD, Khan MS, Darzi AW. Measurement of surgical dexterity using motion analysis of simple bench tasks. *World journal of surgery* 2003 Apr;27(4): pp. 390-394.

[8] Moorthy K, Munz Y, Dosis A, Bello F, Chang A, Darzi A. Bimodal assessment of laparoscopic suturing skills: construct and concurrent validity. *Surgical endoscopy* 2004 Nov;18(11): pp. 1608-1612.

[9] Francis NK, Hanna GB, Cuschieri A. The performance of master surgeons on the Advanced Dundee Endoscopic Psychomotor Tester: contrast validity study. *Archives of surgery (Chicago, Ill.: 1960)* 2002 Jul;137(7): pp. 841-844.

[10] Egi H, Okajima M, Yoshimitsu M, et al. Objective assessment of endoscopic surgical skills by analyzing direction-dependent dexterity using the Hiroshima University Endoscopic Surgical Assessment Device (HUESAD). *Surgery today* 2008;38(8): pp. 705-710.

[11] Yamaguchi S, Yoshida D, Kenmotsu H, et al. Objective assessment of laparoscopic suturing skills using a motion-tracking system. *Surgical endoscopy* 2011 Mar;25(3): pp. 771-775.

[12] Brost, A.Rui Liao, Joachim Hornegger, Norbert Strobel: 3-D Respiratory Motion Compensation during EP Procedures by Image-Based 3-D Lasso Catheter Model Generation and Tracking. MICCAI (1) 2009: 394-401.

[13] Barbu, A., V. Athitsos, B. Georgescu, et al. Hierarchical Learning of Curves: Application to Guidewire Localization in Fluoroscopy. CVPR, 2007.

Evaluation of Robot Assistance in Neurosurgical Applications

G. Kronreif, W. Ptacek, M. Kornfeld, M. Fürst

Austrian Center for Medical Innovation and Technology – ACMIT
Integrated Microsystems Austria GmbH
gernot.kronreif@acmit.at

INTRODUCTION

Neurosurgery was one of the first clinical applications of robotics and continues to be a topic of current interest. Neurosurgical stereotactic applications require spatial accuracy and precision targeting to reach the anatomy of interest while minimizing collateral damage [1]. Apart from robotic assistance, there are other methods available and used in clinical practice, e.g. stereotactic frames and neuro-navigation systems. An analysis of usability aspects as well as of accuracy for these different methods has been accomplished in a detailed study with inclusion of clinicians with different experience levels. Accuracy tests have been performed with a special designed phantom under clinical conditions. Test scenarios have been designed according to a realistic clinical work-flow for brain biopsy process. Validation of accuracy has been performed according to EN ISO 9283 - evaluation of usability was done based on the PROMEDIKS-method [2]. This paper presents the results for the accuracy evaluation as well as a discussion of the results and further steps.

MATERIALS AND METHODS

Three different methods can be used for needle-based neurosurgical interventions and have been evaluated in the present study:

- Stereotactic frame,
- Neuro-navigation, and
- Robot assisted procedure.

In *Stereotaxy* – a technique used since the 1950's – a coordinate frame is being attached to the patient's skull and serves as a reference system for planning and execution. The high accuracy of the method qualifies Stereotaxy for diagnosis and therapy of deep lesions, treatment of movement disorders, or vascular malformations. *Neuro-navigation* belongs to the family of image guided treatment. Essentially, this method is based on real-time quantitative spatial fusion of images of the patient's brain with a virtual coordinate system for the purpose of guiding the surgeon's instrument or probe to a selected target. Tracking of tools and target area with different (mainly optical) tracking systems complete a classical neuro-navigation setup. *Robot assisted procedures* finally did not reach the state of a routine setup yet and are, compared to the two aforementioned methods, not used that frequently. To some extent, the use of a robot system for neurosurgery can be seen as a combination of the two methods described above. In most of the known setups the robot is taking over the role of the stereotactic frame by bringing the tool to the right position and orientation, based on a preoperative imaging and planning. In contrast to classical stereotaxy, the robot (mostly) is not being attached to the patient skull, but in a permanently known position and orientation relative to the planning coordinate frame. Robotic systems designed for neuro-surgical interventions include the Minerva (EPFL Lausanne), the PathFinder (Amstrong Healthcare) or the NeuroMate (Integrated Surgical Systems, now Renishaw-Mayfield). The robot system used in the present study however is a robot which originally has been developed for US- and CT-based procedures in interventional radiology – the B-RobII system. The combination of high dexterity and small size seems to be a perfect prerequisite for this robot to be used in neurosurgical applications which should be proven in the reported evaluation study.

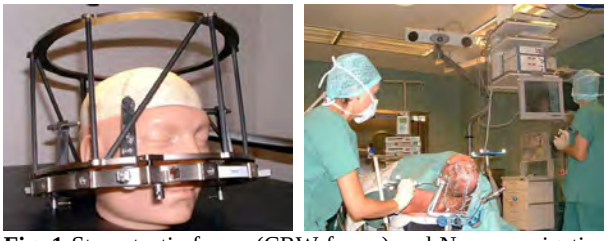

Fig. 1 Stereotactic frame (CRW frame) and Neuro-navigation system (Medtronic Treon) in OR-setup. Source: LNK Wagner-Jauregg, Austria

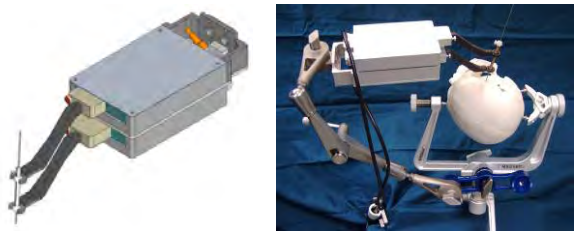

Fig. 2 Robot system B-RobII – schematic view and robot in neurosurgical setup

The B-RobII robot system [3], [4] basically consists of two high-precision positioning modules, each of which having two degrees-of-freedom (DOF) in x-y-configuration. For needle angulation a parallelogram structure is established by relative motion of two parallel "fingers" connected to each other by means of spherical joints The integrated design allows high

dexterity regardless of the small footprint of the system. The robot allows any possible combination of 2-DOF needle angulation (±35◦) and 2-DOF positioning (±20 mm for each axis) as well as maintaining a software-defined pivot point for angulation (cf. Fig. 2).

Evaluation of Accuracy

Evaluation of the targeting accuracy of the three aforementioned methods was performed according to EN ISO 9238 (Manipulating industrial robots -- Performance criteria and related test methods). This international standard is setting different performance criteria for (industrial) robots and suggesting test procedures in order to obtain appropriate parameter values. Due to the nature of the investigated application scenario of neurosurgery, focus for evaluation was on measurement of „accuracy of pose“ only – the measured accuracy however includes all sources of inaccuracy, e.g. registration and target selection. A dedicated measurement phantom has been developed which aims to simulate the different targeting options for brain biopsies as good as possible (cf. Fig 3). Targets have been simulated by spheres with 10mm diameter and are arranged in different heigths in order to simulate different trajectory lengths.

Fig. 3 Measurement setup for stereotactic frame and evaluation of targeting accuracy

RESULTS

Trials have been performed under clinical conditions at “Landesnervenklinik Wagner-Jauregg” in Linz, Austria.

Evaluation of Accuracy

Measurement has been performed for each target (Zyl1, Zyl2, Zyl3) separately. The table below shows the mean values (in mm) for pose accuracy according to EN ISO 9238 for each target and in total.

Table 1 Targeting accuracy for different methods and different target regions

Method	Zyl1	Zyl2	Zyl3	Total
Stereotaxy	1.70	1.45	1.30	1.52
Neuro-navigation	2.42	3.37	2.70	2.83
Robot assistance	0.99	1.02	1.34	1.11

The measured targeting accuracy is in line with data from literature, which shows a targeting accuracy of ± 2mm for Stereotaxy and ± 3mm for neuro-navigation. Experiments also have shown that accuracy for stereotactic frame can be improved to sub-millimetric accuracy by proper maintenance of the mechanical system and an exact needle guide on one hand, as well as by accurate transfer of planning data to the frame scales on the other. Reachable accuracy for the neuro-navigation very much depends on how much time and effort will be used in order to align the needle/needle guide according to the targeting information provided by the navigation software. Measurements for the robot assistance show – in contrast to Stereotaxy and neuro-navigation – a clear relation between trajectory length and accuracy.

DISCUSSION

As mentioned above, spatial accuracy is of paramount importance for neurosurgical interventions. This study shows that the reachable accuracy is similar for Stereotaxy and robotic assistance. Trials also have shown that the influence of both skill level and effort for transferring the preoperative planning data into action is significant for Stereotaxy and neuro-navigation, whereas this human factor is not such prominent for robotic assistance.

Combined with the findings from the usability evaluation for all three methods (not reported in this paper), a combination between robotic assistance (good accuracy) and neuro-navigation (usability aspects) seems to be a useful way to perform needle-based interventions in the brain. A first cadaver study for such a combined setup has been performed recently with very promising results (cf Fig. 4).

Fig. 4 Combined setup neuro-navigation (VectroVision, BrainLAB) and B-RobII during cadaver trial

REFERENCES

[1] Cleary K, Nguyen C. State of the art in surgical robotics: clinical applications and technology challenges. Computer Aided Surgery, 2001;6:312–328.

[2] Backhaus C. Entwicklung einer Methodik zur Analyse und Bewertung der Gebrauchstauglichkeit von Medizintechnik. PROMEDIKS – Prozessorientierte Medizintechnik in klinischen Systemen. Dissertation, Technische Univ. Berlin, 2004.

[3] Cleary K, Melzer A, Watson V, Kronreif G, Stoianovici D. Interventional robotic systems: Applications and technology state-of the-art. Minimally Invasive Therapy. 2006; 15:2; 101–113.

[4] Kronreif G, Fürst M, Ptacek W, Kornfeld M, Kettenbach J. Robotic Platform B-RobII: In vitro Tests and Results. Proc. 4th International Conference on Computer Aided Surgery around the Head, 2007, Innsbruck, Austria.

Author Index

W

Y

Z